CALIFORNIA INSTITUTE OF TECHNOLOGY

EARTHQUAKE ENGINEERING RESEARCH LABORATORY

STATISTICAL SYSTEM IDENTIFICATION AND APPLICATIONS TO SEISMIC RESPONSE OF STRUCTURES

BY

CHI-MING YANG

REPORT NO. EERL 96-02

PASADENA, CALIFORNIA

1996

Statistical System Identification and Applications to Seismic Response of Structures

Thesis by

Chi-Ming Yang

In Partial Fulfillment of the Requirements

for the Degree of

Doctor of Philosophy

California Institute of Technology

Pasadena, California

1996

(Submitted May 28, 1996)

Acknowledgements

I would like to express my sincere appreciation to my advisor, Professor James L. Beck, for his enthusiastic guidance of my research and continuous support and encouragement throughout my graduate study at Caltech. I am especially grateful for many useful meetings and discussions with him during the weekends and even evenings. The generous financial support provided by Caltech during these years to help me concentrate on the research is also deeply appreciated.

The willingness of the faculty members in the examining committee of my thesis – Professors James K. Knowles, Thomas K. Caughey, Paul C. Jennings, and John F. Hall – to spend their valuable time reviewing the thesis and giving me suggestions is very much appreciated. The courses I took from them are no doubt the best I have ever received during the course of my education.

Many individuals associated with Caltech have assisted me in various aspects during my stay at Caltech : Sharon Beckenbach, Denise Okamoto, Jackie Beard, Philip Roché, Jennifer Packman, Dar-Yun Chiang, Cheh-Ming Liu, Ching-Tung Huang, and Eduardo Chan. Many thanks go to these nice people.

I want to express my special gratitude to my girl friend, Helen, for her patience, faithful companionship, and continuous encouragement. The numerous talks between us are very inspiring and have also provided me with new perspectives of various facets of life.

Finally, I am deeply grateful to my parents in Taiwan, to whom this thesis is dedicated, for their continuous and unconditional encouragement and support for all these years during the pursuit of my graduate study in the United States. I am also greatly indebted to my brother for taking care of the family while I am away from home.

Abstract

A pragmatic and versatile statistical system identification framework is presented and applied to seismic response records of structures. The framework is based on the interpretation of probability as a measure of plausibility and on Bayesian statistical inference. Various classical system identification techniques can be derived and viewed as the special cases of the framework. However, the framework can provide a more informative interpretation of the identified optimal model.

When the number of sampled input and output data from structures is large, useful asymptotic approximations of the analytical results are available. These asymptotic approximations are incorporated into the framework by introducing the definitions of system identifiability and model identifiability. New asymptotic approximation results are derived for the system un-identifiable case.

From the viewpoint of asymptotic approximations, the system identification problem is a non-trivial global optimization problem. Two generalized trajectory methods, the homotopy scheme and the relaxation scheme, are presented which can be combined to provide a very robust numerical procedure for global optimization. Both methods can also be applied to find the roots of a set of nonlinear algebraic equations.

Structural model updating is useful because it can be applied to structural health monitoring and is also desirable since the theoretically based stiffness matrix of a structure can be improved by using the measured structural response data. However, no well-accepted solution to this difficult problem has emerged primarily because it is an ill-conditioned and non-unique inverse problem. A single-stage structural model updating approach using the least-squares prediction-error system identification method and a substructuring technique is proposed and applied to simulated and real structural response data.

Contents

List of Figures

List of Tables

Chapter 1

Introduction

1.1 Motivation and Objectives

For centuries, strong earthquakes happening around the world have caused a tremendous loss of lives and property in human society. Although the occurrence of strong earthquakes cannot be prevented, society has been trying to devise effective approaches to reduce the impact of future strong earthquakes. Researchers and professionals in the field of earthquake engineering have been making significant and continual contributions to this goal for several decades. From the perspective of earthquake engineering, it is essential for civil structures such as buildings, bridges, and dams to have adequate capability to resist future strong earthquakes in order to avoid collapse or reduce structural damage. Numerous studies and experimental work have been conducted to study the behavior of structures during strong earthquakes. The results of analysis are incorporated in various design codes to regulate earthquake-resistant design of different types of civil structures.

To study the seismic response characteristics of structures, mathematical models are needed to describe the relation between the input and output of structures when subject to earthquakes. The predictive capability of a structural model can be assessed by using measured input and output of the structure. System identification is employed in the field of earthquake engineering to improve mathematical models of structures by using measured structural response and possibly measured earthquake ground motions. In classical system identification approaches, a single "best" model among a chosen class of models is identified by minimizing some least-squares fit between the measured structural response and the model response. Even though these techniques have been applied to real seismic response records for a long time, some of their fundamental limitations and discrepancies still need to be resolved.

First of all, the identified "best" model can only be interpreted in the classical least-squares sense in these system identification methods. It is not clear how to determine a "best" model when different "best" models are identified from separate sets of measurement data. Furthermore, the accuracy of the estimated "best" model and the prediction accuracy of this model cannot be assessed in these methods. If there is more than one "best" model in the chosen class of models, the correct way to incorporate these "best" models is also not clear in these approaches. These fundamental limitations and discrepancies of classical system identification techniques are due to a lack of a unified and versatile system identification framework which can provide more knowledgeable interpretation of the identification results and handle the various aforementioned difficulties.

An innovative statistical system identification framework was proposed by Beck [1-2]. The framework is based on the interpretation of probability as a measure of plausibility and on Bayesian statistical inference. It turns out that various classical system identification techniques can be derived from the framework by making appropriate choices for the class of probabilistic models. However, the framework provides more insight and information about the identified optimal model than classical system identification techniques. Furthermore, all types of uncertainties in structural dynamics can be explicitly incorporated and the situation of multiple optimal models can be handled systematically. When the number of sampled input and output data from structures is large, which is typical in experimental testing and seismic structural response records, useful asymptotic approximations are available to simplify the computation of analytical results. In that case, the system identification problem is converted into a nontrivial global optimization problem.

Global optimization has been a challenge from the perspective of both theoretical studies and numerical approaches for decades. In contrast to finding only local extrema, which can be characterized by the local behavior of the objective function, no practical and general criteria have been derived to guarantee whether a global extremum is found. Because the objective function in the aforementioned asymp-

totic approximations in the statistical system identification framework is not convex, there may be multiple optimal models in the parameter space. Various numerical approaches for global optimization have been devised and proposed in the literature [3-4]. Most methods use special heuristics to improve the efficiency of the search but cannot offer an absolute guarantee of locating the global extrema. However, from the application point of view, it is still worthwhile to explore new and more robust numerical global optimization methods.

Several system identification techniques have been applied by using seismic response records from different types of civil structures to estimate their modal properties such as natural frequencies and mode shape amplitudes [5-12]. In spite of its successful and broad applications, the modal identification technique has some limitations. First of all, no information about the uninstrumented degrees of freedom of a structure can be directly extracted from the measurement data. Therefore, in order to predict the response at these degrees of freedom, some approximation method, such as an interpolation, is needed. Furthermore, modal identification does not estimate the stiffness matrix of a structure directly.

Much attention has been drawn to the challenging problem of structural model updating in the system identification community in recent years. In this case, a finite-element model is modified to be more consistent with vibration data from a structure. Structural model updating is useful because it can be applied to structural health monitoring and it is also desirable, since the theoretically based stiffness matrix of a structure can be updated using the measurement data directly to provide more accurate response predictions. However, no well-accepted solution to the structural model updating problem has emerged primarily because it is an ill-conditioned and non-unique inverse problem.

1.2 Outline of this Dissertation

The statistical system identification framework with intended applications in the field of structural dynamics is presented in Chapter 2. The problem of system identification is first discussed and several different types of classical system identi-

fication techniques are reviewed. Two types of uncertainty in structural modeling, *parameter uncertainty* and *modeling error*, are explained. To describe the uncertainty using probability, a more useful interpretation of probability as a measure of plausibility is explained. The steps in the statistical system identification procedure are outlined after the introduction of Bayesian statistical inference. For illustration, a time-domain prediction-error approach, which is a special case of the framework, is described in detail. Definitions of system identifiability and model identifiability are then presented and the relation between them is also discussed. Finally, asymptotic approximations of the analytic results for both the system identifiable case and the system un-identifiable case are shown.

In Chapter 3, two generalized trajectory methods for global optimization are proposed. The nature of the global optimization problem is first described followed by an overview of several classes of existing global optimization methods. The two generalized trajectory methods, the *homotopy scheme* and the *relaxation scheme*, are explained in detail after introducing the notation and assumptions. An efficient numerical algorithm for tracking both homotopy trajectories and relaxation trajectories is then illustrated. Properties of the homotopy trajectory and the relaxation trajectory are discussed from the perspective of differential topology and some characteristics of the behavior of the homotopy trajectory and the relaxation trajectory are explained. The strategy for dealing with multiple trajectory components is also discussed. Finally, a numerical example is presented to demonstrate the application of both the homotopy scheme and the relaxation scheme to locate all the global extrema of an objective function.

The application of a least-squares prediction-error approach to the problem of structural model updating is presented in Chapter 4. The least-squares prediction-error method is derived by modeling the prediction error as a zero-mean stationary Gaussian stochastic sequence. Calculation of the optimal model parameters and prediction accuracy parameters is demonstrated. Asymptotic approximations for this particular approach are summarized. Modal analysis of linear time-invariant

models with classical normal modes is then reviewed, and some model identifiability results of both linear modal models and linear structural models are presented. An example of applying the relaxation scheme to find the multiple equivalent stiffness models for a uniform six-degrees-of-freedom linear chain model is given. Issues about the uniqueness and accuracy in structural model updating are presented and discussed. A single-stage structural model updating approach using the least-squares prediction-error method and the technique of substructuring is presented. Finally, an analytic expression of the gradient vector of the objective function in the least-squares prediction-error method is derived.

In Chapter 5, four examples are presented to demonstrate the application of the proposed single-stage structural model updating approach to both simulated and real structural response data. In the first example, the identification of the natural frequency and damping factor of a simulated single-degree-of-freedom linear oscillator is considered. The results of identification of the stiffness parameters of a simulated two-story structure with known damping are shown in the second example. Measurement noise is added to study its influence on the identified optimal model. In the third example, the same simulated two-story structure is considered but the damping factors are now part of the unknown model parameters. In the last example, seismic response records of a ten-story building, the Great Western Bank, during the 1984 Morgan Hill Earthquake are used. The seismic response characteristics of the building in both the transverse and longitudinal directions are analyzed and the earthquake-induced base shear force, base overturning moment, interstory shear force, and interstory drift are also estimated.

A summary of the research presented in this dissertation is presented in the first part of Chapter 6 along with some comments and conclusions. Finally, several future research topics are suggested.

References for Chapter 1

1. Beck, J. L., *Statistical System Identification of Structures,* Proceedings of the Fifth International Conference on Structural Safety and Reliability, ASCE, New York, New York, pp. 1395-1402, 1989.
2. Beck, J. L., *System Identification Methods Applied to Measured Seismic Response*, Proceedings of the Eleventh World Conference on Earthquake Engineering, Acapulco, Mexico, 1996.
3. Arora, J. S., Elwakeil, O. A., Chahande, A. I., and Hsieh, C. C., *Global Optimization Methods for Engineering Applications : A Review*, Structural Optimization, No. 9, pp. 137-159, 1995.
4. Törn, A., and Žilinskas, A., *Global Optimization*, Lecture Notes in Computer Science Vol. 350, Springer-Verlag, Berlin, 1989.
5. Beck, J. L., *Determining Models of Structures from Earthquake Records*, Report No. EERL 78-01, California Institute of Technology, Pasadena, California, 1978.
6. Beck, J. L., *System Identification Applied to Strong Motion Records from Structures*, Earthquake Ground Motion and its Effects on Structures, AMD-53, Edited by S. K. Datta, ASME, New York, New York, pp. 109-133, 1982.
7. McVerry, G. H., and Beck, J. L., *Structural Identification of JPL Building 180 Using Optimally Synchronized Earthquake Records*, Report No. EERL 83-01, California Institute of Technology, Pasadena, California, 1983.
8. Werner, S. D., Beck, J. L., and Levine, M. B., *Seismic Response Evaluation of Meloland Road Overpass Using 1979 Imperial Valley Earthquake Records*, Earthquake Engineering and Structural Dynamics, Vol. 15, No. 2, pp. 249-274, 1987.
9. Mason, A. B., Beck, J. L., Chen, J., and Ullmann, R. R., *Modal Parameter Identification of an Off-shore platform from Earthquake Response Records*, Seismic Engineering : Research and Practice, ASCE, New York, New York, pp. 217-226, 1989.
10. Li, Y., and Mau, S. T., *A Case Study of MIMO System Identification Applied to Building Seismic Records*, Earthquake Engineering and Structural Dynamics, Vol. 20, No. 11, pp. 1045-1064, 1991.
11. Beck, J. L., May, B. S., and Polidori, D. C., *Determination of Modal Parameters from Ambient Vibration Data for Structural Health Monitoring*, Proceedings of the First World Conference on Structural Control, International Association for Structural Control, Los Angeles, California, pp. TA3:3 - TA3:12, 1994.
12. Benedetti, D., and Gentile, C., *Identification of Modal Quantities from Two Earthquake Responses*, Earthquake Engineering and Structural Dynamics, Vol. 23, No. 4, pp. 447-462, 1994.

Chapter 2

Statistical System Identification in Structural Dynamics

2.1 System Identification

2.1.1 Introduction

In the field of structural dynamics, one main interest is to study the dynamic behavior of civil structures such as buildings, bridges, and dams under the influence of external excitations like earthquakes and wind. To facilitate such study, mathematical models are used to describe the dynamic behavior of these structures. In constructing models for the structures, various assumptions are made and the theory of mechanics such as Newton's laws is applied. These models describe the mathematical relation between external excitations and structural response and the interaction among different components of complex structures.

Mathematical models of structures are useful for engineering applications if they can describe the behavior and characteristics of structures reasonably well. There are several motivations to have useful mathematical models for civil structures. First of all, the behavior of a structure under the influence of future external excitations can be predicted by using its model. Secondly, the knowledge and expertise acquired in constructing models of existing structures can help when designing new structures. Finally, the model of a structure can be used in other applications such as structural control design and structural health monitoring.

Civil structures and their associated mathematical models are of different nature and cannot be compared directly. Therefore, a model of given structure can never be rigorously validated and claimed as the *true* model of the structure. It is only possible to conclude that one model is more or less plausible than another model

even though no perfect objective judgment can be made. To assess the capability of a model in describing the behavior of a structure, measured inputs and outputs of the structure are an important source of quantitative information. These data can be obtained from experiments conducted on structures or by measuring the response of structures under the influence of natural external excitations.

The objective of system identification in structural dynamics is to improve mathematical models of the dynamics of structures by using measured response and possibly measured external excitations. Unfortunately, the dynamic behavior of large scale civil structures cannot be studied as complete systems in the laboratory due to their huge dimension and mass. Even in field experiments, it is also difficult to shake these structures to generate large structural response. As an alternative, these structures can be instrumented to record their response during earthquakes in order to quantitatively assess their mathematical models. This approach has been demonstrated to be practical and economically feasible.

Several system identification techniques have been applied to recorded seismic response of civil structures to identify modal properties and a large number of structures of different types have been studied as reviewed in [1-2]. Most of the records studied were recorded at various locations in multi-story buildings during earthquakes in California [3-11]. The modal identification methodology has also been applied to recorded seismic response from a highway bridge [12] and an off-shore oil platform [13]. More recently, this methodology has been applied successfully to study the behavior of tall buildings by using ambient vibration records [14]. These studies have shown the level of structural damping and substantial variation of structural stiffness during strong earthquakes.

System identification of a structure is an iterative process and includes three major steps. A class of mathematical models is first constructed to model the structure. The modeling process makes use of existing theory of mechanics and any prior information about the structure. Alternatively, a "black-box" approach which adopts some convenient general mathematical models such as autoregressive and moving-

average (ARMA) models or neural networks has also been used. In the second step, the "best" model within the given class of models is estimated by using the measured input and output of the structure and certain criteria which relate to the accuracy of different models. Finally, an assessment of the identified model is necessary to determine whether the model is adequate for its intended application. If not, a new class of models is selected and the entire identification procedure is repeated.

2.1.2 Classification of System Identification Techniques

A survey of the system identification literature reveals all kinds of methods in different fields of science and technology. Even though the class of mathematical models used in different fields vary a lot, most of these techniques share similar concepts and properties regardless of the particular field. A recent review and evaluation of some system identification techniques for structural dynamics application are given in [15-16]. In structural dynamics, there are various practical issues which make the successful application of system identification techniques to real structures a challenge.

First of all, the measured structural response is usually incomplete relative to the level of detail desired to understand the structural behavior. For example, the number of measured degrees of freedom is usually much less than the number of model parameters of interest, such as those relating to the distribution of stiffness. This is mainly due to the cost of instrument deployment. Also, some response quantity such as nodal rotation cannot be measured reliably, and some measurement may not even be possible because certain locations in a structure are not accessible. Furthermore, all measurement data is inevitably contaminated by measurement noise. Finally, any chosen mathematical model can only describe the behavior of a structure approximately.

All the system identification techniques in structural dynamics can be roughly classified in three aspects. Depending on the form and nature of mathematical models, there is distinction between *parametric* and *non-parametric* identification. In *recursive* identification, the estimation of model parameters and the measurement of

input and output of a structure is conducted simultaneously. On the other hand, the estimation of model parameters is performed after a segment of measured data has been collected in *non-recursive* identification. Finally, *time-domain* and *frequency-domain* identification differ in the domain where the measured input and output of a structure are used for identification.

2.1.3 Parametric and Non-Parametric Identification

In parametric identification, mathematical models of a structure are constructed based on the theory of mechanics. Then, the measured input and output of the structure are used to estimate the parameters of the model which is the "best" within the given class of models based on certain criterion. A central aspect is the criterion for choosing the "best" model in the model set. Usually, it involves a measure of how well a mathematical model can fit the structural response. The main feature of parametric identification is that the identified parameters have clear physical meaning. Most system identification techniques which have been developed are classified as parametric.

Parametric identification can be used to estimate some physical characteristics of a structure such as the equivalent viscous damping which cannot be derived directly from theory. These techniques can also be used to assess and improve finite element models which are used for designing new structures or predicting the dynamic response of existing structures. However, for many complex nonlinear dynamic systems, it is not yet clear how to derive appropriate mathematical models from the existing theory of mechanics. Therefore, some attention has been devoted to non-parametric identification. However, non-parametric identification has limited usefulness in improving analytic modeling required in structural design.

Non-parametric identification refers to techniques which do not assume any theoretical knowledge or model of a structure. Instead, they adopt a "black-box" approach and try to estimate a general functional relationship, such as transfer functions, between the input and output of a structure. Traditionally, non-parametric identification techniques used the Volterra series or the Wiener-Kernel approach [17].

However, these approaches have restrictions on the type of input signal which can be used and on the nature of dynamic systems to be identified. Furthermore, the evaluation of higher-order terms in the functional expansion requires a prohibitive amount of numerical effort.

More recent development in non-parametric identification has been devoted to alleviate some of the aforementioned problems associated with traditional approaches [18-19]. It was realized that it is more efficient to use a parameterized form of the involved functional relationship. Usually, the functional is approximated by a series of orthogonal, e.g., Chebyshev, polynomials. Therefore, it is still required to estimate the coefficients in the series of the polynomial expansion. The conceptual difference with respect to parametric identification is that these coefficients are not physical parameters based on the theory of mechanics and their number can grow as required by the estimation procedure.

Based on the idea and research of biological neural networks, artificial neural networks have been adopted in the structural dynamics community as a new non-parametric identification approach [20]. In this type of method, the relation between the input and output of a structure is represented by a set of neurons which are connected to each other with links. Each neuron performs certain processing of its inputs and sends output to adjacent neurons. Non-parametric identification with neural networks is achieved by systematically adjusting the weights of links in the network by using certain *training* or *learning* algorithms until desirable relation between the input and output of network is accomplished.

2.1.4 Recursive and Non-Recursive Identification

Recursive identification is also referred to as *on-line*, *real-time*, *sequential*, or *adaptive* identification in the literature. In recursive identification, an updated estimate of the model parameters of a structure is made at each sampling instant. In theory, recursive identification techniques can be helpful in applications such as adaptive structural control and real-time structural health monitoring in which the estimation of time variation of model parameters is essential. A review of several well-

known recursive identification techniques such as *least-square*, *instrumental variable*, and *extended Kalman Filter* can be found in general texts on system identification [21-22]. The application of recursive identification to identify degrading structures is presented in [23].

Perhaps the most widely adopted recursive identification technique is the extended Kalman Filter. The Kalman Filter was originally developed as a tool to estimate the states of a linear and time-invariant dynamic system subject to stochastic input disturbance and measurement noise. In applying the Kalman Filter algorithm to system identification, an extended state vector is constructed which includes the model parameters to be estimated. Therefore, the model parameters and states of the structure are estimated simultaneously. But the stability and convergence of the extended Kalman Filter depend on the initial guess for the model parameters and for the disturbance and noise variance matrices. To improve convergence and ensure statistical consistency, a weighted global iteration procedure and an adaptive filtering procedure have been proposed for the extended Kalman Filter algorithm [3,24-25].

To successfully track the time variation of model parameters, recursive identification algorithms need to have excellent convergence capability. Convergence is especially difficult to achieve in the presence of measurement noise and uncertainty of structural modeling which is the case in structural dynamics. On the other hand, non-recursive identification methods estimate model parameters by using a segment of measured input and output of a structure. Since more information is incorporated in the identification process, the estimated model parameters are more reliable even though they only represent the averaged value during an interval of time. To investigate the time-varying behavior of structures parameters using non-recursive identification, overlapping subintervals in time can be used to estimate the model parameters successively. This technique has been proven to be useful in practice.

2.1.5 Time-Domain and Frequency-Domain Identification

The governing equations of the mathematical model of a structures are generally expressed in the time domain. However, the governing equations of simple mathemat-

ical models, such as those that are linear and time-invariant, can be transformed into the frequency domain by the Fourier integral transform. But, for complex dynamic systems which have nonlinear or hysteretic behavior, only time-domain mathematical models are usually available. In general, the choice between time-domain and frequency-domain mathematical models is dictated by the prior knowledge of the structure and the intended use of the model. Actually, time-domain and frequency-domain mathematical models complement each other and describe the behavior of a structure from different perspectives.

In time-domain identification, measured input and output time histories from a structure are used to estimate model parameters. This approach is natural since all the data is measured directly in the time domain. Beck and Jennings [26] developed a very efficient time-domain identification technique to estimate the modal parameters of linear time-invariant models of a structure. The methodology has been extended by Beck to handle multiple excitation inputs and implemented in a computer program called MODE-ID. MODE-ID is a least-squares output-error method based on matching the structural response and the corresponding model output using an efficient "modal sweep" optimization algorithm. More recently, this method has been extended to identify structural models with non-classical modes of vibration [27]. Identification techniques using the least-squares equation-error approach have also been developed [28-29].

When linear and time-invariant mathematical models are used in identification, it is also feasible to transform the measured input and output of a structure to the frequency domain and estimate the model parameters. McVerry [30] developed a frequency-domain identification technique to estimate the modal parameters by a least-squares fit over a specified frequency band between the unsmoothed and complex-valued finite Fourier transform of the measured output and the corresponding model output. A similar approach which incorporates spectral smoothing is presented in [31]. Without using the measured input, Benedetti and Gentile [32] used the amplitude ratio of the Fourier transform of structural response measured

at two different locations to estimate modal parameters.

2.1.6 Structural Model Updating

Some special system identification techniques have been developed for the purpose of structural model updating which can be applied to structural health monitoring or damage detection. Structural damage in a structure can be assessed in terms of local reduction in the structural stiffness. Usually, the identification of stiffness is done in two stages. In the first stage, modal parameters, such as natural frequencies and the mode shape amplitudes, of a structure are estimated by using modal identification methods. In the second stage, the estimated modal parameters are used to identify the structural stiffness. Unfortunately, there is no well accepted solution and several approaches have been proposed. These methods include minimizing the error norm of the eigenvalue problem which relates modal parameters with the mass and stiffness matrix [33], using a least-squares fit of the measured modal parameters and corresponding model values [34-35], and using the sensitivity of modal parameters to the local change of structural stiffness [36].

2.2 Uncertainty in Structural Modeling

2.2.1 Types of Uncertainty

Although seismic structural response records can help earthquake engineering researchers understand the dynamic behavior of civil structures during strong earthquakes, the analysis of these records does not match the rate these records are collected. This situation may be due to insufficient funding for these type of studies. On the other hand, system identification tools for extracting the dynamic characteristics of structures from seismic response records are still not widely available for researchers and engineers. This situation leaves a great deal of uncertainty about the detailed dynamic behavior of structures and their capability to resist strong earthquakes.

The underlying motivation for applying system identification to measured seismic response of structures is that it is currently not possible to accurately predict

this response by using mathematical models of structures. This is due to inherent uncertainty in constructing the mathematical models. Once a class of models has been chosen to describe the behavior of a structure, there are model parameters which need to be assigned values in order to choose a particular model from the class of models. There are two types of uncertainty when modeling a structure, *parameter uncertainty* and *modeling error*. Parameter uncertainty arises simply because the most appropriate values of the model parameters to be specified are not known *a priori*. For example, the material properties of structural members, such as the Young's modulus E and the effective moment of inertia I, are uncertain because of manufacturing and construction process.

For any given mathematical model of a structure, the predicted response may differ from the actual structural response because any mathematical model is only an approximation of the actual behavior of the structure. It is always possible that some secondary dynamics of the structure is not modeled explicitly in the given mathematical model. This type of uncertainty is referred to as *modeling error*. For example, the modeling of the material constitutive behavior, e.g., stiffness, damping, nonlinearity, and time-varying behavior, is only approximate. Even when a reliable constitutive model is available at the structural component level, the complexity of component interactions, e.g., there are no exactly pinned or rigid beam-column connections, makes it difficult to build up a complete mathematical model based on theory. Also, there is discrepancy due to the spatial discretization of a distributed structural system when applying the finite element formulation. Modeling error can be described in terms of *prediction accuracy* which represents the uncertain error in the response prediction given by any mathematical model.

2.2.2 Description of Uncertainty

Traditionally, probability is defined to be the limiting relative frequency of occurrence of a repeatable random event in the long run [37]. It turns out that this definition is unnecessarily restrictive because there are many cases where it is desirable to quantify uncertainty but the interpretation of probability using relative

frequency makes no sense. Since parameter uncertainty and modeling error are not repeatable events, the classical interpretation of probability is not applicable in describing the uncertainty in structural modeling. However, another more useful interpretation of probability as a measure of plausibility is more appropriate to describe *the uncertainty in modeling civil structures.*

Starting from the observation that human brain does plausible reasoning in a fairly definite way, it was shown that there is only a single set of rules for doing plausible reasoning which is consistent and in qualitative correspondence with common sense [38]. It turns out that these rules match the axioms in classical probability theory and they can be deduced without resort to the concept of repeatable event and frequency of occurrence. Therefore, a re-interpretation of the probability concept can greatly extend the power of probability and statistical methods for applications in science and engineering.

Actually, there have been two principal lines of thoughts about plausible reasoning in the literature [2]. One is based on decision theory and views probability as a personal expression of an individual's degree of belief about a certain proposition given some information [39]. The other line of thought emphasizes that plausibility should be uniquely determined by objective criteria, such as the *Principle of Maximum Entropy*, once the incomplete information available has been studied in a suitable explicit form [40]. Nevertheless, both lines of thoughts end up with the same set of mathematical relations for plausible reasoning.

In this dissertation, the notation $P(a|b)$ is used to represent a measure of the plausibility of proposition a given the information stated in proposition b. Propositions a and b may refer to hypotheses of mathematical models of civil structures or they may refer to observations or measurement of data. It was demonstrated that to quantify plausibility, one is led to the calculus of mathematical (Boolean) logic together with the following three additional axioms [41]:

$$1) \quad 0 \leq P(a|b) \leq 1 \text{ and } P(a|a) = 1,$$

$$2) \quad P(a|b) + P(\text{not } a|b) = 1, \text{ and}$$

$$3) \quad P(a, b|c) = P(a|b, c)P(b|c),$$

where "," represents the propositional conjunction "and." From this point of view, the calculus of plausibility is a generalization of the calculus of mathematical logic since the latter assumes that the information given in proposition b is complete enough to deduce that either "$b \Rightarrow a$", i.e., $P(a|b) = 1$, or that "$b \Rightarrow$ not a", i.e., $P(a|b) = 0$.

2.3 Statistical System Identification

2.3.1 Bayesian Statistical Inference

In classical statistical inference problems, one is to decide on the basis of measurement or observation which probability distribution in a given family of distribution functions could represent the distribution of some random quantity. It is implicitly assumed that there is a *true* probability distribution in the given family of distribution functions, but this point of view is questionable. Several types of *point* estimate such as *maximum likelihood*, *minimax*, and *methods of moments* have been proposed in the literature trying to estimate the true probability distribution. The difficulty with these types of estimate is that their quality is unknown.

To overcome this discrepancy, the idea of *confidence interval* is used. Unfortunately, confidence intervals need to be interpreted by using the limiting concept of a repeatable event in the long run and so they do not indicate the quality of estimate given only finite observation data. The difficulty of classical statistical inference approaches is rooted in the interpretation of probability as the limiting relative frequency of occurrence of a repeatable random event. By using the plausibility interpretation of probability, a more powerful Bayesian statistical inference framework has been proposed in the literature [38].

In Bayesian statistical inference, the observation of some quantities, such as the input and output of structures, are used to update the probability of other unobservable quantities, such as those relating to models of material constitutive behavior. For illustration, the axioms of probability give the following relation:

$$P(a, b|c) = P(a|b, c)P(b|c) = P(b|a, c)P(a|c).$$

By rearrangement, the Bayes' formula is obtained:

$$P(b|a, c) = \frac{P(a|b, c)P(b|c)}{P(a|c)} = kP(a|b, c)P(b|c) \propto P(a|b, c)P(b|c),$$

where k is a constant if proposition a is observed. $P(b|c)$ is called the *prior* probability of proposition b since it represents the probability of proposition b *before* the observation of proposition a. $P(b|a, c)$ is called the *posterior* probability of proposition b because it indicates the probability of proposition b *after* the observation of proposition a. $P(a|b, c)$ is called the *likelihood function* of proposition b for given observation of proposition a and represents the influence of observation data on the plausibility of proposition b.

A Bayesian statistical inference framework is appealing because it provides a systematic approach to explicitly introduce the prior probability of some propositions and prescribes how their posterior probability is obtained when observations become available. Indeed, the inference framework provides continual update of the probability of certain propositions as more observations are taken. For example, after an initial observation of a, a_1, becomes available, the posterior probability of b is given by:

$$P(b|a_1, c) \propto P(a_1|b, c)P(b|c).$$

After another independent observation of a, a_2, is taken, the posterior probability of

b given observations a_1 and a_2 becomes:

$$\begin{aligned} P(b|a_1, a_2, c) &\propto P(a_1, a_2|b, c)P(b|c), \\ &\propto P(a_2|a_1, b, c)P(a_1|b, c)P(b|c), \\ &\propto P(a_2|b, c)P(b|a_1, c). \end{aligned}$$

It is noted that the posterior probability $P(b|a_1, c)$ plays the role of prior probability when deriving the posterior probability $P(b|a_1, a_2, c)$ as the observation a_2 becomes available. Obviously, this procedure can be repeated when more observations are taken.

2.3.2 Statistical System Identification Framework

In classical system identification techniques, the prediction accuracy of the identified model is typically not quantified. When the identified model is used to predict the structural response, the accuracy of prediction is usually judged only based on how well the identified model fits the available measurement data. Furthermore, most system identification techniques only identify one "best" model from the given class of models, but it is also important to assess the precision of the identified model. A *posterior* sensitivity study of the criterion for choosing the model gives some clues but does not solve the problem. Another approach is to use expensive Monte Carlo simulation to estimate the statistical properties of the identified model [42-43]. However, if there are multiple "best" models in the given class of models based on the measurement data, it is not clear how to proceed in these techniques.

Because of parameter uncertainty and modeling error, the process of system identification is best addressed within a probabilistic framework. But this involves dealing with the probability of mathematical models, which are of course not repeatable events. Beck [2,44] proposed a statistical system identification framework based on the interpretation of probability as a measure of plausibility and on Bayesian statistical inference. The framework addresses all of the previously mentioned practical

difficulties in the application of system identification techniques to real structures. One of the main aspects of system identification is the criterion for choosing the "best" model within the given class of mathematical models. In the statistical system identification framework, the choice of this criterion is done in a very natural way. *Furthermore, it provides an integrated approach to handle the situation when* there are multiple "best" models.

The statistical system identification procedure is an iterative process and includes four major steps:

1. Specify a class of deterministic mathematical models, which describe the modeled dynamics of a structure,

2. Embed the class of deterministic models within a class of probabilistic models which provide a probabilistic description of the uncertain prediction accuracy,

3. Determine the prior probability of model parameters based on all the available information and knowledge, and

4. Use the measured input and output of the structure to infer the posterior probability of model parameters.

The statistical system identification framework has several features and advantages over classical system identification techniques. First of all, the framework explicitly treats all types of uncertainty in structural dynamics including parameter uncertainty, modeling error, measurement noise, and uncertain external excitation. Furthermore, the framework can be applied to any type of mathematical models, e.g., parametric, non-parametric, time-domain, frequency-domain, etc. Besides, no spurious concepts such as the "true" model are used in the framework, and the framework does not depend on the concept of ensemble average or need to be interpreted in the long run. Therefore, the statistical system identification framework is pragmatic and versatile for practical applications to civil structures.

By making appropriate choices for the class of probabilistic models, several classical system identification techniques can be viewed as the special cases of the statistical system identification framework. But the statistical system identification framework provides more information and insight than the classical system identification techniques. For example, the classical least-squares output-error method can be derived if the uncertain prediction accuracy is modeled as a stationary Gaussian white noise sequence with zero mean. The least-squares output-error approach has been the dominant method in the application of system identification to real structures because it does not rely on the measurement of all the degrees of freedom of a structure.

2.3.3 Time-Domain Prediction-Error Approach

The statistical system identification framework is very general and is applicable for any type of mathematical models. The framework can also be applied in other fields such as soil mechanics and seismology by using suitable models to describe the dynamics of systems and external excitations. For illustration, a particular statistical system identification technique developed by Beck [2] is presented. It is assumed that a class of mathematical models $\mathcal{M}$ has been chosen to model a structure. The $N_{\underline{a}}$ model parameters $\underline{a} \in S_{\underline{a}} \subset R^{N_{\underline{a}}}$ need to be assigned values in order to indicate a particular model in $\mathcal{M}$. The model output and system input is only required at discrete time. This is typical of modern seismic records which are recorded using digital instruments.

The class of models $\mathcal{M}$ provides a functional relationship between the model output $\underline{x}(n;\underline{a}) \in R^{N_o}$ at time $n\Delta t$ and the system input $Z_1^n = \{\underline{z}(m) \in R^{N_I} : m = 1,\ldots,n\}$:

$$\underline{x}(n;\underline{a}) = \underline{x}(n;\underline{a}, Z_1^n, \mathcal{M}),$$

where $\underline{x}(n;\underline{a})$ contains N_o model output quantities and $\underline{z}$ contains N_I system input quantities. In the following, the dependence of model output $\underline{x}$ on the system input

Z_1^n and the class of models $\mathcal{M}$ will be suppressed in the notation for simplicity. Only the observed model response quantities are contained in $\underline{x}(n;\underline{a})$. For example, if the acceleration response of a structure is measured, $\underline{x}(n;\underline{a})$ contain the acceleration predicted by the class of models $\mathcal{M}$ at the observed degrees of freedom. When earthquake excitation is considered, the system input Z_1^n consists of the ground acceleration induced by earthquakes.

To embed the class of deterministic models $\mathcal{M}$ within a class of probabilistic models, the *prediction error* $\underline{e}(n;\underline{a})$ is defined as the difference between the model output $\underline{x}(n;\underline{a})$ and the measured system output $\underline{y}(n)$, i.e.,

$$\underline{y}(n) = \underline{x}(n;\underline{a}) + \underline{e}(n;\underline{a}). \tag{2.3.1}$$

The prediction error actually accounts for the effects of both measurement noise and modeling error. But for modern structural response measuring instruments, the measurement noise is usually negligible compared with the modeling error. Therefore, the measured system output is essentially equal to the actual system output.

A class of probabilistic models $\mathcal{P}$ is chosen to describe the uncertainty in the prediction error. $\mathcal{P}$ is parameterized by $N_{\underline{\sigma}}$ prediction accuracy parameters $\underline{\sigma} \in S_{\underline{\sigma}} \subset R^{N_{\underline{\sigma}}}$, and prescribes a function h_M which gives the probability distribution of a sequence of M prediction errors $E_1^M = \{\underline{e}(n;\underline{a}) \in R^{N_o} : n = 1,\ldots,M\}$, i.e.,

$$p(E_1^M|\underline{\sigma},\mathcal{P}) = h_M(\underline{e}(1),\ldots,\underline{e}(M);\underline{\sigma}). \tag{2.3.2}$$

After the classes of models $\mathcal{M}$ and $\mathcal{P}$ are chosen, a class of probabilistic models $\mathcal{M}_{\mathcal{P}}$ can be defined and parameterized by the parameters $\underline{\alpha} = [\underline{a}^T, \underline{\sigma}^T]^T \in S_{\underline{\alpha}} \subset R^{N_{\underline{\alpha}}}$ where $N_{\underline{\alpha}} = N_{\underline{a}} + N_{\underline{\sigma}}$. The class of models $\mathcal{M}_{\mathcal{P}}$ prescribes a function f_M which gives the probability distribution of the system output $Y_1^M = \{\underline{y}(n) \in R^{N_o} : n = 1,\ldots,M\}$, i.e.,

$$\begin{aligned} p(Y_1^M|\underline{\alpha}, Z_1^M, \mathcal{M}_\mathcal{P}) &= f_M(\underline{y}(1), \ldots, \underline{y}(M); \underline{\alpha}, Z_1^M), \\ &= h_M(\underline{y}(1) - \underline{x}(1; \underline{a}), \ldots, \underline{y}(M) - \underline{x}(M; \underline{a}); \underline{\sigma}). \end{aligned} \tag{2.3.3}$$

The function f_M is determined by substituting (2.3.1) in (2.3.2).

To account for the parameter uncertainty of $\underline{\alpha}$, a *prior* probability distribution $\pi(\underline{\alpha})$ over the set $S_{\underline{\alpha}}$ of all possible parameter values of $\underline{\alpha}$ is chosen, i.e.,

$$p(\underline{\alpha}|\mathcal{M}_\mathcal{P}) = \pi(\underline{\alpha}).$$

The choice of $\pi(\underline{\alpha})$ reflects prior engineering judgment about the relative plausibility of different models in the class of models $\mathcal{M}_\mathcal{P}$. For simplicity, $\pi(\underline{\alpha})$ is usually approximated by using a smooth and slowly-moving function.

The probability distribution $p(Y_1^M|\underline{\alpha}, Z_1^M, \mathcal{M}_\mathcal{P})$ in (2.3.3) prescribes the prediction accuracy of the system output for a particular model in the class of models $\mathcal{M}_\mathcal{P}$. Before using any measured system input and output, the probability distribution of the predicted system output Y_1^M based on the class of models $\mathcal{M}_\mathcal{P}$ is given by:

$$\begin{aligned} p(Y_1^M|Z_1^M, \mathcal{M}_\mathcal{P}) &= \int_{S_{\underline{\alpha}}} p(Y_1^M, \underline{\alpha}|Z_1^M, \mathcal{M}_\mathcal{P}) d\underline{\alpha}, \\ &= \int_{S_{\underline{\alpha}}} p(Y_1^M|\underline{\alpha}, Z_1^M, \mathcal{M}_\mathcal{P}) p(\underline{\alpha}|\mathcal{M}_\mathcal{P}) d\underline{\alpha}, \\ &= \int_{S_{\underline{\alpha}}} f_M(Y_1^M; \underline{\alpha}, Z_1^M) \pi(\underline{\alpha}) d\underline{\alpha}. \end{aligned} \tag{2.3.4}$$

The probability distribution in (2.3.4) is a weighted average of each individual probability distribution given in (2.3.3) over the entire class of models $\mathcal{M}_\mathcal{P}$. The weighting of each individual probability distribution is given by the prior probability of each model.

Let $\mathcal{D}_N$ denote a set of measured system input $\hat{Z}_1^N = \{\underline{\hat{z}}(n) \in R^{N_I} : n =$

$1, \ldots, N\}$ and system output $\hat{Y}_1^N = \{\hat{\underline{y}}(n) \in R^{N_o} : n = 1, \ldots, N\}$ recorded at discrete time. Based on the new information contained in $\mathcal{D}_N$, a *posterior* probability distribution of parameters $\underline{\alpha}$ can be derived by using the Bayes' formula:

$$\begin{aligned} p(\underline{\alpha}|\mathcal{D}_N, \mathcal{M}_\mathcal{P}) &= kp(\hat{Y}_1^N|\underline{\alpha}, \hat{Z}_1^N, \mathcal{M}_\mathcal{P})p(\underline{\alpha}|\mathcal{M}_\mathcal{P}), \\ &= kf_N(\hat{Y}_1^N; \underline{\alpha}, \hat{Z}_1^N)\pi(\underline{\alpha}), \end{aligned} \tag{2.3.5}$$

where the normalizing constant k can be evaluated by using (2.3.4) and is given by:

$$k^{-1} = P(\hat{Y}_1^N|\hat{Z}_1^N, \mathcal{M}_\mathcal{P}).$$

Given the measured data $\mathcal{D}_N$, the probability distribution of the predicted system output Y_1^M in (2.3.4) can be replaced by an *updated* probability distribution of the predicted system output for the next $(M - N)$ sampling time and a prescribed future system input Z_{N+1}^M by using (2.3.5) as follows:

$$\begin{aligned} p(Y_{N+1}^M|\mathcal{D}_N, Z_{N+1}^M, \mathcal{M}_\mathcal{P}) &= \int_{S_{\underline{\alpha}}} p(Y_{N+1}^M, \underline{\alpha}|\mathcal{D}_N, Z_{N+1}^M, \mathcal{M}_\mathcal{P})d\underline{\alpha}, \\ &= \int_{S_{\underline{\alpha}}} p(Y_{N+1}^M|\underline{\alpha}, Z_{N+1}^M, \mathcal{M}_\mathcal{P})p(\underline{\alpha}|\mathcal{D}_N, \mathcal{M}_\mathcal{P})d\underline{\alpha}, \\ &= k\int_{S_{\underline{\alpha}}} p(\hat{Y}_1^N, Y_{N+1}^M|\underline{\alpha}, \hat{Z}_1^N, Z_{N+1}^M, \mathcal{M}_\mathcal{P})p(\underline{\alpha}|\mathcal{M}_\mathcal{P})d\underline{\alpha}, \\ &= k\int_{S_{\underline{\alpha}}} f_M(\hat{Y}_1^N, Y_{N+1}^M; \underline{\alpha}, \hat{Z}_1^N, Z_{N+1}^M)\pi(\underline{\alpha})d\underline{\alpha}. \end{aligned} \tag{2.3.6}$$

The updated probability distribution in (2.3.6) can be viewed as a weighted average of each individual probability distribution $p(Y_{N+1}^M|\underline{\alpha}, Z_{N+1}^M, \mathcal{M}_\mathcal{P})$ over the entire class of models $\mathcal{M}_\mathcal{P}$ just as in (2.3.4). But, the weighting of each individual probability distribution is now given by the posterior probability of each model given the measured data $\mathcal{D}_N$.

2.4 Identifiability and Asymptotic Approximations

2.4.1 System and Model Identifiability

It is noted that the exact updated probability distribution given in (2.3.6) does not require parameter identification in the usual sense. However, the difficulty with the analytic expression in (2.3.6) is that the multi-dimensional integral cannot be evaluated analytically nor numerically if the dimension of the parameter space $S_{\underline{\alpha}}$ is too high. Fortunately, the multi-dimensional integral in (2.3.6) can be approximated to simplify the computation if the number N of sampled system input and output is large which is usually the case with dynamic tests or records of structural response during earthquakes.

Assume the vector of parameters $\hat{\underline{\alpha}} = [\hat{\underline{a}}^T, \hat{\underline{\sigma}}^T]^T \in S_{\underline{\alpha}}$ *globally* maximizes $f_N(\hat{Y}_1^N; \underline{\alpha}, \hat{Z}_1^N)$, which is the likelihood function in the inference equation (2.3.5), and the attained global maximum is at an isolated point. Consider any parameters $\underline{\alpha}$ in the neighborhood of $\hat{\underline{\alpha}}$. In most situations,

$$\ln\left(\frac{f_N(\hat{Y}_1^N; \underline{\alpha}, \hat{Z}_1^N)}{f_N(\hat{Y}_1^N; \hat{\underline{\alpha}}, \hat{Z}_1^N)}\right) = \mathcal{O}(N). \tag{2.4.1}$$

It is clear from (2.4.1) that the function $f_N(\hat{Y}_1^N; \underline{\alpha}, \hat{Z}_1^N)$ is very peaked at $\hat{\underline{\alpha}}$ for a large number N of measured system input and output. Besides, the contribution of these parameters which only locally maximize $f_N(\hat{Y}_1^N; \underline{\alpha}, \hat{Z}_1^N)$ will eventually diminish as N increases. Furthermore, if the prior probability distribution $\pi(\underline{\alpha})$ is a smooth and slowly-varying function, the posterior probability distribution in (2.3.5) is also very peaked at $\hat{\underline{\alpha}}$. In that case, $\hat{\underline{\alpha}}$ is an approximate *local* maximizer of the posterior probability distribution $p(\underline{\alpha}|\mathcal{D}_N, \mathcal{M}_\mathcal{P})$ and the accuracy is $\mathcal{O}(N^{-1})$.

Motivated by the above observations, the *optimal* parameters $\hat{\underline{\alpha}}$ for the class of models $\mathcal{M}_\mathcal{P}$ given the measured data $\mathcal{D}_N$ are defined to be the values of parameters $\underline{\alpha} \in S_{\underline{\alpha}}$ which *globally* maximize the function $f_N(\hat{Y}_1^N; \underline{\alpha}, \hat{Z}_1^N)$. Since the defined optimal parameters are equivalent to the maximum likelihood estimates in classical statistical inference, the traditional maximum likelihood estimation approach can

be justified and interpreted within the more general statistical system identification framework. Let $S_{\underline{\alpha}}^{opt}(\mathcal{D}_N) \subset S_{\underline{\alpha}}$ represent the set of all optimal parameters, the following definition of *system identifiability* is introduced in [45]:

- A parameter α_i of $\underline{\alpha}$ is *globally system identifiable* for the class of models $\mathcal{M}_{\mathcal{P}}$ and the measured data $\mathcal{D}_N$ if $S_{\underline{\alpha}}^{opt}(\mathcal{D}_N)$ contains only one vector of optimal parameters, or, if not, then:

$$\hat{\underline{\alpha}}^{(1)}, \hat{\underline{\alpha}}^{(2)} \in S_{\underline{\alpha}}^{opt}(\mathcal{D}_N) \Longrightarrow \hat{\alpha}_i^{(1)} = \hat{\alpha}_i^{(2)}.$$

- A parameter α_i of $\underline{\alpha}$ is *system identifiable* for the class of models $\mathcal{M}_{\mathcal{P}}$ and the measured data $\mathcal{D}_N$ if there exists a positive number ϵ_i such that:

$$\hat{\underline{\alpha}}^{(1)}, \hat{\underline{\alpha}}^{(2)} \in S_{\underline{\alpha}}^{opt}(\mathcal{D}_N) \Longrightarrow |\hat{\alpha}_i^{(1)} - \hat{\alpha}_i^{(2)}| > \epsilon_i \text{ or } \hat{\alpha}_i^{(1)} = \hat{\alpha}_i^{(2)}.$$

- A parameter α_i of $\underline{\alpha}$ is *locally system identifiable* for the class of models $\mathcal{M}_{\mathcal{P}}$ and the measured data $\mathcal{D}_N$ if it is system identifiable but not globally system identifiable.

- A parameter α_i of $\underline{\alpha}$ is *system un-identifiable* for the class of models $\mathcal{M}_{\mathcal{P}}$ and the measured data $\mathcal{D}_N$ if it is not system identifiable.

Furthermore, the above definition can be extended as follows:

- The vector of parameters $\underline{\alpha}$ is (globally) system identifiable if all of the parameters α_i are (globally) system identifiable.

- The vector of parameters $\underline{\alpha}$ is locally system identifiable if it is system identifiable but at least one parameter α_i is only locally system identifiable.

- The vector of parameters $\underline{\alpha}$ is system un-identifiable if at least one parameter α_i is system un-identifiable.

- The class of models $\mathcal{M}_{\mathcal{P}}$ is (globally) locally system identifiable given the measured data $\mathcal{D}_N$ if $\underline{\alpha}$ is (globally) locally system identifiable.
- The class of models $\mathcal{M}_{\mathcal{P}}$ is system un-identifiable given the measured data $\mathcal{D}_N$ if $\underline{\alpha}$ is system un-identifiable.

If the class of models $\mathcal{M}_{\mathcal{P}}$ is system identifiable given the measured data $\mathcal{D}_N$ and $S_{\underline{\alpha}}$ is bounded, there is only a finite number of optimal parameters in $S_{\underline{\alpha}}^{opt}(\mathcal{D}_N)$.

It is of interest to note that any two different optimal parameters $\hat{\underline{\alpha}}^{(1)}$ and $\hat{\underline{\alpha}}^{(2)}$ in $S_{\underline{\alpha}}^{opt}(\mathcal{D}_N)$ need not produce the same model output given the measured system input $\hat{Z}_1^N$, i.e.,

$$\hat{\underline{\alpha}}^{(1)} = [\hat{\underline{a}}^{(1)^T}, \hat{\underline{\sigma}}^{(1)^T}]^T \in S_{\underline{\alpha}}^{opt}(\mathcal{D}_N) \text{ and } \hat{\underline{\alpha}}^{(2)} = [\hat{\underline{a}}^{(2)^T}, \hat{\underline{\sigma}}^{(2)^T}]^T \in S_{\underline{\alpha}}^{opt}(\mathcal{D}_N)$$

$$\not\Longrightarrow \underline{x}(n; \hat{\underline{a}}^{(1)}) = \underline{x}(n; \hat{\underline{a}}^{(2)}).$$

However, it is true that for given optimal parameters $\hat{\underline{\alpha}}$ in $S_{\underline{\alpha}}^{opt}(\mathcal{D}_N)$, any other parameters $\underline{\alpha}$ in $S_{\underline{\alpha}}$ which produce the same model output as $\hat{\underline{\alpha}}$ are also optimal parameters, i.e.,

$$\underline{x}(n; \underline{a}) = \underline{x}(n; \hat{\underline{a}}) \text{ and } \hat{\underline{\alpha}} = [\hat{\underline{a}}^T, \hat{\underline{\sigma}}^T]^T \in S_{\underline{\alpha}}^{opt}(\mathcal{D}_N)$$

$$\Longrightarrow \underline{\alpha} = [\underline{a}^T, \hat{\underline{\sigma}}^T]^T \in S_{\underline{\alpha}}^{opt}(\mathcal{D}_N).$$

Due to the complex nature of system identifiability as explained above, the definition of another type of identifiability becomes necessary. Let $\hat{\underline{\alpha}} = [\hat{\underline{a}}^T, \hat{\underline{\sigma}}^T]^T$ be a vector of optimal parameters in $S_{\underline{\alpha}}^{opt}(\mathcal{D}_N)$ and $S_{\hat{\underline{a}}}(\hat{Z}_1^N)$ contain all the model parameters $\underline{a}$ which produce the same model output as the model specified by $\hat{\underline{a}}$, i.e.,

$$\underline{x}(n;\underline{a}) = \underline{x}(n;\hat{\underline{a}}) \iff \underline{a} \in S_{\hat{\underline{a}}}(\hat{Z}_1^N).$$

Then, the following definition of model identifiability is introduced:

- A parameter a_i of $\underline{a}$ is *globally model identifiable* at $\hat{\underline{a}}$ given the measured system input $\hat{Z}_1^N$ if $S_{\hat{\underline{a}}}(\hat{Z}_1^N)$ contains only one vector of model parameters, or, if not, then:

$$\hat{\underline{a}}^{(1)}, \hat{\underline{a}}^{(2)} \in S_{\hat{\underline{a}}}(\hat{Z}_1^N) \Longrightarrow \hat{a}_i^{(1)} = \hat{a}_i^{(2)}.$$

- A parameter a_i of $\underline{a}$ is *model identifiable* at $\hat{\underline{a}}$ given the measured system input $\hat{Z}_1^N$ if there exists a positive number ϵ_i such that:

$$\hat{\underline{a}}^{(1)}, \hat{\underline{a}}^{(2)} \in S_{\hat{\underline{a}}}(\hat{Z}_1^N) \Longrightarrow |\hat{a}_i^{(1)} - \hat{a}_i^{(2)}| > \epsilon_i \text{ or } \hat{a}_i^{(1)} = \hat{a}_i^{(2)}.$$

- A parameter a_i of $\underline{a}$ is *locally model identifiable* at $\hat{\underline{a}}$ given the measured system input $\hat{Z}_1^N$ if it is model identifiable but not globally model identifiable.

- A parameter a_i of $\underline{a}$ is *model un-identifiable* at $\hat{\underline{a}}$ given the measured system input $\hat{Z}_1^N$ if it is not model identifiable.

Similarly, the above definition can be extended as follows:

- The vector of model parameters $\underline{a}$ is (globally) model identifiable at $\hat{\underline{a}}$ if all of the parameters a_i are globally model identifiable at $\hat{\underline{a}}$.

- The vector of model parameters $\underline{a}$ is locally model identifiable at $\hat{\underline{a}}$ if it is model identifiable but at least one parameter a_i is only locally model identifiable at $\hat{\underline{a}}$.

- The vector of model parameters $\underline{a}$ is model un-identifiable at $\hat{\underline{a}}$ if at least one parameter a_i is model un-identifiable at $\hat{\underline{a}}$.

- The class of models $\mathcal{M}$ is (globally) locally model identifiable at $\hat{\underline{a}}$ given the measured system input $\hat{Z}_1^N$ if $\underline{a}$ is (globally) locally model identifiable at $\hat{\underline{a}}$.

- The class of models $\mathcal{M}$ is model un-identifiable at $\hat{\underline{a}}$ given the measured system input $\hat{Z}_1^N$ if $\underline{a}$ is model un-identifiable at $\hat{\underline{a}}$.

If the class of models $\mathcal{M}$ is model identifiable at $\hat{\underline{a}}$ given the measured system input $\hat{Z}_1^N$ and $S_{\underline{a}}$ is bounded, there is only a finite number of model parameters in $S_{\hat{\underline{a}}}(\hat{Z}_1^N)$.

It is noted that if the vector of model parameters $\underline{a}$ is not globally model identifiable at $\hat{\underline{a}}$ given the measured system input $\hat{Z}_1^N$, the parameters $\underline{\alpha}$ cannot be globally system identifiable given the measured data $\mathcal{D}_N$. Furthermore, in the locally identifiable case, the number of optimal parameters in $S_{\underline{\alpha}}^{opt}(\mathcal{D}_N)$ must be at least as large as the number of model parameters in $S_{\hat{\underline{a}}}(\hat{Z}_1^N)$. Therefore, a system identifiability problem can be theoretically decomposed into multiple model identifiability subproblems. But the difficulty is that the number of model identifiability subproblems is not known *a priori*.

2.4.2 Asymptotic Approximations in System Identifiable Cases

Assume the vector of parameters $\underline{\alpha}$ is system identifiable given the measured data $\mathcal{D}_N$. Hence, if $S_{\underline{\alpha}}$ is bounded, there is a finite number of optimal parameters in $S_{\underline{\alpha}}^{opt}(\mathcal{D}_N)$. Denote these optimal parameters by $\hat{\underline{\alpha}}^{(k)}, k = 1, \ldots, K$ and assume that they all lie in the interior of $S_{\underline{\alpha}}$. Each $\hat{\underline{\alpha}}^{(k)}$ globally maximizes the likelihood function $f_N(\hat{Y}_1^N; \underline{\alpha}, \hat{Z}_1^N)$ and so locally maximizes the posterior probability distribution $p(\underline{\alpha}|\mathcal{D}_N, \mathcal{M}_{\mathcal{P}})$ if the prior probability distribution $\pi(\underline{\alpha})$ is a smooth and slowly-varying function.

By expanding $\ln f_N(\hat{Y}_1^N; \underline{\alpha}, \hat{Z}_1^N)$ in a second-order Taylor series about the optimal parameters $\hat{\underline{\alpha}}^{(k)}$, the following approximation of $f_N(\hat{Y}_1^N; \underline{\alpha}, \hat{Z}_1^N)$ in the neighborhood of $\hat{\underline{\alpha}}^{(k)}$ can be obtained:

$$f_N(\hat{Y}_1^N; \underline{\alpha}, \hat{Z}_1^N) \approx f_N(\hat{Y}_1^N; \underline{\hat{\alpha}}^{(k)}, \hat{Z}_1^N) \exp\left[-\frac{1}{2}(\underline{\alpha} - \underline{\hat{\alpha}}^{(k)})^T A_N(\underline{\hat{\alpha}}^{(k)})(\underline{\alpha} - \underline{\hat{\alpha}}^{(k)})\right], \tag{2.4.2}$$

where the $N_{\underline{\alpha}} \times N_{\underline{\alpha}}$ Hessian matrix $A_N(\underline{\hat{\alpha}}^{(k)})$ of $\ln f_N(\hat{Y}_1^N; \underline{\alpha}, \hat{Z}_1^N)$ is assumed to be positive-definite and is given by:

$$[A_N(\underline{\hat{\alpha}}^{(k)})]_{ij} = -\left.\frac{\partial^2 \ln f_N(\hat{Y}_1^N; \underline{\alpha}, \hat{Z}_1^N)}{\partial\alpha_i \partial\alpha_j}\right|_{\underline{\alpha}=\underline{\hat{\alpha}}^{(k)}}.$$

Because the elements of $A_N(\underline{\alpha})$ are $\mathcal{O}(N)$ in most cases, $f_N(\hat{Y}_1^N; \underline{\alpha}, \hat{Z}_1^N)$ is very peaked at each vector of optimal parameters $\underline{\hat{\alpha}}^{(k)}$ for a large number N of sampled measurement. By using Laplace's method [46] for asymptotic expansion of multi-dimensional integrals and (2.4.2), $p(\underline{\alpha}|\mathcal{D}_N, \mathcal{M}_\mathcal{P})$ can be approximated by:

$$p(\underline{\alpha}|\mathcal{D}_N, \mathcal{M}_\mathcal{P}) \approx \sum_{k=1}^{K} w_k G(\underline{\alpha}; \underline{\hat{\alpha}}^{(k)}, A_N^{-1}(\underline{\hat{\alpha}}^{(k)})), \tag{2.4.3}$$

where

$$G(\underline{\alpha}; \underline{\hat{\alpha}}^{(k)}, A_N^{-1}(\underline{\hat{\alpha}}^{(k)})) = \frac{1}{(2\pi)^{N_{\underline{\alpha}}/2}|A_N^{-1}(\underline{\hat{\alpha}}^{(k)})|^{1/2}} \exp\left[-\frac{1}{2}(\underline{\alpha} - \underline{\hat{\alpha}}^{(k)})^T A_N(\underline{\hat{\alpha}}^{(k)})(\underline{\alpha} - \underline{\hat{\alpha}}^{(k)})\right],$$

and

$$w_k = \frac{w_k'}{\sum_{l=1}^{K} w_l'} \quad , \quad w_k' = |A_N(\underline{\hat{\alpha}}^{(k)})|^{-1/2} \pi(\underline{\hat{\alpha}}^{(k)}). \tag{2.4.4}$$

From (2.4.3), it is noted that $p(\underline{\alpha}|\mathcal{D}_N, \mathcal{M}_\mathcal{P})$ turns out to coincide with a scaled $N_{\underline{\alpha}}$-dimensional Gaussian distribution for $\underline{\alpha}$ with mean $\underline{\hat{\alpha}}^{(k)}$ and covariance matrix $A_N^{-1}(\underline{\hat{\alpha}}^{(k)})$ in the neighborhood of $\underline{\hat{\alpha}}^{(k)}$. Furthermore, each vector of optimal param-

eters $\underline{\alpha}$ in $S_{\underline{\alpha}}^{opt}(\mathcal{D}_N)$ may be interpreted as a locally most probable model within the class of models $\mathcal{M}_{\mathcal{P}}$ given the measured data $\mathcal{D}_N$, and the covariance matrix can be used to examine how precisely the optimal parameters are identified.

By using the asymptotic approximation of $p(\underline{\alpha}|\mathcal{D}_N, \mathcal{M}_{\mathcal{P}})$ in (2.4.3), an asymptotic expansion of the analytical integral for the updated probability distribution given in (2.3.6) can be obtained [2]:

$$p(Y_{N+1}^M|\mathcal{D}_N, Z_{N+1}^M, \mathcal{M}_{\mathcal{P}}) \approx \sum_{k=1}^{K} w_k p(Y_{N+1}^M|\hat{\underline{\alpha}}^{(k)}, Z_{N+1}^M, \mathcal{M}_{\mathcal{P}}), \tag{2.4.5}$$

where

$$\begin{aligned} p(Y_{N+1}^M|\hat{\underline{\alpha}}^{(k)}, Z_{N+1}^M, \mathcal{M}_{\mathcal{P}}) &= \frac{p(\hat{Y}_1^N, Y_{N+1}^M|\hat{\underline{\alpha}}^{(k)}, \hat{Z}_1^N, Z_{N+1}^M, \mathcal{M}_{\mathcal{P}})}{p(\hat{Y}_1^N|\hat{\underline{\alpha}}^{(k)}, \hat{Z}_1^N, \mathcal{M}_{\mathcal{P}})}, \\ &= \frac{f_M(\hat{Y}_1^N, Y_{N+1}^M; \hat{\underline{\alpha}}^{(k)}, \hat{Z}_1^N, Z_{N+1}^M)}{f_N(\hat{Y}_1^N; \hat{\underline{\alpha}}^{(k)}, \hat{Z}_1^N)}. \end{aligned}$$

Therefore, the continuous weighted average of the updated probability distribution in (2.3.6) is approximated by a discrete weighted average of the updated probability distribution for each vector of optimal parameters in the class of models $\mathcal{M}_{\mathcal{P}}$ given the measured data $\mathcal{D}_N$. The weighting of each optimal parameter vector is equal to the volume of $p(\underline{\alpha}|\mathcal{D}_N, \mathcal{M}_{\mathcal{P}})$ under its corresponding Gaussian-shaped peak. It is noted from (2.4.4) and (2.4.5) that the prior probability distribution $\pi(\underline{\alpha})$ is not required over the entire parameter space $S_{\underline{\alpha}}$. Indeed, only the relative values at each vector of optimal parameters $\hat{\underline{\alpha}}^{(k)}$ need to be specified.

It should be emphasized that the exact updated probability distribution in (2.3.6) does not require parameter estimation in the usual sense. However, the asymptotic approximation in (2.4.5) does. Therefore, the system identification problem is converted to a nontrivial global optimization problem. Because the optimal parameters are equivalent to the traditional maximum likelihood estimates, these

estimates can be interpretated in terms of an asymptotic approximation to the exact probability distribution in (2.3.6). However, the asymptotic approximation in (2.4.5) is still applicable when there are multiple vectors of optimal parameters. But this situation cannot be dealt with in the classic maximum likelihood estimation.

2.4.3 Asymptotic Approximations in System Un-Identifiable Cases

Suppose the class of models $\mathcal{M}_{\mathcal{P}}$ is system un-identifiable given the measured data $\mathcal{D}_N$ and the prior probability distribution $\pi(\underline{\alpha})$ is a smooth and slowly-varying function. It is assumed that $S_{\underline{\alpha}}^{opt}(\mathcal{D}_N)$ contains a finite collection of smooth and non-intersecting d-dimensional manifolds or hyper-surfaces in the parameter space $S_{\underline{\alpha}}$ and let $\mathcal{H}_d$ denote any one of these manifolds. Based on the definition, each vector of optimal parameters $\hat{\underline{\alpha}}$ in $\mathcal{H}_d$ globally maximizes $f_N(\hat{Y}_1^N; \underline{\alpha}, \hat{Z}_1^N)$ (or $\ln f_N(\hat{Y}_1^N; \underline{\alpha}, \hat{Z}_1^N)$).

Consider a local *parameterization* of a neighborhood $\mathcal{N}_{\hat{\underline{\alpha}}}$ of $\hat{\underline{\alpha}}$ on the manifold $\mathcal{H}_d$ by a smooth function $\underline{\phi}_{\hat{\underline{\alpha}}} : U \longmapsto \mathcal{N}_{\hat{\underline{\alpha}}}$, where U is an open set in R^d and $\underline{\phi}_{\hat{\underline{\alpha}}}(\underline{0}) = \hat{\underline{\alpha}}$. Since $\underline{\phi}_{\hat{\underline{\alpha}}}(\underline{u}) \in \mathcal{N}_{\hat{\underline{\alpha}}}$, $\forall \underline{u} \in U$, the following is true:

$$\nabla \ln f_N(\hat{Y}_1^N; \underline{\phi}_{\hat{\underline{\alpha}}}(\underline{u}), \hat{Z}_1^N) = \underline{0}, \ \forall \underline{u} \in U, \tag{2.4.6}$$

where the gradient is with respect to $\underline{\alpha}$. By differentiating (2.4.6) with respect to $\underline{u}$ and evaluating at $\underline{u} = \underline{0}$, (2.4.7) is obtained:

$$[\nabla\nabla \ln f_N(\hat{Y}_1^N; \hat{\underline{\alpha}}, \hat{Z}_1^N)][\nabla \underline{\phi}_{\hat{\underline{\alpha}}}(\underline{0})] = \underline{0}. \tag{2.4.7}$$

Let $A_N(\hat{\underline{\alpha}})$ denote the $N_{\underline{\alpha}} \times N_{\underline{\alpha}}$ Hessian matrix $-\nabla\nabla \ln f_N(\hat{Y}_1^N; \hat{\underline{\alpha}}, \hat{Z}_1^N)$ of $\ln f_N(\hat{Y}_1^N; \hat{\underline{\alpha}}, \hat{Z}_1^N)$ which must be positive semi-definite. By definition, the *tangent space*, $\mathcal{T}_{\hat{\underline{\alpha}}}(\mathcal{H}_d)$, of the manifold $\mathcal{H}_d$ at $\hat{\underline{\alpha}}$ is the *image* or *range* of the linear map $\nabla \underline{\phi}_{\hat{\underline{\alpha}}}(\underline{0})$. Therefore, it is clear from (2.4.7) that the tangent space $\mathcal{T}_{\hat{\underline{\alpha}}}(\mathcal{H}_d)$ is a sub-space of the *null space* of $A_N(\hat{\underline{\alpha}})$. Since the manifold $\mathcal{H}_d$ is d-dimensional, the tangent space $\mathcal{T}_{\hat{\underline{\alpha}}}(\mathcal{H}_d)$ is also d-dimensional. It is assumed for simplicity here that the null space of $A_N(\hat{\underline{\alpha}})$ is also d-dimensional and, therefore, the tangent space $\mathcal{T}_{\hat{\underline{\alpha}}}(\mathcal{H}_d)$ and

the null space of $A_N(\underline{\hat{\alpha}})$ are identical.

By expanding $\ln f_N(\hat{Y}_1^N; \underline{\alpha}, \hat{Z}_1^N)$ in a second-order Taylor series about the optimal parameters $\underline{\hat{\alpha}}$, the following approximation of $f_N(\hat{Y}_1^N; \underline{\alpha}, \hat{Z}_1^N)$ in the neighborhood of $\underline{\hat{\alpha}}$ can be obtained:

$$f_N(\hat{Y}_1^N; \underline{\alpha}, \hat{Z}_1^N) \approx f_N(\hat{Y}_1^N; \underline{\hat{\alpha}}, \hat{Z}_1^N) \exp\left[-\frac{1}{2}(\underline{\alpha} - \underline{\hat{\alpha}})^T A_N(\underline{\hat{\alpha}})(\underline{\alpha} - \underline{\hat{\alpha}})\right]. \tag{2.4.8}$$

Because the null space of $A_N(\underline{\hat{\alpha}})$ is d-dimensional, $A_N(\underline{\hat{\alpha}})$ has exactly d zero eigenvalues. Since $A_N(\underline{\hat{\alpha}})$ is symmetric, it is always possible to find a set of *orthonormal* eigenvectors for $A_N(\underline{\hat{\alpha}})$. Let $\{\lambda_1, \ldots, \lambda_d, \lambda_{d+1}, \ldots, \lambda_{N_{\underline{\alpha}}}\}$ and $\{\underline{v}_1, \ldots, \underline{v}_d, \underline{v}_{d+1}, \ldots, \underline{v}_{N_{\underline{\alpha}}}\}$ denote the set of eigenvalues and corresponding orthonormal eigenvectors of $A_N(\underline{\hat{\alpha}})$ in which $\lambda_1 = \ldots = \lambda_d = 0$ and $\lambda_{d+1}, \ldots, \lambda_{N_{\underline{\alpha}}}$ are positive and are $\mathcal{O}(N)$ in most cases.

Let

$$T_{\underline{\hat{\alpha}}} = [T^0_{\underline{\hat{\alpha}}}, T^+_{\underline{\hat{\alpha}}}], \quad T^0_{\underline{\hat{\alpha}}} = [\underline{v}_1, \ldots, \underline{v}_d], \quad T^+_{\underline{\hat{\alpha}}} = [\underline{v}_{d+1}, \ldots, \underline{v}_{N_{\underline{\alpha}}}],$$

and

$$\Lambda_N(\underline{\hat{\alpha}}) = \begin{bmatrix} 0 & 0 \\ 0 & \Lambda^+_N(\underline{\hat{\alpha}}) \end{bmatrix}, \quad \Lambda^+_N(\underline{\hat{\alpha}}) = diag[\lambda_{d+1}, \ldots, \lambda_{N_{\underline{\alpha}}}].$$

Since $T_{\underline{\hat{\alpha}}}$ is an orthogonal matrix, i.e., $T^T_{\underline{\hat{\alpha}}} = T^{-1}_{\underline{\hat{\alpha}}}$, and $\Lambda_N(\underline{\hat{\alpha}}) = T^T_{\underline{\hat{\alpha}}} A_N(\underline{\hat{\alpha}}) T_{\underline{\hat{\alpha}}}$. Therefore, by applying the following linear coordinate transformation in the neighborhood of $\underline{\hat{\alpha}}$:

$$\underline{\alpha} - \underline{\hat{\alpha}} = T_{\underline{\hat{\alpha}}} \underline{\beta} = [T^0_{\underline{\hat{\alpha}}}, T^+_{\underline{\hat{\alpha}}}] \begin{Bmatrix} \underline{\beta}^0 \\ \underline{\beta}^+ \end{Bmatrix}, \tag{2.4.9}$$

(2.4.8) can be rewritten as:

$$f_N(\hat{Y}_1^N; \underline{\alpha}, \hat{Z}_1^N) \approx f_N(\hat{Y}_1^N; \underline{\hat{\alpha}}, \hat{Z}_1^N) \exp(-\frac{1}{2}\underline{\beta}^{+T} \Lambda_N^+(\underline{\hat{\alpha}})\underline{\beta}^+). \tag{2.4.10}$$

Because the eigenvalues $\lambda_{d+1}, \ldots, \lambda_{N_{\underline{\alpha}}}$ are $\mathcal{O}(N)$, it is noted from (2.4.10) that $f_N(\hat{Y}_1^N; \underline{\alpha}, \hat{Z}_1^N)$ is very peaked at each vector of optimal parameters $\underline{\hat{\alpha}}$ for a large number N of sampled measurement when compared with any other parameters $\underline{\alpha}$ in the neighborhood $\mathcal{N}_{\underline{\hat{\alpha}}}^+$ of $\underline{\hat{\alpha}}$ which is not on the manifold $\mathcal{H}_d$. Furthermore, the vector $\underline{\alpha} - \underline{\hat{\alpha}}$ is a linear combination of the eigenvectors $\underline{v}_{d+1}, \ldots, \underline{v}_{N_{\underline{\alpha}}}$ of $A_N(\underline{\hat{\alpha}})$. Since the integration of $p(\underline{\alpha}|\mathcal{D}_N, \mathcal{M}_\mathcal{P})$ over the entire parameter space $S_{\underline{\alpha}}$ is equal to unity, the following approximation can be obtained by using (2.4.10) and assuming that $\mathcal{H}_d$ is the only manifold in $S_{\underline{\alpha}}^{opt}(\mathcal{D}_N)$ for the time being:

$$\begin{aligned}
1 &= \int_{S_{\underline{\alpha}}} p(\underline{\alpha}|\mathcal{D}_N, \mathcal{M}_\mathcal{P}) d\underline{\alpha}, \\
&= k \int_{S_{\underline{\alpha}}} f_N(\hat{Y}_1^N; \underline{\alpha}, \hat{Z}_1^N) \pi(\underline{\alpha}) d\underline{\alpha}, \\
&\approx k \int_{\mathcal{H}_d} \left\{ \int_{\mathcal{N}_{\underline{\hat{\alpha}}}^+} f_N(\hat{Y}_1^N; \underline{\alpha}, \hat{Z}_1^N) \pi(\underline{\alpha}) d\underline{\beta}^+ \right\} da_{\mathcal{H}_d}, \\
&\approx k f_N(\hat{Y}_1^N; \underline{\hat{\alpha}}, \hat{Z}_1^N) \\
&\qquad \times \int_{\mathcal{H}_d} \left\{ \int_{\mathcal{N}_{\underline{\hat{\alpha}}}^+} \exp(-\frac{1}{2}\underline{\beta}^{+T} \Lambda_N^+(\underline{\hat{\alpha}})\underline{\beta}^+) d\underline{\beta}^+ \right\} \pi(\underline{\hat{\alpha}}) da_{\mathcal{H}_d}.
\end{aligned} \tag{2.4.11}$$

Both the linear coordinate transformation (2.4.9) and the fact that the transformation matrix $T_{\underline{\hat{\alpha}}}$ is orthogonal have been incorporated in deriving (2.4.11). The integrals in (2.4.11) perform an integration over the manifold $\mathcal{H}_d$ and the neighborhood $\mathcal{N}_{\underline{\hat{\alpha}}}^+$. The symbol $da_{\mathcal{H}_d}$ represents an infinitesimal component of the manifold $\mathcal{H}_d$. In the simplest case when $\mathcal{H}_d$ is a smooth curve, $da_{\mathcal{H}_d}$ is just an infinitesimal arclength which is usually denoted by dl in calculus. In (2.4.11), $f_N(\hat{Y}_1^N; \underline{\hat{\alpha}}, \hat{Z}_1^N)$ can be pulled outside the integrals because all the optimal parameters $\underline{\hat{\alpha}}$ in $\mathcal{H}_d$ give the same global minimum of $f_N(\hat{Y}_1^N; \underline{\alpha}, \hat{Z}_1^N)$.

Furthermore, the inner integral in (2.4.11) can be easily computed by noting that the integrand is nothing but a scaled $(N_{\underline{\alpha}} - d)$-dimensional Gaussian distribution for $\underline{\beta}^+$ with zero mean and covariance matrix $(\Lambda_N^+(\underline{\hat{\alpha}}))^{-1}$. Therefore,

$$\int_{\mathcal{N}_{\underline{\hat{\alpha}}}^+} \exp(-\frac{1}{2}\underline{\beta}^{+T}\Lambda_N^+(\underline{\hat{\alpha}})\underline{\beta}^+)d\underline{\beta}^+ \approx (2\pi)^{(N_{\underline{\alpha}}-d)/2}|\Lambda_N^+(\underline{\hat{\alpha}})|^{-1/2}. \tag{2.4.12}$$

By substituting (2.4.12) into (2.4.11), the following approximation is obtained:

$$1 \approx k(2\pi)^{(N_{\underline{\alpha}}-d)/2} f_N(\hat{Y}_1^N; \underline{\hat{\alpha}}, \hat{Z}_1^N) \int_{\mathcal{H}_d} w'(\underline{\hat{\alpha}}) da_{\mathcal{H}_d}, \tag{2.4.13}$$

where $w'(\underline{\hat{\alpha}}) = |\Lambda_N^+(\underline{\hat{\alpha}})|^{-1/2}\pi(\underline{\hat{\alpha}})$.

By using the same approximation approach as in deriving (2.4.11), the exact updated probability distribution in (2.3.6) can be approximated by using (2.4.12) and (2.4.13) as follows:

$$\begin{aligned}
&p(Y_{N+1}^M|\mathcal{D}_N, Z_{N+1}^M, \mathcal{M}_\mathcal{P}) \\
&= \int_{S_{\underline{\alpha}}} p(Y_{N+1}^M|\underline{\alpha}, Z_{N+1}^M, \mathcal{M}_\mathcal{P}) p(\underline{\alpha}|\mathcal{D}_N, \mathcal{M}_\mathcal{P}) d\underline{\alpha}, \\
&= k\int_{S_{\underline{\alpha}}} p(Y_{N+1}^M|\underline{\alpha}, Z_{N+1}^M, \mathcal{M}_\mathcal{P}) f_N(\hat{Y}_1^N; \underline{\alpha}, \hat{Z}_1^N)\pi(\underline{\alpha}) d\underline{\alpha}, \\
&\approx k\int_{\mathcal{H}_d} \left\{ \int_{\mathcal{N}_{\underline{\hat{\alpha}}}^+} p(Y_{N+1}^M|\underline{\alpha}, Z_{N+1}^M, \mathcal{M}_\mathcal{P}) f_N(\hat{Y}_1^N; \underline{\alpha}, \hat{Z}_1^N)\pi(\underline{\alpha}) d\underline{\beta}^+ \right\} da_{\mathcal{H}_d}, \\
&\approx k\int_{\mathcal{H}_d} f_N(\hat{Y}_1^N; \underline{\hat{\alpha}}, \hat{Z}_1^N) \\
&\qquad \times \left\{ \int_{\mathcal{N}_{\underline{\hat{\alpha}}}^+} \exp(-\frac{1}{2}\underline{\beta}^{+T}\Lambda_N^+(\underline{\hat{\alpha}})\underline{\beta}^+) d\underline{\beta}^+ \right\} p(Y_{N+1}^M|\underline{\hat{\alpha}}, Z_{N+1}^M, \mathcal{M}_\mathcal{P})\pi(\underline{\hat{\alpha}}) da_{\mathcal{H}_d}, \\
&\approx k(2\pi)^{(N_{\underline{\alpha}}-d)/2} f_N(\hat{Y}_1^N; \underline{\hat{\alpha}}, \hat{Z}_1^N) \int_{\mathcal{H}_d} p(Y_{N+1}^M|\underline{\hat{\alpha}}, Z_{N+1}^M, \mathcal{M}_\mathcal{P})|\Lambda_N^+(\underline{\hat{\alpha}})|^{-1/2}\pi(\underline{\hat{\alpha}}) da_{\mathcal{H}_d},
\end{aligned}$$

$$\approx \frac{\int_{\mathcal{H}_d} w'(\hat{\underline{\alpha}}) p(Y_{N+1}^M|\hat{\underline{\alpha}}, Z_{N+1}^M, \mathcal{M}_\mathcal{P}) da_{\mathcal{H}_d}}{\int_{\mathcal{H}_d} w'(\hat{\underline{\alpha}}) da_{\mathcal{H}_d}}.$$

Therefore, an asymptotic approximation of the exact updated probability distribution in (2.3.6) can be obtained as follows:

$$p(Y_{N+1}^M|\mathcal{D}_N, Z_{N+1}^M, \mathcal{M}_\mathcal{P}) \approx \int_{\mathcal{H}_d} w(\hat{\underline{\alpha}}) p(Y_{N+1}^M|\hat{\underline{\alpha}}, Z_{N+1}^M, \mathcal{M}_\mathcal{P}) da_{\mathcal{H}_d}, \tag{2.4.14}$$

where

$$w(\hat{\underline{\alpha}}) = \frac{w'(\hat{\underline{\alpha}})}{\int_{\mathcal{H}_d} w'(\hat{\underline{\alpha}}) da_{\mathcal{H}_d}} \text{ and } w'(\hat{\underline{\alpha}}) = |\Lambda_N^+(\hat{\underline{\alpha}})|^{-1/2} \pi(\hat{\underline{\alpha}}). \tag{2.4.15}$$

If there is more than one manifold in the set of optimal parameters $S_{\underline{\alpha}}^{opt}(\mathcal{D}_N)$, the asymptotic approximation given in (2.4.14) and (2.4.15) can be generalized as follows:

$$p(Y_{N+1}^M|\mathcal{D}_N, Z_{N+1}^M, \mathcal{M}_\mathcal{P}) \approx \int_{\cup\mathcal{H}_d} w(\hat{\underline{\alpha}}) p(Y_{N+1}^M|\hat{\underline{\alpha}}, Z_{N+1}^M, \mathcal{M}_\mathcal{P}) da_{\mathcal{H}_d}, \tag{2.4.16}$$

and

$$w(\hat{\underline{\alpha}}) = \frac{w'(\hat{\underline{\alpha}})}{\int_{\cup\mathcal{H}_d} w'(\hat{\underline{\alpha}}) da_{\mathcal{H}_d}} \quad , \quad w'(\hat{\underline{\alpha}}) = |\Lambda_N^+(\hat{\underline{\alpha}})|^{-1/2} \pi(\hat{\underline{\alpha}}). \tag{2.4.17}$$

The integration in (2.4.16) and (2.4.17) is now performed over the union of all the manifolds $\mathcal{H}_d$'s in $S_{\underline{\alpha}}^{opt}(\mathcal{D}_N)$.

The multi-dimensional integral for the exact updated probability distribution in

(2.3.6) is therefore approximated by a continuous weighted average of the updated probability distribution for all of the optimal parameters in the class of models $\mathcal{M}_{\mathcal{P}}$ given the measured data $\mathcal{D}_N$. Although integration is still needed in the asymptotic approximations (2.4.16) and (2.4.17), the order of integration has been reduced from $N_{\underline{\alpha}}$ dimensions in (2.3.6) to d dimensions in (2.4.16) and (2.4.17). It is also noted that the prior probability distribution $\pi(\underline{\alpha})$ is not required over the entire parameter space $S_{\underline{\alpha}}$. Indeed, only the relative values at the optimal parameters $\hat{\underline{\alpha}}$ in the $\mathcal{H}_d$ manifolds need to be specified.

References for Chapter 2

1. Beck, J. L., *System Identification Applied to Strong Motion Records from Structures*, Earthquake Ground Motion and its Effects on Structures, AMD-53, Edited by S. K. Datta, ASME, New York, New York, pp. 109-133, 1982.
2. Beck, J. L., *System Identification Methods Applied to Measured Seismic Response*, Proceedings of the Eleventh World Conference on Earthquake Engineering, Acapulco, Mexico, 1996.
3. Beck, J. L., *Determining Models of Structures from Earthquake Records*, Report No. EERL 78-01, California Institute of Technology, Pasadena, California, 1978.
4. McVerry, G. H., and Beck, J. L., *Structural Identification of JPL Building 180 Using Optimally Synchronized Earthquake Records*, Report No. EERL 83-01, California Institute of Technology, Pasadena, California, 1983.
5. Li, Y., and Mau, S. T., *A Case Study of MIMO System Identification Applied to Building Seismic Records*, Earthquake Engineering and Structural Dynamics, Vol. 20, No. 11, pp. 1045-1064, 1991.
6. Şafak, E., *Identification of Linear Structures Using Discrete-Time Filters*, ASCE Journal of Engineering Mechanics, Vol. 117, No. 10, pp. 3064-3085, 1991.
7. Li, Y., and Mau, S. T., *Anatomy of the Loma Prieta Earthquake Records of Two Steel Buildings Using MIMO System Identification*, Proceedings of the Ninth Conference on Engineering Mechanics, ASCE, New York, New York, pp. 689-692, 1992.
8. Nisar, A., Werner, S. D., and Beck, J. L., *Assessment of UBC Seismic Design Provisions Using Recorded Building Motions*, Proceedings of the Tenth World Conference on Earthquake Engineering, A. A. Balkema, Rotterdam, Netherlands, pp. 5723-5728, 1992.
9. Durrani, A. J., Mau, S. T., AbouHashish, A. A., and Li, Y., *Earthquake Response of Flat-Slab Buildings*, ASCE Journal of Structural Engineering, Vol. 120, No. 3, pp. 947-964, 1994.
10. Mau, S. T., and Aruna, V., *Story-Drift, Shear, and OTM Estimation from Building Seismic Records*, ASCE Journal of Structural Engineering, Vol. 120, No. 11, pp. 3366-3385, 1994.
11. Loh, C. H., and Tou, I. C., *A System Identification Approach to the Detection of Changes in both Linear and Non-linear Structural Parameters*, Earthquake Engineering and Structural Dynamics, Vol. 24, No. 1, pp. 85-97, 1995.
12. Werner, S. D., Beck, J. L., and Levine, M. B., *Seismic Response Evaluation of Meloland Road Overpass Using 1979 Imperial Valley Earthquake Records*, Earthquake Engineering and Structural Dynamics, Vol. 15, No. 2, pp. 249-274, 1987.

13. Mason, A. B., Beck, J. L., Chen, J., and Ullmann, R. R., *Modal Parameter Identification of an Off-shore platform from Earthquake Response Records*, Seismic Engineering : Research and Practice, ASCE, New York, New York, pp. 217-226, 1989.

14. Beck, J. L., May, B. S., and Polidori, D. C., *Determination of Modal Parameters from Ambient Vibration Data for Structural Health Monitoring*, Proceedings of the First World Conference on Structural Control, International Association for Structural Control, Los Angeles, California, pp. TA3:3 - TA3:12, 1994.

15. Ghanem, R., and Shinozuka, M., *Structural System Identification I : Theory*, ASCE Journal of Engineering Mechanics, Vol. 121, No. 2, pp. 255-264, 1995.

16. Shinozuka, M., and Ghanem, R., *Structural System Identification II : Experimental Verification*, ASCE Journal of Engineering Mechanics, Vol. 121, No. 2, pp. 265-273, 1995.

17. Udwadia, F. E., and Marmarelis, P. Z., *The Identification of Building Structural Systems II. The Nonlinear Case*, Bulletin of the Seismological Society of America, Vol. 66, No. 1, pp. 153-171, 1976.

18. Masri, S. F., *A Hybrid Parametric/Non-parametric Approach for the Identification of Nonlinear Systems*, Probabilistic Engineering Mechanics, Vol. 9, Nos. 1-2, pp. 47-57, 1994.

19. Benedettini, F., Capecchi, D., and Vestroni, F., *Identification of Hysteretic Oscillators Under Earthquake Loading by Non-parametric Models*, ASCE Journal of Engineering Mechanics, Vol. 121, No. 5, pp. 606-612, 1995.

20. Chassiakos, A. G., and Masri, S. F., *Modeling Unknown Structural Systems Through the Use of Neural Networks*, Earthquake Engineering and Structural Dynamics, Vol. 25, No. 2, pp. 117-128, 1996.

21. Goodwin, G. C., and Sin, K. S., *Adaptive Filtering, Prediction, and Control*, Prentice-Hall, Englewood Cliffs, New Jersey, 1984.

22. Ljung, L., *System Identification : Theory for the User*, Prentice-Hall, Englewood Cliffs, New Jersey, 1987

23. Lin, C. C., Soong, T. T., and Natke, H. G., *Real-Time System Identification of Degrading Structures*, ASCE Journal of Engineering Mechanics, Vol. 116, No. 10, pp. 2258-2274, 1990.

24. Hoshiya, M., and Saito, E., *Structural Identification by Extended Kalman Filter*, ASCE Journal of Engineering Mechanics, Vol. 110, No. 12, pp. 1757-1770, 1984.

25. Koh, C. G., and See, L. M., *Identification and Uncertainty Estimation of Structural Parameters*, ASCE Journal of Engineering Mechanics, Vol. 120, No. 6, pp. 1219-1236, 1994.

26. Beck, J. L., and Jennings, P. C., *Structural Identification Using Linear Models and Earthquake Records*, Earthquake Engineering and Structural Dynamics, Vol. 8, No. 2, pp. 145-160, 1980.

27. Tan, R. Y., and Cheng, W. M., *System Identification of a Non-classically Damped Linear System*, Computers and Structures, Vol. 46, No. 1, pp. 67-75, 1993.

28. Masri, S. F., Miller, R. K., Saud, A. F., and Caughey, T. K., *Identification of Nonlinear Vibrating Structures; Part I : Formulation*, ASME Journal of Applied Mechanics, Vol. 54, No. 4, pp. 918-922, 1987.

29. Hjelmstad, K. D., Banan, M. R., and Banan, M. R., *Time- Domain Parameter Estimation Algorithm for Structures I : Computational Aspects*, ASCE Journal of Engineering Mechanics, Vol. 121, No. 3, pp. 424-434, 1995.

30. McVerry, G. H., *Structural Identification in the Frequency Domain from Earthquake Records*, Earthquake Engineering and Structural Dynamics, Vol. 8, No. 2, pp. 161-180, 1980.

31. Zhao, Q., Sawada, T., Hirao, K., and Nariyuki, Y., *Localized Identification of MDOF Structures in the Frequency Domain*, Earthquake Engineering and Structural Dynamics, Vol. 24, No. 3, pp. 325-338, 1995.

32. Benedetti, D., and Gentile, C., *Identification of Modal Quantities from Two Earthquake Responses*, Earthquake Engineering and Structural Dynamics, Vol. 23, No. 4, pp. 447-462, 1994.

33. Liu, P. L., *Identification and Damage Detection of Trusses Using Modal Data*, ASCE Journal of Structural Engineering, Vol. 121, No. 4, pp. 599-608, 1995.

34. Beck, R. T., *Fundamental Problems in the Application of Structural Identification Procedures to Damage Detection*, Report No. EERL 91-03, California Institute of Technology, Pasadena, California, 1991.

35. Casas, J. R., and Aparicio, A. C., *Structural Damage Identification from Dynamic Test Data*, ASCE Journal of Structural Engineering, Vol. 120, No. 8, pp. 2437-2450, 1994.

36. Hassiotis, S., and Jeong, G. D., *Identification of Stiffness Reductions Using Natural Frequencies*, ASCE Journal of Engineering Mechanics, Vol. 121, No. 10, pp. 1106-1113, 1995.

37. Hogg, R. V., and Craig, A. T., *Introduction to Mathematical Statistics*, Macmillan Publishing, New York, New York, 1978.

38. Jaynes, E. T., *How Does the Brain Do Plausible Reasoning?*, Maximum Entropy and Bayesian Methods in Science and Engineering, Volume 1 : Foundations, Edited by G. J. Erickson, and C. R. Smith, Kluwer Academic Publishers, Boston, Massachusetts, pp. 1-24, 1988.

39. De Finetti, B., *Theory of Probability : A Critical Introductory Treatment*, Wiley, New York, New York, 1974.

40. Jaynes, E. T., *The Relation of Bayesian and Maximum Entropy Methods*, Maximum Entropy and Bayesian Methods in Science and Engineering, Volume 1 : Foundations, Edited by G. J. Erickson, and C. R. Smith, Kluwer Academic Publishers, Boston, Massachusetts, pp. 25-30, 1988.

41. Cox, R. T., *The Algebra of Probable Inference*, Johns Hopkins Press, Baltimore, Maryland, 1961.

42. Agbabian, M. S., Masri, S. F., Miller, R. K., and Caughey, T. K., *System Identification Approach to Detection of Structural Changes*, ASCE Journal of Engineering Mechanics, Vol. 117, No. 2, pp. 370-390, 1991.

43. Banan, M. R., Banan, M. R., and Hjelmstad, K. D., *Time- Domain Parameter Estimation Algorithm for Structures II : Numerical Simulation Studies*, ASCE Journal of Engineering Mechanics, Vol. 121, No. 3, pp. 435-447, 1995.

44. Beck, J. L., *Statistical System Identification of Structures*, Proceedings of the Fifth International Conference on Structural Safety and Reliability, ASCE, New York, New York, pp. 1395-1402, 1989.

45. Katafygiotis, L. S., *Treatment of Model Uncertainties in Structural Dynamics*, Report No. EERL 91-01, California Institute of Technology, Pasadena, California, 1991.

46. Papadimitriou, C., Beck, J. L., and Katafygiotis, L. S., *Asymptotic Expansions for Reliabilities and Moments of Uncertain Dynamic Systems*, Report No. EERL 95-05, California Institute of Technology, Pasadena, California, 1995.

Chapter 3

Generalized Trajectory Methods for Finding Multiple Extrema and Roots of Functions

3.1 Global Optimization Problem

3.1.1 Introduction

Many problems in engineering and science can be formulated as global optimization problems. In some applications, not only the global extrema but also all the local extrema are significant and need to be found. In any case, determination of these local extrema can be one step in a procedure to find the global extrema. Since the objective functions in many practical applications are not convex, they may have multiple local and global extremal points in the region of interest. Finding all these multiple extrema is a challenging computational problem. Also, in contrast to local extrema, which can be characterized by the local behavior of the objective function, no practical and general criteria exist to determine whether a global extremum has been found. Therefore, global optimization remains a major challenge from both mathematical and computational points of view.

In this dissertation, two generalized trajectory methods are presented which can be combined to provide robust computation of the multiple local extrema of an objective function. The first trajectory method is the homotopy scheme which provides a robust algorithm to find a stationary point of the objective function. The second trajectory method, which is called the relaxation scheme, starts at one stationary point and systematically connects the stationary points in a region by a network of trajectories. Both the homotopy and relaxation schemes actually solve the stationarity conditions and so they can also be used to find the roots of a set of nonlinear algebraic equations.

3.1.2 Overview of Existing Methods

A large number of publications have appeared in the literature during the past three decades on the subject of global optimization which present a variety of deterministic and stochastic methods [1-2]. A common feature of these global optimization methods is that some sort of global search strategy is incorporated in the algorithms. These strategies are essential due to the lack of "local" criteria for ascertaining global extrema, which may be located anywhere in the region of interest and so they can be found only by systematic search of the region.

The challenge is to perform this search in an efficient manner, since it is not computationally feasible to search exhaustively over a fine mesh unless the dimension of the space is small. Most proposed global optimization methods use heuristics to improve the efficiency of the search and do not offer an absolute guarantee of finding the global extrema. Increasing the reliability of finding these extrema while maintaining efficiency is the major challenge in research into global optimization methods.

Random Search Methods

Random search methods typically use random sampling of the objective function as the global search strategy along with some local optimization approaches to yield candidate global extrema, although *pure* random search methods simply use the "best" sampled values of the objective function as the estimated global extrema. A simple extension of pure random search is the *single-start* method which performs a single local optimization from the best sampled point. On the other hand, the *multi-start* methods use each sampled point to start a local optimization search.

One further improvement of pure random search is to find and label sampled points in the region of attraction of a local extremum and then start a local search from just one point in each identified group of sampled points. This kind of strategy is called *clustering* and can avoid locating a particular local extremum several times. Different clustering techniques have been proposed such as density clustering,

multilevel clustering, and vector quantization multi-start clustering [1]. A different clustering method using topographical information about the objective function by *directed graphs* is given in [3].

Covering Methods

The basic idea of covering methods for global optimization is to divide the region of interest into subregions and discard *infeasible* subregions which cannot contain the global extrema. The remaining *feasible* subregions are split into smaller subregions, and so on. Several algorithms have been used to check whether a given subregion is feasible or not. Some are based on the limit on the rate of change of function, i.e., the Lipschitz condition [4-6]. Another approach, which does not need the derivative of the objective function, uses *interval arithmetic* to estimate the upper and lower bounds on the objective function and to decide the feasibility of a given subregion [7].

Trajectory Methods

The basic idea of *trajectory* methods for global optimization is to search for global extrema by following certain trajectories in the region of interest. Most algorithms in this category make use of the solution trajectory of certain ordinary differential equations [2,8]. These differential equations are devised so that their equilibrium points correspond to the stationary points of the objective function. By choosing suitable initial conditions, some of the local extrema can be reached by following the solution trajectory of the differential equations. It is unlikely, however, that all the local extrema can be located by following just one solution trajectory.

Penalty Methods

Penalty methods combine local optimization methods with some technique to avoid duplicate convergence to a local extremum. After some local optimization method has been used to find a local extremum, a so-called *tunneling* process is introduced to other irrelevant local extrema in its neighborhood in order to locate a new starting point for another local optimization search which is expected to reach a

better local extremum [9]. *Tunneling* is accomplished by finding a root to a tunneling function which is constructed using the objective function and some penalty function. Unfortunately, finding such a root is also a global search problem which may be as difficult as the original optimization problem. Furthermore, tunneling is difficult and not robust for high dimensional optimization problems.

Decomposition Methods

In *decomposition* methods, variables of the objective function are partitioned into two groups. The original global optimization problem is then transformed and split into a *primal* subproblem and an associated *dual* subproblem that provides upper and lower bounds respectively on the global optimum. These kinds of methods are only applicable to global optimization problems involving quadratic and/or polynomial terms in the objective function [10].

Stochastic Methods

Stochastic methods for global optimization use stochastic models to model the objective function. The search for global extrema is then governed by optimizing using some criterion of rationality. This derived optimization task is usually easier than the original optimization problem. Since statistical elements are incorporated in the algorithm, the probability of finding global extrema can be explicitly estimated.

Simulated annealing is the most well-known stochastic method for global optimization. The idea comes from statistical mechanics based on the observation that when certain liquids are cooled slowly, they develop orderly stable molecular structures as solids. When applied to global optimization problems, the artificial annealing is kept slow to avoid getting trapped at local extrema. Initially this procedure was applied to combinatorial optimization problems such as the traveling salesman problem, but the idea has since been extended to continuous function optimization problems [11].

3.2 Generalized Trajectory Methods

3.2.1 General Formulation and Assumptions

Let $f(\underline{x})$ be a sufficiently smooth scalar function, the *objective function*, where $\underline{x} \in \mathcal{B} \subset R^{N_{\underline{x}}}$ where $\mathcal{B}$ is an open region. The problem of interest is to find the points in $\mathcal{B}$ which give the greatest local maximum (GLM) and the least local minimum (LLM) of $f(\underline{x})$, if any. In many applications, prior knowledge of the objective function and the choice of the region $\mathcal{B}$ can be used to conclude that the largest or smallest value of $f(\underline{x})$ on the closure $\bar{\mathcal{B}}$ of $\mathcal{B}$ is achieved in $\mathcal{B}$. In this case, the GLM or LLM of $f(\underline{x})$ in $\mathcal{B}$ gives the *global maximum* or *minimum* of $f(\underline{x})$ over $\bar{\mathcal{B}}$. In any case, to find the global maximum over $\bar{\mathcal{B}}$, one strategy is to calculate the GLM in $\mathcal{B}$ and the largest value of $f(\underline{x})$ on the boundary of $\mathcal{B}$ and then take the maximum of these values. A similar strategy to find the global minimum over $\bar{\mathcal{B}}$ employs the LLM in $\mathcal{B}$. Therefore, for these reasons, it is desirable to develop algorithms which compute the GLM and LLM of $f(\underline{x})$ in $\mathcal{B}$. Clearly, these points can be found if all the stationary ("critical") points of $f(\underline{x})$ in the region $\mathcal{B}$ are located, where it is assumed in this dissertation that their number is finite, so that they can each be checked for a local extremum.

Stationary points of the objective function $f(\underline{x})$ satisfy the $N_{\underline{x}}$ conditions:

$$\nabla f(\underline{x}) = \underline{0}. \tag{3.2.1}$$

Therefore, the problem of finding all the stationary points of $f(\underline{x})$ in $\mathcal{B}$ is reduced to the problem of finding all the roots in $\mathcal{B}$ of the system of nonlinear algebraic equations given in (3.2.1). The basic idea of the proposed generalized trajectory method is to embed (3.2.1) in a new set of algebraic equations:

$$\underline{g}(\underline{x}, \lambda) = \underline{0}, \ \lambda \in R, \tag{3.2.2}$$

where $\underline{g}(\underline{x}, \lambda) \in R^{N_{\underline{x}}}$ and all the roots of (3.2.1) also satisfy (3.2.2) for some particular

value of λ, say $\lambda = 1$. Under some generic regularity assumptions on $\underline{g}$, the solutions of (3.2.2) are one-dimensional manifolds or trajectories in $R^{N_{\underline{x}}+1}$. All the roots of (3.2.1) can then be found by tracking these trajectories defined by (3.2.2).

Two special forms of (3.2.2) are used in the proposed generalized trajectory methods for global optimization. If stationary points of $f(\underline{x})$ exist in $\mathcal{B}$ but they are difficult to find using local optimization methods due to the lack of suitable initial guesses, a *homotopy* scheme can be used to find at least one stationary point. To find other stationary points in $\mathcal{B}$, a *relaxation* scheme starting at an initial stationary point can then be applied.

3.2.2 Homotopy Schemes

Several different names, such as *embedding, invariant embedding*, and *parameter continuation*, have been associated with the *homotopy* scheme, which is used in this dissertation as a generic term for this group of methods. The essence of a homotopy scheme is to smoothly transform a known solution to a simple problem into a solution of a target problem which is difficult to solve by embedding the simple and target problems in a more general problem. The function describing the transition between the two problems is called a *homotopy*, and the transformation is parameterized by a *homotopy parameter.* The simple solution can be evolved into the target solution by continuously varying the homotopy parameter. This often provides a novel way to find the solutions of difficult problems.

In early algorithms to track the solutions of the transformed problems, the homotopy parameter was only allowed to vary monotonically. It was assumed that the solutions of the transformed problems would change continuously as the homotopy parameter increased or decreased. But it was soon discovered that this may not always be the case, especially for complicated problems. Most modern algorithms allow the homotopy parameter to increase and decrease as the homotopy transformation proceeds.

The major feature of homotopy schemes is that they usually have a greatly

expanded domain of convergence in the sense that it is possible to have solutions of the simple and target problems far apart and still have convergence. This property makes homotopy schemes drastically different from local iterative methods which need good initial guesses in order to converge. Homotopy schemes are therefore particularly suitable for highly nonlinear problems for which good initial solution estimates are difficult to obtain.

Recently, there have been some applications of these schemes to engineering and applied science problems. They have been used, for example, to solve the forward kinematics problem of relatively complex variable-geometry trusses [12]. Multiple solutions for system identification problems in structural dynamics were solved by a homotopy algorithm [13]. Wayburn and Seader [14] used homotopy schemes in chemical engineering to solve the equilibrium equations of distillation columns. A multi-objective control-structure optimization problem was solved by using homotopy [15]. Also, Chen *et al.* applied homotopy schemes to generalized eigenvalue problems with applications to hydrodynamic stability analysis [16].

There are two canonical homotopy schemes for finding a stationary point of $f(\underline{x})$. The first scheme is called *Newton homotopy* and is given by defining $\underline{g}$ in (3.2.2) as:

$$\underline{g}_N(\underline{x}, \lambda) = \nabla f(\underline{x}) - (1 - \lambda)\nabla f(\underline{x}_0) = \underline{0}, \tag{3.2.3}$$

where $\underline{x}_0$ is a fixed arbitrary point in $\mathcal{B}$. When $\lambda = 0$, (3.2.3) gives the following simple problem:

$$\underline{g}_N(\underline{x}, 0) = \nabla f(\underline{x}) - \nabla f(\underline{x}_0) = \underline{0}. \tag{3.2.4}$$

It is apparent that one of the solutions of (3.2.4) is just $\underline{x}_0$. On the other hand, the original problem given in (3.2.1) is obtained when $\lambda = 1$.

The solution trajectory of a Newton homotopy as λ varies from 0 is called the

Newton flow or Newton trajectory through $\underline{x}_0$. Furthermore, the algebraic equations (3.2.3) can be differentiated with respect to λ and rewritten in the form of a system of ordinary differential equations in $\underline{x}(\lambda)$, which are called the *Newton equations.* The strategy of finding stationary points of $f(\underline{x})$ by solving the Newton equations is called *Global Newton method* or *Branin's method.* Some relations between the Newton trajectory orientation and the direction given by the Newton equations are presented in [17].

The second canonical homotopy scheme is called *Fixed-Point homotopy* and is given by defining $\underline{g}$ in (3.2.2) as:

$$\underline{g}_F(\underline{x}, \lambda) = (1 - \lambda)M_F(\underline{x} - \underline{x}_0) + \lambda \nabla f(\underline{x}) = \underline{0}, \tag{3.2.5}$$

where $\underline{x}_0$ is a fixed arbitrary point in $\mathcal{B}$ and M_F is a non-singular $N_{\underline{x}} \times N_{\underline{x}}$ matrix. When $\lambda = 0$, (3.2.5) gives the following simple problem:

$$\underline{g}_F(\underline{x}, 0) = M_F(\underline{x} - \underline{x}_0) = \underline{0}, \tag{3.2.6}$$

which has only one solution, i.e., $\underline{x}_0$. Again, the original problem given in (3.2.1) is obtained when $\lambda = 1$. The Fixed-Point homotopy is used in the numerical example presented later.

The application of homotopy schemes to global optimization problems is therefore quite straightforward. An arbitrary point x_0 is chosen and the homotopy trajectory defined by either (3.2.3) or (3.2.5) is traced by allowing λ to change from 0. Whenever the homotopy trajectory reaches $\lambda = 1$, a stationary point of $f(\underline{x})$ is found. It is noted that the homotopy trajectory may cross $\lambda = 1$ several times. Therefore, it is sometimes possible to locate more than one stationary point by tracking a single homotopy trajectory. On the other hand, if there are no stationary points inside region $\mathcal{B}$, the homotopy trajectory will typically reach the boundary of $\mathcal{B}$ without $\lambda = 1$ being achieved.

3.2.3 Relaxation Schemes

Homotopy schemes are useful when no stationary point has been found and a good initial estimate of the location of a stationary point is difficult. Suppose, however, that at least one stationary point has been found. To determine other stationary points in $\mathcal{B}$, if any, trajectory methods of another type which is called the *relaxation* scheme can be used. The basic idea of the relaxation scheme is to have a special case of (3.2.2) which is as simple as possible and which needs only the information of one stationary point.

One simple relaxation scheme is given by defining $\underline{g}$ in (3.2.2) as:

$$\underline{g}_R(\underline{x}, \lambda) = \nabla f(\underline{x}) - (1 - \lambda)\underline{v} = \underline{0}, \tag{3.2.7}$$

where $\underline{v}$ is a given normalized constant vector in $R^{N_{\underline{x}}}$. It is apparent that all the stationary points of $f(\underline{x})$ satisfy $\underline{g}_R(\underline{x}, 1) = \underline{0}$. To apply relaxation schemes, an arbitrary constant vector $\underline{v}$ is chosen and the relaxation trajectory defined by (3.2.7) is traced from the known stationary point by allowing λ to change from 1. Whenever the relaxation trajectory crosses $\lambda = 1$, another stationary point is found. Like homotopy trajectories, more than one stationary point can be located by tracking a single relaxation trajectory.

Mathematically, the gradient at each point on the relaxation trajectory defined by (3.2.7) is a multiple of the constant vector $\underline{v}$. This is also true for the Newton trajectory and the constant vector in that case is $\nabla f(\underline{x}_0)$. The difference between those two schemes is that the constant vector can be arbitrarily chosen in the relaxation scheme given in (3.2.7) but it cannot in the homotopy scheme given in (3.2.3).

This feature can be used systematically to find multiple stationary points. In particular, $\underline{v}$ can be chosen to be the vectors $\{\underline{e}_1, \underline{e}_2, \ldots, \text{or } \underline{e}_{N_{\underline{x}}}\}$ which form the standard orthonormal basis for $R^{N_{\underline{x}}}$. If $\underline{v}$ is equal to $\underline{e}_i$, the mathematical interpretation of (3.2.7) is that in order to find other stationary points of $f(\underline{x})$, the ith stationarity constraint on the gradient of $f(\underline{x})$ is released (relaxed) while all the other constraints

remain enforced. The vector $\underline{v}$ can be systematically set to each basis vector in turn in order to relax a different constraint on the gradient of $f(\underline{x})$ each time. Therefore, multiple relaxation trajectories can be tracked from each stationary point.

3.2.4 Trajectory Tracking Algorithm

Both homotopy and relaxation trajectories need to be tracked by numerical algorithms in order to locate stationary points of the objective function. Therefore, only a finite number of discrete points on a trajectory can be computed. To step from one point on a trajectory to an adjacent point on the same trajectory, some iterative scheme is required. The basic idea is to generate an initial guess for that adjacent point and then use some local iteration method to converge to the trajectory point. Different algorithms for trajectory following have been proposed [18-22]. Special algorithms suitable for parallel computers are also available [23-24].

All these algorithms need to compute either the tangent vector of the trajectory or the Hessian matrix of the objective function, both of which are numerically expensive for complicated problems. Therefore, it is desirable to have numerical algorithms which avoid such computations. This motivates the following new and efficient algorithm to track both homotopy and relaxation trajectories, which is illustrated in Figure 3.1.

Let $\underline{p} = [\underline{x}^T, \lambda]^T$, so (3.2.2) can be rewritten as:

$$\underline{g}(\underline{p}) = \underline{0},\ \underline{p} \in \mathcal{B} \times R. \tag{3.2.8}$$

Suppose Γ is one component of the solution trajectory of (3.2.8) and $\underline{p}_i$ is the current point on Γ. To find an adjacent point $\underline{p}_{i+1}$ on the same trajectory, $\underline{p}^0$ is used as an initial approximation. To render $\underline{p}^0$, the secant direction which is determined by points $\underline{p}_{i-1}$ and $\underline{p}_i$ is used. If $\underline{u}$ is the unit vector in that secant direction, then $\underline{p}^0$ is chosen so that $\underline{p}^0 = \underline{p}_i + \delta\underline{u}$ where δ is a given small number which controls the closeness of $\underline{p}^0$. It is noted that secant directions are much easier to compute than tangent directions.

Since $\underline{p}_{i+1}$ is on Γ, it must satisfy (3.2.8). But some additional constraint needs to be imposed in order to precisely determine the position of $\underline{p}_{i+1}$. In the proposed algorithm, $\underline{p}_{i+1}$ is chosen to be a root of the following set of equations:

$$\begin{cases} \underline{g}(\underline{p}) = \underline{0}\,, \\ \underline{u} \cdot (\underline{p} - \underline{p}_i) - \delta = 0 \end{cases} . \tag{3.2.9}$$

The second equation in (3.2.9) is the imposed constraint for $\underline{p}_{i+1}$ and its geometrical meaning is that the projection of vector $\underline{p}_{i+1} - \underline{p}_i$ in the $\underline{u}$ direction is equal to δ. Therefore, this constraint prescribes how far the step should be along Γ.

Equations (3.2.9) are just a set of $N_{\underline{x}}+1$ algebraic equations with $N_{\underline{x}}+1$ variables. Given an initial guess $\underline{p}^0$, (3.2.9) can be solved by using any local numerical iteration method for finding roots of set of equations. Since the root $\underline{p}_{i+1}$ should not be far away from the initial guess $\underline{p}^0$ if δ is small enough, convergence is almost guaranteed. In the proposed trajectory tracking algorithm, (3.2.9) is first transformed to a nonlinear least-squares optimization problem which is then solved by either the Gauss-Newton or Levenberg-Marquardt method. These numerical algorithms are available in most general purpose computational software packages.

A suitable choice of δ is essential to prevent divergence of the tracking algorithm and to minimize overstepping of a stationary point. Both the curvature of a trajectory and the accuracy requirement of tracking influence the selection of δ. In practice, a suitably small default value of δ is chosen for a problem. If stepping from one point on a trajectory to an adjacent point on the same trajectory is not achieved in certain number of local iterations, the default value of δ is halved and a new initial guess $\underline{p}^0$ is rendered to restart the search for roots of (3.2.9). Once convergence has been achieved, δ is reset to its default value to find the next trajectory point.

3.2.5 Computation and Classification of Stationary Points

As discussed before, one stationary point of $f(\underline{x})$ is found whenever the trajectory crosses $\lambda = 1$. Stationary points cannot be located accurately by simply stepping

through discrete points on the trajectory. Local iteration must be performed in order to compute the stationary point accurately. It is clear that stationary points satisfy (3.2.1) and can be found by local iteration using the last point on the trajectory in the tracking process as the initial guess.

It is well-known that stationary points can be local maxima, local minima, or saddle points. If the Hessian matrix $H(\underline{x}^*) = \nabla\nabla f(\underline{x}^*)$ at a stationary point $\underline{x}^*$ is non-singular, $\underline{x}^*$ is called a regular stationary point and the following second-order optimality conditions can be applied:

$$\begin{aligned} H(\underline{x}^*) \text{ is positive-definite} &\implies \underline{x}^* \text{ is a local minimum,} \\ H(\underline{x}^*) \text{ is negative-definite} &\implies \underline{x}^* \text{ is a local maximum,} \\ H(\underline{x}^*) \text{ is indefinite} &\implies \underline{x}^* \text{ is a saddle point.} \end{aligned}$$

Most stationary points of problems in real applications should be regular. Regular stationary points are also isolated from each other. If non-regular stationary points are present, more elaborate classification criteria are available based on higher order derivatives of $f(\underline{x})$ [25].

3.3 Properties of Homotopy and Relaxation Trajectories

3.3.1 Differential Topology Aspects

The function $\underline{g}(\underline{x}, \lambda)$ in (3.2.2) can be viewed as a smooth map from $\mathcal{B} \times R$ to $R^{N_{\underline{x}}}$. A point $[\underline{x}^{*^T}, \lambda^*]^T \in \mathcal{B} \times R$ is called a *regular point* if the *Jacobian* $J(\underline{x}, \lambda)$ of $\underline{g}(\underline{x}, \lambda)$ at point $[\underline{x}^{*^T}, \lambda^*]^T$ is surjective ("onto"), i.e., the rank of $J(\underline{x}^*, \lambda^*)$ is equal to $N_{\underline{x}}$. In this case, by the Implicit Function Theorem, there is a unique and smooth one-dimensional solution trajectory of (3.2.2) in the neighborhood of $[\underline{x}^{*^T}, \lambda^*]^T$ which passes through $[\underline{x}^{*^T}, \lambda^*]^T$. A point in $\mathcal{B} \times R$ is called a *critical point* if it is not a regular point. A point $\underline{y}^* \in R^{N_{\underline{x}}}$ is called a *regular value* if all the pre-images of $\underline{y}^*$ in $\mathcal{B} \times R$ are regular points. A point in $R^{N_{\underline{x}}}$ is called a *critical value* if it is not a

regular value.

If $\underline{y}^* \in R^{N_{\underline{x}}}$ is a regular value, the Pre-Image Theorem in differential topology asserts that the pre-images of $\underline{y}^*$ form one-dimensional manifolds or trajectories in $\mathcal{B} \times R$. Therefore, the solution of (3.2.2) will be smooth one-dimensional trajectories if $\underline{0} \in R^{N_{\underline{x}}}$ is a regular value of the map $\underline{g}(\underline{x}, \lambda)$. Fortunately, Sard's Theorem [26] in differential topology asserts that almost all the points in $R^{N_{\underline{x}}}$ are regular values, i.e., all the critical value in $R^{N_{\underline{x}}}$ is a set of measure zero. Furthermore, the Parameterized Sard's Theorem [27] can be applied to the Fixed-Point homotopy scheme and the relaxation scheme to conclude that it is almost certain that $\underline{0} \in R^{N_{\underline{x}}}$ is a regular value for almost every point $\underline{x}_0 \in \mathcal{B}$ and vector $\underline{v} \in R^{N_{\underline{x}}}$.

Therefore, it is almost certain that the homotopy and relaxation trajectories are smooth and non-intersecting one-dimensional curves in $\mathcal{B} \times R$. A singularity occurs along a trajectory if there is a bifurcation in which two or more trajectories intersect at a single point. Unfortunately, bifurcations can not be treated with a simple analytic approach because of the huge variety of different types of bifurcation [28-31]. Each type has its own distinct properties and needs to be classified and studied separately.

There have been some attempts to deal with some simple types of bifurcation using numerical procedures. One strategy is to derive either necessary or sufficient conditions for the tangent directions of smooth trajectories intersecting at a simple bifurcation point [32-33]. Another approach is to perform an exhaustive search in the neighborhood of a bifurcation point for points on all the related bifurcating trajectories [34-35]. Both methods require extensive computational effort and can be justified only when the computation of bifurcation points and intersecting trajectories is essential to the problem at hand.

The philosophy taken in this work is that it is not worthwhile to handle bifurcations explicitly by analytic approaches because bifurcation is so rare. Anyway, a trajectory is not followed exactly but is only tracked approximately by any numerical algorithm, so the computed trajectory is actually a perturbation of the exact

trajectory. Since bifurcation is intrinsically unstable, any small perturbation of the trajectory will destroy the bifurcation. Therefore, the basic idea is to avoid direct attack on the bifurcation problem and invest effort in improving the robustness of the proposed global optimization algorithm by using multiple relaxation trajectories.

3.3.2 Trajectory Behavior

The *Jacobian* matrix of the Fixed-Point homotopy scheme defined in (3.2.5) is given by:

$$\nabla \underline{g}_F(\underline{x}, \lambda) = [(1-\lambda)M_F + \lambda \nabla\nabla f(\underline{x}),\ -M_F(\underline{x} - \underline{x}_0) + \nabla f(\underline{x})]. \tag{3.3.1}$$

At the starting point $\underline{p}_0 = [\underline{x}_0^T, 0]^T$ on the homotopy trajectory, the Jacobian matrix is equal to:

$$\nabla \underline{g}_F(\underline{x}_0, 0) = [M_F,\ \nabla f(\underline{x}_0)]. \tag{3.3.2}$$

Since the matrix M_F is nonsingular, the Jacobian matrix in (3.3.2) has full rank. Therefore, $\underline{p}_0$ is a regular point and there is a unique and smooth one-dimensional solution trajectory of (3.2.5) in the neighborhood of $\underline{p}_0$ and passing through $\underline{p}_0$. Assume this trajectory segment is parameterized by its arc length s in the neighborhood of $\underline{p}_0$, i.e.,

$$\begin{cases} \underline{x} = \underline{x}(s), & \underline{x}(0) = \underline{x}_0 \\ \lambda = \lambda(s), & \lambda(0) = 0 \end{cases} \tag{3.3.3}$$

then (3.2.5) can be differentiated with respect to s at $\underline{p}_0$ and the result is:

$$M_F \dot{\underline{x}}(0) + \dot{\lambda}(0) \nabla f(\underline{x}_0) = \underline{0}. \tag{3.3.4}$$

It is clear from (3.3.4) that

$$\begin{bmatrix} \dot{\underline{x}}(0) \\ \dot{\lambda}(0) \end{bmatrix} \propto \begin{bmatrix} -M_F^{-1}\nabla f(\underline{x}_0) \\ 1 \end{bmatrix}. \tag{3.3.5}$$

Therefore, the unit tangent vector of the homotopy trajectory at the starting point $\underline{p}_0$ can be computed from (3.3.5) and used as the starting value for the unit vector $\underline{u}$ in the trajectory tracking algorithm.

If the nonsingular matrix M_F in (3.2.5) is symmetric, the function $\underline{g}_F(\underline{x}, \lambda)$ can be integrated with respect to $\underline{x}$ and the result is:

$$G_F(\underline{x}, \lambda) = \int_{\underline{x}} \underline{g}_F(\underline{x}, \lambda) d\underline{x} = (1-\lambda)\frac{1}{2}(\underline{x} - \underline{x}_0)^T M_F(\underline{x} - \underline{x}_0) + \lambda f(\underline{x}). \tag{3.3.6}$$

It is clear from (3.3.6) that the homotopy $G_F(\underline{x}, \lambda)$ is made up of a simple quadratic function $\frac{1}{2}(\underline{x}-\underline{x}_0)^T M_F(\underline{x}-\underline{x}_0)$ and the objective function $f(\underline{x})$. Assume that there is no bifurcation of the homotopy trajectory, then it is most likely that the homotopy trajectory will reach a local maximum of $f(\underline{x})$ if matrix M_F is negative-definite since the simple quadratic function has a unique global maximum at $\underline{x}_0$. On the other hand, a local minimum of $f(\underline{x})$ will be reached by following the homotopy trajectory if matrix M_F is positive-definite.

The *Jacobian* matrix of the relaxation scheme defined in (3.2.7) is given by:

$$\nabla \underline{g}_R(\underline{x}, \lambda) = [\nabla\nabla f(\underline{x}), \underline{v}]. \tag{3.3.7}$$

If $\underline{x}^*$ is a regular stationary point of $f(\underline{x})$, the Jacobian matrix at $\underline{p}^* = [\underline{x}^{*^T}, 1]^T$ is equal to:

$$\nabla \underline{g}_R(\underline{x}^*, 1) = [\nabla\nabla f(\underline{x}^*), \underline{v}]. \tag{3.3.8}$$

Since the Hessian matrix $\nabla\nabla f(\underline{x}^*)$ is nonsingular because $\underline{x}^*$ is regular, the Jacobian

matrix in (3.3.8) has full rank. Therefore, $\underline{p}^*$ is a regular point and there is a unique and smooth one-dimensional solution trajectory of (3.2.7) in the neighborhood of $\underline{p}^*$ and passing through $\underline{p}^*$. Assume this trajectory segment is parameterized by its arc length s in the neighborhood of $\underline{p}^*$, i.e.,

$$\begin{cases} \underline{x} = \underline{x}(s), & \underline{x}(0) = \underline{x}^* \\ \lambda = \lambda(s), & \lambda(0) = 1 \end{cases} \tag{3.3.9}$$

then (3.2.7) can be differentiated with respect to s at $\underline{p}^*$ and the result is:

$$\nabla\nabla f(\underline{x}^*)\dot{\underline{x}}(0) + \dot{\lambda}(0)\underline{v} = \underline{0}. \tag{3.3.10}$$

It is clear from (3.3.10) that

$$\begin{bmatrix} \dot{\underline{x}}(0) \\ \dot{\lambda}(0) \end{bmatrix} \propto \begin{bmatrix} -(\nabla\nabla f(\underline{x}^*))^{-1}\underline{v} \\ 1 \end{bmatrix}. \tag{3.3.11}$$

Therefore, the unit tangent vector of the relaxation trajectory at the starting point $\underline{p}^*$ can be computed from (3.3.11) and used as the starting value for the unit vector $\underline{u}$ in the trajectory tracking algorithm.

3.3.3 Multiple Trajectory Components

Under generic regularity assumptions, a generalized trajectory is a smooth one-dimensional curve in $R^{N_{\underline{x}}+1}$ based on the Pre-Image Theorem of differential topology. But it is quite possible that a trajectory has more than one component. In that case, not all the stationary points of the objective function lie on a single connected trajectory component. To find all the stationary points, all the separate components of the trajectory need to be found. There is no guaranteed complete solution for this task. This remains as the major problem with the generalized trajectory method.

Conditions on the objective function which guarantee only one trajectory component were given in [36]. But those conditions have only mathematical merit since

they are too strong and difficult to apply in most applications. There have been several proposals to deal with multiple trajectory components for general objective functions. One approach is to connect the separate trajectory components using certain one-dimensional curves which connect the trajectories through *touching points* [37-38]. Since not every trajectory component has a *touching point*, it is not guaranteed that all the trajectory components can be so connected.

Another approach is trying to connect different trajectory components at plus and minus infinity [39-40]. The problem with this method is that connection at infinity is not always possible because some trajectory components may be closed and remain bounded. Furthermore, reaching plus and minus infinity at the same point by different trajectory components is not always guaranteed. To connect bounded trajectory components, complex bifurcation techniques can be helpful [41]. Another approach [42] is to investigate empirical criteria for choosing the simple solution in the Fixed-Point homotopy scheme in the hope that there is only one trajectory component.

In this dissertation, a new approach is proposed to deal with multiple trajectory components. Instead of using only one relaxation scheme and dealing with the problem of connecting separate trajectory components, multiple applications of the relaxation scheme are used in a systematic way. Thus, for every stationary point found, a multiple of relaxation trajectories is traced. For example, for each stationary point $\underline{x}^*$ that is found, $\underline{v}$ in (3.2.7) can be chosen in succession as the orthonormal basis vectors $\{\underline{e}_1, \underline{e}_2, \ldots, \underline{e}_{N_{\underline{x}}}\}$ to generate $N_{\underline{x}}$ relaxation trajectories through $\underline{x}^*$. The application of multiple relaxation generates redundancy and increases the chance of finding all the stationary points. Furthermore, the multiple trajectories issuing from a stationary point can be traced simultaneously on a parallel computer to increase efficiency in high dimensional spaces.

3.4 Numerical Example

In this example, the goal is to find all the points giving the global maximum of the objective function:

$$f(\underline{x}) = \sum_{i=1}^{4} w_i G(\underline{x}; \underline{m}_i, \Sigma_i), \quad \underline{x} = [x_1, x_2]^T \in \mathcal{B} \subset R^2, \tag{3.4.1}$$

where w_i is a weighting factor and

$$G(\underline{x}; \underline{m}_i, \Sigma_i) = \frac{1}{2\pi\sqrt{|\Sigma_i|}} \exp\left[-\frac{1}{2}(\underline{x} - \underline{m}_i)^T \Sigma_i^{-1} (\underline{x} - \underline{m}_i)\right], \tag{3.4.2}$$

is the two-dimensional Gaussian distribution function with mean $\underline{m}_i$ and covariance matrix Σ_i. The weighting factors w_i and means $\underline{m}_i$ used in this example are given in Table 3.1. The covariance matrices Σ_i are equal to 2×2 identity matrices and the region of interest $\mathcal{B}$ is set to be $[-5, 5] \times [-5, 5]$.

The three-dimensional mesh plot of the objective function $f(\underline{x})$ is given in Figure 3.2 and the corresponding contour plot is shown in Figure 3.3. It is clear from the plots that the objective function has nine stationary points in $\mathcal{B}$. Four of them give local maxima as marked by "×" in Figure 3.3 and one of them gives a local minimum as marked by "∗" in Figure 3.3. The remaining four are saddle points as marked by "o" in Figure 3.3. Two of the local maximum points are also global maximum points with the same largest function value. The local minimum is not a global minimum because $f(\underline{x})$ takes on smaller values on the boundary of $\mathcal{B}$.

The Fixed-Point homotopy scheme defined in (3.2.5) is first applied to find one stationary point of the objective function. The matrix M_F is set equal to the negative of the 2×2 identity matrix since it is desired that the homotopy trajectory converges to a local maximum of the objective function. Three different initial guesses:

$$P_1 = [-1, 0]^T, \; P_2 = [-4, 1]^T, \text{ and } P_3 = [-2, 4]^T,$$

are used in the Fixed-Point homotopy scheme and the homotopy trajectories are shown in Figure 3.4. It is noted that all three trajectories reach the same local

maximum point $A = [-2, 2]^T$. The three-dimensional plots of these trajectories are depicted in Figure 3.5 where the variation of the homotopy parameter λ along the homotopy trajectory is illustrated.

Using the stationary point A, the relaxation scheme is applied to find the other stationary points of the objective function in $\mathcal{B}$. By relaxing the constraint on each gradient component of the objective function, two relaxation trajectories Γ_1 and Γ_2 going through A are tracked and four more stationary points, B, C, D, and E are located as shown in Figure 3.6. By checking their Hessian matrices, points B and D are found to be saddle points while points C and E give local maxima.

Starting from point B, the relaxation trajectory Γ_3 is tracked and two more stationary points F and G are found. Point F gives a local minimum while point G is a saddle point. By following the relaxation trajectory Γ_4 from point C, two more stationary points H and I are reached. Point H is a saddle point and point I gives a local maximum. It is noted that these stationary points can also be reached by tracking the relaxation trajectories Γ_5 and Γ_6.

All the relaxation trajectories through the stationary points which have been found so far have now been tracked and no new stationary points are found. It is concluded that the nine points summarized in Table 3.2 are the only stationary points of the objective function in region $\mathcal{B}$. Furthermore, point C and point E are local maximum with the same largest function value. Therefore, they give the greatest local maxima and, in fact, they give the global maximum of the given objective function in the region $\mathcal{B}$ because the boundary values of $f(\underline{x})$ are all less than this value.

References for Chapter 3

1. Arora, J. S., Elwakeil, O. A., Chahande, A. I., and Hsieh, C. C., *Global Optimization Methods for Engineering Applications : A Review*, Structural Optimization, No. 9, pp. 137-159, 1995.
2. Törn, A., and Žilinskas, A., *Global Optimization*, Lecture Notes in Computer Science Vol. 350, Springer-Verlag, Berlin, 1989.
3. Törn, A., and Viitanen, S., *Topographical Global Optimization*, Recent Advances in Global Optimization, Edited by C. A. Floudas, and P. M. Pardalos, Princeton University Press, Princeton, New Jersey, pp. 384-398, 1992.
4. Printér, J., *Lipschitzian Global Optimization : Some Prospective Applications*, Recent Advances in Global Optimization, Edited by C. A. Floudas, and P. M. Pardalos, Princeton University Press, Princeton, New Jersey, pp. 399-432, 1992.
5. Jones, D. R., Perttunen, C. D., and Stuckman, B. E., *Lipschitzian Optimization Without the Lipschitz Constant*, Journal of Optimization Theory and Applications, Vol. 79, No. 1, pp. 157-181, 1993.
6. Sergeyev, Ya. D., and Grishagin, V. A., *A Parallel Method for Finding the Global Minimum of Univariate Functions*, Journal of Optimization Theory and Applications, Vol. 80, No. 3, pp. 513-536, 1994.
7. Moore, R., Hansen, E., and Leclerc, A., *Rigorous Methods for Global Optimization*, Recent Advances in Global Optimization, Edited by C. A. Floudas, and P. M. Pardalos, Princeton University Press, Princeton, New Jersey, pp. 321-342, 1992.
8. Schäffler, S., and Warsitz, H., *A Trajectory-Following Method for Unconstrained Optimization*, Journal of Optimization Theory and Applications, Vol. 67, No. 1, pp. 133-140, 1990.
9. Levy, A. V., and Montalvo, A., *The Tunneling Algorithm for the Global Minimization of Functions*, SIAM Journal on Scientific and Statistical Computing, Vol. 6, No. 1, pp. 15-29, 1985.
10. Floudas, C. A., and Visweswaran, V., *Primal-Relaxed Dual Global Optimization Approach*, Journal of Optimization Theory and Applications, Vol. 78, No. 2, pp. 187-225, 1993.
11. Rabinowitz, F. M., *Algorithm 744 : A Stochastic Algorithm for Global Optimization with Constraints*, ACM Transactions on Mathematical Software, Vol. 22, No. 2, pp. 194-213, 1995.
12. Arun, V., Reinholtz, C. F., and Watson, L. T., *Application of New Homotopy Continuation Techniques to Variable Geometry Trusses*, Transactions of the ASME Journal of Mechanical Design, Vol. 114, pp. 422-427, 1992.

13. Beck, R. T., *Fundamental Problems in the Application of Structural Identification Procedures to Damage Detection*, Report No. EERL 91-03, California Institute of Technology, Pasadena, California, 1991.

14. Wayburn, T. L., and Seader, J. D., *Homotopy Continuation Methods for Computer-Aided Process Design*, Computers and Chemical Engineering, Vol. 11, No. 1, pp. 7-25, 1987.

15. Rakowska, J., Haftka, R. T., and Watson, L. T., *Multi-Objective Control-Structure Optimization via Homotopy Methods*, SIAM Journal of Optimization, Vol. 3, No. 3, pp. 654-667, 1993.

16. Chen, G., Keller, H. B., Lui, S. H., and Roux, B., *Parallel Homotopy Algorithm for Large Sparse Generalized Eigenvalue Problems : Application to Hydrodynamic Stability Analysis*, Parallel Processing : CONPAR 92 - VAPP V, Edited by L. Bougé, M. Cosnard, Y. Robert, and D. Trystram, Springer-Verlag, Berlin, pp. 331-342, 1992.

17. Garcia, C. B., and Gould, F. J., *Relations Between Several Path Following Algorithms and Local and Global Newton Methods*, SIAM Review, Vol. 22, No. 3, pp. 263-274, 1980.

18. Allgower, E., and Georg, K., *Simplicial and Continuation Methods for Approximating Fixed Points and Solutions to Systems of Equations*, SIAM Review, Vol. 22, No. 1, pp. 28-85, 1980.

19. Watson, L. T., Billups, S. C., and Morgan, A. P., *Algorithm 652 - HOMPACK : A Suite of Codes for Globally Convergent Homotopy Algorithms*, ACM Transactions on Mathematical Software, Vol. 13, No. 3, pp. 281-310, 1987.

20. Watson, L. T., and Haftka, R. T., *Modern Homotopy Methods in Optimization*, Computer Methods in Applied Mechanics and Engineering, Vol. 74, pp. 289-305, 1989.

21. Desa, C., Irani, K. M.,Ribbens, C. J., Watson, L. T., and Walker, H. F., *Preconditioned Iterative Methods for Homotopy Curve Tracking*, SIAM Journal on Scientific and Statistical Computing, Vol. 13, No. 1, pp. 30-46, 1992.

22. Keller, H. B., *Lectures on Numerical Methods in Bifurcation Problems*, Springer-Verlag, Heidelberg, 1987.

23. Allison, D. C. S., Irani, K. M., Ribbens, C. J., and Watson, L. T., *High-Dimensional Homotopy Curves Tracking on a Shared-Memory Multiprocessor*, Journal of Supercomputing, Vol. 5, No. 4, pp. 347-366, 1992.

24. Chakraborty, A., Allison, D. C. S., Ribbens, C. J., and Watson, L. T., *The Parallel Complexity of Embedding Algorithms for the Solution of Systems of Nonlinear Equations*, IEEE Transactions on Parallel and Distributed Systems, Vol. 4, No. 4, pp. 458-465, 1993.

25. Schäffler, S., *Classification of Critical Stationary Points in Unconstrained Optimization*, SIAM Journal of Optimization, Vol. 2, No. 1, pp. 1-6, 1992.

26. Guillemin, V., and Pollack, A., *Differential Topology*, Prentice-Hall, Englewood Cliffs, New Jersey, 1974.

27. Chow, S. N., Mallet-Paret, J., and Yorke, J. A., *Finding Zeros of Maps : Homotopy Methods That Are Constructive With Probability One*, Mathematics of Computation, Vol. 32, No. 143, pp. 887-899, 1978.

28. Kuznetsov, Y. A., *Elements of Applied Bifurcation Theory*, Springer-Verlag, New York, 1995.

29. Golubitsky, M., and Schaeffer, D. G., *Singularities and Groups in Bifurcation Theory*, Vol. I, Springer-Verlag, New York, 1985.

30. Rabier, P., *Lectures on Topics in One-Parameter Bifurcation Problems*, Springer-Verlag, Heidelberg, 1985.

31. Chow, S. N., and Hale, J. K., *Methods of Bifurcation Theory*, Springer-Verlag, New York, 1982.

32. Doedel, E., Keller, H. B., and Kernevez, J. P., *Numerical Analysis and Control of Bifurcation Problems : (I) Bifurcation in Finite Dimensions*, International Journal of Bifurcation and Chaos, Vol. 1, No. 3, pp. 493-520, 1991.

33. Jäger, E., *Bifurcation in Degenerate Directions*, Bifurcation : Analysis, Algorithms, Applications, Edited by T. Kupper, R. Seydel, and H. Troger, Birkäuser Verlag, Boston, Massachusetts, pp. 131-138, 1987.

34. Kearfott, R. B., *Some General Bifurcation Techniques*, SIAM Journal on Scientific and Statistical Computing, Vol. 4, No. 1, pp. 52-68, 1983.

35. Fujii, F., and Choong, K. K., *Branch Switching in Bifurcation of Structures*, ASCE Journal of Engineering Mechanics, Vol. 118, No. 8, pp. 1578-1596, 1992.

36. Diener, I., *On the Global Convergence of Path-Following Methods to Determine All Solutions to a System of Nonlinear Equations*, Mathematical Programming, No. 39, pp. 181-188, 1987.

37. Diener, I., *Trajectory Nets Connecting All Critical Points of a Smooth Function*, Mathematical Programming, No. 36, pp. 340-352, 1986.

38. Diener, I., and Schaback, R., *An Extended Continuous Newton Method*, Journal of Optimization Theory and Applications, Vol. 67, No. 1, pp. 57-77, 1990.

39. Seader, J. D., Kuno, M., Lin, W. J., Johnson, S. A., Unsworth, K., and Wiskin, J. W., *Mapped Continuation Methods for Computing All Solutions to General Systems of Nonlinear Equations*, Computers and Chemical Engineering, Vol. 14, No. 1, pp. 71-85, 1990.

40. Sun, A. C., and Seider, W. D., *Homotopy-Continuation Algorithm for Global Optimization*, Recent Advances in Global Optimization, Edited by C. A. Floudas, and P. M. Pardalos, Princeton University Press, Princeton, New Jersey, pp. 561-592, 1992.

41. Henderson, M. E., and Keller, H. B., *Complex Bifurcation from Real Paths*, SIAM Journal of Applied Mathematics, Vol. 50, No. 2, pp. 460-482, 1990.

42. Kuno, M., and Seader, J. D., *Computing All Real Solutions to Systems of Nonlinear Equations With a Global Fixed-Point Homotopy*, Industrial and Engineering Chemistry Research, Vol. 27, pp. 1320-1329, 1988.

Table 3.1: Weighting Factors and Means of the Two-Dimensional Gaussian Distribution Function in (3.4.2).

i	w_i	$\underline{m_i}$
1	1.0	$[2.5, 2.5]^T$
2	1.0	$[-2.5, -2.5]^T$
3	0.5	$[2.0, -2.0]^T$
4	0.5	$[-2.0, 2.0]^T$

Table 3.2: Locations and Types of the Stationary Points of the Objective Function in (3.4.1).

Stationary Point	Location	Type
A	$[-2, 2]^T$	local maximum
B	$[0.061, 2.229]^T$	saddle point
C	$[2.5, 2.5]^T$	global maximum
D	$[-2.229, -0.061]^T$	saddle point
E	$[-2.5, -2.5]^T$	global maximum
F	$[0, 0]^T$	local minimum
G	$[-0.061, -2.229]^T$	saddle point
H	$[2.229, 0.061]^T$	saddle point
I	$[2, -2]^T$	local maximum

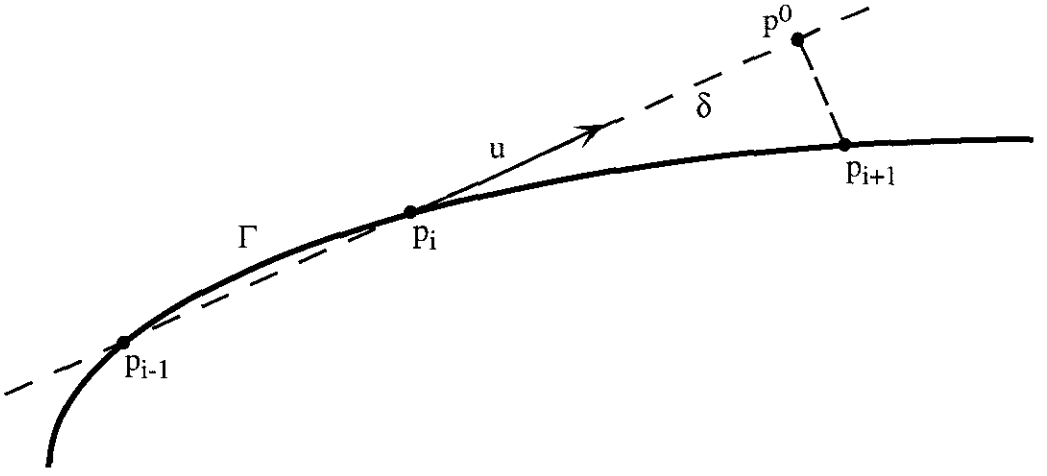

Figure 3.1: Illustration of the Trajectory Tracking Algorithm.

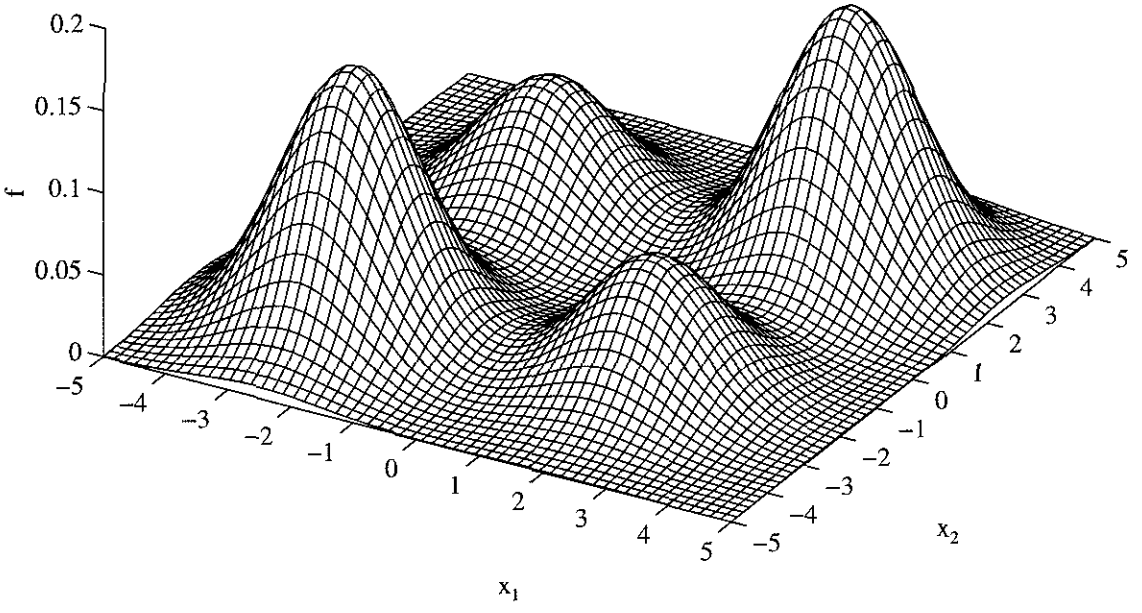

Figure 3.2: Three-Dimensional Mesh Plot of the Objective Function in (3.4.1).

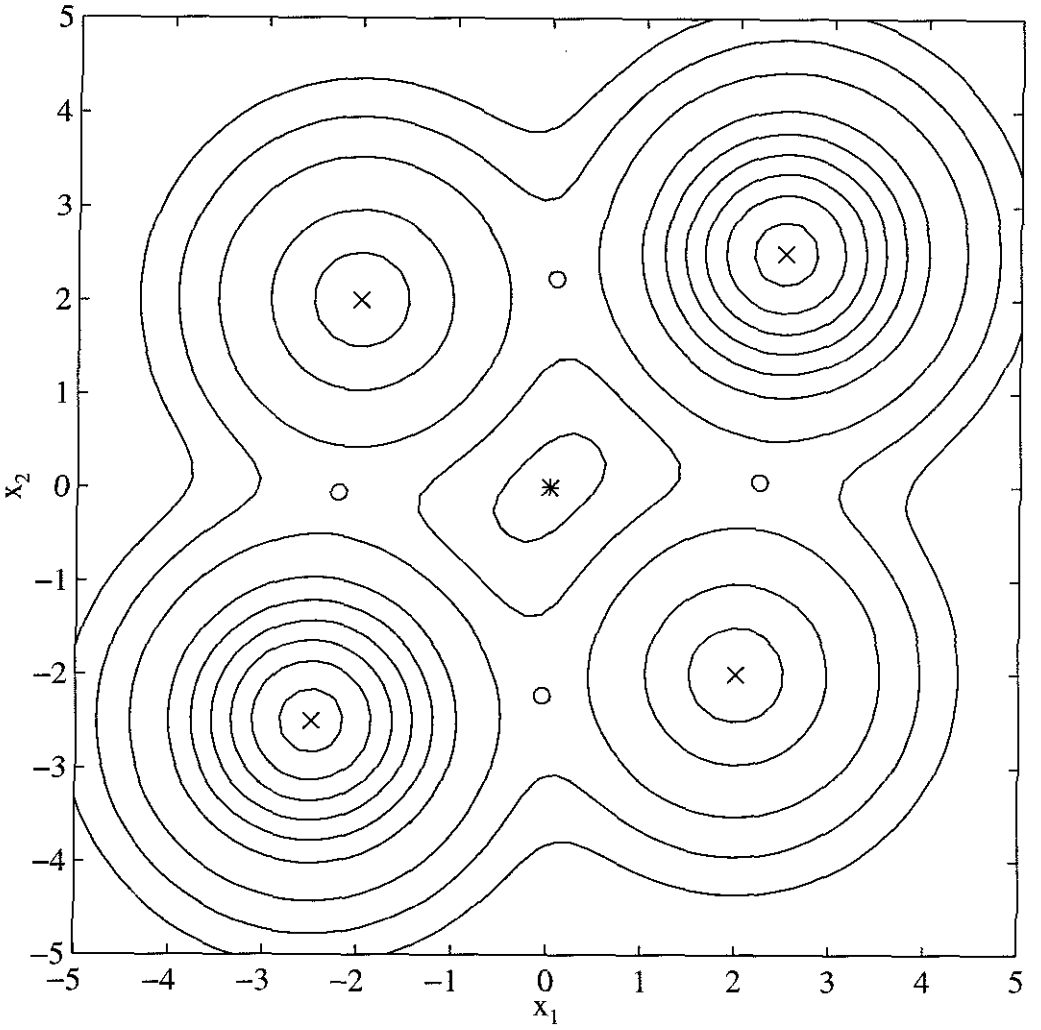

Figure 3.3: Contour Plot of the Objective Function in (3.4.1).

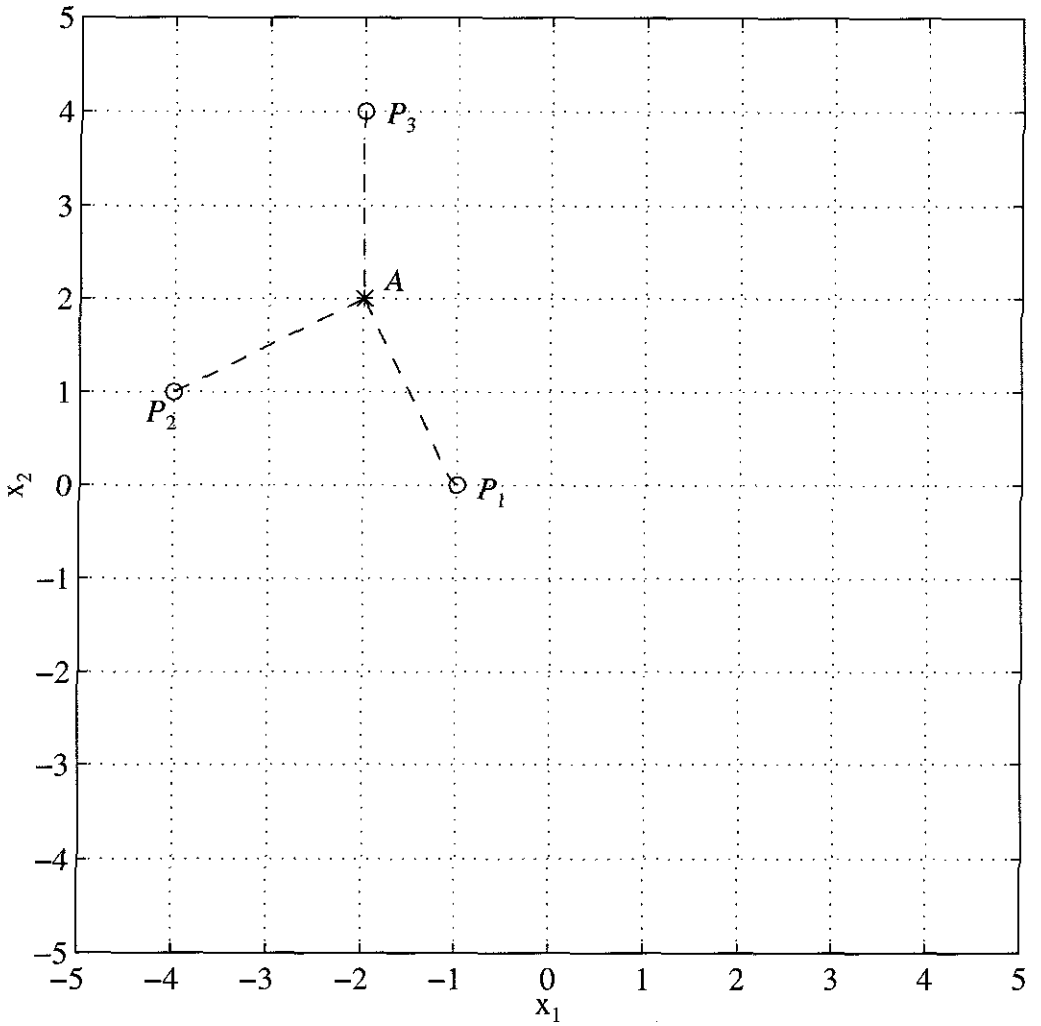

Figure 3.4: Fixed-Point Homotopy Trajectories in the Search of the Global Extrema of the Objective Function in (3.4.1).

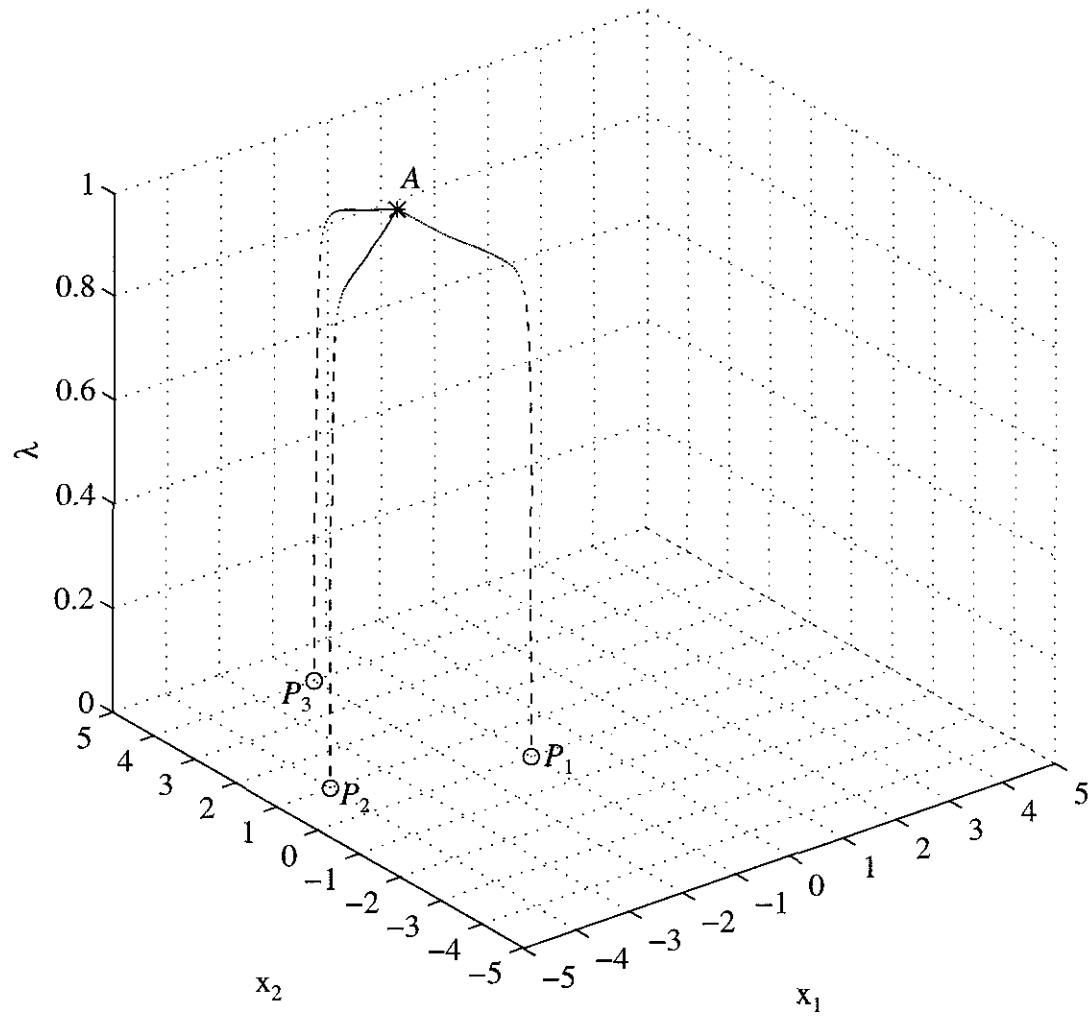

Figure 3.5: Three-Dimensional Plot of the Fixed-Point Homotopy Trajectories in Figure 3.4.

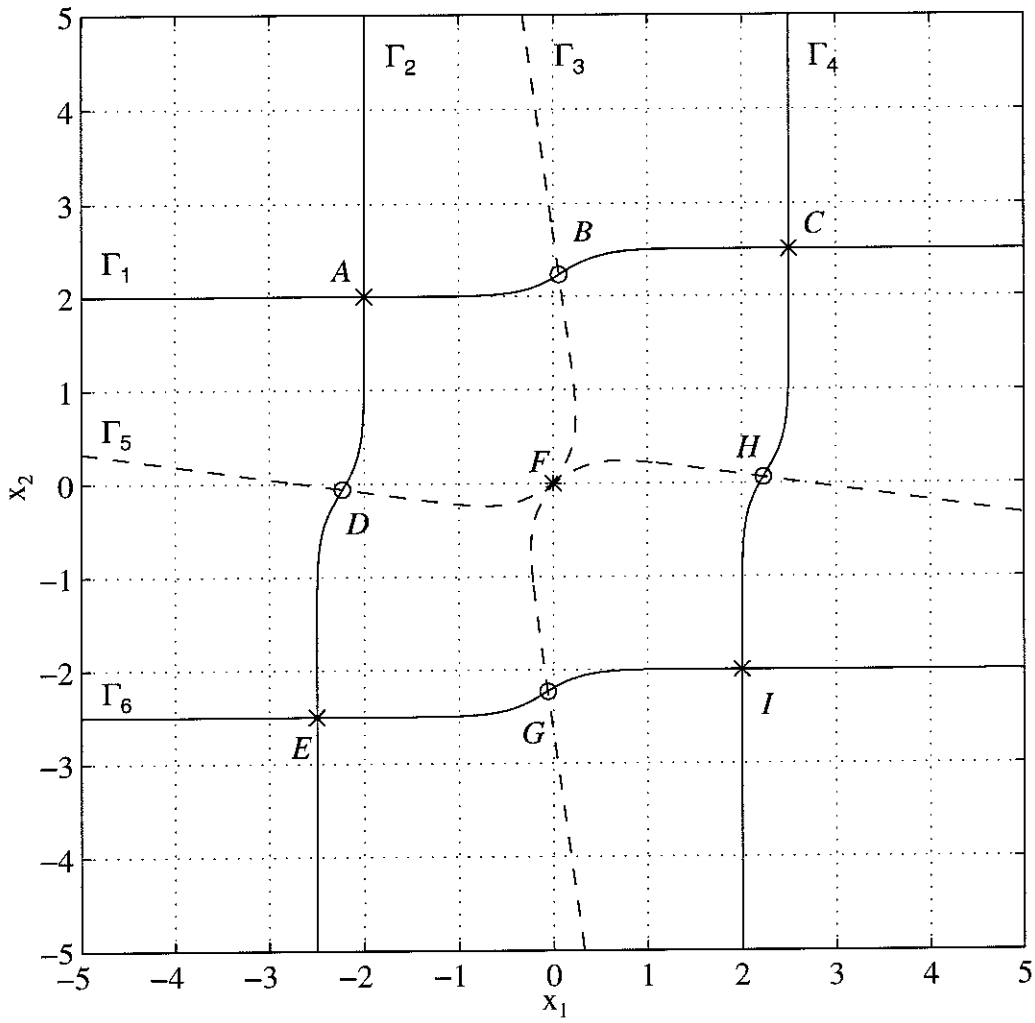

Figure 3.6: Relaxation Trajectories in the Search of the Global Extrema of the Objective Function in (3.4.1).

Chapter 4

Least-Squares Prediction-Error Approach and Structural Model Updating

4.1 Least-Squares Prediction-Error Approach

4.1.1 Probabilistic Prediction-Error Model

In the time-domain prediction-error approach presented in Section 2.3.3, a class of probabilistic models $\mathcal{P}$ is chosen in order to describe the uncertainty in the prediction error E_1^M. By making appropriate choices for the class of models $\mathcal{P}$, several classical system identification methods, such as the least-squares output-error method, *can be derived and interpreted as the special cases of the statistical system* identification framework. However, by viewing these methods within the statistical system identification framework, the prediction accuracy of the identified "best" model and the precision of the identified model parameters can be evaluated.

For illustration, the derivation of a least-squares prediction-error approach based on [1] is presented. Consider a choice for the class of models $\mathcal{P}$ which assumes the prediction error E_1^M is a zero-mean stationary $(N_o M)$-dimensional Gaussian stochastic sequence with both temporal and spatial independent components, i.e.,

$$h_M(E_1^M; \underline{\alpha}) = \prod_{i=1}^{N_o} \left[\frac{1}{(\sqrt{2\pi}\sigma_i)^M} \exp\left(-\frac{1}{2\sigma_i^2} \sum_{n=1}^{M} [e_i(n)]^2 \right) \right].$$

Therefore,

$$f_M(Y_1^M; \underline{\alpha}, Z_1^M) = \prod_{i=1}^{N_o} \left[\frac{1}{(\sqrt{2\pi}\sigma_i)^M} \exp\left(-\frac{1}{2\sigma_i^2} \sum_{n=1}^{M} [y_i(n) - x_i(n; \underline{a})]^2 \right) \right]. \qquad (4.1.1)$$

The assumption of temporal independence implies that if one knows the prediction error at other time instants, this does not influence one's uncertainty of the prediction error at a specific time instant. The assumption of spatial independence means that if one knows the prediction error for the structural response at certain degree of freedom in a structure, this does not affect one's uncertainty of the prediction error for the structural response at other degrees of freedom. From the point of view of Bayesian probability, the probability density function in (4.1.1) is just a particular choice for modeling the incomplete knowledge of the actual structural response. For simplicity, it is also assumed that the uncertainty of the prediction error at each time instant has the same probability distribution.

For this particular class of models $\mathcal{P}$, $N_{\underline{\sigma}}$ is equal to N_o and the prediction accuracy parameters $\underline{\sigma}$ are the set of independent standard deviations $\{\sigma_1, \ldots, \sigma_{N_o}\}$ of the $(N_o M)$-dimensional Gaussian distribution given in (4.1.1). In the special situation where there is only one type of measured structural response, such as acceleration which is typically measured in practice, and the structural response at all the measured degrees of freedom is of the same order of magnitude, all of the standard deviations σ_i's can be assumed to be equal for simplicity. Therefore, there is only a single prediction accuracy parameter σ and (4.1.1) can be simplified as follows:

$$f_M(Y_1^M; \underline{\alpha}, Z_1^M) = \frac{1}{(\sqrt{2\pi}\sigma)^{N_o M}} \exp\left(-\frac{1}{2\sigma^2} \sum_{i=1}^{N_o} \sum_{n=1}^{M} [y_i(n) - x_i(n; \underline{a})]^2\right). \qquad (4.1.2)$$

The following derivation is done only for the case in which all of the standard deviations σ_i's are assumed to be equal. The results can be extended to the more general case.

4.1.2 Calculation of the Optimal Parameters

As explained in Section 2.4.1, the optimal parameters $\hat{\underline{\alpha}} = [\hat{\underline{a}}^T, \hat{\sigma}]^T$ for the class of models $\mathcal{M}_{\mathcal{P}}$ given the measured data $\mathcal{D}_N$ are determined by finding the global

maximum of the function $f_N(\hat{Y}_1^N; \underline{\alpha}, \hat{Z}_1^N)$ (or $\ln f_N(\hat{Y}_1^N; \underline{\alpha}, \hat{Z}_1^N)$) in the parameter space $S_{\underline{\alpha}}$, where $\ln f_N(\hat{Y}_1^N; \underline{\alpha}, \hat{Z}_1^N)$ can be calculated from (4.1.2) as follows:

$$\ln f_N(\hat{Y}_1^N; \underline{\alpha}, \hat{Z}_1^N) = -N_o N \ln(\sqrt{2\pi}\sigma) - \frac{1}{2\sigma^2} \sum_{i=1}^{N_o} \sum_{n=1}^{N} [\hat{y}_i(n) - x_i(n; \underline{a})]^2. \tag{4.1.3}$$

Assume the model parameters $\underline{a}$ are fixed for the time being, the maximum value of $\ln f_N(\hat{Y}_1^N; \underline{\alpha}, \hat{Z}_1^N)$ in (4.1.3) is achieved when σ satisfies:

$$\sigma^2 = \hat{\sigma}^2(\underline{a}) = \frac{1}{N_o N} \sum_{i=1}^{N_o} \sum_{n=1}^{N} [\hat{y}_i(n) - x_i(n; \underline{a})]^2. \tag{4.1.4}$$

Therefore, the optimal prediction accuracy parameter for given model parameters $\underline{a}$ is equal to the RMS of the prediction error at all of the measured DOF of a structure.

To find the optimal model parameters $\hat{\underline{a}}$, (4.1.4) is substituted into (4.1.3) and the result is:

$$\ln f_N(\hat{Y}_1^N; \underline{a}, \hat{\sigma}(\underline{a}), \hat{Z}_1^N) = -\frac{N_o N}{2} \ln[2\pi e \hat{\sigma}^2(\underline{a})]. \tag{4.1.5}$$

It is clear from (4.1.5) that the optimal model parameters $\hat{\underline{a}}$ can be calculated by minimizing the function $J_E(\underline{a})$ defined by:

$$J_E(\underline{a}) = \hat{\sigma}^2(\underline{a}), \tag{4.1.6}$$

with respect to $\underline{a}$. It is noted that $J_E(\underline{a})$ is just the arithmetic average of the RMS prediction error at all the measured DOF of a structure. The optimal prediction accuracy parameter $\hat{\sigma}$ is then given by (4.1.4) when $\underline{a} = \hat{\underline{a}}$, i.e.,

$$\hat{\sigma}^2(\hat{\underline{a}}) = \frac{1}{N_o N} \sum_{i=1}^{N_o} \sum_{n=1}^{N} [\hat{y}_i(n) - x_i(n; \hat{\underline{a}})]^2. \tag{4.1.7}$$

From (4.1.6), it is noted that the optimal standard deviation $\hat{\sigma}$ is unique even in the

case when there are multiple optimal model parameters $\hat{\underline{a}}$ in the parameter space $S_{\underline{a}}$.

Since the optimal model parameters $\hat{\underline{a}}$ are determined by minimizing the objective function $J_E(\underline{a})$ given in (4.1.6), the derived least-squares prediction-error approach is essentially equivalent to the classical least-squares output-error system identification method. For civil structures, the model output $x_i(n;\underline{a})$ is generally a nonlinear function of the model parameters $\underline{a}$ even if the structure is modeled by using a class of linear models. Hence, there may be multiple optimal model parameters because the objective function $J_E(\underline{a})$ is generally non-convex and so might attain its minimum value at more than one vector of model parameters $\hat{\underline{a}}$ in the parameter space $S_{\underline{a}}$.

4.1.3 Asymptotic Approximations in System Identifiable Cases

Suppose the class of models $\mathcal{M}_{\mathcal{P}}$ is system identifiable given the measured data $\mathcal{D}_N$ and $S_{\underline{\alpha}}$ is bounded, then $S_{\underline{\alpha}}^{opt}(\mathcal{D}_N)$ contains a finite number K of optimal parameters $\hat{\underline{\alpha}}^{(k)} = [\hat{\underline{a}}^{(k)^T}, \hat{\sigma}]^T, k = 1, \ldots, K$. For each vector of optimal parameters $\hat{\underline{\alpha}}^{(k)}$, the probability distribution of the predicted system output for the next $(M-N)$ sampling time and a prescribed future system input Z_{N+1}^M can be obtained from (4.1.2) and is equal to a $[N_o(M-N)]$-dimensional Gaussian distribution given by:

$$p(Y_{N+1}^M|\hat{\underline{\alpha}}^{(k)}, Z_{N+1}^M, \mathcal{M}_{\mathcal{P}}) = \frac{1}{(\sqrt{2\pi}\hat{\sigma})^{N_o(M-N)}} \exp\left(-\frac{1}{2\hat{\sigma}^2}\sum_{i=1}^{N_o}\sum_{n=N+1}^{M}[y_i(n) - x_i(n;\hat{\underline{a}}^{(k)})]^2\right). \quad (4.1.8)$$

Therefore, the asymptotic approximation of the updated probability distribution of the predicted system output y_i at time instant m, $(N < m \leq M)$, can be obtained from (2.4.5) and is equal to:

$$p(y_i(m)|\mathcal{D}_N, Z_{N+1}^m, \mathcal{M}_{\mathcal{P}}) \approx \sum_{k=1}^{K} w_k \frac{1}{\sqrt{2\pi}\hat{\sigma}}$$

$$\times \exp\left(-\frac{1}{2\hat{\sigma}^2}[y_i(m) - x_i(m;\underline{\hat{a}}^{(k)})]^2\right),$$

$$\approx \sum_{k=1}^{K} w_k G(y_i(m); x_i(m;\underline{\hat{a}}^{(k)}), \hat{\sigma}^2). \tag{4.1.9}$$

In (4.1.9), the weight w_k corresponding to the optimal parameters $\underline{\hat{\alpha}}^{(k)}$ can be determined by using (2.4.4) which is repeated below:

$$w_k = \frac{w_k^{'}}{\sum_{l=1}^{K} w_l^{'}} \quad , \quad w_k^{'} = |A_N(\underline{\hat{\alpha}}^{(k)})|^{-1/2}\pi(\underline{\hat{\alpha}}^{(k)}). \tag{4.1.10}$$

In the above, $G(y_i(m); x_i(m;\underline{\hat{a}}^{(k)}), \hat{\sigma}^2)$ denotes a Gaussian distribution for $y_i(m)$ with mean $x_i(m;\underline{\hat{a}}^{(k)})$ and variance $\hat{\sigma}^2$. It should be noted from (4.1.9) that unless the class of models $\mathcal{M}_{\mathcal{P}}$ is globally system identifiable given the measured data $\mathcal{D}_N$, i.e., $K = 1$, the asymptotic approximation of $p(y_i(m)|\mathcal{D}_N, Z_{N+1}^m, \mathcal{M}_{\mathcal{P}})$ is not a Gaussian distribution even though each term in (4.1.9) is a Gaussian distribution.

The asymptotic approximation of the mean of the predicted system output $y_i(m)$ can be determined by using (4.1.9) and is equal to:

$$\begin{aligned} E[y_i(m)] &= \int_{-\infty}^{\infty} y_i(m) p(y_i(m)|\mathcal{D}_N, Z_{N+1}^m, \mathcal{M}_{\mathcal{P}}) dy_i(m), \\ &\approx \sum_{k=1}^{K} w_k \left\{ \int_{-\infty}^{\infty} y_i(m) G(y_i(m); x_i(m;\underline{\hat{a}}^{(k)}), \hat{\sigma}^2) dy_i(m) \right\}, \\ &= \sum_{k=1}^{K} w_k x_i(m;\underline{\hat{a}}^{(k)}). \end{aligned} \tag{4.1.11}$$

Based on (4.1.11), the mean $E[y_i(m)]$ is a weighted sum of the model output for each optimal model with parameters $\underline{\hat{a}}^{(k)}$. Similarly, the asymptotic approximation of the variance of the predicted system output $y_i(m)$ can be obtained by making use of the result in (4.1.11) as follows:

$$
\begin{aligned}
Var[y_i(m)] &= E[y_i^2(m)] - E[y_i(m)]^2, \\
&\approx \sum_{k=1}^{K} w_k \left\{ \int_{-\infty}^{\infty} y_i^2(m) G(y_i(m); x_i(m; \underline{\hat{a}}^{(k)}), \hat{\sigma}^2) dy_i(m) \right\} - E[y_i(m)]^2, \\
&= \sum_{k=1}^{K} w_k [\hat{\sigma}^2 + x_i^2(m; \underline{\hat{a}}^{(k)})] - E[y_i(m)]^2, \\
&= \hat{\sigma}^2 + \sum_{k=1}^{K} w_k x_i^2(m; \underline{\hat{a}}^{(k)}) - E[y_i(m)]^2. \qquad (4.1.12)
\end{aligned}
$$

To determine the weights w_k's in (4.1.9), the Hessian matrix $A_N(\underline{\alpha})$ of $\ln f_N(\hat{Y}_1^N; \underline{\alpha}, \hat{Z}_1^N)$ needs to be evaluated at each vector of optimal parameters $\underline{\hat{\alpha}}^{(k)}$. The components of $A_N(\underline{\hat{\alpha}}^{(k)})$ can be determined by using the definition:

$$
[A_N(\underline{\hat{\alpha}}^{(k)})]_{jl} = - \left. \frac{\partial^2 \ln f_N(\hat{Y}_1^N; \underline{\alpha}, \hat{Z}_1^N)}{\partial \alpha_j \partial \alpha_l} \right|_{\underline{\alpha} = \underline{\hat{\alpha}}^{(k)}}. \qquad (4.1.13)
$$

By combining the results in (4.1.3) and (4.1.4), the following is obtained:

$$
\ln f_N(\hat{Y}_1^N; \underline{\alpha}, \hat{Z}_1^N) = -N_o N \left[\ln(\sqrt{2\pi}\sigma) + \frac{\hat{\sigma}^2(\underline{a})}{2\sigma^2} \right]. \qquad (4.1.14)
$$

It can be shown by using (4.1.13) and (4.1.14) that $A_N(\underline{\hat{\alpha}}^{(k)})$ is a block diagonal matrix, i.e.,

$$
A_N(\underline{\hat{\alpha}}^{(k)}) = \begin{bmatrix} B_N(\underline{\hat{\alpha}}^{(k)}) & 0 \\ 0 & C_N(\underline{\hat{\alpha}}^{(k)}) \end{bmatrix}.
$$

The $N_{\underline{a}} \times N_{\underline{a}}$ matrix $B_N(\underline{\hat{\alpha}}^{(k)})$ corresponds to the model parameters $\underline{a}$ and the scalar $C_N(\underline{\hat{\alpha}}^{(k)})$ corresponds to the prediction accuracy parameter σ. Moreover, the components of $B_N(\underline{\hat{\alpha}}^{(k)})$ and $C_N(\underline{\hat{\alpha}}^{(k)})$ can be computed by using the following formulas:

$$
[B_N(\underline{\hat{\alpha}}^{(k)})]_{jl} = \frac{N_o N}{2\hat{\sigma}^2} \left. \frac{\partial^2 \hat{\sigma}^2(\underline{a})}{\partial a_j \partial a_l} \right|_{\underline{a} = \underline{\hat{a}}^{(k)}}, \qquad (4.1.15)
$$

$$C_N(\hat{\underline{\alpha}}^{(k)}) = \frac{2N_oN}{\hat{\sigma}^2}. \tag{4.1.16}$$

It is noted from (4.1.16) that the value of $C_N(\hat{\underline{\alpha}}^{(k)})$ is the same for each vector of optimal parameters $\hat{\underline{\alpha}}^{(k)}$.

As explained in Section 2.4.2, the posterior probability distribution of the parameters $\underline{\alpha}$ given the measured data $\mathcal{D}_N$ in the neighborhood of optimal parameters $\hat{\underline{\alpha}}^{(k)}$ can be asymptotically approximated by a scaled $N_{\underline{\alpha}}$-dimensional Gaussian distribution with mean $\hat{\underline{\alpha}}^{(k)}$ and covariance matrix $A_N^{-1}(\hat{\underline{\alpha}}^{(k)})$. Since the Hessian matrix $A_N(\hat{\underline{\alpha}}^{(k)})$ is block diagonal, the (marginal) posterior probability distributions of the model parameters $\underline{a}$ in the neighborhood of $\hat{\underline{a}}^{(k)}$ is Gaussian with covariance matrix $B_N^{-1}(\hat{\underline{\alpha}}^{(k)})$. Similarly, the (marginal) posterior probability distribution of the prediction accuracy parameter σ in the neighborhood of $\hat{\sigma}$ is also Gaussian with variance $C_N^{-1}(\hat{\underline{\alpha}}^{(k)})$. Furthermore, the determinant of the Hessian matrix $A_N(\hat{\underline{\alpha}}^{(k)})$ is equal to the product of the determinant of matrix $B_N(\hat{\underline{\alpha}}^{(k)})$ and the value of $C_N(\hat{\underline{\alpha}}^{(k)})$. Since the value of $C_N(\hat{\underline{\alpha}}^{(k)})$ is the same for each vector of optimal parameters $\hat{\underline{\alpha}}^{(k)}$, (4.1.10) can be simplified as follows:

$$w_k = \frac{v_k}{\sum_{l=1}^{K} v_l} \quad , \quad v_k = |B_N(\hat{\underline{\alpha}}^{(k)})|^{-1/2}\pi(\hat{\underline{\alpha}}^{(k)}).$$

4.1.4 Asymptotic Approximations in System Un-Identifiable Cases

Suppose the class of models $\mathcal{M}_{\mathcal{P}}$ is system un-identifiable given the measured data $\mathcal{D}_N$ and the prior probability distribution $\pi(\underline{\alpha})$ is a smooth and slowly-varying function. It is assumed that $S_{\underline{\alpha}}^{opt}(\mathcal{D}_N)$ contains a finite collection of smooth and non-intersecting d-dimensional manifolds or hyper-surfaces $\mathcal{H}_d$'s in the parameter space $S_{\underline{\alpha}}$. For each vector of optimal parameters $\hat{\underline{\alpha}} = [\hat{\underline{a}}^T, \hat{\sigma}]^T$ in the manifolds $\mathcal{H}_d$'s, the probability distribution of the predicted system output for the next $(M-N)$ sampling time and a prescribed future system input Z_{N+1}^M can be obtained from (4.1.2) and is equal to a $[N_o(M-N)]$-dimensional Gaussian distribution given by:

$$p(Y_{N+1}^{M}|\underline{\hat{\alpha}}, Z_{N+1}^{M}, \mathcal{M}_{\mathcal{P}}) = \frac{1}{(\sqrt{2\pi}\hat{\sigma})^{N_o(M-N)}} \exp\left(-\frac{1}{2\hat{\sigma}^2}\sum_{i=1}^{N_o}\sum_{n=N+1}^{M}[y_i(n) - x_i(n;\underline{\hat{a}})]^2\right). \quad (4.1.17)$$

Therefore, the asymptotic approximation of the updated probability distribution of the predicted system output y_i at time instant m, $(N < m \leq M)$, can be obtained from (2.4.16) and is equal to:

$$\begin{aligned} p(y_i(m)|\mathcal{D}_N, Z_{N+1}^{m}, \mathcal{M}_{\mathcal{P}}) &\approx \int_{\cup\mathcal{H}_d} w(\underline{\hat{\alpha}}) \frac{1}{\sqrt{2\pi}\hat{\sigma}} \\ &\quad \times \exp\left(-\frac{1}{2\hat{\sigma}^2}[y_i(m) - x_i(m;\underline{\hat{a}})]^2\right) da_{\mathcal{H}_d}, \\ &\approx \int_{\cup\mathcal{H}_d} w(\underline{\hat{\alpha}}) G(y_i(m); x_i(m;\underline{\hat{a}}), \hat{\sigma}^2) da_{\mathcal{H}_d}. \end{aligned} \quad (4.1.18)$$

In (4.1.18), the weight $w(\underline{\hat{\alpha}})$ corresponding to the optimal parameters $\underline{\hat{\alpha}}$ can be determined by using (2.4.17) which is repeated below:

$$w(\underline{\hat{\alpha}}) = \frac{w'(\underline{\hat{\alpha}})}{\int_{\cup\mathcal{H}_d} w'(\underline{\hat{\alpha}}) da_{\mathcal{H}_d}}, \quad w'(\underline{\hat{\alpha}}) = |\Lambda_N^{+}(\underline{\hat{\alpha}})|^{-1/2}\pi(\underline{\hat{\alpha}}). \quad (4.1.19)$$

As before, $G(y_i(m); x_i(m;\underline{\hat{a}}), \hat{\sigma}^2)$ denotes a Gaussian distribution for $y_i(m)$ with mean $x_i(m;\underline{\hat{a}})$ and variance $\hat{\sigma}^2$. It is noted from (4.1.18) that the asymptotic approximation of $p(y_i(m)|\mathcal{D}_N, Z_{N+1}^{m}, \mathcal{M}_{\mathcal{P}})$ is not a Gaussian distribution even though the integrand in (4.1.18) is Gaussian.

The asymptotic approximation of the mean of the predicted system output $y_i(m)$ can be determined by using (4.1.18) and is equal to:

$$E[y_i(m)] = \int_{-\infty}^{\infty} y_i(m) p(y_i(m)|\mathcal{D}_N, Z_{N+1}^{m}, \mathcal{M}_{\mathcal{P}}) dy_i(m),$$

$$\begin{aligned} &\approx \int_{\cup\mathcal{H}_d} w(\hat{\underline{\alpha}}) \left\{ \int_{-\infty}^{\infty} y_i(m) G(y_i(m); x_i(m; \hat{\underline{a}}), \hat{\sigma}^2) dy_i(m) \right\} da_{\mathcal{H}_d}, \\ &= \int_{\cup\mathcal{H}_d} w(\hat{\underline{\alpha}}) x_i(m; \hat{\underline{a}}) da_{\mathcal{H}_d}. \end{aligned} \tag{4.1.20}$$

Based on (4.1.20), the mean $E[y_i(m)]$ is a continuous weighted average of the model output for each vector of optimal model parameters $\hat{\underline{a}}$. Similarly, the asymptotic approximation of the variance of the predicted system output $y_i(m)$ can be obtained by making use of the result in (4.1.20) as follows:

$$\begin{aligned} Var[y_i(m)] &= E[y_i^2(m)] - E[y_i(m)]^2, \\ &\approx \int_{\cup\mathcal{H}_d} w(\hat{\underline{\alpha}}) \left\{ \int_{-\infty}^{\infty} y_i^2(m) G(y_i(m); x_i(m; \hat{\underline{a}}), \hat{\sigma}^2) dy_i(m) \right\} da_{\mathcal{H}_d} \\ &\qquad - E[y_i(m)]^2, \\ &= \int_{\cup\mathcal{H}_d} w(\hat{\underline{\alpha}}) [\hat{\sigma}^2 + x_i^2(m; \hat{\underline{a}})] da_{\mathcal{H}_d} - E[y_i(m)]^2, \\ &= \hat{\sigma}^2 + \int_{\cup\mathcal{H}_d} w(\hat{\underline{\alpha}}) x_i^2(m; \hat{\underline{a}}) da_{\mathcal{H}_d} - E[y_i(m)]^2. \end{aligned} \tag{4.1.21}$$

To determine the weight $w(\hat{\underline{\alpha}})$ in (4.1.18), the Hessian matrix $A_N(\underline{\alpha})$ of $\ln f_N(\hat{Y}_1^N; \underline{\alpha}, \hat{Z}_1^N)$ needs to be evaluated at all of the optimal parameters $\hat{\underline{\alpha}}$ in the manifolds $\mathcal{H}_d$'s. All of the related formulas derived for the system identifiable case to calculate the Hessian matrix $A_N(\underline{\alpha})$ are still applicable for the system un-identifiable case. However, the scalar $C_N(\hat{\underline{\alpha}})$ is positive, therefore, the matrix $B_N(\hat{\underline{\alpha}})$ must have d zero eigenvalues under the assumption that the null space of $A_N(\hat{\underline{\alpha}})$ is d-dimensional. Furthermore, the determinant of $\Lambda_N^+(\hat{\underline{\alpha}})$ is equal to the product of all the positive eigenvalues of matrix $B_N(\hat{\underline{\alpha}})$ and the value of $C_N(\hat{\underline{\alpha}})$. Since the value of $C_N(\hat{\underline{\alpha}})$ is the same for each vector of optimal parameters $\hat{\underline{\alpha}}$, (4.1.19) can be simplified as follows:

$$w(\hat{\underline{\alpha}}) = \frac{v(\hat{\underline{\alpha}})}{\int_{\cup\mathcal{H}_d} v(\hat{\underline{\alpha}}) da_{\mathcal{H}_d}} \quad , \quad v(\hat{\underline{\alpha}}) = [\Delta^+(\hat{\underline{\alpha}})]^{-1/2} \pi(\hat{\underline{\alpha}}),$$

where $\Delta^+(\hat{\underline{\alpha}})$ denotes the product of all the positive eigenvalues of matrix $B_N(\hat{\underline{\alpha}})$.

4.2 Identifiability of Linear Modal and Structural Models

4.2.1 Linear Time-Invariant Models

The modal identification technique using the class of linear time-invariant models with classical normal modes has been applied to seismic response records of different types of structures such as buildings and bridges to estimate their modal properties. The results of identification show that a small number of linear classical modes can reasonably approximate both the translational and torsional vibration of tall buildings when the earthquake-induced ground acceleration is not very high so that there is no significant structural yielding and damage. In that case, the identified modal properties of structures are reasonably close to the corresponding values derived from theoretically based finite element models. Therefore, the class of linear time-invariant models is usually adopted as a first step towards system identification of structures.

Strictly speaking, all civil structures are spatially continuous and therefore continuous mathematical models such as partial differential equations are suitable to describe their behavior. But it is usually difficult to solve these partial differential equations either analytically or numerically. Therefore, in the analysis and design of most structures, it is usually assumed that a finite number of suitable degrees of freedom can be chosen to represent the possible configuration of a structure. By applying principles of mechanics, such as Newton's laws and the principle of virtual work, and finite element modeling, a set of ordinary differential equations in terms of the chosen degrees of freedom can be derived which approximates the dynamic behavior of the structure.

Assume N_{dof} suitable degrees of freedom are chosen to describe the configuration of a structure. It is also assumed that the structure is subject to ground acceleration induced by earthquakes and the ground acceleration $\ddot{z}(t)$ is considered to be uniform across the base, which is the case when the size of the base of the structure is small compared with the wave length of the incident seismic waves. Therefore, the vibration of the structure can be described by using the following set of ordinary

differential equations:

$$M\underline{\ddot{q}}(t) + C\underline{\dot{q}}(t) + K\underline{q}(t) = -M\underline{r}\ddot{z}(t), \quad \text{i.c. } \underline{q}(0) \text{ and } \underline{\dot{q}}(0). \tag{4.2.1}$$

The $N_{dof} \times N_{dof}$ matrices $M, C,$ and$K$ are the mass, damping, and stiffness matrix respectively, where the mass matrix M and stiffness matrix K are symmetric and positive-definite, except if there are degrees of freedom with no associated inertia such as in the lumped mass approach, then the mass matrix is positive-semidefinite.

In theory, the damping matrix C can be constructed from the damping of each individual structural component. However, the energy dissipation characteristics of structural material are not well understood and a portion of damping in structures also comes from joints and other non-structural elements. Therefore, the damping of structures is usually defined directly at the structural level rather than in terms of individual components. It is a well-known result that the class of linear time-invariant models possesses classical normal modes, i.e., the mode shapes are the same in both the undamped and the damped case, if and only if the damping matrix C satisfies the following condition [2]:

$$CM^{-1}K = KM^{-1}C, \tag{4.2.2}$$

or, equivalently, $M^{-1}C$ and $M^{-1}K$ commute. This type of damping is usually referred to as *classical* or *proportional* damping. Instead of specifying the damping matrix itself, the damping is prescribed directly in terms of the damping factor of each classical normal mode.

The vector $\underline{q}(t)$ contains the relative structural displacement at each degree of freedom with respect to the base of a structure. The vector $\underline{r}$ contains the pseudo-static influence coefficients for all the degrees of freedom and this can be determined from the geometry of the structure and the direction of ground motion. In the special case where only the vibration of a structure in one direction is considered and

the ground motion is also parallel to that direction, all of the components of $\underline{r}$ are just equal to one. Typically, the initial conditions $\underline{q}(0)$ and $\dot{\underline{q}}(0)$ are assumed to be zero if the structure is considered to be at rest prior to the ground motion. In this dissertation, the initial conditions will be assumed to be equal to zero.

4.2.2 Modal Analysis

In general, the set of ordinary differential equations in (4.2.1) is coupled and needs to be solved simultaneously which will be very expensive if there are many degrees of freedom in the structural model. Under the assumption of classical damping, the set of coupled equations can be transformed into a new set of uncoupled equations by using a particular coordinate transformation. Let ω_j and $\underline{\phi}^{(j)}$ denote the jth natural frequency and corresponding mode shape of the structural model and they satisfy the following generalized eigenvalue problem:

$$K\underline{\phi}^{(j)} = \omega_j^2 M\underline{\phi}^{(j)}, \quad j = 1, \ldots, N_{dof}. \tag{4.2.3}$$

Since both the mass matrix and stiffness matrix are symmetric, it can be shown that different mode shapes $\underline{\phi}^{(j)}$ and $\underline{\phi}^{(l)}$ are orthogonal with respect to the mass matrix and the stiffness matrix, i.e.,

$$\underline{\phi}^{(j)^T} M\underline{\phi}^{(l)} = \underline{\phi}^{(j)^T} K\underline{\phi}^{(l)} = 0, \quad \text{if } j \neq l. \tag{4.2.4}$$

The orthogonality properties in (4.2.4) still hold even in the case of repeated natural frequencies. Since mode shapes are determined only to within a constant multiplier, they can be scaled in any convenient way. Usually, mode shapes are normalized so that they are *orthonormal* with respect to the mass matrix. The *modal matrix* Φ of the structural model is a $N_{dof} \times N_{dof}$ matrix whose individual column is the corresponding mode shape, i.e.,

$$\Phi = [\underline{\phi}^{(1)}, \ldots, \underline{\phi}^{(N_{dof})}].$$

Therefore, by combining the results in (4.2.3) and (4.2.4), the following relations are obtained:

$$\Phi^T M \Phi = I \text{ and } \Phi^T K \Phi = \Omega, \tag{4.2.5}$$

where $\Omega = diag[\omega_1^2, \ldots, \omega_{N_{dof}}^2]$.

Under the assumption of classical damping, the mode shapes are also the generalized eigenvectors of the mass matrix and the damping matrix. Therefore, the mode shapes also have the following orthogonality property:

$$\underline{\phi}^{(j)^T} C \underline{\phi}^{(l)} = 0, \text{ if } j \neq l.$$

Let the damping factor ζ_j of the jth classic normal mode be defined by:

$$\zeta_j = \frac{\underline{\phi}^{(j)^T} C \underline{\phi}^{(j)}}{2\omega_j}.$$

Then, the following relation is obtained:

$$\Phi^T C \Phi = \Lambda, \tag{4.2.6}$$

where $\Lambda = diag[2\zeta_1\omega_1, \ldots, 2\zeta_{N_{dof}}\omega_{N_{dof}}]$.

By using the orthogonality properties in (4.2.4), it can be shown that the mode shapes are also linear independent vectors in $R^{N_{dof}}$. Therefore, they qualify as a basis for the vector space $R^{N_{dof}}$ and the displacement vector $\underline{q}(t)$ can be expressed as a linear combination of the mode shapes, i.e.,

$$\underline{q}(t) = \Phi \underline{\eta}(t). \tag{4.2.7}$$

The components of the vector $\underline{\eta}(t)$ are usually referred to as *principal* or *normal*

coordinates of the structural model. By substituting (4.2.7) into (4.2.1), premultiplying by Φ^T, and using (4.2.5) and (4.2.6), the following set of ordinary differential equations is obtained:

$$\ddot{\underline{\eta}}(t) + \Lambda\dot{\underline{\eta}}(t) + \Omega\underline{\eta}(t) = -\underline{p}\ddot{z}(t), \tag{4.2.8}$$

where $\underline{p}$ is the vector of modal participation factors and is given by $\underline{p} = \Phi^T M \underline{r}$.

Since the matrices Λ and Ω are diagonal, the set of ordinary differential equations in (4.2.8) contains a set of N_{dof} uncoupled equations in terms of the principal coordinates $\underline{\eta}(t)$, i.e.,

$$\ddot{\eta}_j(t) + 2\zeta_j\omega_j\dot{\eta}_j(t) + \omega_j^2\eta_j(t) = -p_j\ddot{z}(t), \quad j = 1, \ldots, N_{dof}. \tag{4.2.9}$$

Let $\underline{q}^{(j)}(t)$ represent the contribution to the displacement vector $\underline{q}(t)$ from the jth classic normal mode, i.e.,

$$\underline{q}^{(j)}(t) = \underline{\phi}^{(j)}\eta_j(t).$$

Therefore, (4.2.7) and (4.2.9) can be rewritten as:

$$\underline{q}(t) = \sum_{j=1}^{N_{dof}} \underline{q}^{(j)}(t), \tag{4.2.10}$$

and

$$\ddot{\underline{q}}^{(j)}(t) + 2\zeta_j\omega_j\dot{\underline{q}}^{(j)}(t) + \omega_j^2\underline{q}^{(j)}(t) = -\underline{\beta}^{(j)}\ddot{z}(t), \quad j = 1, \ldots, N_{dof}, \tag{4.2.11}$$

where $\underline{\beta}^{(j)}$ is the vector of *effective* modal participation factors for the jth mode and is given by $\underline{\beta}^{(j)} = p_j\underline{\phi}^{(j)}$ [3]. It is noted that the effective modal participation factors

are independent of the normalization chosen for the mode shapes. Furthermore, the effective participation factors satisfy the following constraints:

$$\sum_{j=1}^{N_{dof}} \underline{\beta}^{(j)} = \Phi \underline{p} = \Phi \Phi^T M \underline{r} = \underline{r}. \tag{4.2.12}$$

It is a fact that the contribution of higher modes to the structural response is usually negligible when compared with the dominant modes. This is because the higher modes are intrinsically more difficult to excite and typical earthquake ground accelerations also do not have enough energy in the high frequency range. Therefore, it is usually assumed that only the first $N_m (< N_{dof})$ dominant modes contribute to the structural response and (4.2.10) can be approximated by:

$$\underline{q}(t) \approx \sum_{j=1}^{N_m} \underline{q}^{(j)}(t). \tag{4.2.13}$$

By solving each ordinary differential equation in (4.2.11) and using (4.2.13), the seismic response of a structure is obtained.

4.2.3 Model Identifiability of Linear Modal Models

When the modal analysis approach presented in Section 4.2.2 is adopted to analyze the response of linear time-invariant models, the model parameters involved are the natural frequencies ω_j's, damping factors ζ_j's, and effective modal participation factors $\underline{\beta}^{(j)}$'s. Since all of the model parameters in this case are related directly to the classical normal modes, this type of linear time-invariant models is usually referred to as *modal* models. System identification techniques which use the class of modal models are classified as *modal identification* methods. It is of interest to note that modal models can be derived without the need to develop a structural model involving the mass, damping, and stiffness matrices and this is the major advantage of the modal identification approach.

Because usually the structural response at a small number $N_o (< N_{dof})$ of degrees of freedom is measured, only those effective modal participation factors which

correspond to the measured degrees of freedom can be estimated in modal identification. A theoretical study of the model identifiability of the class of modal models is given in [3]. It is shown that the class of modal models is globally model identifiable given any finite-duration input if and only if the following conditions are satisfied:

1. There are no repeated modes, i.e., no two modes have the same natural frequency and damping factor.

2. For each mode, there exists at least one measured degree of freedom such that the associated effective modal participation factor is not zero.

It is clear that if the first condition is not satisfied, the effective modal participation factors of the repeated modes at a measured degree of freedom cannot be determined uniquely. On the other hand, if the second condition is not satisfied, the particular mode will have no contribution to the model output and therefore the associated natural frequency and damping factor cannot be determined.

Because the energy content of typical ground acceleration records falls off at the high frequency range and higher modes are intrinsicly difficult to excite, the contribution of higher modes to seismic structural response is usually negligible. Therefore, the higher modes cannot be identified reliably if they are included in the modal model. Furthermore, there is a decrease in the signal-to-noise ratio for higher modes in modal identification of real structures because of an increase in the noise at the high frequency range. Therefore, it is concluded that only the modal parameters of the first $N_m (< N_{dof})$ dominant modes can be estimated reliably from seismic structural response data and these modal parameters are also globally system identifiable if the measurement noise and modeling error are not too large [3].

A very efficient computer program MODE-ID based on the least-squares output-error method was developed by Beck for modal identification using real seismic structural response records. In MODE-ID, the estimation of the modal parameters of the dominant modes is accomplished by using a modal minimization procedure which consists of the following steps:

1. Successive modal sweeps consist of a sequence of minimization with respect to the modal parameters of a single mode.

2. For each modal minimization, the original minimization problem is simplified so that only the natural frequency and the damping factor of a mode are considered as parameters.

3. A sequence of alternating one-dimensional minimization with respect to the natural frequency and the damping factor is performed until convergence.

4. Additional sweeps are performed if necessary until the change in the fit between the model output and measured structural response is insignificant.

In spite of the broad application of modal identification techniques to real seismic response records, modal identification has its own limitations. First of all, no direct information can be extracted from the measured data regarding the unmeasured degrees of freedom of a structure. More specifically, the effective modal participation factors at the unmeasured degrees of freedom can not be estimated directly from the measured data. Therefore, it is not possible to predict the future structural response at these unmeasured degrees of freedom and estimate the level of earthquake-induced force such as the base shear. As an approximation, the mode shape amplitudes at the unmeasured degrees of freedom are estimated by using simple interpolation or extrapolation based on the identified mode shape information at the measured degrees of freedom. Even though this method is straightforward, it is not a very rigorous approach.

Another limitation of modal identification is related to the constraints on the natural frequencies and effective modal participation factors. In modal identification, the natural frequencies are only required to be positive and in ascending order. For the effective modal participation factors, they are only required to satisfy (4.2.12). However, when prior knowledge is used to impose certain constraints on the stiffness matrix, corresponding constraints will also be imposed on the natural frequencies and effective modal participation factors. For example, the class of linear chain

models constitutes a subclass of the linear time-invariant models with particular tridiagonal stiffness matrices. This prior knowledge is not easily utilized when a modal identification approach is used.

4.2.4 Model Identifiability of Linear Structural Models

Instead of using the modal parameters $\{\omega_j, \zeta_j, \underline{\beta}^{(j)} : j = 1, \ldots, N_{dof}\}$, the elements in the damping matrix C and the stiffness matrix K can also be designated as the model parameters $\underline{a}$ for the class of linear time-invariant models. It is implicitly assumed here that the mass matrix M is known. Because all of the model parameters in this case have clear physical meaning on the structural level, this type of model is referred to as a *structural* model. Moreover, it can be shown that knowing all the modal parameters and given the mass matrix, a unique damping matrix C and stiffness matrix K can be determined by the following formulas:

$$C = M\Phi\Lambda\Phi^T M = M\left(\sum_{j=1}^{N_{dof}} 2\zeta_j\omega_j\underline{\phi}^{(j)}\underline{\phi}^{(j)^T}\right)M, \tag{4.2.14}$$

and

$$K = M\Phi\Omega\Phi^T M = M\left(\sum_{j=1}^{N_{dof}} \omega_j^2\underline{\phi}^{(j)}\underline{\phi}^{(j)^T}\right)M. \tag{4.2.15}$$

A theoretical study of the model identifiability of the class of structural models was presented in [3]. It was proven that a subclass of structural models whose corresponding modal models satisfy the two conditions for global model identifiability in Section 4.2.3 is locally model identifiable if and only if the structural response is measured at no less than half of the total number of degrees of freedom. Furthermore, the subclass of structural models is globally model identifiable if and only if the structural response is measured at every degree of freedom. Because of the highly restrictive conditions on the number of measured degrees of freedom in a structure, the subclass of structural models is too general to guarantee unique determination of a model from its input and output unless all of the degrees of freedom are measured.

If the subclass of structural models is further restricted, more relaxed conditions for model identifiability can be obtained but this may also reduce the modeling capability for real structures. One such example is the class of linear chain models. In this case, the damping matrix and the stiffness matrix have the property of being tridiagonal. Moreover, they have only N_{dof} independent parameters compared with $2N_{dof} - 1$ independent parameters for a general symmetric and tridiagonal matrix of order N_{dof}. The class of linear chain models is often used as simplified models for planar-frame buildings with N_{dof} stories.

A theoretical study of the problem of determining the damping matrix and the stiffness matrix of the class of linear chain models given the horizontal ground motion and the model response at only one degree of freedom was presented in [4-5]. It was shown that the class of linear chain models is globally model identifiable if the model response at the first floor is available. Furthermore, the class of models is only locally model identifiable if the model response at any other floor is available. In addition, upper bounds on the number of equivalent solutions of interstory stiffness were estimated for the local model identifiability case. The degree of non-uniqueness of the stiffness matrix is found to monotonically increase as the model response at a higher and higher floor is measured. In the case of forced vibration tests in which shakers are used to excite the building, results on the global model identifiability of some of the damping and stiffness parameters of the class of linear chain models were given in [6].

Based on the results in [4], there are at most $N_{dof}!$ different equivalent solutions of interstory stiffness when the model response at the roof is available. However, there is no immediate answer to the problem of determining the exact number of solutions or of calculating these solutions. A novel numerical approach which systematically searches the parameter space of interstory stiffness was presented to find all the solutions of interstory stiffness [7]. The idea is based on the global model identifiability of the natural frequencies and effective modal participation factors. Since these modal parameters are uniquely determined given any ground motion, all

the equivalent solutions of interstory stiffness must produce the same corresponding modal parameters as the nominal interstory stiffness. Therefore, different solutions of interstory stiffness can be found by systematically relaxing the constraints on matching these modal parameters.

Actually, the mentioned model identifiability problem of the class of linear chain models can also be solved by using the relaxation scheme presented in Section 3.2.3. For illustration, consider a class of six-degrees-of-freedom linear chain models which is used to model a six-story building as shown in Figure 4.1. The mass matrix M and stiffness matrix K are given by:

$$M = m_o \begin{bmatrix} 1 & & & & & 0 \\ & 1 & & & & \\ & & \ddots & & & \\ & & & & & \\ 0 & & & & & 1 \end{bmatrix} \quad \text{and} \quad K = k_o \begin{bmatrix} \theta_1 + \theta_2 & -\theta_2 & & & & 0 \\ -\theta_2 & \theta_2 + \theta_3 & -\theta_3 & & & \\ & -\theta_3 & \ddots & & & \\ & & & & \theta_5 + \theta_6 & -\theta_6 \\ 0 & & & & -\theta_6 & \theta_6 \end{bmatrix},$$

where m_o is the mass of each floor and k_o is some nominal interstory stiffness. These two parameters are assumed to be known and the stiffness matrix K is parameterized by the vector of stiffness parameters, $\underline{\theta} = [\theta_1, \ldots, \theta_6]^T$. In the particular case considered here, the ground motion and the model response at the roof, i.e., q_6, are assumed to be available. The problem is to determine the number of equivalent stiffness models consistent with these data.

Udwadia [4] showed that there is at most $6! = 720$ equivalent stiffness models in this case. Later, it was shown in [7] that there are only eight equivalent stiffness models if the nominal stiffness model is assumed to be parameterized by $\underline{\theta} = [1, 1, 1, 1, 1, 1]^T$, i.e., a uniform linear chain model. It turns out that all of these equivalent stiffness models have the same natural frequencies as the nominal stiffness model. Let $\omega_1, \ldots, \omega_6$ denote the six natural frequencies of a stiffness model and $\omega_1^o, \ldots, \omega_6^o$ be the corresponding natural frequencies of the nominal stiffness model.

Therefore, to find all of the equivalent stiffness models, the roots of the following set of nonlinear algebraic equations need to be found:

$$\begin{cases} \omega_1(\underline{\theta}) - \omega_1^0 = 0, \\ \qquad \vdots \\ \omega_6(\underline{\theta}) - \omega_6^0 = 0 \end{cases} . \tag{4.2.16}$$

As pointed out in Chapter 3, the homotopy scheme and the relaxation scheme can be used to search for all of the roots of a set of nonlinear algebraic equations such as (4.2.16). Since one of the roots of (4.2.16), i.e., the uniform stiffness model, is assumed to be known already, the relaxation scheme is applied to find all the other roots of (4.2.16). The stiffness parameters for the eight computed equivalent stiffness models are summarized in Table 4.1. These computed models are the same as the results in [7].

Twelve relaxation trajectories were tracked in searching for these eight equivalent stiffness models. These relaxation trajectories are labeled as $\Gamma_1, \ldots, \Gamma_{12}$ and all of the different equivalent stiffness models which can be reached by each trajectory are summarized in Table 4.2. A "•" mark is placed in Table 4.2 to indicate a particular equivalent stiffness model can be reached by a certain relaxation trajectory while blanks mean the opposite. For each relaxation trajectory, the relaxed natural frequency is indicated in the last column of Table 4.2. In Table 4.2, a "∗" mark is used to designate a relaxation trajectory which is a closed curve.

The connectivity of the network spanned by the twelve relaxation trajectories can be reorganized as shown in Table 4.3, which is useful in determining whether all the possible relaxation trajectories have been tried from each equivalent stiffness model which has been found. Table 4.3 shows that all of the 48 possible cases for relaxing each natural frequency at a time from each found equivalent stiffness model has been covered by the 12 relaxation trajectories that are tracked.

4.3 Structural Model Updating

4.3.1 Introduction

Partially due to the aforementioned limitations of modal identification, research on the challenging problem of *structural model updating* has gained a lot of attention in the system identification community in the last few years. The major motivation to study structural model updating is to find suitable ways to match a theoretically based model of a structure with measured structural response data. This problem is important because structural model updating has the potential to be implemented as a tool for structural health monitoring which can provide early warning of damage of structural components [8-10]. From the perspective of system identification, structural model updating is essentially a system identification problem in which the stiffness matrix of a structure is to be estimated by using the measured data.

There are two major inherent difficulties in structural model updating using real seismic structural response records. The first constraint is that the structural response is usually measured at only a few degrees of freedom in a structure. If there is no constraint on the structure of the stiffness matrix other than it is symmetric and positive definite, the structural response must be measured at no less than half of all the degrees of freedom in order for the stiffness matrix to be at least locally model identifiable as discussed in Section 4.2.4. This requirement will impose a severe restriction on the number of degrees of freedom allowed in the structural models which subsequently causes the damping and stiffness distribution of a structure to be modeled very poorly. Therefore, there is a mismatch between the desired detail in the stiffness matrix and the sparse structural response records.

Another constraint in structural model updating is related to the accuracy of stiffness matrix estimation and can be explained from the viewpoint of modal identification. It is recalled from (4.2.15) that the stiffness matrix is more sensitive to the modal parameters of higher modes than to the modal parameters of the dominant lower modes. As discussed in Section 4.2.3, only the modal parameters of the dominant modes can be estimated reliably from real seismic structural response records.

Since the modal parameters of the higher modes cannot be identified accurately, the estimation of the stiffness matrix will not be accurate even when the stiffness matrix is locally model identifiable in theory. These two constraints in structural model updating are discussed in more detail in the following.

Because the natural frequencies ω_j's and effective modal participation factors $\underline{\beta}^{(j)}$'s of a stiffness matrix K are related by (4.2.3), the free parameters in the stiffness matrix also need to satisfy these constraints, that is, the stiffness matrix must generate a set of compatible natural frequencies and effective modal participation factors. The total number of constraints in (4.2.3) depends on N_m, the number of modes considered, and N_o, the number of measured degrees of freedom in a structure. However, there may be some redundancy among these constraints because of the particular structure of the stiffness matrix and the relations given in (4.2.12). Therefore, if $N_m < N_{dof}$, there are $N_m(N_o + 1)$ constraints in theory. But, if $N_m = N_{dof}$, there are only $N_m(N_o + 1) - N_o$ constraints in theory.

Apparently, if the number of free parameters in the stiffness matrix is larger than the total number of constraints, the stiffness matrix becomes un-identifiable and so cannot be determined uniquely given a set of compatible natural frequencies and effective modal participation factors. To give precise description of the stiffness distribution in a structure, the stiffness matrix needs to be at least locally unique or identifiable. Hence, for a given number of modes and measured degrees of freedom in a structure, there is a limit on the number of free parameters allowed in the stiffness matrix in order to make the stiffness matrix at least locally identifiable.

As discussed in Section 4.2.3, only the modal parameters of the dominant modes can be estimated reliably from seismic structural response records. Based on the formula in (4.2.15), the stiffness matrix is more sensitive to the modal parameters of higher modes than to the modal parameters of the dominant lower modes. Therefore, only the modal parameters of the dominant modes can be used in order to make accurate estimation of the stiffness matrix. Otherwise, the estimated stiffness matrix will be unreliable even if in theory it is locally identifiable.

The goal of structural model updating is to estimate a stiffness matrix which can provide detailed description of the stiffness distribution in a structure. Therefore, the more parameters in the stiffness matrix the better. However, because of the aforementioned constraints, there is a trade-off between the uniqueness and accuracy of the stiffness matrix and the detail of description of the stiffness distribution in a structure. If the stiffness matrix has too many parameters, the stiffness matrix will become un-identifiable and its estimation is also not reliable. On the other hand, even if a stiffness matrix with few parameters can be uniquely and accurately identified from the seismic structural response records, it may not suitably describe the stiffness distribution in a structure.

The number of dominant modes whose modal parameters can be estimated reliably from seismic structural response records depends on the frequency content of the ground motion and the type of structure. For typical buildings, the number of dominant modes in one direction is usually below five. In order to have more detailed description of the stiffness distribution in a structure without sacrificing the accuracy of stiffness estimation, an alternative way is to increase the number of measured degrees of freedom in a structure so that more mode shape information can be incorporated when determining the stiffness matrix. But this may not be feasible in all situations because of economic reasons or technical limitations. In any case, the limit on the number of free parameters of the stiffness matrix is not known *a priori* and needs to be explored.

4.3.2 Single-Stage Approach

Basically, the structural model updating problem has been explored by using two types of approaches. The first type of approach is to decompose the problem into two stages as in [10]. In the first stage, modal parameters of the dominant modes are identified by using the modal identification technique. In the second stage, several methods have been proposed to adjust the stiffness matrix. One way is to minimize the fit between the calculated modal parameters and the corresponding identified modal parameters. Another method is to minimize the fit between the calculated

modal response time histories and the corresponding identified modal response time histories which can be artificially constructed from the identified modal parameters. The main issue in these two-stage structural model updating approaches is that there is no well-accepted guideline in selecting the weight for each dominant mode. Different combination of weights will give different estimates of the stiffness matrix.

Another type of approach is to estimate the stiffness matrix using the measured seismic structural response time histories directly without identifying the modal parameters first. Unlike the two-stage approaches, the estimation of the stiffness matrix is accomplished in a single stage. The advantage of the one-stage approach is that the estimated stiffness matrix depends on the structural response time history directly and therefore only one class of probabilistic models $\mathcal{M}_{\mathcal{P}}$ is needed in the statistical system identification framework. The problem of explicitly choosing weights for each dominant mode does not arise. Furthermore, the identified *posterior* stiffness matrix is based on the directly measurable structural response time history rather than the modal parameters which can only be estimated indirectly by using modal identification techniques.

To obtain a reliable and locally unique estimate of the stiffness matrix, a so-called *substructuring* approach is used to reduce the number of parameters in the stiffness matrix. The given structure is conceptually decomposed into a small number of $N_{\underline{\theta}}$ substructures. The contribution of stiffness from different individual substructures is specified by using a vector of normalized and non-dimensional stiffness parameters $\underline{\theta} = [\theta_1, \ldots, \theta_{N_{\underline{\theta}}}]^T$ so that the stiffness matrix K is given by:

$$K = K_0 + \sum_{l=1}^{N_{\underline{\theta}}} \theta_l K_l, \tag{4.3.1}$$

where K_0 represents that part of the stiffness matrix which is considered accurately known and so need not be parameterized, and K_l represents the stiffness matrix of the lth substructure. All of the stiffness matrices K_l's are symmetric and positive semi-definite $N_{dof} \times N_{dof}$ matrices. The stiffness parameters θ_l's are usually scaled

appropriately so that they are of the same order.

As discussed in Section 4.2.1, the damping of linear time-invariant models is usually prescribed directly in terms of the damping factor of each mode. Therefore, the damping factors of the first N_m dominant modes are also considered as part of the model parameters $\underline{a}$. Therefore, there are two types of model parameters: stiffness parameters θ_l's and modal parameters ζ_j's. Let $\underline{\zeta} = [\zeta_1, \ldots, \zeta_{N_m}]^T$, then the vector of model parameters is $\underline{a} = [\underline{\theta}^T, \underline{\zeta}^T]^T$ and there are $N_{\underline{a}} = N_{\underline{\theta}} + N_m$ model parameters in total.

For real seismic structural response, only the absolute acceleration is usually measured because it can be done readily with an inertial ("seismic mass") transducer. By subtracting the corresponding measured ground acceleration, the relative acceleration of the structural response can be obtained. Let $\mathcal{L}^o$ denote the set of integers corresponding to the numbering of the measured degrees of freedom of the structure. For each $i \in \mathcal{L}^o$, let $\hat{b}_i(n)$ denote the measured relative acceleration at the ith degree of freedom of the structure at time instant n. The corresponding model output at the same degree of freedom and time instant is $\ddot{q}_i(n; \underline{a})$. In the least-squares prediction-error approach described in Section 4.1, the optimal model parameters $\hat{\underline{a}}$ are determined by minimizing the objective function $J_E(\underline{a})$ given in (4.1.6). Let $s_i(\underline{a})$ be the sum of squares of the prediction error of the relative acceleration at the ith degree of freedom of the structure, i.e.,

$$s_i(\underline{a}) = \sum_{n=1}^{N} [\hat{b}_i(n) - \ddot{q}_i(n; \underline{a})]^2. \tag{4.3.2}$$

By using (4.1.6) and (4.3.2), $J_E(\underline{a})$ can be rewritten as follows:

$$J_E(\underline{a}) = \frac{1}{N_o N} \sum_{i \in \mathcal{L}^o} s_i(\underline{a}). \tag{4.3.3}$$

When the class of linear structural models is locally system identifiable given the measured data and the set of allowable model parameters $S_{\underline{a}}$ is bounded, there is

a finite number of optimal model parameters $\hat{\underline{a}}$. The generalized trajectory methods presented in Chapter 3 can then be applied to find the least local minimum (LLM) of $J_E(\underline{a})$ in the parameter space $S_{\underline{a}}$, which in most cases gives the global minimum of $J_E(\underline{a})$ over the parameter space $S_{\underline{a}}$. In particular, the Fixed-Point homotopy scheme:

$$\underline{g}_F(\underline{a}, \lambda) = (1 - \lambda)M_F(\underline{a} - \underline{a}_o) + \lambda \nabla J_E(\underline{a}) = \underline{0}, \tag{4.3.4}$$

can be applied to locate the first vector of optimal model parameters, and then the relaxation scheme:

$$\underline{g}_R(\underline{a}, \lambda) = \nabla J_E(\underline{a}) - (1 - \lambda)\underline{v} = \underline{0}, \tag{4.3.5}$$

can be applied to systematically search the parameter space $S_{\underline{a}}$ for other optimal model parameters, if any.

4.3.3 Calculation of $\nabla J_E(\underline{a})$

In order to use the homotopy scheme in (4.3.4) and the relaxation scheme in (4.3.5) to find all of the optimal model parameters $\hat{\underline{a}}$, the gradient vector of the objective function $J_E(\underline{a})$ is needed. To reduce numerical round-off error and increase the accuracy in tracking the homotopy and the relaxation trajectories, this gradient vector needs to be calculated by using analytical expressions instead of finite-difference approximations. From (4.3.3), the gradient vector of $J_E(\underline{a})$ can be calculated as follows:

$$\nabla J_E(\underline{a}) = \frac{1}{N_o N} \sum_{i \in \mathcal{L}^o} \nabla s_i(\underline{a}). \tag{4.3.6}$$

Furthermore, the gradient vector of $s_i(\underline{a})$ can be computed from (4.3.2) as:

$$\nabla s_i(\underline{a}) = -2 \sum_{n=1}^{N} [\hat{b}_i(n) - \ddot{q}_i(n; \underline{a})] \nabla \ddot{q}_i(n; \underline{a}). \tag{4.3.7}$$

The discrete-time model output $\ddot{q}_i(n;\underline{a})$ and its associated gradient vector $\nabla\ddot{q}_i(n;\underline{a})$ can be obtained by solving the governing continuous-time equations of motion using any suitable numerical time integration scheme such as the Newmark average-acceleration scheme. From (4.2.13), the model acceleration response $\ddot{q}_i(t;\underline{a})$ is given by:

$$\ddot{q}_i(t;\underline{a}) = \sum_{j=1}^{N_m} \ddot{q}_i^{(j)}(t;\underline{a}),$$

where the contribution to the model acceleration response from the jth mode $\ddot{q}_i^{(j)}(t;\underline{a})$ satisfies the differential equation given in (4.2.11), i.e.,

$$\ddot{q}_i^{(j)}(t;\underline{a}) + 2\zeta_j\omega_j\dot{q}_i^{(j)}(t;\underline{a}) + \omega_j^2 q_i^{(j)}(t;\underline{a}) = -\beta_i^{(j)}\ddot{z}(t). \tag{4.3.8}$$

It is noted from (4.3.8) that $\ddot{q}_i^{(j)}(t;\underline{a})$ depends only on the modal parameters of the jth mode but not the modal parameters of any other modes. Therefore,

$$\frac{\partial\ddot{q}_i^{(j)}(t;\underline{a})}{\partial\zeta_k} = \frac{\partial\ddot{q}_i^{(j)}(t;\underline{a})}{\partial\omega_k} = \frac{\partial\ddot{q}_i^{(j)}(t;\underline{a})}{\partial\beta_i^{(k)}} = 0, \quad \text{if } j \neq k. \tag{4.3.9}$$

The differential equation which $\frac{\partial\ddot{q}_i^{(j)}(t;\underline{a})}{\partial\zeta_j}$ must satisfy can be obtained by differentiating (4.3.8) with respect to ζ_j:

$$\frac{d^2}{dt^2}\left[\frac{\partial q_i^{(j)}(t;\underline{a})}{\partial\zeta_j}\right] + 2\zeta_j\omega_j\frac{d}{dt}\left[\frac{\partial q_i^{(j)}(t;\underline{a})}{\partial\zeta_j}\right] + 2\omega_j\dot{q}_i^{(j)}(t;\underline{a}) + \omega_j^2\frac{\partial q_i^{(j)}(t;\underline{a})}{\partial\zeta_j} = 0. \tag{4.3.10}$$

To compute $\frac{\partial\ddot{q}_i^{(j)}(t;\underline{a})}{\partial\theta_l}$, the chain rule and (4.3.9) are used. Therefore,

$$\frac{\partial\ddot{q}_i^{(j)}(t;\underline{a})}{\partial\theta_l} = \frac{\partial\ddot{q}_i^{(j)}(t;\underline{a})}{\partial\omega_j}\frac{\partial\omega_j}{\partial\theta_l} + \frac{\partial\ddot{q}_i^{(j)}(t;\underline{a})}{\partial\beta_i^{(j)}}\frac{\partial\beta_i^{(j)}}{\partial\theta_l}. \tag{4.3.11}$$

Similarly, by differentiating (4.3.8) with respect to ω_j and $\beta_i^{(j)}$, $\frac{\partial \ddot{q}_i^{(j)}(t;\underline{a})}{\partial \omega_j}$ and $\frac{\partial \ddot{q}_i^{(j)}(t;\underline{a})}{\partial \beta_i^{(j)}}$ satisfy the following differential equations respectively:

$$\frac{d^2}{dt^2}\left[\frac{\partial q_i^{(j)}(t;\underline{a})}{\partial \omega_j}\right]+2\zeta_j\omega_j\frac{d}{dt}\left[\frac{\partial q_i^{(j)}(t;\underline{a})}{\partial \omega_j}\right]+2\zeta_j\dot{q}_i^{(j)}(t;\underline{a})+\omega_j^2\frac{\partial q_i^{(j)}(t;\underline{a})}{\partial \omega_j}+2\omega_j q_i^{(j)}(t;\underline{a})=0, \tag{4.3.12}$$

and

$$\frac{d^2}{dt^2}\left[\frac{\partial q_i^{(j)}(t;\underline{a})}{\partial \beta_i^{(j)}}\right]+2\zeta_j\omega_j\frac{d}{dt}\left[\frac{\partial q_i^{(j)}(t;\underline{a})}{\partial \beta_i^{(j)}}\right]+\omega_j^2\frac{\partial q_i^{(j)}(t;\underline{a})}{\partial \beta_i^{(j)}}=-\ddot{z}(t). \tag{4.3.13}$$

By solving the set of three differential equations (4.3.10), (4.3.12), (4.3.13), and using (4.3.11), the gradient vector of the model acceleration response $\nabla\ddot{q}_i^{(j)}(t;\underline{a})$ can be computed as:

$$\nabla\ddot{q}_i^{(j)}(t;\underline{a})=[\frac{\partial \ddot{q}_i^{(j)}(t;\underline{a})}{\partial\theta_1},\ldots,\frac{\partial \ddot{q}_i^{(j)}(t;\underline{a})}{\partial\theta_{N_{\underline{\theta}}}},0,\ldots,\frac{\partial \ddot{q}_i^{(j)}(t;\underline{a})}{\partial\zeta_j},\ldots,0]^T,$$

and

$$\nabla\ddot{q}_i(t;\underline{a})=\sum_{j=1}^{N_m}\nabla\ddot{q}_i^{(j)}(t;\underline{a}).$$

4.3.4 Calculation of the $\frac{\partial\omega_j}{\partial\theta_l}$ and $\frac{\partial\beta_i^{(j)}}{\partial\theta_l}$

To compute $\frac{\partial\omega_j}{\partial\theta_l}$ and $\frac{\partial\beta_i^{(j)}}{\partial\theta_l}$ in (4.3.11), recall that the natural frequency ω_j and mode shape $\underline{\phi}^{(j)}$ satisfy the generalized eigenvalue problem:

$$K(\underline{\theta})\underline{\phi}^{(j)}=\omega_j^2M\underline{\phi}^{(j)}. \tag{4.3.14}$$

It is assumed that there is no repeated natural frequency, therefore ω_j and $\underline{\phi}^{(j)}$

are smooth functions of the stiffness parameters $\underline{\theta}$. By differentiating (4.3.14) with respect to θ_l and using (4.3.1), the following is obtained:

$$[K(\underline{\theta}) - \omega_j^2 M]\frac{\partial \underline{\phi}^{(j)}}{\partial \theta_l} = \frac{\partial \omega_j^2}{\partial \theta_l} M\underline{\phi}^{(j)} - K_l\underline{\phi}^{(j)}. \tag{4.3.15}$$

Pre-multiplying (4.3.15) with $\underline{\phi}^{(j)^T}$, and using (4.2.4) and (4.3.14), gives:

$$\frac{\partial \omega_j^2}{\partial \theta_l} = \underline{\phi}^{(j)^T} K_l \underline{\phi}^{(j)} \quad \text{or} \quad \frac{\partial \omega_j}{\partial \theta_l} = \frac{1}{2\omega_j}\underline{\phi}^{(j)^T} K_l \underline{\phi}^{(j)}. \tag{4.3.16}$$

Because there is no repeated natural frequency, the matrix $[K(\underline{\theta}) - \omega_j^2 M]$ has rank $N_{dof}-1$ and therefore has a one-dimensional null space which is actually spanned by the mode shape $\underline{\phi}^{(j)}$. Since the coefficient matrix $[K(\underline{\theta}) - \omega_j^2 M]$ in (4.3.15) is singular, $\frac{\partial \underline{\phi}^{(j)}}{\partial \theta_l}$ can not be solved from (4.3.15) without more constraints on $\frac{\partial \underline{\phi}^{(j)}}{\partial \theta_l}$. Recall that $\underline{\phi}^{(j)}$ is normalized with respect to the mass matrix, i.e.,

$$\underline{\phi}^{(j)^T} M \underline{\phi}^{(j)} = 1. \tag{4.3.17}$$

By differentiating (4.3.17), the following is obtained:

$$\underline{\phi}^{(j)^T} M \frac{\partial \underline{\phi}^{(j)}}{\partial \theta_l} = 0. \tag{4.3.18}$$

Consider the combined set of equations (4.3.15) and (4.3.18), i.e.,

$$\begin{bmatrix} K(\underline{\theta}) - \omega_j^2 M \\ \underline{\phi}^{(j)^T} M \end{bmatrix} \frac{\partial \underline{\phi}^{(j)}}{\partial \theta_l} = \begin{bmatrix} \frac{\partial \omega_j^2}{\partial \theta_l} M\underline{\phi}^{(j)} - K_l\underline{\phi}^{(j)} \\ 0 \end{bmatrix}. \tag{4.3.19}$$

The $(N_{dof}+1)\times N_{dof}$ coefficient matrix in (4.3.19) is of rank N_{dof} since the submatrix $[K(\underline{\theta}) - \omega_j^2 M]$ has $N_{dof} - 1$ linearly independent rows which are orthogonal to $\underline{\phi}^{(j)}$ and from (4.3.17), the row vector $\underline{\phi}^{(j)^T} M$ is not orthogonal to $\underline{\phi}^{(j)}$. Therefore, $\frac{\partial \underline{\phi}^{(j)}}{\partial \theta_l}$ can be obtained by solving the set of equations (4.3.19).

An efficient way to solve (4.3.19) is to transform the following $(N_{dof}+1) \times (N_{dof}+1)$ matrix:

$$\begin{bmatrix} K(\underline{\theta}) - \omega_j^2 M & \frac{\partial \omega_j^2}{\partial \theta_l} M\underline{\phi}^{(j)} - K_l \underline{\phi}^{(j)} \\ \underline{\phi}^{(j)^T} M & 0 \end{bmatrix},$$

to the row-reduced echelon form by using elementary row operations [11]. The resulting row-reduced echelon form is:

$$\begin{bmatrix} I & \frac{\partial \underline{\phi}^{(j)}}{\partial \theta_l} \\ 0 & 0 \end{bmatrix},$$

where I is the identity matrix of order N_{dof}.

To compute $\frac{\partial \beta_i^{(j)}}{\partial \theta_l}$, recall that:

$$\beta_i^{(j)} = p_j \phi_i^{(j)} = \phi_i^{(j)} \underline{\phi}^{(j)^T} M \underline{r}. \tag{4.3.20}$$

Differentiation of (4.3.20) with respect to θ_l yields:

$$\frac{\partial \beta_i^{(j)}}{\partial \theta_l} = \left(\frac{\partial \underline{\phi}^{(j)}}{\partial \theta_l} \right)_i \underline{\phi}^{(j)^T} M \underline{r} + \phi_i^{(j)} \left(\frac{\partial \underline{\phi}^{(j)}}{\partial \theta_l} \right)^T M \underline{r}.$$

References for Chapter 4

1. Beck, J. L., *System Identification Methods Applied to Measured Seismic Response*, Proceedings of the Eleventh World Conference on Earthquake Engineering, Acapulco, Mexico, 1996.
2. Caughey, T. K., and O'Kelly, M. E. J., *Classical Normal Modes in Damped Linear Dynamic Systems*, ASME Journal of Applied Mechanics, Vol. 32, No. 3, pp. 583-588, 1965.
3. Beck, J. L., *Determining Models of Structures from Earthquake Records*, Report No. EERL 78-01, California Institute of Technology, Pasadena, California, 1978.
4. Udwadia, F. E., and Sharma, D. K., *Some Uniqueness Results Related to Building Structural Identification*, SIAM Journal on Applied Mathematics, Vol. 34, No. 1, pp. 104-118, 1978.
5. Udwadia, F. E., Sharma, D. K., and Shah, P. C., *Uniqueness of Damping and Stiffness Distributions in the Identification of Soil and Structural Systems*, ASME Journal of Applied Mechanics, Vol. 45, No. 1, pp. 181-187, 1978.
6. Udwadia, F. E., *Some Uniqueness Results Related to Soil and Building Structural Identification*, SIAM Journal on Applied Mathematics, Vol. 45, No. 4, pp. 674-685, 1985.
7. Katafygiotis, L. S., *Treatment of Model Uncertainties in Structural Dynamics*, Report No. EERL 91-01, California Institute of Technology, Pasadena, California, 1991.
8. Beck, J. L., and Katafygiotis, L. S., *Probabilistic System Identification and Health Monitoring of Structures*, Proceedings of the Tenth World Conference on Earthquake Engineering, A. A. Balkema, Rotterdam, Netherlands, pp. 3721-3726, 1992.
9. Beck, J. L., Vanik, M. W., and Katafygiotis, L. S., *Determination of Stiffness Changes from Modal Parameters Changes for Structural Health Monitoring*, Proceedings of the First World Conference on Structural Control, International Association for Structural Control, Los Angeles, California, pp. TA3:13-TA3:22, 1994.
10. Beck, R. T., *Fundamental Problems in the Application of Structural Identification Procedures to Damage Detection*, Report No. EERL 91-03, California Institute of Technology, Pasadena, California, 1991.
11. Strang, G., *Linear Algebra and its Applications*, Harcourt Brace Jovanovich, Orlando, Florida, 1988.

Table 4.1: Equivalent Stiffness Models for a Uniform Six-Degrees-of-Freedom Linear Chain Model.

No.	θ_1	θ_2	θ_3	θ_4	θ_5	θ_6
1	1.0000	1.0000	1.0000	1.0000	1.0000	1.0000
2	1.5848	0.6963	1.2875	0.7574	1.1766	0.7898
3	1.9970	0.7980	0.7095	1.3848	0.7113	0.8980
4	2.0000	1.0000	1.0000	0.5000	1.0000	1.0000
5	2.0932	1.0476	0.7240	0.7374	0.6705	1.2738
6	2.2911	0.6304	0.9321	1.1774	0.9515	0.6631
7	2.4913	0.8777	0.6514	1.1106	0.6672	0.9475
8	2.8252	0.6753	0.8826	0.9021	0.8753	0.7520

Table 4.2: Relaxation Trajectories and Reachable Equivalent Stiffness Models.

	Equivalent Stiffness Model								Relaxed
Trajectory	1	2	3	4	5	6	7	8	ω
$^*\Gamma_1$	•	•	•	•	•	•	•	•	ω_1
$^*\Gamma_2$	•	•	•	•	•	•	•	•	ω_2
$^*\Gamma_3$	•	•	•			•			ω_3
$^*\Gamma_4$	•	•	•			•			ω_4
$^*\Gamma_5$	•		•		•		•		ω_5
Γ_6	•				•				ω_6
$^*\Gamma_7$		•		•		•		•	ω_5
Γ_8		•		•					ω_6
Γ_9			•				•		ω_6
$^*\Gamma_{10}$				•	•		•	•	ω_3
$^*\Gamma_{11}$				•	•		•	•	ω_4
Γ_{12}						•		•	ω_6

Table 4.3: Connectivity Table of Relaxation Trajectory Network.

Stiffness Model	Relaxed Natural Frequency					
	ω_1	ω_2	ω_3	ω_4	ω_5	ω_6
1	Γ_1	Γ_2	Γ_3	Γ_4	Γ_5	Γ_6
2	Γ_1	Γ_2	Γ_3	Γ_4	Γ_7	Γ_8
3	Γ_1	Γ_2	Γ_3	Γ_4	Γ_5	Γ_9
4	Γ_1	Γ_2	Γ_{10}	Γ_{11}	Γ_7	Γ_8
5	Γ_1	Γ_2	Γ_{10}	Γ_{11}	Γ_5	Γ_6
6	Γ_1	Γ_2	Γ_3	Γ_4	Γ_7	Γ_{12}
7	Γ_1	Γ_2	Γ_{10}	Γ_{11}	Γ_5	Γ_9
8	Γ_1	Γ_2	Γ_{10}	Γ_{11}	Γ_7	Γ_{12}

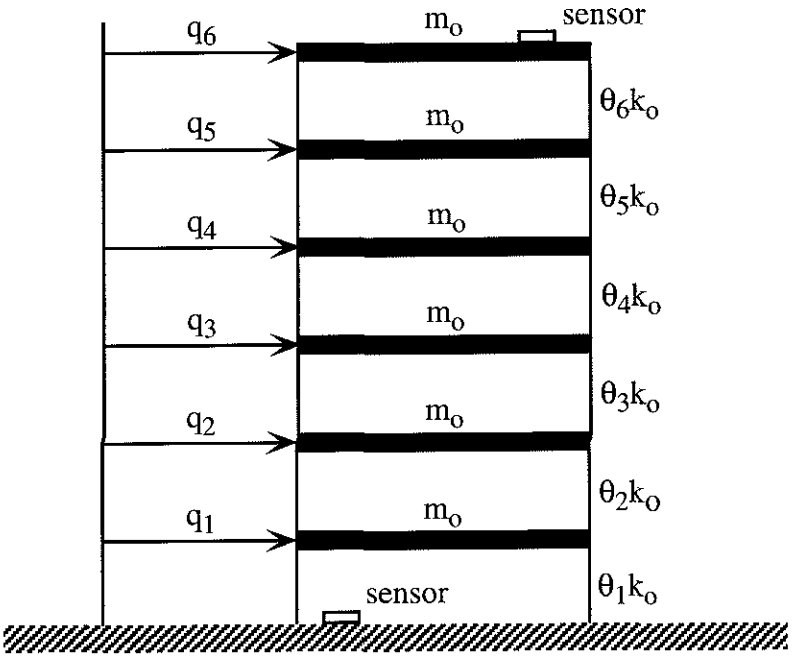

Figure 4.1: Six-Degrees-of-Freedom Linear Chain Model of a Six-Story Building.

Chapter 5

Applications to Simulated and Real Structural Response Data

5.1 Single-Degree-of-Freedom System

In this example, the class of single-degree-of-freedom linear oscillators is chosen to model a single-degree-of-freedom system subject to earthquake ground motion $\ddot{z}(t)$. The equation of motion of a single-degree-of-freedom linear oscillator is given by:

$$\ddot{q}(t) + 2\zeta\omega\dot{q}(t) + \omega^2 q(t) = -\ddot{z}(t).$$

Therefore, the vector of model parameters $\underline{a}$ for the class of models considered contains the natural frequency $f = \frac{\omega}{2\pi}$ and the damping factor ζ, i.e., $\underline{a} = [f, \zeta]^T$. The particular earthquake ground acceleration record used is the S00E component of the 1940 Imperial Valley earthquake recorded at the El Centro Imperial Valley Irrigation District. Because that ground acceleration record has strong components in the frequency range between 1 Hz and 3 Hz, the system to be identified is assumed to have natural frequency f_o equal to 2 Hz and damping factor ζ_o equal to 5% of critical. No modeling error and measurement noise is considered in this example. Thus, in contrast to real structural systems, the system considered lies in the chosen class of models.

By using the first 10 seconds of the selected ground acceleration record, the relative acceleration of the system is simulated and treated as the measured response. Then, the objective function $J_E(\underline{a})$ is calculated for different values of the natural frequency f and damping factor ζ. Because of the absence of modeling error and measurement noise, it is clear that $J_E(\underline{a})$ has a unique global minimum at $[f_o, \zeta_o]^T$

and the minimum value of $J_E(\underline{a})$ is equal to zero. A contour plot of $J_E(\underline{a})$ with the natural frequency f in the range between 1 Hz and 3 Hz and the damping factor ζ in the range between 1% and 14% is shown in Figure 5.1. The corresponding three-dimensional mesh plot of $J_E(\underline{a})$ is also shown in Figure 5.1.

It is noted from Figure 5.1 that the value of $J_E(\underline{a})$ is generally decreasing with increasing damping factor and the fluctuation with respect to the natural frequency is not noticeable when the damping factor is large. This is due to the fact that the response of a linear oscillator is less sensitive to the natural frequency and damping factor as the damping factor increases. On the other hand, the value of $J_E(\underline{a})$ is larger when a linear oscillator has a small damping factor. This is also expected because the response of a linear oscillator grows when its damping factor is smaller. The exception is when the natural frequency of a linear oscillator is close to f_o. In that case, the value of $J_E(\underline{a})$ increases as the damping factor deviates from ζ_o. Another feature of $J_E(\underline{a})$ is that its value depends on the natural frequency in some periodic fashion when the damping factor is small.

To identify the system's natural frequency f_o and damping factor ζ_o, the Fixed-Point homotopy scheme is applied to search for the global minimum of $J_E(\underline{a})$ in the parameter space specified above. The initial guess of $[f_o, \zeta_o]^T$ for twelve different homotopy trajectories $\{\Gamma_1, \ldots, \Gamma_{12}\}$ are summarized in Table 5.1. All of these homotopy trajectories successfully reach both f_o and ζ_o. Plots of these homotopy trajectories are shown in Figures 5.2 - 5.4. In these plots, a "$*$" mark is placed at each initial guess of $[f_o, \zeta_o]^T$, and a "o" mark is placed at $[f_o, \zeta_o]^T$.

For comparison, the popular Quasi-Newton method for optimization is also applied to identify f_o and ζ_o using the same 12 initial guesses as the homotopy scheme. It turns out that the search is successful with only three initial guesses which correspond to the initial guesses for homotopy trajectories Γ_5, Γ_7, and Γ_9. A possible reason for the poor performance of the Quasi-Newton method in this example is that a suitable initial search direction is not found and the method lacks a mechanism to resume the search when the search becomes not promising. On the other hand, the

homotopy scheme is robust in the sense that if the homotopy trajectory reaches a region in which no convergence to a solution is possible as the homotopy parameter λ approaches 1, the homotopy trajectory automatically makes a turn to avoid contradiction so that the homotopy parameter starts decreasing and new search directions can be devised. This feature is demonstrated in the three-dimensional plots of the homotopy trajectories shown in Figures 5.2 - 5.4.

5.2 Two-Story Structure with Known Damping

5.2.1 Without Measurement Noise

Consider the class of two-degrees-of-freedom linear chain models with classical normal modes which is used to model a two-story structure subject to earthquake ground motion $\ddot{z}(t)$ as illustrated in Figure 5.5. The two masses m_1 and m_2 of the structure are assumed to be known and equal to m_o. The damping factor of each mode of the structure is also assumed known and set equal to 5% of critical. The two stiffness parameters k_1 and k_2 of the structure are unknown and are parameterized by using two normalized non-dimensional parameters θ_1 and θ_2 such that $k_1 = \theta_1 k_o$ and $k_2 = \theta_2 k_o$, where k_o is a nominal stiffness. The equations of motion of a two-degrees-of-freedom linear chain model are given by:

$$M\underline{\ddot{q}}(t) + C\underline{\dot{q}}(t) + K\underline{q}(t) = -M\underline{1}\ddot{z}(t),$$

where

$$\underline{q}(t) = [q_1(t), q_2(t)]^T,\ M = \begin{bmatrix} m_o & 0 \\ 0 & m_o \end{bmatrix},\ \text{and } K = k_o \begin{bmatrix} \theta_1 + \theta_2 & -\theta_2 \\ -\theta_2 & \theta_2 \end{bmatrix}.$$

The vector of model parameters $\underline{a}$ for the class of two-degrees-of-freedom linear chain models contains the two stiffness parameters θ_1 and θ_2, i.e., $\underline{a} = \underline{\theta} = [\theta_1, \theta_2]^T$. The values of m_o and k_o are chosen such that the two natural frequencies of the structure are equal to 1 Hz and 2.6 Hz for $\underline{\theta}_o = [1, 1]^T$. By using the first 10

seconds of the same earthquake ground acceleration record as in Section 5.1, the relative acceleration of the structure at the top degree of freedom is simulated and considered as the measured response. The objective function $J_E(\underline{\theta})$ is then calculated for different values of θ_1 and θ_2. A contour plot of $J_E(\underline{\theta})$ with $\underline{\theta}$ in the range $[0.7, 3.2] \times [0.3, 1.9]$ is shown in Figure 5.6. The corresponding three-dimensional mesh plot of $J_E(\underline{\theta})$ is also shown in Figure 5.6.

It is noted that there exists one major "banana valley" in Figure 5.6. This feature can be explained in terms of the dependence of the two natural frequencies ω_1 and ω_2 of a two-degrees-of-freedom linear chain model on the stiffness parameters $\underline{\theta}$. It can be shown that ω_1 and ω_2 are given by:

$$\begin{cases} \omega_1 = c\sqrt{\theta_1 + 2\theta_2 - \sqrt{\theta_1^2 + 4\theta_2^2}} \ , \text{ and} \\ \omega_2 = c\sqrt{\theta_1 + 2\theta_2 + \sqrt{\theta_1^2 + 4\theta_2^2}} \ , \end{cases} \tag{5.2.1}$$

where $c = \sqrt{\frac{k_o}{2m_o}}$. By plotting the contour line for ω_1 using the formula given in (5.2.1), it turns out that the contour line for ω_1 is essentially parallel to the valley and therefore ω_1 along the valley basically remains unchanged. Moreover, the valley goes through the structure's parameter values, i.e., $\underline{\theta}_o$. Therefore, ω_1 along the floor of the valley is very close to the first natural frequency of the structure. Furthermore, the variation of the modal participation factor of the first mode for the top degree of freedom is slow along the valley. Hence, the response of the first mode of any model along the valley is similar. Since the response of the first mode dominates the total response, all of the models along the valley have a response similar to the structure's and so $J_E(\underline{\theta})$ has a small value along the floor of the valley. Note also that the minor "banana valley" appears in Figure 5.6 is where the natural frequency of the first mode matches 1.5 Hz.

It has been proved that there exists an "output-equivalent" structure which also lies along the valley and gives exactly the same two natural frequencies and modal participation factors as the specified structure [1]. The equivalent structure has

stiffness parameters $\underline{\theta}_e = [2, \frac{1}{2}]^T$. So, $J_E(\underline{\theta})$ has two global minima and its minimum value is equal to zero. To identify the specified structure and the equivalent structure, both the Quasi-Newton method and the Fixed-Point homotopy scheme are applied to search for the two global minima of $J_E(\underline{\theta})$, i.e., $\underline{\theta}_o$ and $\underline{\theta}_e$. Four different initial guesses of $\underline{\theta}_o$ and $\underline{\theta}_e$ are chosen. The result is that all four homotopy trajectories $\{\Gamma_1, \ldots, \Gamma_4\}$ successfully reach either $\underline{\theta}_o$ or $\underline{\theta}_e$. Plots of these homotopy trajectories are shown in Figure 5.7 with a "$*$" mark placed at each initial guess of $\underline{\theta}_o$ or $\underline{\theta}_e$ and a "$\circ$" mark placed at both $\underline{\theta}_o$ and $\underline{\theta}_e$. It turns out that the Quasi-Newton method is successful with only one initial guess which corresponds to the initial guess of the homotopy trajectory Γ_2. Since the other three initial guesses are quite far away from the floor of the major "banana valley," the Quasi-Newton method may have difficulty in selecting a suitable initial search direction and therefore cannot converge.

As explained in Chapter 3, the relaxation scheme can be applied to systematically search the parameter space and find other local minima of $J_E(\underline{\theta})$ from any given local minima (or more generally, any stationary point) of $J_E(\underline{\theta})$. In particular, each of the following stationarity conditions on $J_E(\underline{\theta})$:

$$\frac{\partial J_E(\underline{\theta})}{\partial \theta_1} = 0 \tag{5.2.2}$$

and

$$\frac{\partial J_E(\underline{\theta})}{\partial \theta_2} = 0 \tag{5.2.3}$$

can be relaxed alternately to generate two relaxation trajectories from each given local minima of $J_E(\underline{\theta})$. Plots of these two relaxation trajectories are shown in Figures 5.8 and 5.9. From these plots, it is demonstrated that any one of the global minima of $J_E(\underline{\theta})$ can be reached by either relaxation trajectory given the other global minimum of $J_E(\underline{\theta})$. It is noted that these two relaxation trajectories are roughly parallel to the major "banana valley" and are quite close to each other. This is because the valley is very narrow. Furthermore, there exists a saddle point $\underline{\theta}_s$, which is marked by "$\times$"

in Figures 5.8 and 5.9, between $\underline{\theta}_o$ and $\underline{\theta}_e$ along the valley. The particular model corresponding to the saddle point has stiffness parameters $\underline{\theta}_s = [1.307, 0.654]^T$.

5.2.2 With Measurement Noise

To simulate more realistic situations, a Gaussian white noise sequence is added to the simulated acceleration of the two-story structure in Section 5.2.1 and the resulting signal is treated as the measured response. Because of the existence of noise, both the specified structure and the equivalent structure cannot exactly generate the measured response. The optimal model $\hat{\underline{\theta}}$ in the given class of models needs to be found by searching for the global minimum (which is not zero) of the objective function $J_E(\underline{\theta})$. A series of case studies is performed to determine the change of $\hat{\underline{\theta}}$ due to different levels of noise. The standard deviation of the added Gaussian white noise sequence is chosen to be a certain fraction of the RMS acceleration of the second mode of the structure which is equal to 36.5 cm/sec/sec. Also, the sensitivity of $\hat{\underline{\theta}}$ to the level of noise is investigated by comparing the value $J_E(\hat{\underline{\theta}})$ with a reference value $J_E(\underline{\theta}_s)$, where $\underline{\theta}_s$ is the saddle point in Figures 5.8 and 5.9.

For the level of noise between 0% and 460%, two optimal models $\hat{\underline{\theta}}^{(1)}$ and $\hat{\underline{\theta}}^{(2)}$ are found and the values of $\hat{\underline{\theta}}^{(1)}$, which is closer to $\underline{\theta}_o$, are shown in Figure 5.10 by using the mark "×" for lower levels of noise. The modal parameters of $\hat{\underline{\theta}}^{(1)}$ are summarized in Table 5.2. The highest level of noise corresponds to 73% of the RMS of the total structural acceleration. When no noise is added, $\hat{\underline{\theta}}^{(1)}$ coincides with $\underline{\theta}_o$. As the level of noise increases, $\hat{\underline{\theta}}^{(1)}$ start moving away from $\underline{\theta}_o$ along the major "banana valley." This is expected since, as long as the noise is not too much, the second mode is influenced more by the noise than the first mode. Therefore, the first natural frequency of the optimal model is very close to the structure's. But the second natural frequency of the optimal model is larger than the structure's because of the slight shift of the frequency content of the measured response towards the high frequency range due to noise.

In Figure 5.11, $J_E(\hat{\underline{\theta}})$ and $J_E(\underline{\theta}_s)$ are plotted as a function of the level of noise. A "×" mark is used to denote the value $J_E(\hat{\underline{\theta}})$ for lower levels of noise and a "+"

mark is used to denote the value $J_E(\underline{\theta}_s)$ in Figure 5.11. When no noise is added, $J_E(\hat{\underline{\theta}})$ is equal to zero. As the level of noise increases, both $J_E(\hat{\underline{\theta}})$ and $J_E(\underline{\theta}_s)$ increase but at the same time the two values are also getting closer to each other. The result is that the floor of the major "banana valley" becomes flatter as the level of noise increases. From the numerical point of view, this makes the estimation of the second mode less reliable and subsequently the estimation of the optimal model $\hat{\underline{\theta}}$ also is less reliable. From the standpoint of system identification, the second mode becomes less observable and so the identification of the structure becomes more like an un-identifiable case.

As the level of noise reaches 260%, two additional local minima $\tilde{\underline{\theta}}^{(1)}$ and $\tilde{\underline{\theta}}^{(2)}$ of $J_E(\underline{\theta})$ suddenly emerge. The values of $\tilde{\underline{\theta}}^{(1)}$, which is further away from $\underline{\theta}_o$ than $\hat{\underline{\theta}}^{(1)}$, are shown by using the "o" mark in Figure 5.10 for noise levels just above 260%. The modal parameters of $\tilde{\underline{\theta}}^{(1)}$ are summarized in Table 5.3. The value $J_E(\tilde{\underline{\theta}})$ for these same noise levels is also shown in Figure 5.11 by using the "o" mark. $\tilde{\underline{\theta}}^{(1)}$ and $\tilde{\underline{\theta}}^{(2)}$ correspond to two particular models whose first natural frequency is close to the first natural frequency of $\hat{\underline{\theta}}^{(1)}$ and $\hat{\underline{\theta}}^{(2)}$ but whose second natural frequency is slightly higher. These two models also produce a good fit to the measured response but the fit is not as good as the one produced by $\hat{\underline{\theta}}^{(1)}$ and $\hat{\underline{\theta}}^{(2)}$, until the level of noise is greater than 360%, when the two local minima at $\tilde{\underline{\theta}}^{(1)}$ and $\tilde{\underline{\theta}}^{(2)}$ actually become the global minima. The consequence is a sudden jump in the stiffness parameters of the optimal models at a level of noise of about 360%, as illustrated in Figure 5.10. Based on this observation, it is possible to have four optimal models at the same time for a certain level of noise.

The results of identification of the specified two-story structure are presented in detail for two cases. In the first case, the level of noise is equal to 100% and represents the situation of less noisy measurement. In the second case, the level of noise is increased to 300% to account for situations with much higher noise. The topology of the function $J_E(\underline{\theta})$ for these two cases is very similar to the case in Section 5.2.1 except for the details of the variation inside the major "banana valley." In the

first case, two optimal models $\hat{\underline{\theta}}^{(1)}$ and $\hat{\underline{\theta}}^{(2)}$ are identified by using the Fixed-Point homotopy scheme as shown by the "o" mark in Figure 5.12. The two optimal models have stiffness parameters $\hat{\underline{\theta}}^{(1)} = [0.999, 1.002]^T$ and $\hat{\underline{\theta}}^{(2)} = [2.005, 0.499]^T$ respectively. Furthermore, $\hat{\underline{\theta}}^{(1)}$ and $\hat{\underline{\theta}}^{(2)}$ are "connected" by the two relaxation trajectories and there is a saddle point in between as shown in Figure 5.13 by using the mark "×." The particular model corresponding to the saddle point has stiffness parameters $\underline{\theta} = [1.307, 0.654]^T$.

In the second case, the Fixed-Point homotopy scheme identifies two local minima $\tilde{\underline{\theta}}^{(1)}$ and $\tilde{\underline{\theta}}^{(2)}$ of $J_E(\underline{\theta})$ and two optimal models $\hat{\underline{\theta}}^{(1)}$ and $\hat{\underline{\theta}}^{(2)}$ as shown in Figure 5.14. In Figure 5.14, a "•" mark is placed at $\tilde{\underline{\theta}}^{(1)}$ and $\tilde{\underline{\theta}}^{(2)}$, and a "o" mark is placed at $\hat{\underline{\theta}}^{(1)}$ and $\hat{\underline{\theta}}^{(2)}$. The two optimal models have stiffness parameters $\hat{\underline{\theta}}^{(1)} = [0.997, 1.011]^T$ and $\hat{\underline{\theta}}^{(2)} = [2.021, 0.498]^T$ respectively. The relaxation scheme is applied at each local minimum or optimal model which is found by the Fixed-Point homotopy scheme. Actually, both relaxation trajectories connect the two local minima and two optimal models as shown in Figures 5.15 and 5.16. It is interesting to note that in this case there are three saddle points, marked by "×"in Figures 5.15 and 5.16, separating the two local minima and two optimal models. The particular models corresponding to these saddle points have stiffness parameters $\underline{\theta} = [0.936, 1.237]^T$, $\underline{\theta} = [1.308, 0.654]^T$, and $\underline{\theta} = [2.473, 0.468]^T$ respectively. The measured acceleration and the output of the two optimal models are shown in Figure 5.17 for comparison and the Fourier amplitude spectra of the actual and measured accelerations are shown in Figure 5.18.

5.3 Two-Story Structure with Unknown Damping

5.3.1 Without Measurement Noise

The two-story structure identified in Section 5.3 is again considered and is modeled using the class of two-degrees-of-freedom linear chain models. But, instead of assuming the two damping factors of the structure are known, the two damping factors are now considered as part of the model parameters. Therefore, the vector of model parameters $\underline{a}$ contains the two stiffness parameters and two damping factors,

i.e., $\underline{a} = [\underline{\theta}^T, \underline{\zeta}^T]^T = [\theta_1, \theta_2, \zeta_1, \zeta_2]^T$. The two-story structure to be identified is again chosen to have stiffness parameters $\underline{\theta}_o = [1, 1]^T$ and damping factors $\underline{\zeta}_o = [5\%, 5\%]^T$. By using the first 10 seconds of the same earthquake ground acceleration record as in Sections 5.1 and 5.2, the relative acceleration of the structure at the top degree of freedom is calculated and used as the measured response. As explained in Section 5.2.1, there exists an equivalent structure which has the same damping factors $\underline{\zeta}_o$ as the specified structure but different stiffness parameters $\underline{\theta}_e = [2, \frac{1}{2}]^T$. Hence, the objective function $J_E(\underline{a})$ has two global minima and its minimum value is equal to zero.

The Fixed-Point homotopy scheme is applied to search for the two global minima of $J_E(\underline{a})$ using four different initial guesses for the model parameters of the specified structure and the equivalent structure. The initial guesses for $\underline{\theta}_o$ and $\underline{\theta}_e$ are chosen to be close to these used in Section 5.2.1 in order to compare the behavior of the homotopy trajectories, but the initial guesses of $\underline{\zeta}_o$ also need to be chosen in this example. All four homotopy trajectories successfully reach either one of the global minima of $J_E(\underline{a})$ as shown in Figure 5.19. In Figure 5.19, a "$*$" mark is placed at each initial guess for $\underline{\theta}_o$, $\underline{\theta}_e$, and $\underline{\zeta}_o$ while a "o" mark is placed at each global minimum of $J_E(\underline{a})$. Since there is a total of four parameters, giving a four-dimensional space, the projection of each homotopy trajectory on the $\zeta_1 - \zeta_2$ plane and $\theta_1 - \theta_2$ plane is shown.

From Figure 5.19, it is noted that the projection of homotopy trajectory on the $\theta_1 - \theta_2$ plane is similar to these in Section 5.2.1 except for trajectory Γ_4. This result shows that considering the two damping factors as part of the model parameters has little effect on the homotopy trajectory as far as the projection on the $\theta_1 - \theta_2$ plane is concerned. This is reasonable since damping factors have less influence on the response than stiffness parameters which control the natural frequencies and modal participation factors. It is also demonstrated in Figure 5.19 that the convergence of ζ_2 is much slower than ζ_1 and the convergence of each damping factor is "monotonic" except for trajectory Γ_4. The robustness of the homotopy scheme is

best demonstrated by trajectory Γ_4. The initial trajectory orientation is actually not promising in reaching either global minimum of $J_E(\underline{a})$, but the trajectory can make turns and eventually reaches one of the global minima of $J_E(\underline{a})$.

The relaxation scheme is then applied to search the parameter space for all the local minima of $J_E(\underline{a})$ in the region considered by relaxing each of the following stationarity conditions on $J_E(\underline{a})$ alternately:

$$\frac{\partial J_E(\underline{a})}{\partial \theta_1} = 0 \text{ and } \frac{\partial J_E(\underline{a})}{\partial \theta_2} = 0, \tag{5.3.1}$$

$$\frac{\partial J_E(\underline{a})}{\partial \zeta_1} = 0 \text{ and } \frac{\partial J_E(\underline{a})}{\partial \zeta_2} = 0. \tag{5.3.2}$$

Four relaxation trajectories are generated and the projection of each relaxation trajectory on the $\zeta_1 - \zeta_2$ plane and $\theta_1 - \theta_2$ plane is shown in Figures 5.20 - 5.23. Because of projection, some of the trajectories seem to terminate prematurely. What really happens to these trajectories is that they simply reach the boundary of the specified parameter space. It is noted that there exists a saddle point, which is marked by "×," between the two global minima of $J_E(\underline{a})$. The particular model corresponding to the saddle point has stiffness parameters $\underline{\theta} = [1.304, 0.652]^T$ and damping factors $\underline{\zeta} = [5.19\%, 14.06\%]^T$.

It is noted from Figures 5.20 and 5.21 that the two global minima of $J_E(\underline{a})$ and the saddle point are connected by the two relaxation trajectories which are generated by relaxing the constraints in (5.3.1). On the other hand, the two global minima are not connected by the two relaxation trajectories which are generated by relaxing the constraints in (5.3.2). Still, one global minimum of $J_E(\underline{a})$ can be reached by following the first two relaxation trajectories from the other global minimum of $J_E(\underline{a})$. These two relaxation trajectories are quite close to each other just as the case in Section 5.2.1. This suggests that there may also exist some kind of "banana valleys" in the four-dimensional parameter space in this case.

5.3.2 With Measurement Noise

To simulate more realistic situations, the same Gaussian white noise sequence used in Section 5.2.2 is added to the simulated acceleration of the structure and the resulting signal is considered as the measured response. To investigate the effect of considering the two damping factors as part of the model parameters, the two cases of system identification presented in Section 5.2.2 are again considered.

In the first case, the level of noise is set equal to 100% which corresponds to 16% of the RMS of the total acceleration of the structure. Two optimal models $\underline{\hat{a}}^{(1)}$ and $\underline{\hat{a}}^{(2)}$ are found by using the Fixed-Point homotopy scheme. The projection of these homotopy trajectories are illustrated in Figure 5.24 with a "o" mark placed at both $\underline{\hat{a}}^{(1)}$ and $\underline{\hat{a}}^{(2)}$. The behavior of these homotopy trajectories is similar to the case in Section 5.3.1. The two optimal models have the same damping factors $\underline{\hat{\zeta}} = [4.99\%, 5.77\%]^T$ but different stiffness parameters $\underline{\hat{\theta}}^{(1)} = [0.999, 1.001]^T$ and $\underline{\hat{\theta}}^{(2)} = [2.002, 0.499]^T$ respectively. It is noted that the two optimal models have similar parameter values as the specified structure and the equivalent structure except that the damping factor of the second mode is slightly higher.

In the second case, the level of noise is equal to 300%. It turns out that only two optimal models $\underline{\hat{a}}^{(1)}$ and $\underline{\hat{a}}^{(2)}$ are identified. This result is different from the second case in Section 5.2.2. In this case, no other local minimum of $J_E(\underline{a})$ is found. The projected homotopy trajectories are shown in Figure 5.25 with a "o" mark placed at both $\underline{\hat{a}}^{(1)}$ and $\underline{\hat{a}}^{(2)}$. The behavior of these trajectories is similar to the case in Section 5.3.1 except that the convergence of the damping factor of the second mode is very slow. The two optimal models have the same damping factors $\underline{\hat{\zeta}} = [4.94\%, 9.23\%]^T$ but different stiffness parameters $\underline{\hat{\theta}}^{(1)} = [0.985, 1.046]^T$ and $\underline{\hat{\theta}}^{(2)} = [2.091, 0.493]^T$ respectively. It is noted that the damping factor of the second mode of the two optimal models is much higher than the corresponding damping factor of the structure.

The projection of four relaxation trajectories in this case are shown in Figures 5.26 - 5.29. Unlike the second case in Section 5.2.2, there is only one saddle point,

which is marked by "×" in Figures 5.26 - 5.29, between the two optimal models. The particular model corresponding to the saddle point has stiffness parameters $\underline{\theta} = [1.304, 0.652]^T$ and damping factors $\underline{\zeta} = [5.15\%, 26.61\%]^T$. It is noted that the two optimal models and the saddle point are connected by three relaxation trajectories which are generated by relaxing the two constraints in (5.3.1) and the first constraint in (5.3.2). This is different from the second case in Section 5.2.2. It is also noted from Figures 5.26 and 5.27 that these two relaxation trajectories are quite close to each other just as the case in Section 5.3.1. Therefore, the existence of "banana valleys" in the four-dimensional parameter space is also possible in this case. The measured acceleration and the output of the two optimal models are shown in Figure 5.30 for comparison.

5.4 Ten-Story Building

5.4.1 Background Information

The building considered in this example is the Great Western Bank located at 111 Market Street in San Jose, California. It is a ten-story rectangular reinforced-concrete office building with overall plan dimensions of 190 ft. by 82 ft., a total height of 124 ft. above the ground surface, and a single basement level of 17 ft. below the ground surface. The story height is 12 ft. except for the first story whose height is 16 ft. The building's lateral force resisting system consists of exterior shear walls in the transverse (East-West) direction and moment-resisting frames in the longitudinal (North-South) direction. The foundation of the building consists of a 5 ft. thick reinforced-concrete mat. More detailed configuration information about the building can be found in [2].

The California Division of Mines and Geology (CDMG) has deployed an array of 13 strong motion accelerometers at the Great Western Bank under the California Strong Motion Instrumentation Program (CDMG station number 57355). The deployment of these accelerometers in the building is illustrated in Figure 5.31. This accelerometer array can measure transverse translations, longitudinal translations, and torsional rotations at the roof, fifth floor, and the basement. In addition, the

array also measures the longitudinal translations at the second floor, vertical translations, rocking rotations about the building's longitudinal axis, and transverse deformation of the fifth floor diaphragm. The particular seismic acceleration records of the building used in this example were recorded during the 1984 Morgan Hill Earthquake ($M_s = 6.2$). The building is located about 12 miles west of the epicenter of that earthquake.

There have been some studies of the seismic response characteristics of the building and references to previous studies can be found in [2]. In particular, the modal identification technique has been applied to estimate the modal parameters of the significant modes of the building by using the proven computer program MODE-ID [2]. The identified mode shape amplitudes at the instrumented floors were used to estimate the complete mode shape amplitudes at all the floors by using interpolation. Subsequently, the earthquake-induced base shear force, base overturning moment, lateral interstory shear force, and interstory drift were estimated based on modal superposition using the identified modal periods and damping ratios, as well as the interpolated mode shape amplitudes. An assessment of the UBC seismic design provisions as applied to the building was made by comparing the estimated earthquake-induced responses with the UBC seismic design values.

5.4.2 Structural Model Updating

In this example, instead of using the modal identification approach, the earthquake-induced response of the building is estimated by using a class of structural models with classical normal modes. The results of identification are compared with the corresponding values obtained from the modal identification approach presented in [2]. Based on the results of modal identification, only five significant modes of the building can be identified. They are the first two translational modes in the transverse and longitudinal directions and the fundamental torsional mode. The results also indicate that there is little coupling between the vibration in the transverse and longitudinal directions. Therefore, the seismic response characteristics of the building in the transverse and longitudinal directions are studied separately in

this example. It is also assumed that rocking of the building about the transverse axis can be neglected but rocking about the longitudinal axis needs to be considered.

In modeling the building, the same lumped mass of weight 2700 kips is used for each floor. One degree of freedom is assigned to describe the rigid-floor horizontal translation of each floor. Since only the fifth floor and the roof are instrumented in both directions and only the first two modes in each direction are considered to be significant, the stiffness matrix will become un-identifiable if it is overparameterized as discussed in Chapter 4. In this example, it is not feasible to have one stiffness parameter for each story of the building since then there will be too many parameters. Therefore, a substructuring approach is needed in which the building is decomposed into a small number of substructures and a stiffness parameter scales each substructure stiffness matrix. A convention is established to denote a particular substructure configuration. For example, a notation like "4-6" means that there are two substructures and the first substructure contains the lower four stories and the second substructure contains the upper six stories. Each substructure is modeled by using uniform linear chain models. The stiffness parameters are calibrated such that when their values are all equal to one, the building is modeled as a uniform linear chain model. The nominal stiffness is chosen such that the first two model natural frequencies are close to the values estimated by using MODE-ID and is equal to 3.73×10^5 kips/ft in the transverse direction and 2.17×10^5 kips/ft in the longitudinal direction.

To account for rocking about the longitudinal axis of the building, two different types of models are used in the transverse direction in this example. The first type of model is called the "rocking-base" model in which the vertical motion records at the base of the building are included in the set of output measurement [2]. Therefore, the identified mode shape amplitudes contain contributions from rocking rotations about the base of the building. The second type of model is called the "fixed-base" model in which the vertical motion records at the base of the building are included in the set of input motions for the building [2]. Therefore, the effects of rocking

rotations are contained in the pseudostatic response and the identified mode shape amplitudes will not exhibit any rocking rotations.

5.4.3 Discussion of Identified Model Parameters

The seismic response characteristics of the building in the transverse direction are considered first by using two substructures to model the building. To investigate the change of optimal model parameters due to different substructure configurations, five substructure configurations "3-7", "4-6", "5-5", "6-4", and "7-3" are studied. Two non-dimensional stiffness parameters θ_1 and θ_2 are used to parameterize the two substructures in each configuration. The Fixed-Point homotopy method was used to identify the optimal parameters for the rocking-base model. The optimal damping factors and stiffness parameters, along with the corresponding natural periods and optimal values of J_E, are summarized in Table 5.4. The corresponding natural periods and damping factors obtained by using MODE-ID are shown in the last column of Table 5.4 for comparison.

From Table 5.4, it is noted that the optimal models for the three substructure configurations "5-5", "6-4", and "7-3" are similar and essentially equivalent to uniform linear chain models. This result can be explained by using modal superposition. In order for the model output to have a good fit with the measured acceleration, the first two natural frequencies of a model need to be close to the first two dominant frequencies in the measured acceleration. Furthermore, the ratios between the mode shape amplitudes at the measured degrees of freedom are also important especially for the first mode since it dominates the overall model response. An analysis is done to study the change of the first two natural frequencies and mode shape amplitudes of the five substructure configurations for different values of the stiffness parameters. It turns out that substructure configurations "5-5", "6-4", and "7-3" are similar in that aspect. Therefore, the optimal models for these three substructure configurations are similar. The behavior of substructure configurations "4-6" and "3-7" is different from the other three configurations so that the optimal models for these two configurations are different from uniform chain models. In fact, the optimal model

for configuration "3-7" shows a significant difference between the stiffness of the two substructures.

For all the substructure configurations considered, the identified natural periods are close to the corresponding values estimated by using MODE-ID. The identified damping factors of the first mode are slightly smaller than the values estimated by using MODE-ID. However, the identified damping factors of the second mode are larger, especially for the substructure configuration "3-7". A possible reason is that the optimal modal participation factor of the second mode at the roof is larger when compared with the corresponding value of the other substructure configurations and so the damping is increased to give a better match of the response amplitude. Based on the optimal values of J_E, the output of all of the five optimal models has a similar fit to the measured response, although the output of the optimal model for the substructure configuration "3-7" has a slightly better fit.

The identified optimal damping factors and stiffness parameters, along with the corresponding natural periods and optimal values of J_E for the fixed-base model, are summarized in Table 5.5. The corresponding natural periods and damping factors obtained by using MODE-ID are shown in the last column of Table 5.5 for comparison. When compared with the results in Table 5.4, the lower substructure is much stiffer in the fixed-base case. This is because no rotational spring at the base is used in the rocking-base case to account for rocking so that the stiffness of the lower substructure needs to be smaller in order to account for the rocking flexibility of the base. It is noted that only the identified first natural periods are close to the value estimated by using MODE-ID. The identified second natural periods are shorter. Furthermore, the identified natural periods of the fixed-base model are shorter than the identified natural periods of the rocking-base model. This is reasonable since rocking has significant contribution in the transverse direction so that the apparent stiffness of the rocking-base model is smaller.

The difference between the identified second natural periods and the corresponding value obtained by using MODE-ID is more significant when the fixed-base model

is used. It is noted that the ratio between the first and second natural period estimated by using MODE-ID with the fixed-base model is about 2.43 but the ratio is about 2.84 when the rocking-base model is used. Because of the intrinsic constraints of the class of linear chain models, it turns out that all of the five substructure configurations could not match the target ratio close enough when the fixed-base model is used. Since the first natural period needs to be matched closely in order to have a good fit with the measured response, the second natural period turns out to be not estimated accurately.

The identified damping factors of the first mode are close to the value estimated by using MODE-ID and are also larger than the corresponding values when the rocking-base model is used. This is expected since the overall damping of the rocking-base model is lower because the damping of rocking about the base of the building is lower than the damping of the building itself. It is noted that the identified damping factors of the second mode are much larger than the value estimated by using MODE-ID. This may be due to the inaccurate estimation of the second natural period. By comparing the optimal values of J_E, it is concluded that the optimal model for the substructure configuration "3-7" is slightly better in matching the measured response than the other four configurations. Furthermore, it is noted that the fixed-base model is more capable in matching the measured response than the rocking-base model. This is because rocking is better modeled by using the pseudostatic response as in the fixed-based model.

For illustration, the identified seismic response characteristics of the building in the transverse direction are presented in detail for the substructure configuration "4-6" using both the rocking-base model and the fixed-base model. The projected homotopy trajectories in the identification of the optimal model for these cases are shown in Figures 5.32 and 5.33 respectively. It is noted that the convergence of the damping factor of the second mode is very slow, just as in Section 5.3. The measured acceleration at the fifth floor and the roof, together with the corresponding response of the optimal model, are shown in Figures 5.34 and 5.35 for comparison. Generally

speaking, the phase of the measured acceleration is matched reasonably well by both types of models. But there is still some mismatch in the amplitudes. The time history plots also demonstrate that the match using the fixed-base model is slightly better than the one using the rocking-base model.

The seismic response characteristics of the building in the longitudinal direction are investigated by using five substructure configurations "2-8", "3-7", "4-6", "5-5", and "6-4". The identified optimal damping factors and stiffness parameters, and corresponding natural periods and optimal values of J_E, are summarized in Table 5.6. The corresponding natural periods and damping factors obtained by using MODE-ID are shown in the last column of Table 5.6 for reference. Both identified natural periods are very close to the values estimated by using MODE-ID. The identified damping factors of the first mode are slightly larger than the value estimated by using MODE-ID while the identified damping factors of the second mode are smaller.

It is noted that the optimal models for substructure configurations "3-7", "4-6", and "5-5" are similar in the sense that they have a similar stiffness ratio between the two substructures. This is because the change of the first two natural frequencies and mode shape amplitudes at the instrumented floors due to different values of the stiffness parameters for these three substructure configurations are similar. For the same reason, the two substructure configurations "2-8" and "6-4" give similar optimal models. For all of the five substructure configurations, the model output of the optimal models for the substructure configurations "5-5" and "6-4" can fit the measured response better.

It is also noted from Table 5.6 that the optimal models are not consistent with common intuition since the optimal value of θ_1 is smaller that the optimal value of θ_2. In other words, the stiffness of the lower substructure should not be less than the stiffness of the upper substructure for a typical building such as the Great Western Bank. This discrepancy is mainly due to the modeling error in using the linear chain models. In this case, the ratio between the first and second natural periods estimated by using MODE-ID is about 3.42. Because of the intrinsic internal constraints of

linear chain models, it turns out that, in order for linear chain models to have a close match for the target ratio, the optimal value of θ_1 needs to be smaller than the optimal value of θ_2.

For illustration, the identified seismic response characteristics of the building in the longitudinal direction by using the substructure configuration "5-5" are presented in detail. The projected homotopy trajectories in the identification of the optimal model are shown in Figure 5.36. The measured acceleration at the fifth floor and at the roof and the corresponding response of the optimal model are shown in Figure 5.37 for comparison. Because both natural periods are identified accurately, the phase of the measured acceleration is matched well. However, the match of the amplitude is less satisfactory because the damping factors and mode shape amplitudes at the instrumented floors are not estimated accurately. In this example, the measured acceleration at the 2nd floor is reserved to assess the prediction accuracy of the identified optimal model. The measured acceleration and predicted model acceleration at the 2nd floor are shown in Figure 5.38. From the time history plots, it is demonstrated that there is a good match between these responses.

The seismic response characteristics of the building in both directions are also studied by using more than two substructures to model the building. However, another important issue in structural model updating is noted. For example, the optimal model for the substructure configuration "4-3-3" using the rocking-base model in the transverse direction has the stiffness parameters $[1.16, 0.81, 1.35]^T$. It is noted that the stiffness of the top substructure which includes the top three stories of the building turns out to be the largest. This is again not consistent with common intuition for a typical building in which the distribution of stiffness along the height should be monotonically decreasing except for maybe the first story. Discrepancies of this kind appear in all of the studied substructure configurations which have more than two substructures. A possible cause of this discrepancy is explained in the following.

In structural model updating, the process of searching for the optimal structural

model can be interpreted as adjusting the stiffness of each substructure in order to obtain a best fit between the measured data and model output. However, the sensitivity of the model output at the measured degrees of freedom to the stiffness of each substructure is different. Some substructures have a more "global" influence on the model behavior in the sense that the model output at each degree of freedom in a structure is significantly affected. On the other hand, the influence of other substructures tends to be merely "local" in the sense that only the model output at those degrees of freedom, which are within or near that substructure, will be affected. In this example, a substructure which contains the lower stories generally will have more global influence on the model behavior than a substructure which contains the upper stories.

During the identification process, the adjustment of the stiffness of substructures which have less global influence on the model behavior is usually larger when compared with substructures which have more global influence on the model behavior. For the identified optimal model to have a physically feasible stiffness distribution, the stiffness of all the substructures are crucial regardless of their scope of influence on the model behavior. Therefore, it is quite possible that the resulting optimal stiffness of these insensitive substructures spoils the feasibility of the stiffness distribution given by the optimal model. This possibility can only be ruled out when the modeling error is negligible, which is not usually the case in practice. One way to avoid this discrepancy is to measure the response at the degrees of freedom which are either within or near these insensitive substructures so that more constraints can be exerted to control the stiffness of these substructures. If this is not possible, using larger substructures may also avoid this discrepancy although then the stiffness distribution in the structure may not be modeled appropriately.

5.4.4 Earthquake-Induced Force, Moment, and Drift

In Tables 5.7 - 5.10, the calculated peak interstory shear force and base overturning moment in the transverse direction by using both the rocking-base model and the fixed-base model are summarized. The corresponding values obtained by us-

ing MODE-ID and interpolation for the rocking-base case are also included in these tables for comparison. According to [2], the corresponding fixed-base model quantities obtained by using MODE-ID should be close to the rocking-base model values. From Tables 5.7 - 5.10, it is concluded that the base shear force and base overturning moment estimated by using the fixed-base model are slightly larger than the values estimated by using the rocking-base model. Moreover, the values obtained by using the fixed-base model are slightly smaller than the values inferred by the results from MODE-ID and interpolation. For illustration, the distribution of the peak interstory shear force along the height of the building is shown in Figure 5.39 using the optimal model for the substructure configuration "4-6". The corresponding time histories of the base shear force and base overturning moment and the corresponding UBC design values are shown in Figures 5.40 and 5.41.

The peak interstory shear force and base overturning moment in the longitudinal direction are summarized in Tables 5.11 and 5.12. The corresponding values obtained from MODE-ID and interpolation are also included in these tables for comparison. It is noted that the estimated peak interstory shear force is larger than the value estimated by using MODE-ID, especially for the lower stories of the building. The estimated peak base overturning moment is also larger than the value estimated by using MODE-ID and interpolation. In this aspect, it is concluded that linear chain models are less competent in modeling the structure in the longitudinal direction than in the transverse direction. Nevertheless, the distribution of the peak interstory shear force along the height of the building looks reasonable even though the stiffness of the lower substructure of the optimal models is smaller than the stiffness of the upper substructure. For illustration, the time histories of the base shear force and base overturning moment estimated by using the optimal model for the substructure configuration "5-5" are shown in Figure 5.42. The corresponding UBC design values are also included in Figure 5.42 for reference.

The peak interstory drift in the transverse direction is summarized in Tables 5.13 and 5.14 along with the values obtained by using MODE-ID and interpolation.

When compared with the latter results, the interstory drift at the upper stories of the building is underestimated when using either the rocking-base model or the fixed-based model. This is due to the use of a uniform linear chain model in each substructure. Moreover, the distribution of peak interstory drift along the height of the building is not always monotonic, because of a jump in the stiffness from the lower substructure to the upper substructure. Because rocking rotations about the base of the building are contained in the pseudostatic response when the fixed-base model is used, the discrepancy in estimating the interstory drift by using the linear chain model can be compensated to some extent. Therefore, the estimated interstory drift by using the fixed-base model is more reasonable in the sense that the distribution of interstory drift along the height of the building is more uniform.

The peak interstory drift in the longitudinal direction is summarized in Table 5.15 along with the values obtained by using MODE-ID and interpolation. When compared with the latter results, the interstory drift at the upper stories of the building is underestimated while the interstory drift at the lower stories is overestimated. This is due to the incompetence of linear chain models in modeling the structure in the longitudinal direction. Although the distribution of peak interstory drift along the height of the building is monotonic, there is still a noticeable jump in the distribution of peak interstory drift which is due to a jump in the stiffness from the lower substructure to the upper substructure.

In summary, reasonable response results are obtained in applying the proposed one-stage structural model updating approach to the seismic response records of the Great Western Bank even though some discrepancies are noticed. It is noted that the stiffness distribution of the identified optimal model may become physically unrealistic if too many or too few substructures are used. If the selected class of structural models is less competent in modeling the structure, as in the longitudinal direction in this example, the resulting stiffness distribution of the identified optimal model may also be physically unrealistic. In the case where the building is modeled by using two substructures, the identified modal parameters of the first mode are close to the

corresponding results obtained by using MODE-ID. The fit between the measured data and the model output of the identified optimal models is also reasonable. Furthermore, the estimated earthquake-induced base shear force, interstory shear force, and base overturning moment in the transverse direction are in good agreement with the corresponding values obtained by using MODE-ID and interpolation. However, the estimated interstory drift is less satisfactory due to the use of a uniform linear chain model in each substructure.

References for Chapter 5

1. Beck, J. L., *Determining Models of Structures from Earthquake Records*, Report No. EERL 78-01, California Institute of Technology, Pasadena, California, 1978.

2. Werner, S. D., Nisar, A., and Beck, J. L., *Assessment of UBC Seismic Design Provisions using Recorded Building Motions from Morgan Hill, Mount Lewis, and Loma Prieta Earthquakes*, Technical Report, Dames and Moore, Oakland, California, 1992.

Table 5.1: Initial Guesses of f_o and ζ_o for Homotopy Trajectories $\{\Gamma_1, \ldots, \Gamma_{12}\}$.

Trajectory	f_o (Hz)	ζ_o (%)
Γ_1	1.4	2.0
Γ_2	1.5	9.0
Γ_3	2.7	2.0
Γ_4	2.6	7.0
Γ_5	1.2	3.0
Γ_6	1.7	2.0
Γ_7	2.5	3.0
Γ_8	2.4	9.0
Γ_9	1.6	3.0
Γ_{10}	1.4	6.0
Γ_{11}	2.3	2.0
Γ_{12}	2.8	4.0

Table 5.2: Modal Parameters of $\hat{\underline{\theta}}^{(1)}$ for Different Levels of Noise ($\beta_2^{(1)}, \beta_2^{(2)}$ – Modal Participation Factors at Roof and $\beta_1^{(1)}, \beta_1^{(2)}$ – Modal Participation Factors at the 1st Floor).

Noise (%)	f_1 (Hz)	f_2 (Hz)	$\beta_2^{(1)}$	$\beta_2^{(2)}$	$\beta_1^{(1)}$	$\beta_1^{(2)}$
0	0.984	2.575	1.171	-0.171	0.724	0.276
20	0.984	2.576	1.171	-0.171	0.724	0.276
40	0.984	2.576	1.171	-0.171	0.724	0.276
60	0.984	2.576	1.171	-0.171	0.724	0.276
80	0.984	2.577	1.171	-0.171	0.724	0.276
100	0.984	2.577	1.171	-0.171	0.725	0.275
120	0.984	2.578	1.171	-0.171	0.725	0.275
140	0.984	2.578	1.170	-0.170	0.725	0.275
160	0.984	2.579	1.170	-0.170	0.725	0.275
180	0.984	2.579	1.170	-0.170	0.725	0.275
200	0.984	2.580	1.170	-0.170	0.726	0.274
220	0.984	2.580	1.170	-0.170	0.726	0.274
240	0.984	2.581	1.170	-0.170	0.726	0.274
260	0.984	2.582	1.170	-0.170	0.727	0.273
280	0.984	2.583	1.170	-0.170	0.727	0.273
300	0.984	2.584	1.170	-0.170	0.727	0.273
320	0.984	2.585	1.169	-0.169	0.728	0.272
340	0.984	2.586	1.169	-0.169	0.728	0.272
360	0.985	2.913	1.129	-0.129	0.823	0.177
380	0.985	2.919	1.128	-0.128	0.824	0.176
400	0.985	2.925	1.128	-0.128	0.825	0.175
420	0.985	2.930	1.127	-0.127	0.826	0.174
440	0.985	2.935	1.127	-0.127	0.827	0.173
460	0.985	2.939	1.127	-0.127	0.828	0.172

Table 5.3: Modal Parameters of $\underline{\tilde{\theta}}^{(1)}$ for Different Levels of Noise ($\beta_2^{(1)}, \beta_2^{(2)}$ – Modal Participation Factors at Roof and $\beta_1^{(1)}, \beta_1^{(2)}$ – Modal Participation Factors at the 1st *Floor*).

Noise (%)	f_1 (Hz)	f_2 (Hz)	$\beta_2^{(1)}$	$\beta_2^{(2)}$	$\beta_1^{(1)}$	$\beta_1^{(2)}$
260	0.984	2.851	1.135	-0.135	0.810	0.190
280	0.984	2.873	1.133	-0.133	0.815	0.185
300	0.985	2.887	1.132	-0.132	0.818	0.182
320	0.985	2.898	1.131	-0.131	0.820	0.180
340	0.985	2.906	1.130	-0.130	0.822	0.178
360	0.984	2.587	1.169	-0.169	0.729	0.271
380	0.984	2.589	1.169	-0.169	0.730	0.270
400	0.984	2.591	1.169	-0.169	0.730	0.270
420	0.984	2.593	1.168	-0.168	0.731	0.269
440	0.984	2.596	1.168	-0.168	0.733	0.267
460	0.984	2.600	1.167	-0.167	0.734	0.266

Table 5.4: Optimal Model Parameters (Transverse Direction) [Rocking-Base Model].

	Substructure Configurations					
	"3-7"	"4-6"	"5-5"	"6-4"	"7-3"	MODE-ID
θ_1	1.49	1.07	1.05	1.05	1.05	-
θ_2	0.79	1.01	1.04	1.05	1.07	-
T_1(sec)	0.616	0.615	0.615	0.616	0.616	0.608
T_2(sec)	0.213	0.209	0.207	0.207	0.206	0.214
ζ_1(%)	6.1	6.2	6.3	6.3	6.3	6.9
ζ_2(%)	28.2	10.6	9.6	9.4	9.4	3.7
J_E	0.260	0.261	0.262	0.262	0.262	-

Table 5.5: Optimal Model Parameters (Transverse Direction) [Fixed-Base Model].

	Substructure Configurations					
	"3-7"	"4-6"	"5-5"	"6-4"	"7-3"	MODE-ID
θ_1	2.96	2.03	1.86	1.72	1.60	-
θ_2	1.05	1.07	0.99	0.94	1.04	-
T_1(sec)	0.503	0.505	0.505	0.505	0.506	0.51
T_2(sec)	0.173	0.182	0.189	0.192	0.183	0.21
ζ_1(%)	6.6	6.7	6.9	7.1	7.1	6.8
ζ_2(%)	37.8	32.4	24.4	20.5	28.3	4.2
J_E	0.168	0.169	0.176	0.184	0.191	-

Table 5.6: Optimal Model Parameters (Longitudinal Direction).

	Substructure Configurations					
	"2-8"	"3-7"	"4-6"	"5-5"	"6-4"	MODE-ID
θ_1	0.47	0.61	0.69	0.73	0.75	-
θ_2	1.53	1.42	1.39	1.56	2.51	-
T_1(sec)	0.914	0.914	0.914	0.914	0.914	0.914
T_2(sec)	0.263	0.263	0.264	0.263	0.264	0.267
$\zeta_1(\%)$	4.3	4.3	4.3	4.2	4.1	3.9
$\zeta_2(\%)$	2.4	2.7	2.8	2.9	3.0	4.7
J_E	0.200	0.191	0.188	0.176	0.176	-

Table 5.7: Peak Interstory Shear Force (kips $\times 10^3$) (Transverse Direction) [Rocking-Base Model].

Story	Substructure Configurations					MODE-ID
	"3-7"	"4-6"	"5-5"	"6-4"	"7-3"	
10th	0.48	0.47	0.47	0.47	0.47	0.58
9th	0.96	0.93	0.93	0.93	0.93	1.06
8th	1.41	1.38	1.38	1.38	1.38	1.54
7th	1.84	1.81	1.81	1.81	1.81	1.98
6th	2.23	2.22	2.21	2.21	2.21	2.40
5th	2.57	2.58	2.59	2.59	2.59	2.77
4th	2.85	2.91	2.92	2.92	2.92	3.06
3rd	3.07	3.19	3.20	3.20	3.20	3.35
2nd	3.25	3.41	3.43	3.43	3.43	3.54
1st	3.40	3.58	3.59	3.60	3.60	3.75

Table 5.8: Peak Base Overturning Moment (k-ft $\times 10^5$) (Transverse Direction) [Rocking-Base Model].

	Substructure Configurations					MODE-ID
	"3-7"	"4-6"	"5-5"	"6-4"	"7-3"	
Base	2.78	2.84	2.85	2.85	2.85	3.00

Table 5.9: Peak Interstory Shear Force (kips $\times 10^3$) (Transverse Direction) [Fixed-Base Model].

Story	Substructure Configurations				
	"3-7"	"4-6"	"5-5"	"6-4"	"7-3"
10th	0.54	0.54	0.54	0.54	0.53
9th	1.06	1.06	1.06	1.05	1.04
8th	1.54	1.55	1.54	1.53	1.52
7th	1.98	1.99	1.98	1.97	1.96
6th	2.38	2.39	2.37	2.35	2.36
5th	2.71	2.72	2.70	2.70	2.72
4th	2.98	3.01	3.00	3.01	3.04
3rd	3.19	3.25	3.26	3.28	3.31
2nd	3.37	3.45	3.46	3.49	3.53
1st	3.51	3.60	3.62	3.65	3.70

Table 5.10: Peak Base Overturning Moment (k-ft $\times 10^5$) (Transverse Direction) [Fixed-Base Model].

	Substructure Configurations				
	"3-7"	"4-6"	"5-5"	"6-4"	"7-3"
Base	2.92	2.96	2.96	2.97	2.99

Table 5.11: Peak Interstory Shear Force (kips $\times 10^3$) (Longitudinal Direction).

Story	Substructure Configurations					MODE-ID
	"2-8"	"3-7"	"4-6"	"5-5"	"6-4"	
10th	0.46	0.47	0.47	0.47	0.47	0.47
9th	0.92	0.93	0.94	0.94	0.94	0.92
8th	1.37	1.38	1.39	1.39	1.39	1.31
7th	1.80	1.81	1.82	1.83	1.84	1.66
6th	2.21	2.22	2.23	2.25	2.28	2.00
5th	2.60	2.61	2.62	2.64	2.66	2.29
4th	2.97	2.98	2.99	3.00	3.01	2.54
3rd	3.33	3.33	3.30	3.30	3.30	2.79
2nd	3.65	3.60	3.56	3.56	3.55	2.95
1st	3.87	3.80	3.75	3.75	3.74	3.13

Table 5.12: Peak Base Overturning Moment (k-ft $\times 10^5$) (Longitudinal Direction).

	Substructure Configurations					MODE-ID
	"2-8"	"3-7"	"4-6"	"5-5"	"6-4"	
Base	2.93	2.91	2.90	2.91	2.92	2.62

Table 5.13: Peak Interstory Drift (cm) (Transverse Direction) [Rocking-Base Model].

Story	Substructure Configurations					MODE-ID
	"3-7"	"4-6"	"5-5"	"6-4"	"7-3"	
10th	0.05	0.04	0.04	0.04	0.03	0.20
9th	0.10	0.07	0.07	0.07	0.07	0.20
8th	0.14	0.11	0.11	0.11	0.10	0.20
7th	0.19	0.15	0.14	0.14	0.14	0.21
6th	0.23	0.18	0.17	0.17	0.17	0.21
5th	0.27	0.21	0.20	0.20	0.20	0.22
4th	0.30	0.22	0.23	0.23	0.23	0.22
3rd	0.17	0.24	0.25	0.25	0.25	0.23
2nd	0.18	0.26	0.26	0.26	0.27	0.23
1st	0.18	0.27	0.27	0.27	0.27	0.31

Table 5.14: Peak Interstory Drift (cm) (Transverse Direction) [Fixed-Base Model].

Story	Substructure Configurations				
	"3-7"	"4-6"	"5-5"	"6-4"	"7-3"
10th	0.10	0.10	0.10	0.10	0.10
9th	0.14	0.14	0.15	0.15	0.14
8th	*0.18*	*0.18*	*0.19*	*0.19*	*0.18*
7th	0.22	0.21	0.23	0.23	0.16
6th	0.25	0.25	0.26	0.18	0.18
5th	0.28	0.27	0.18	0.19	0.20
4th	0.30	0.19	0.20	0.21	0.22
3rd	0.15	0.19	0.21	0.22	0.23
2nd	0.15	0.20	0.21	0.23	0.24
1st	0.18	0.22	0.24	0.25	0.27

Table 5.15: Peak Interstory Drift (cm) (Longitudinal Direction).

Story	Substructure Configurations					MODE-ID
	"2-8"	"3-7"	"4-6"	"5-5"	"6-4"	
10th	0.04	0.04	0.05	0.04	0.03	0.21
9th	0.08	0.09	0.09	0.08	0.05	0.25
8th	0.12	0.13	0.14	0.12	0.08	0.28
7th	0.16	0.17	0.18	0.16	0.10	0.32
6th	0.20	0.22	0.22	0.20	0.42	0.36
5th	0.24	0.26	0.26	0.50	0.49	0.39
4th	0.27	0.30	0.61	0.58	0.56	0.43
3rd	0.31	0.77	0.68	0.64	0.62	0.46
2nd	1.09	0.84	0.73	0.69	0.67	0.50
1st	1.14	0.87	0.75	0.71	0.69	0.72

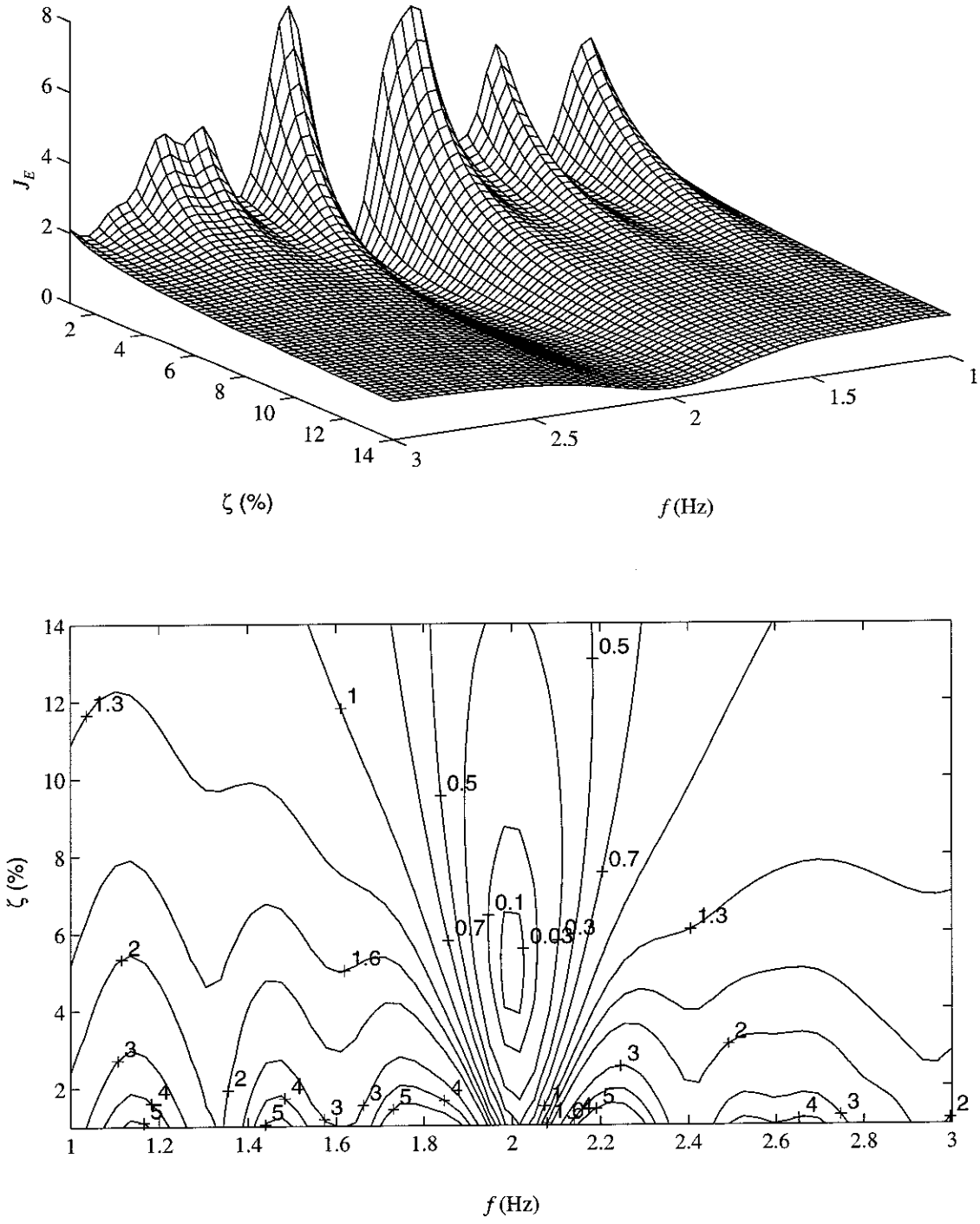

Figure 5.1: Mesh and Contour Plot of $J_E(\underline{a})$ of Single-Degree-of-Freedom Linear Oscillators.

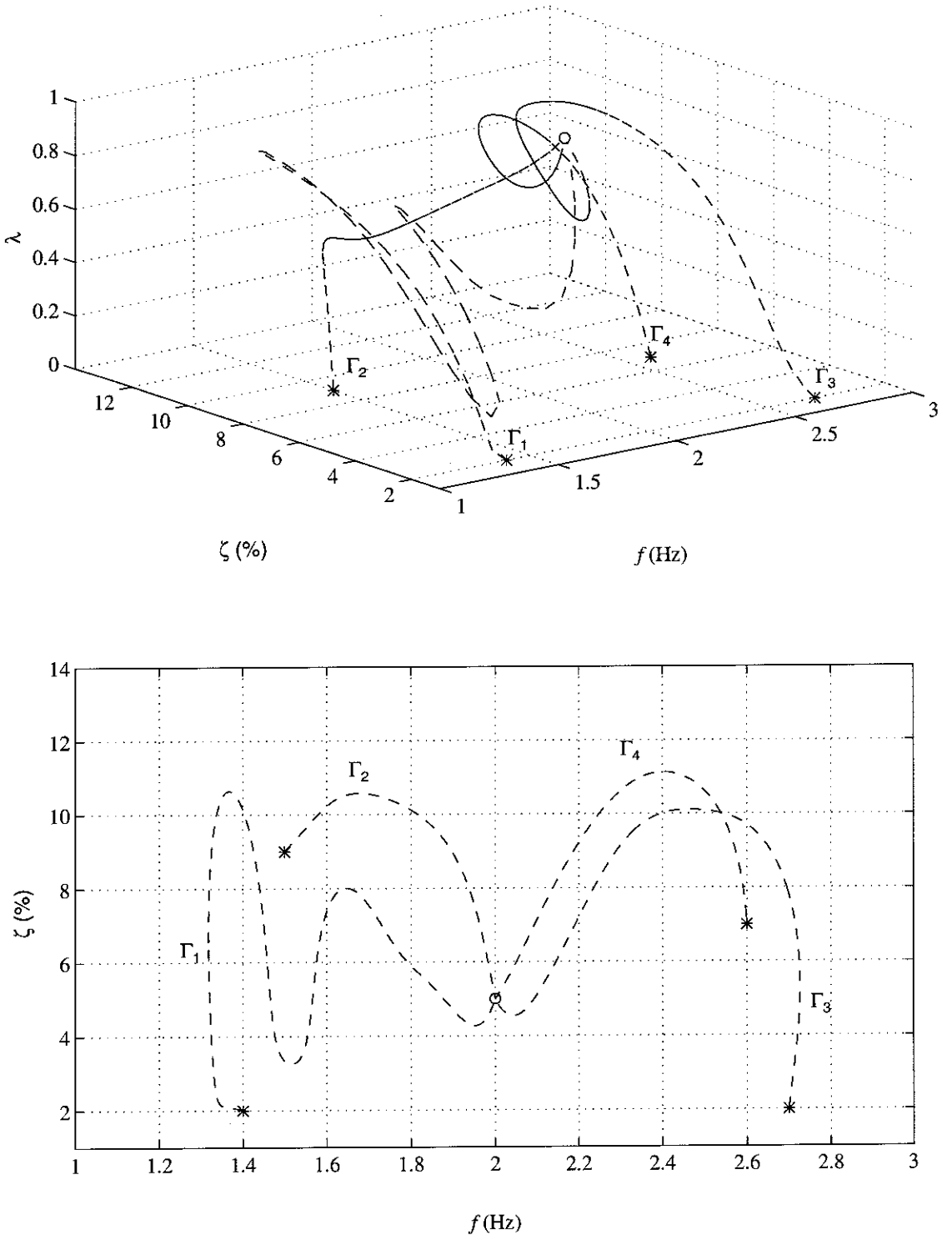

Figure 5.2: Homotopy Trajectories $\{\Gamma_1, \ldots, \Gamma_4\}$ in the Identification of f_o and ζ_o.

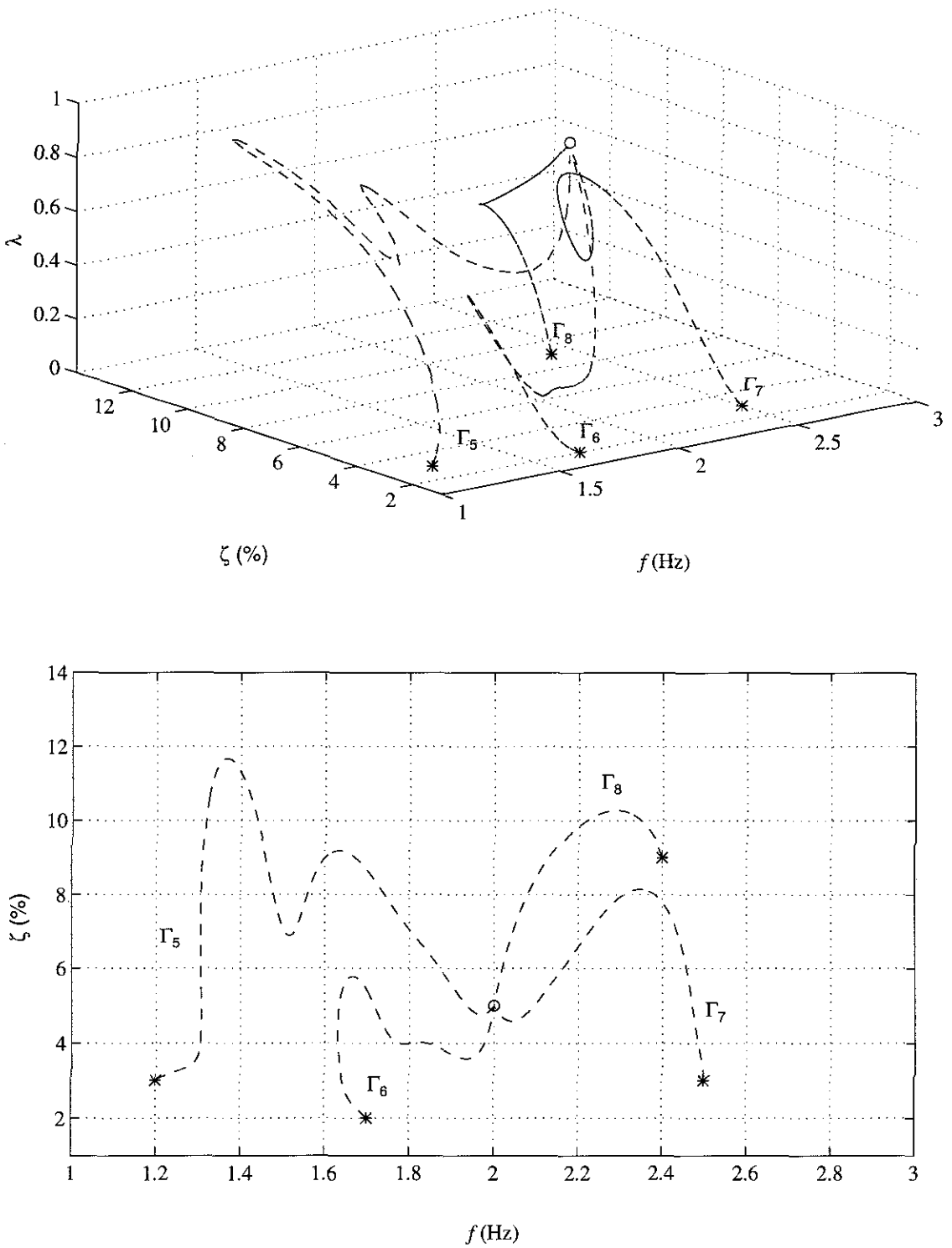

Figure 5.3: Homotopy Trajectories $\{\Gamma_5, \ldots, \Gamma_8\}$ in the Identification of f_o and ζ_o.

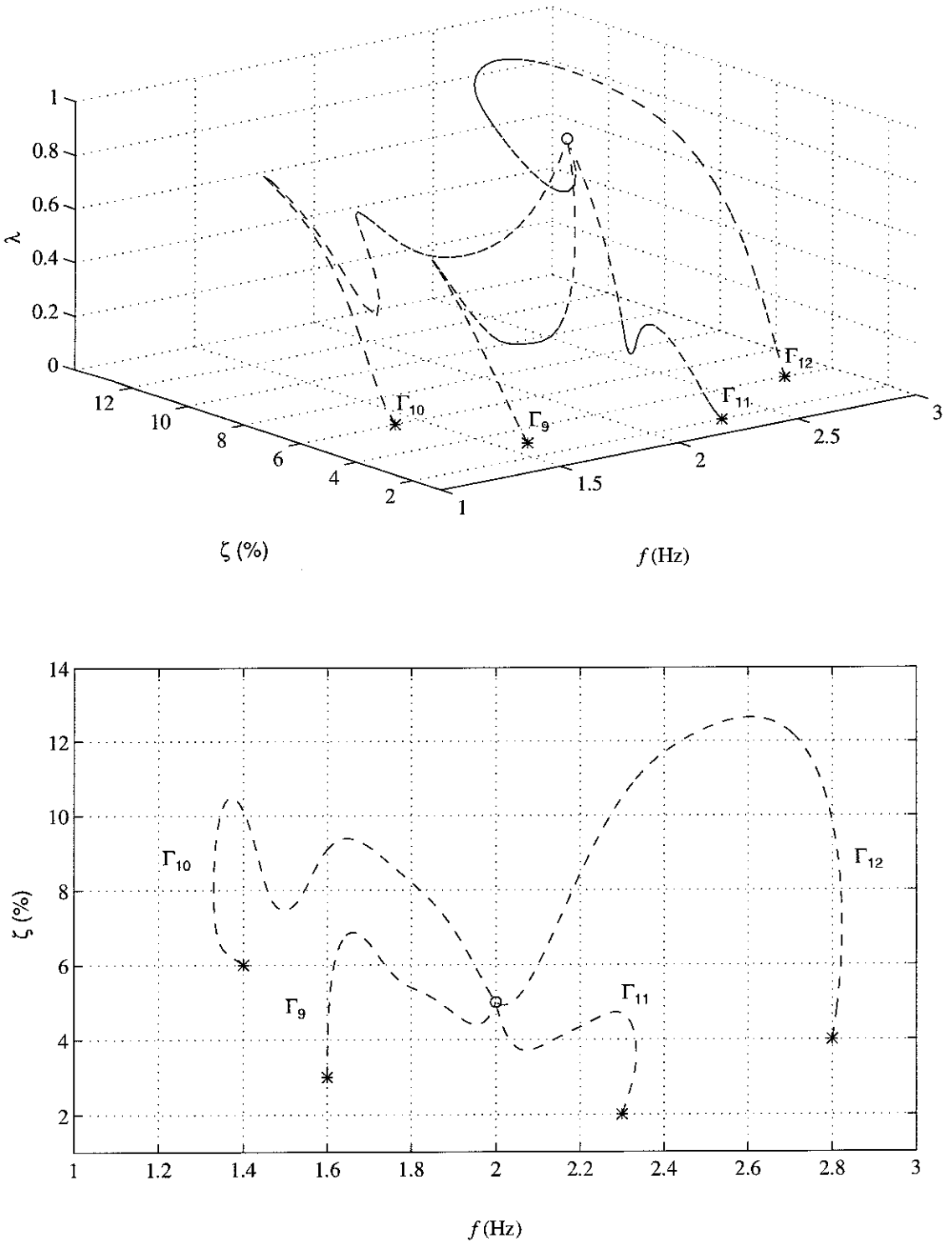

Figure 5.4: Homotopy Trajectories $\{\Gamma_9, \ldots, \Gamma_{12}\}$ in the Identification of f_o and ζ_o.

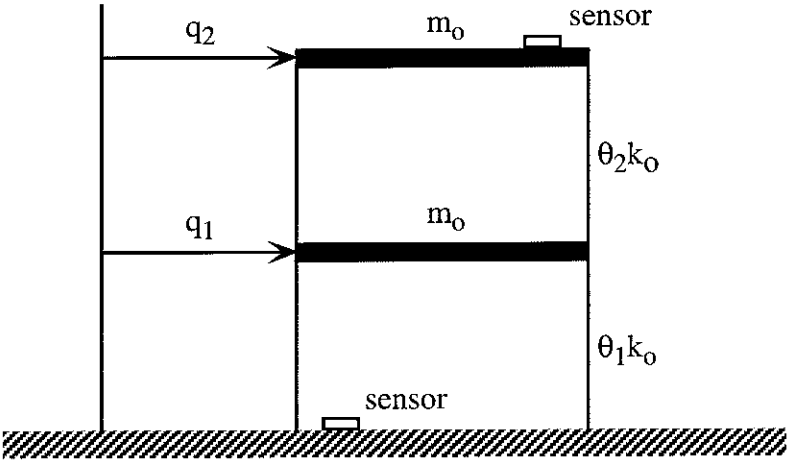

Figure 5.5: Two-Degrees-of-Freedom Linear Chain Model of a Two-Story Structure.

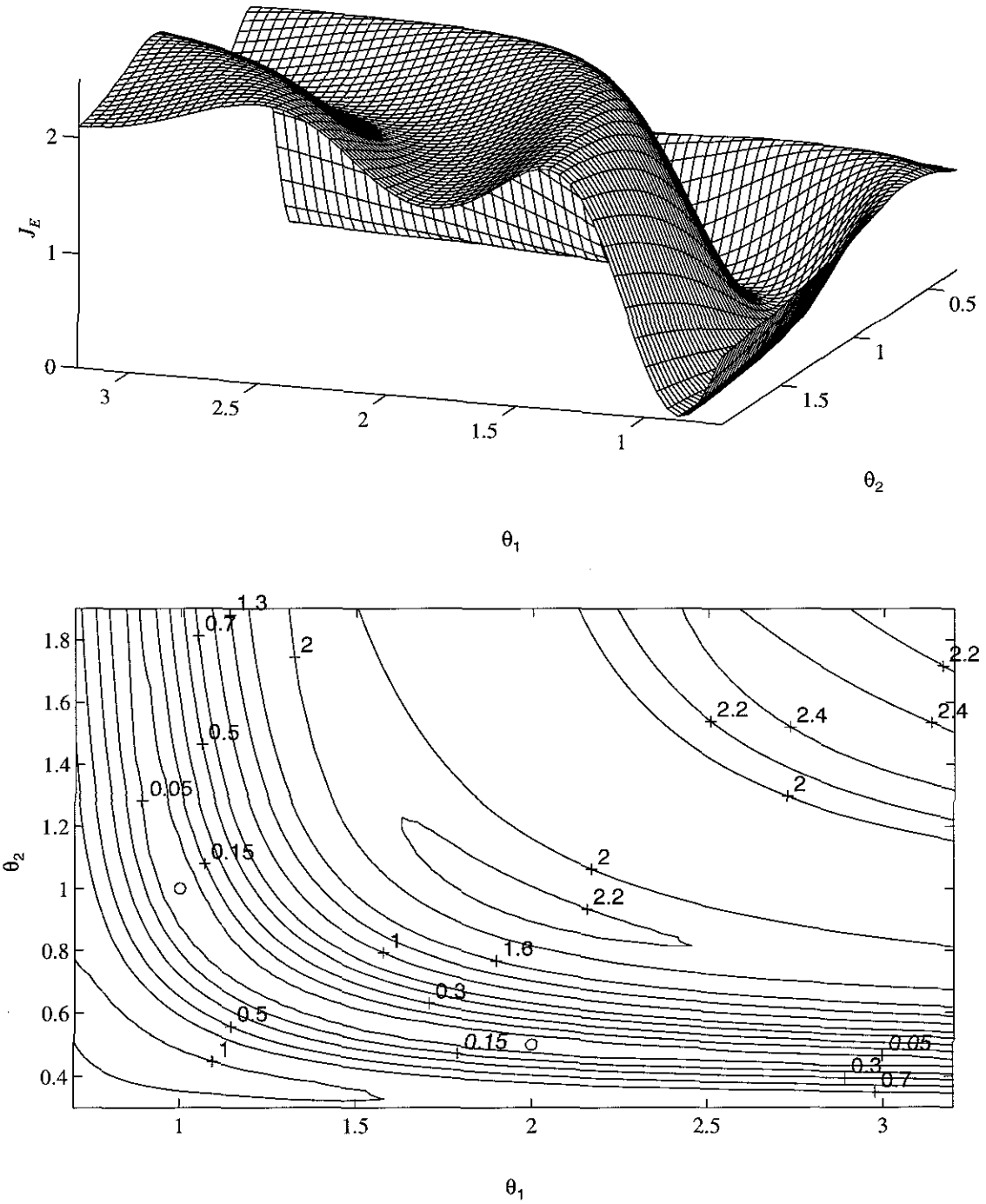

Figure 5.6: Mesh and Contour Plot of $J_E(\underline{\theta})$ of Two-Degrees-of-Freedom Linear Chain Models.

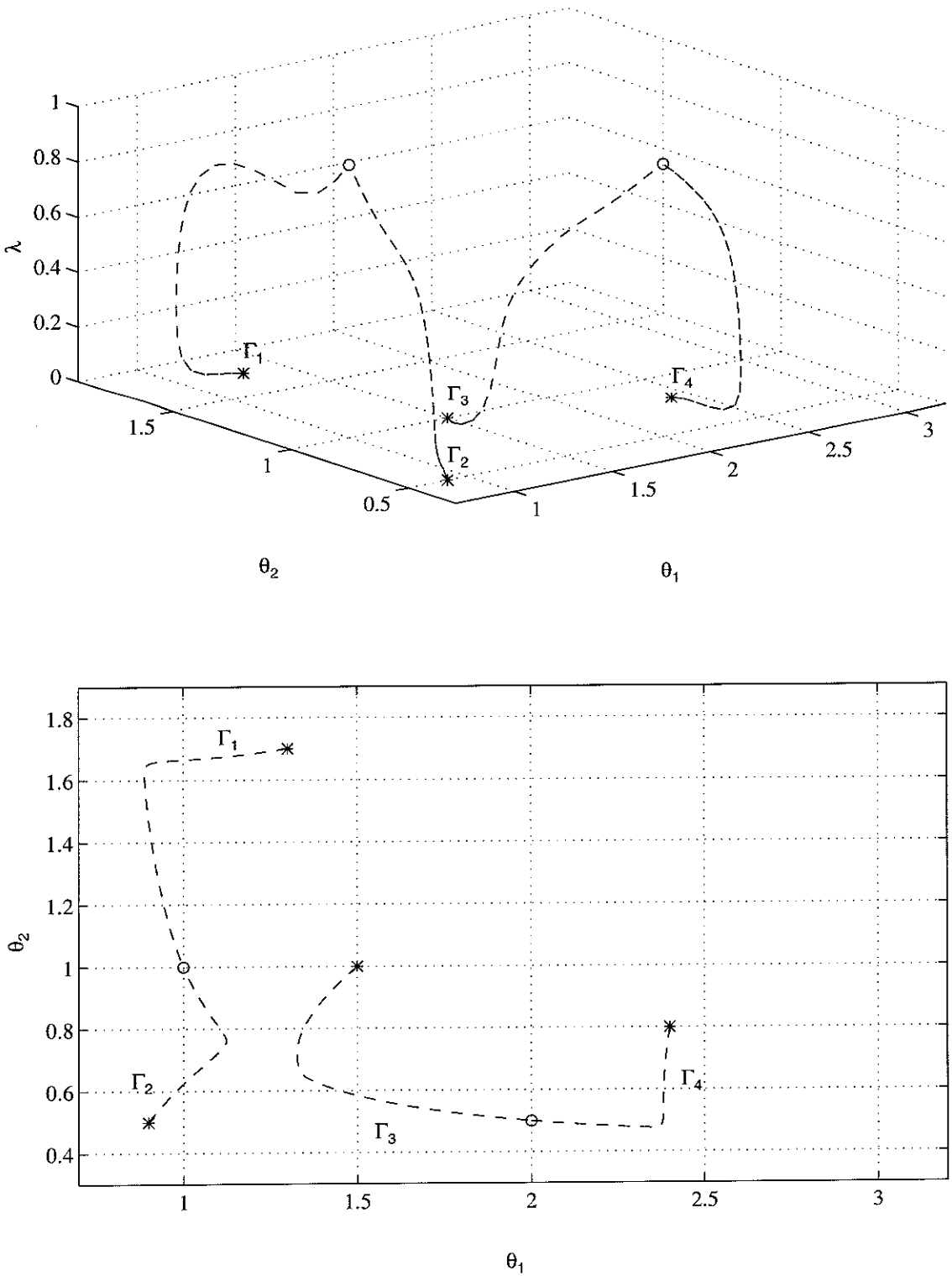

Figure 5.7: Homotopy Trajectories in the Identification of $\underline{\theta}_o$ and $\underline{\theta}_e$ (No Noise).

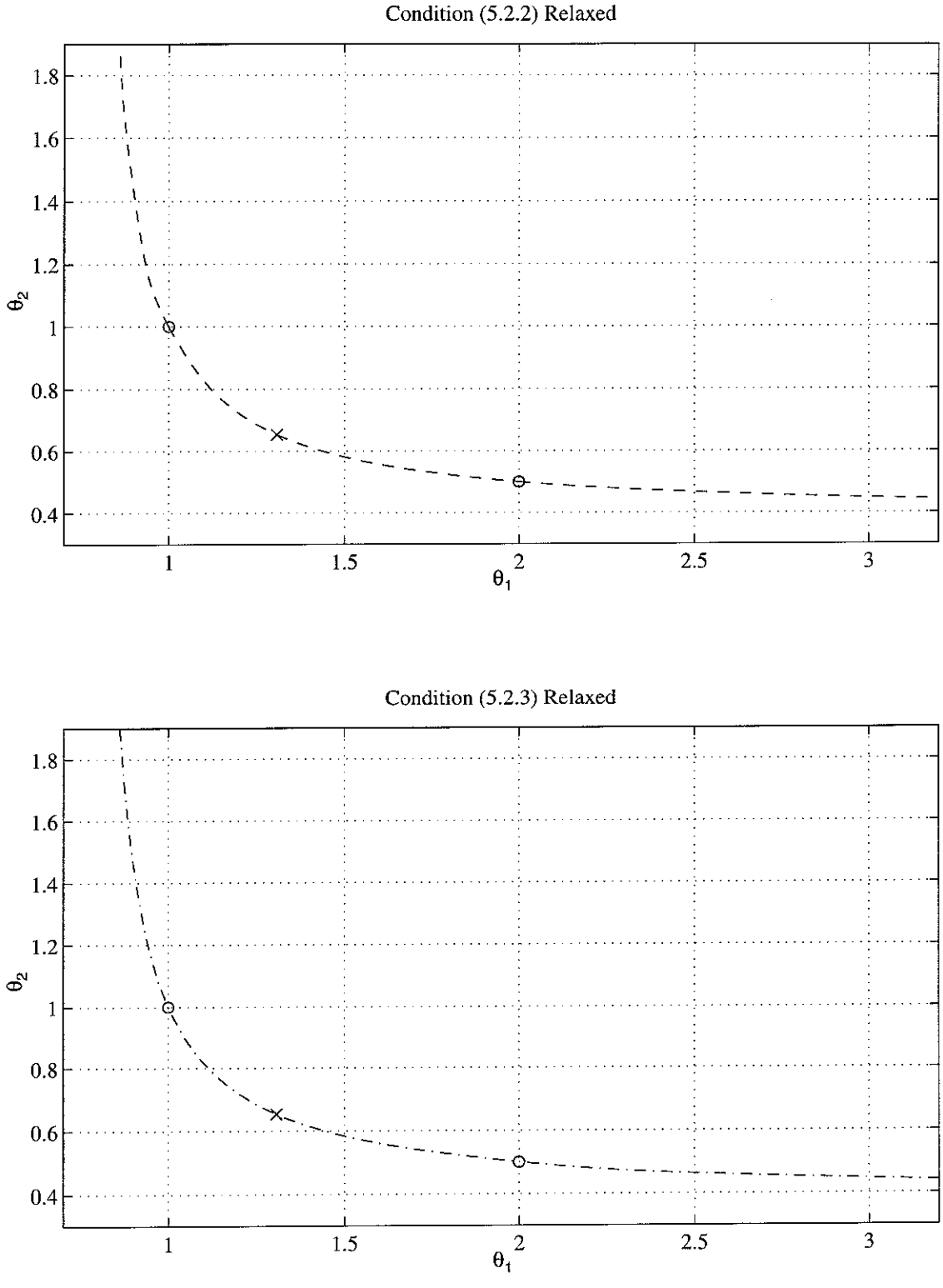

Figure 5.8: Relaxation Trajectories in the Identification of $\underline{\theta}_o$ and $\underline{\theta}_e$ (No Noise).

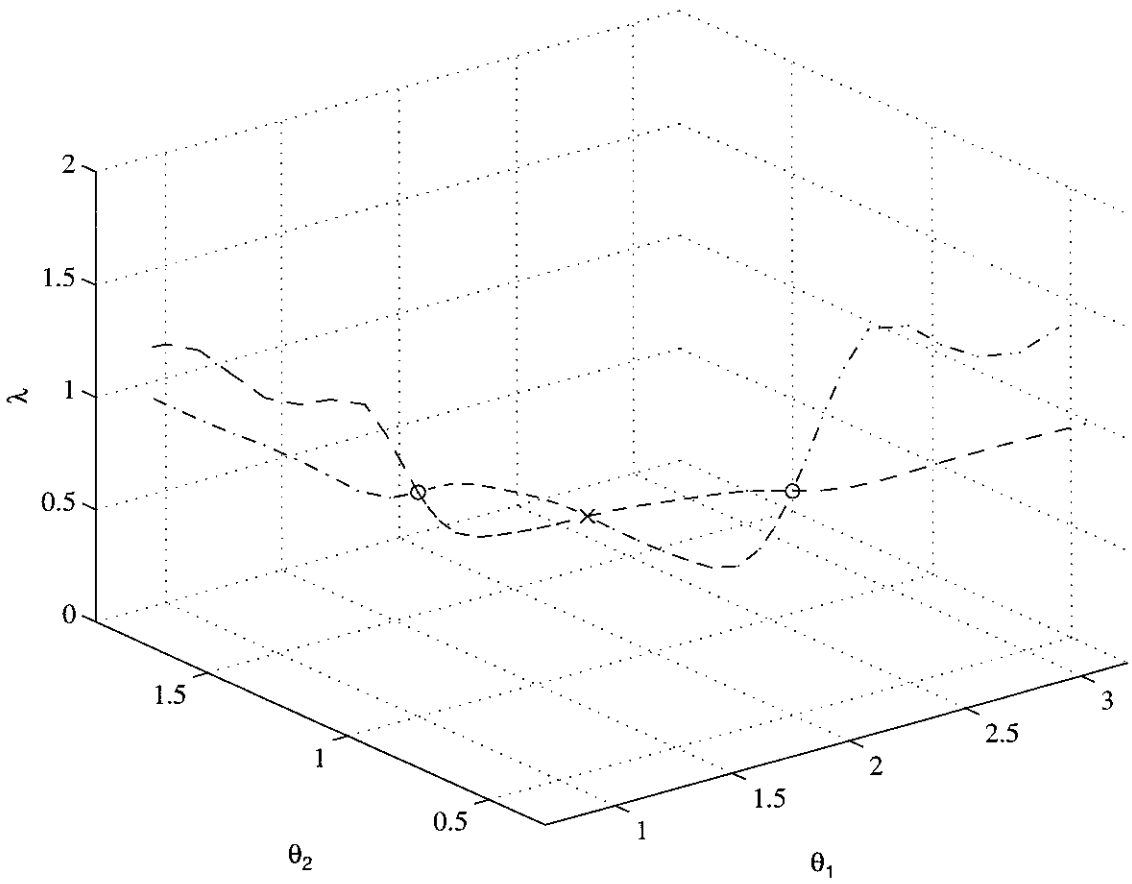

Figure 5.9: Three-Dimensional Plot of the Relaxation Trajectories in Figure 5.8.

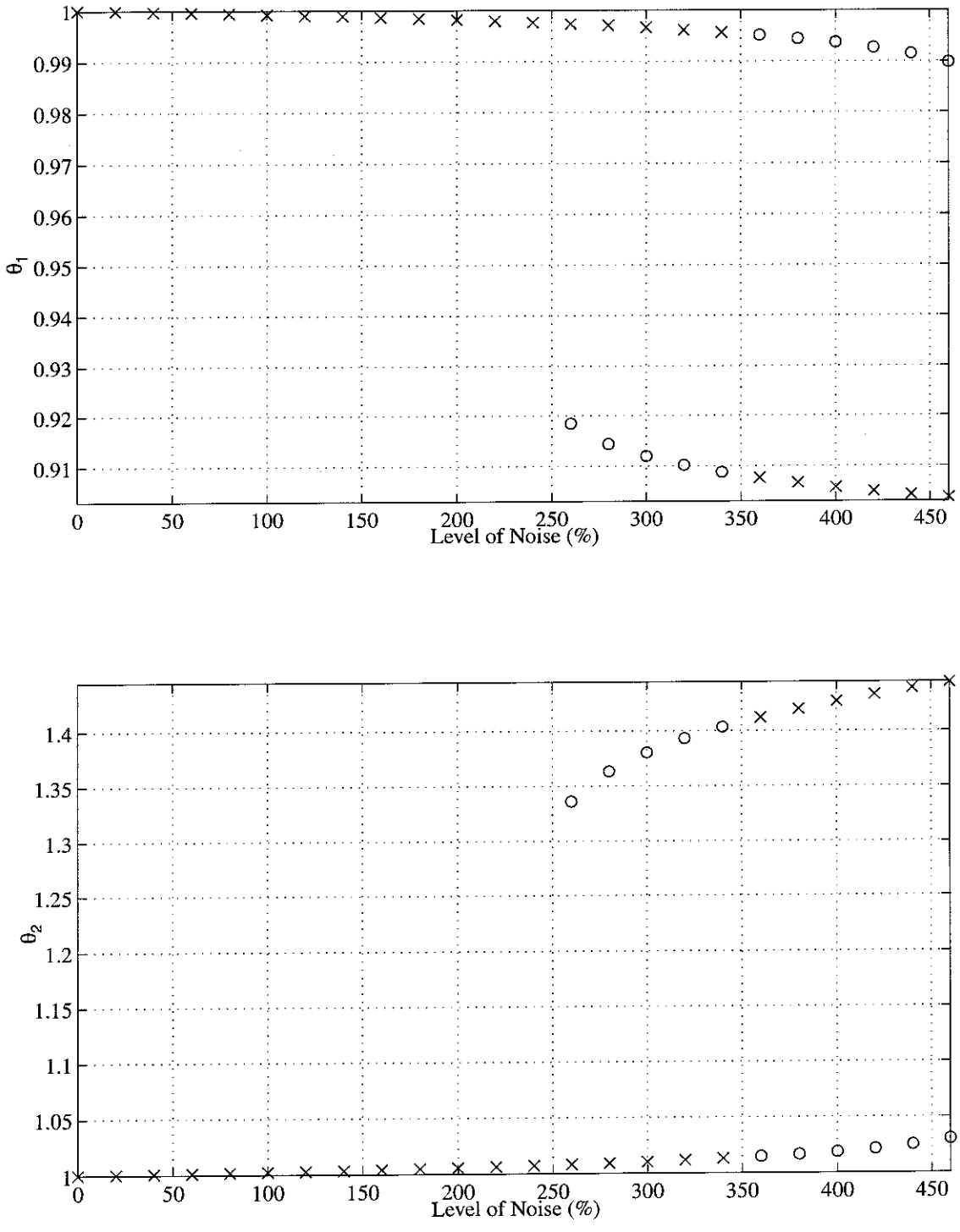

Figure 5.10: Stiffness Parameters of $\underline{\hat{\theta}}^{(1)}$ ("×") and $\underline{\tilde{\theta}}^{(1)}$ ("○") for Different Levels of Noise ["×" – Global Minimum, "○" – Local Minimum].

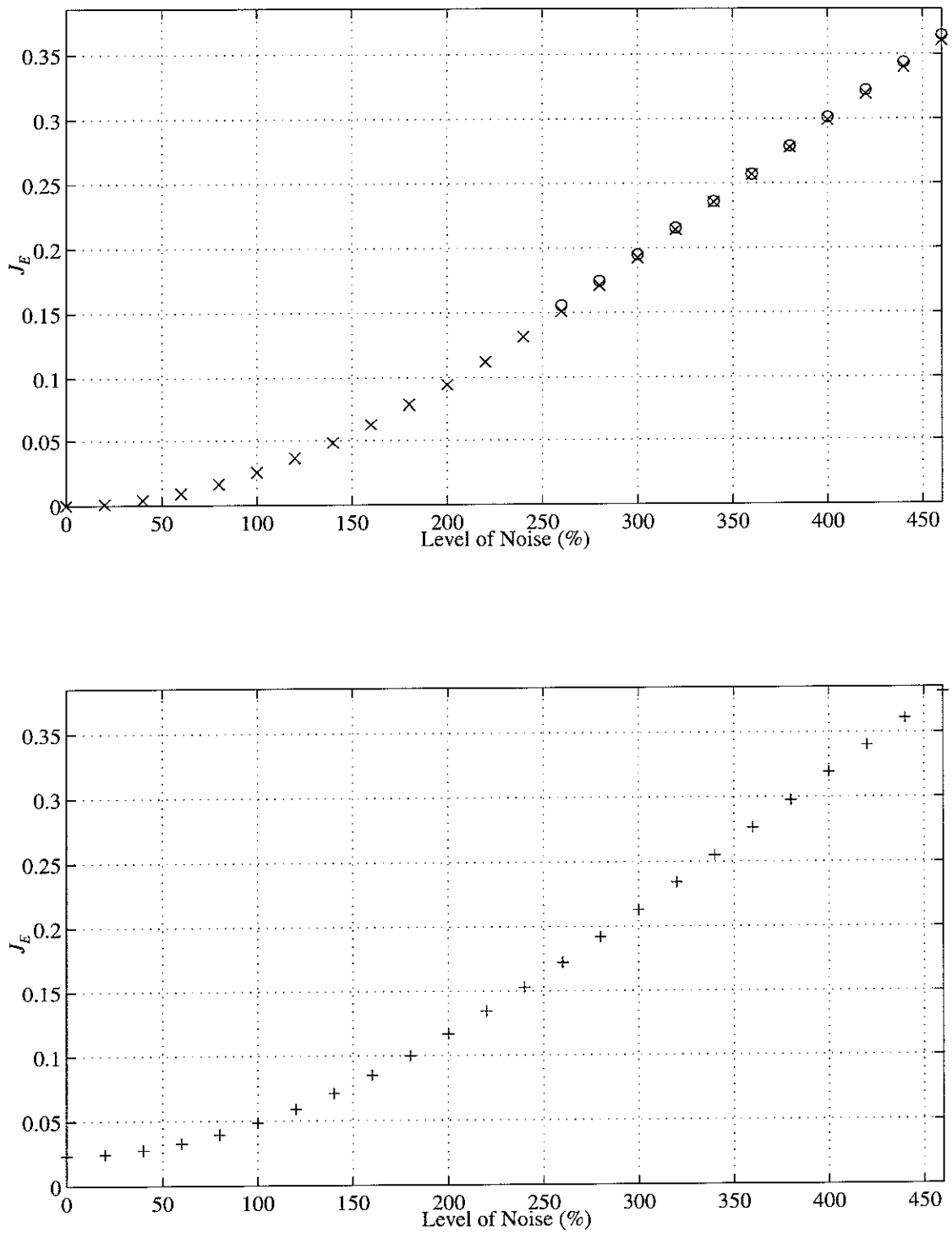

Figure 5.11: $J_E(\underline{\hat{\theta}})$ ("×"), $J_E(\underline{\tilde{\theta}})$ ("○"), and $J_E(\underline{\theta}_s)$ ("+") for Different Levels of Noise ["×" – Global Minimum, "○" – Local Minimum].

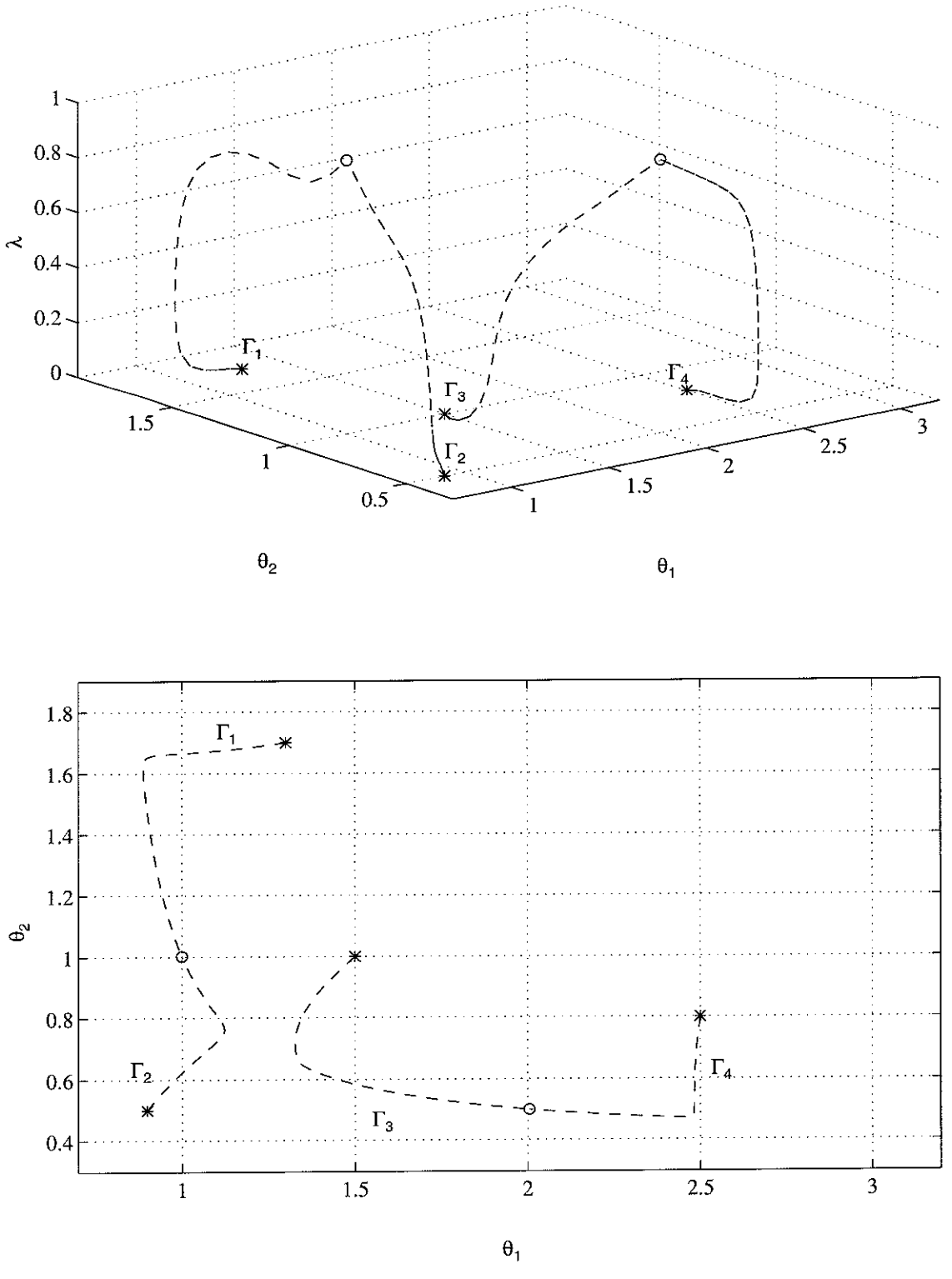

Figure 5.12: Homotopy Trajectories in the Identification of $\hat{\underline{\theta}}$ (100% Noise).

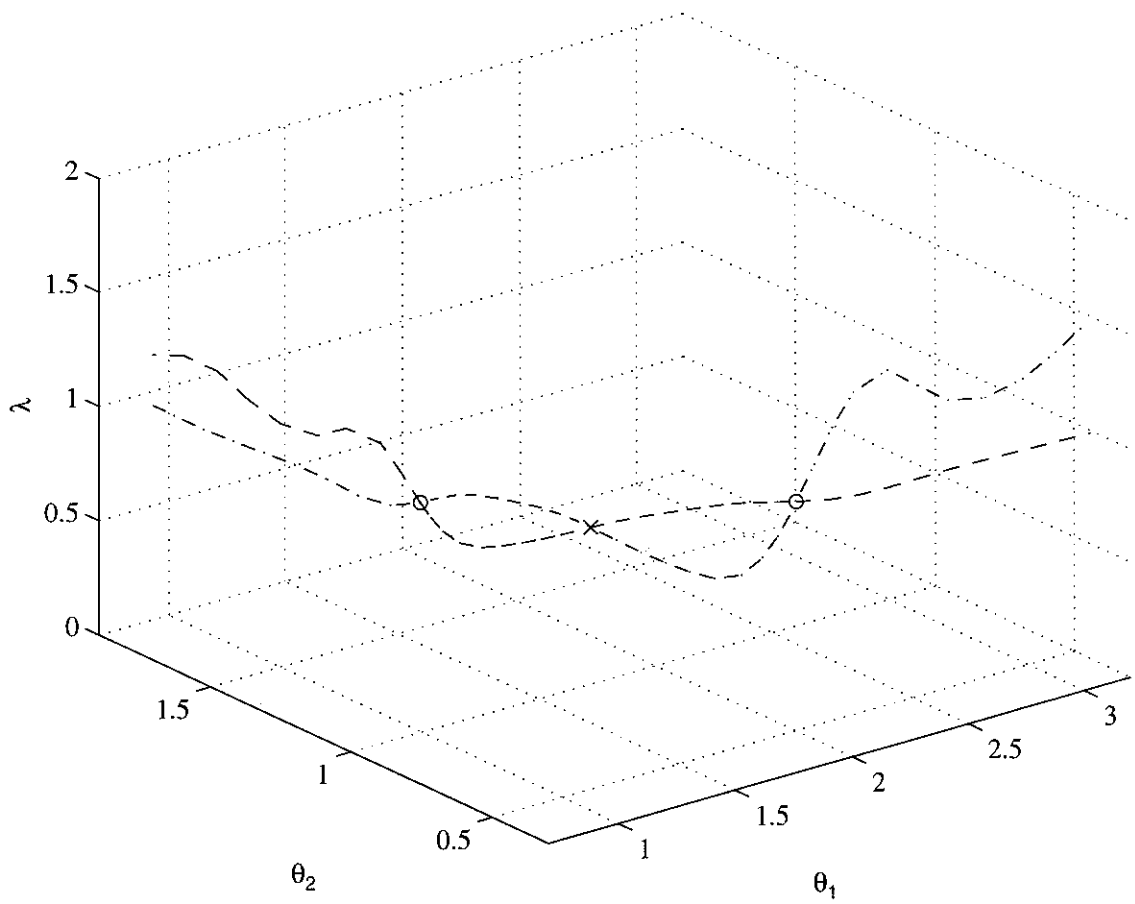

Figure 5.13: Three-Dimensional Plot of the Relaxation Trajectories in the Identification of $\hat{\underline{\theta}}$ (100% Noise).

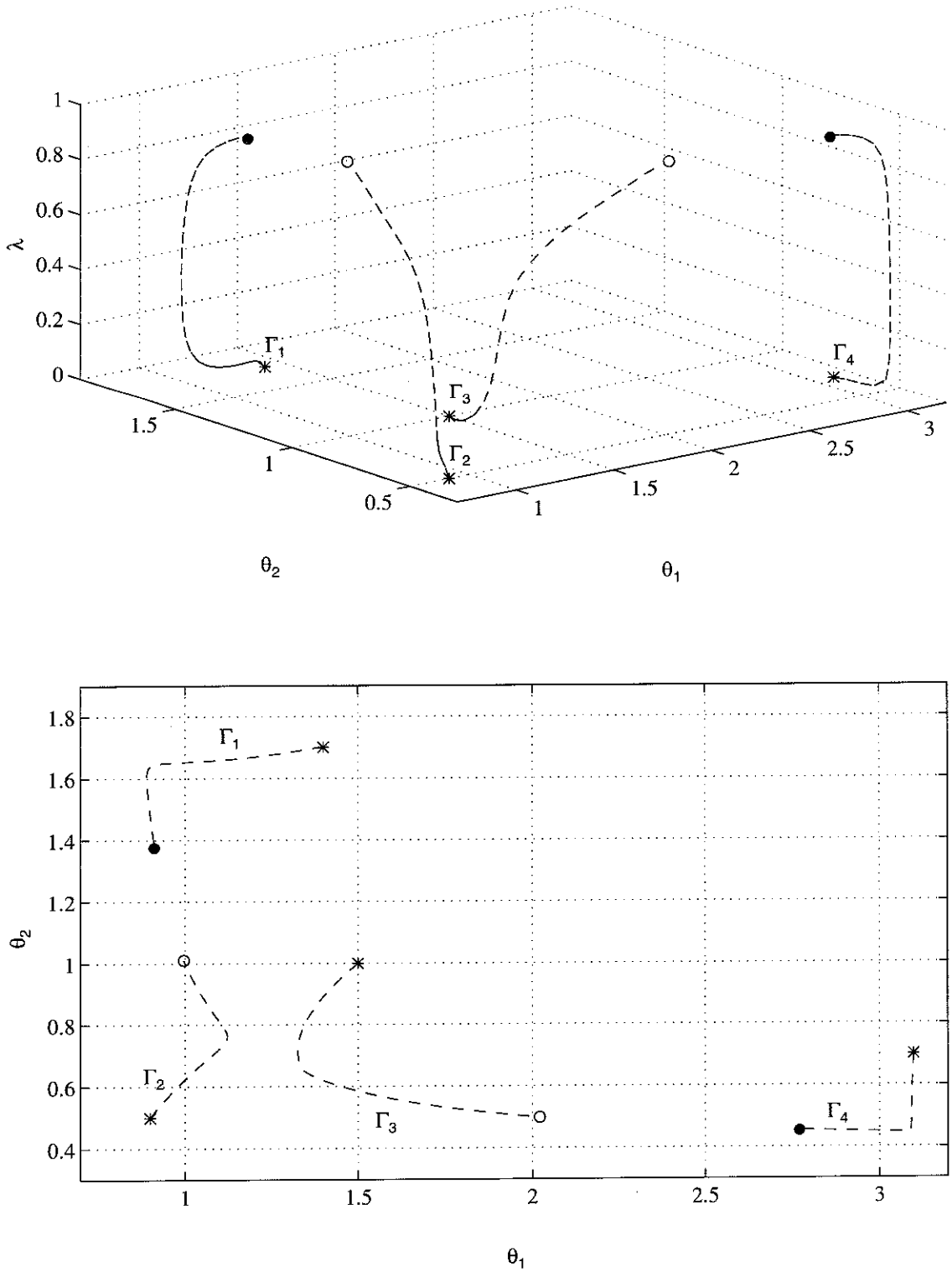

Figure 5.14: Homotopy Trajectories in the Identification of $\hat{\underline{\theta}}$ (300% Noise).

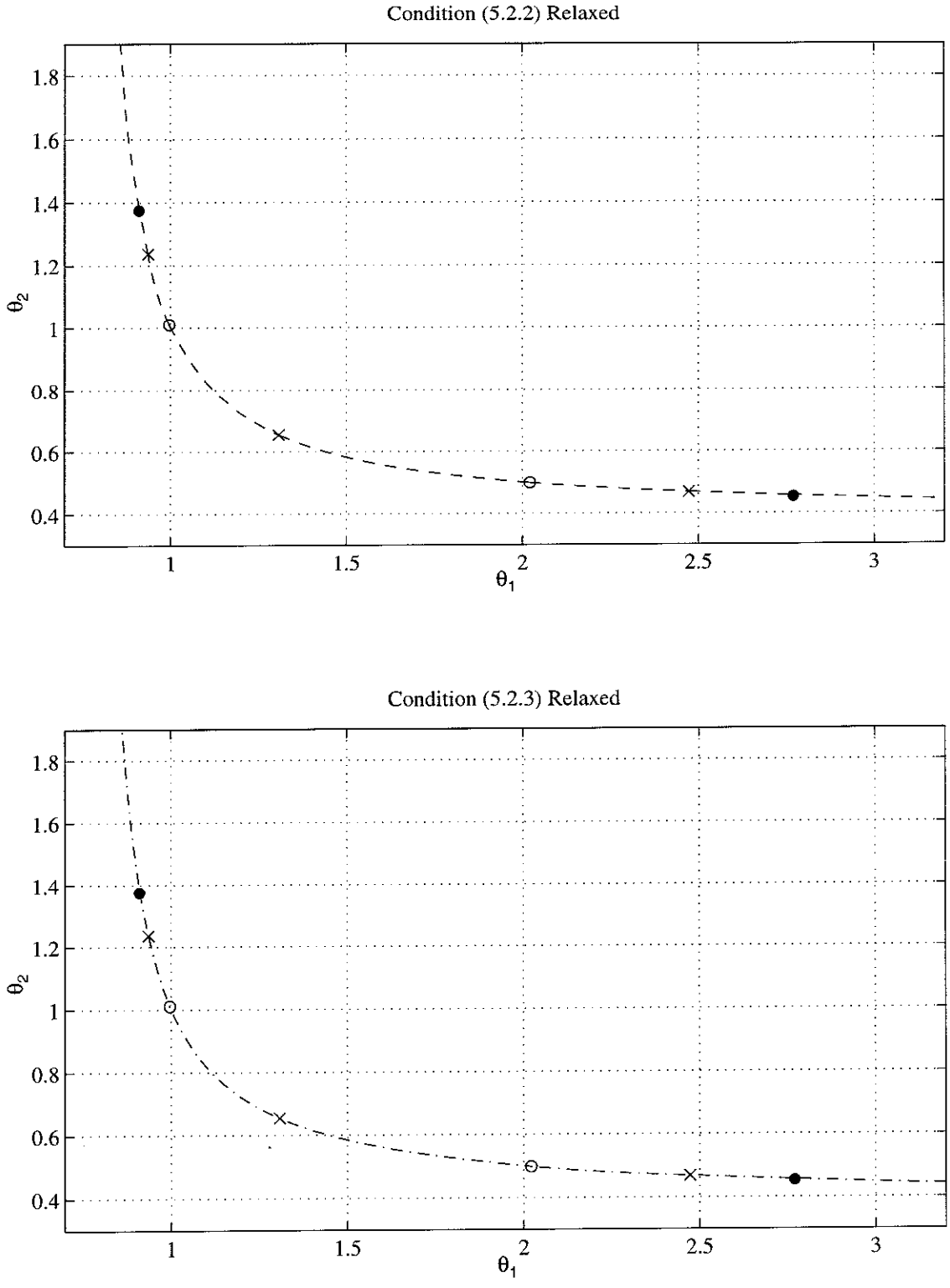

Figure 5.15: Relaxation Trajectories in the Identification of $\hat{\underline{\theta}}$ (300% Noise).

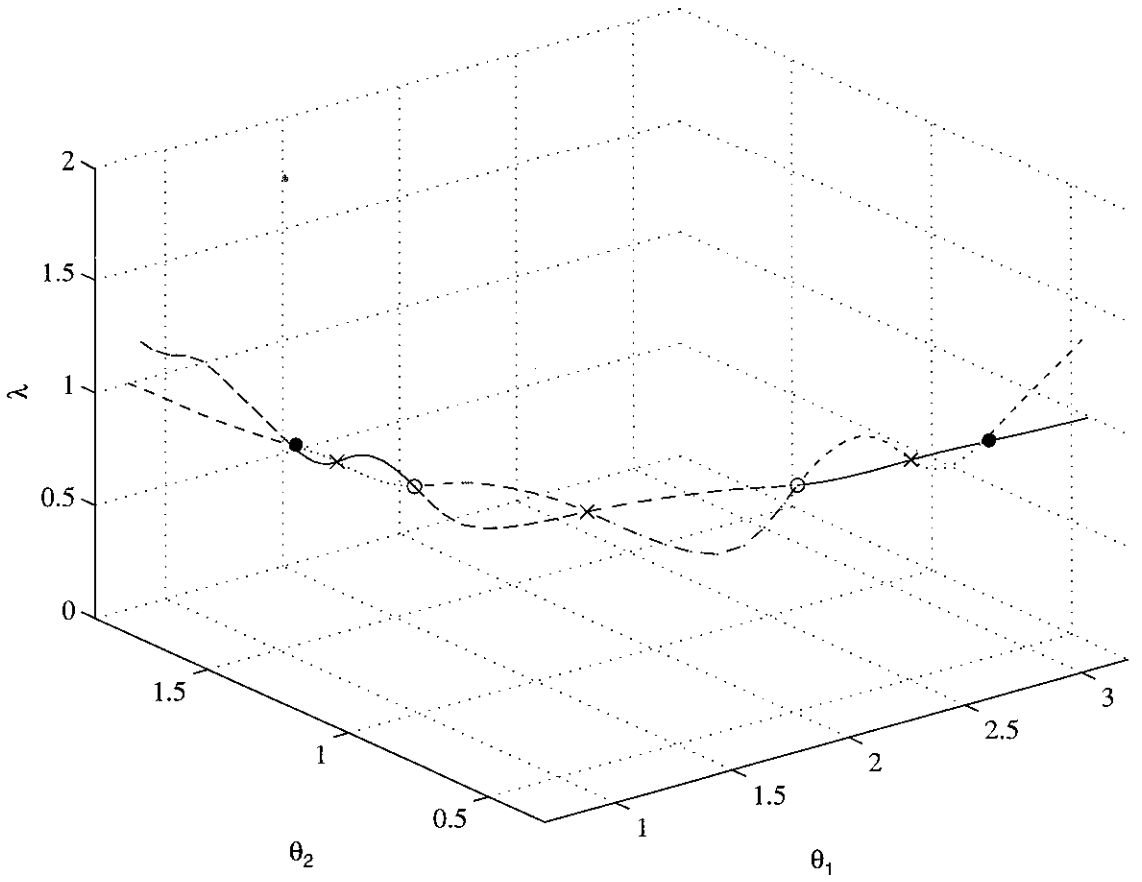

Figure 5.16: Three-Dimensional Plot of the Relaxation Trajectories in Figure 5.15.

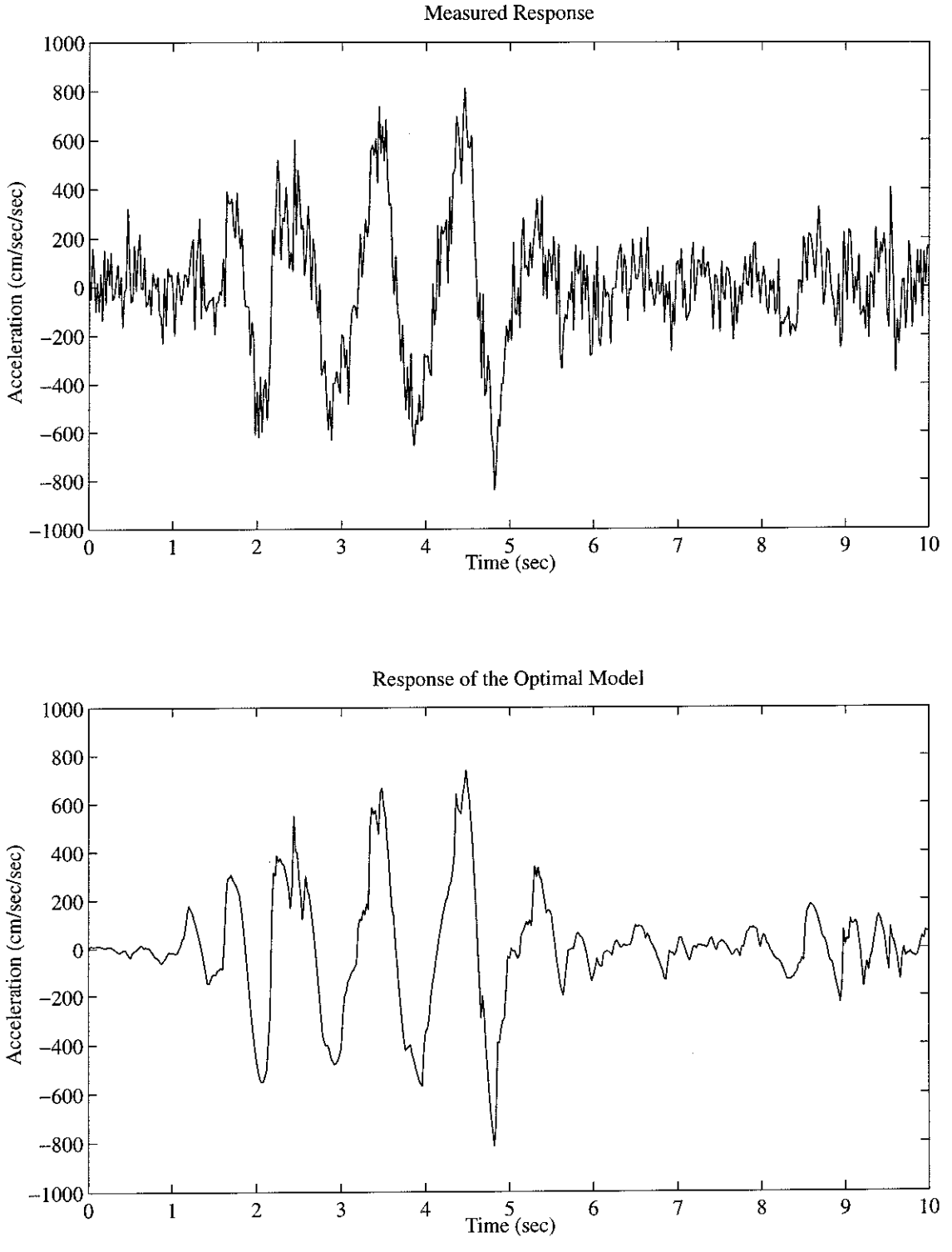

Figure 5.17: Measured "Roof" Response of the Two-Story Structure and the Response of the Optimal Linear Chain Models (300% Noise).

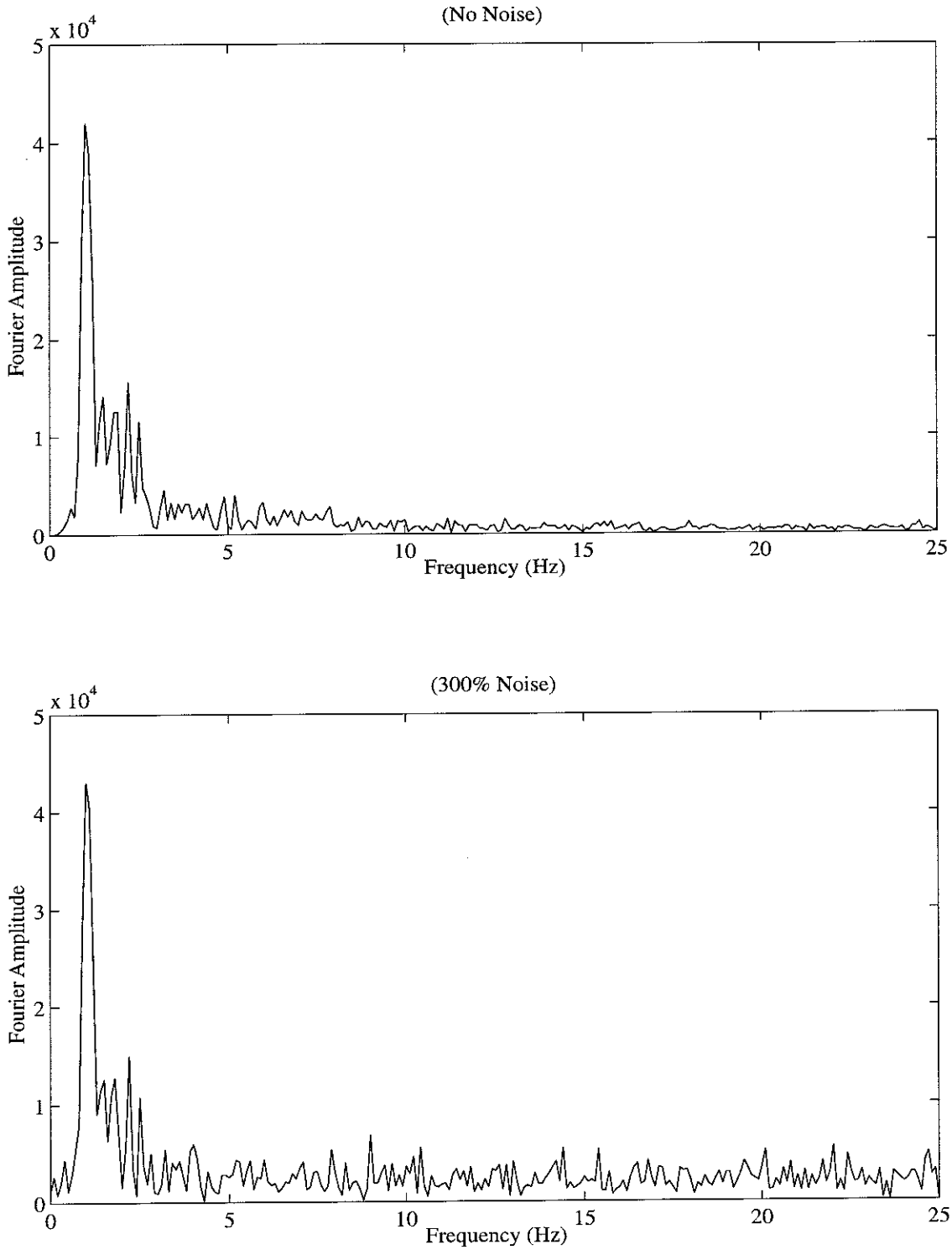

Figure 5.18: Fourier Amplitude Spectrum of the Actual and Measured "Roof" Response.

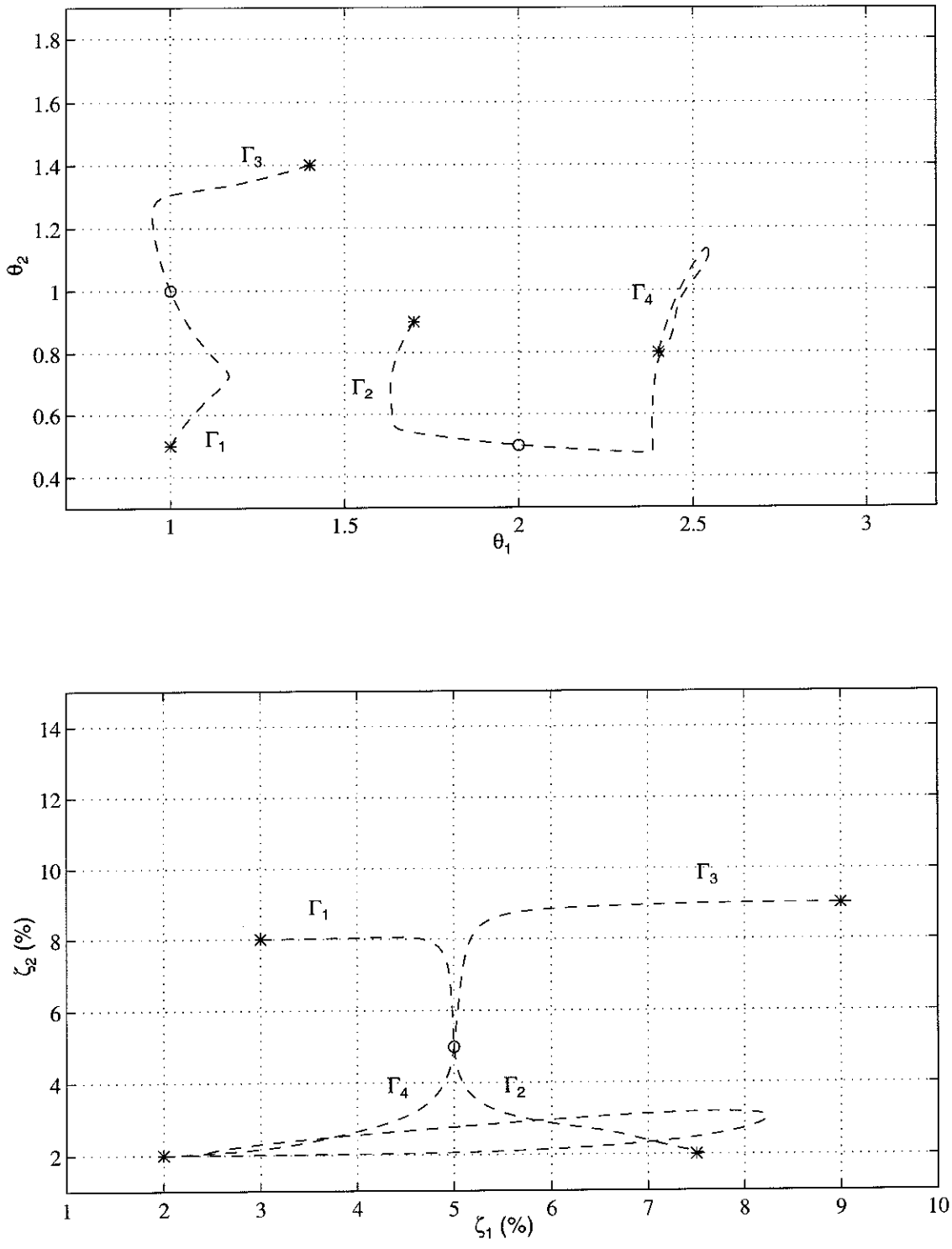

Figure 5.19: Projected Homotopy Trajectories in the Identification of $\underline{\theta}_o$, $\underline{\theta}_e$, and $\underline{\zeta}_o$ (No Noise).

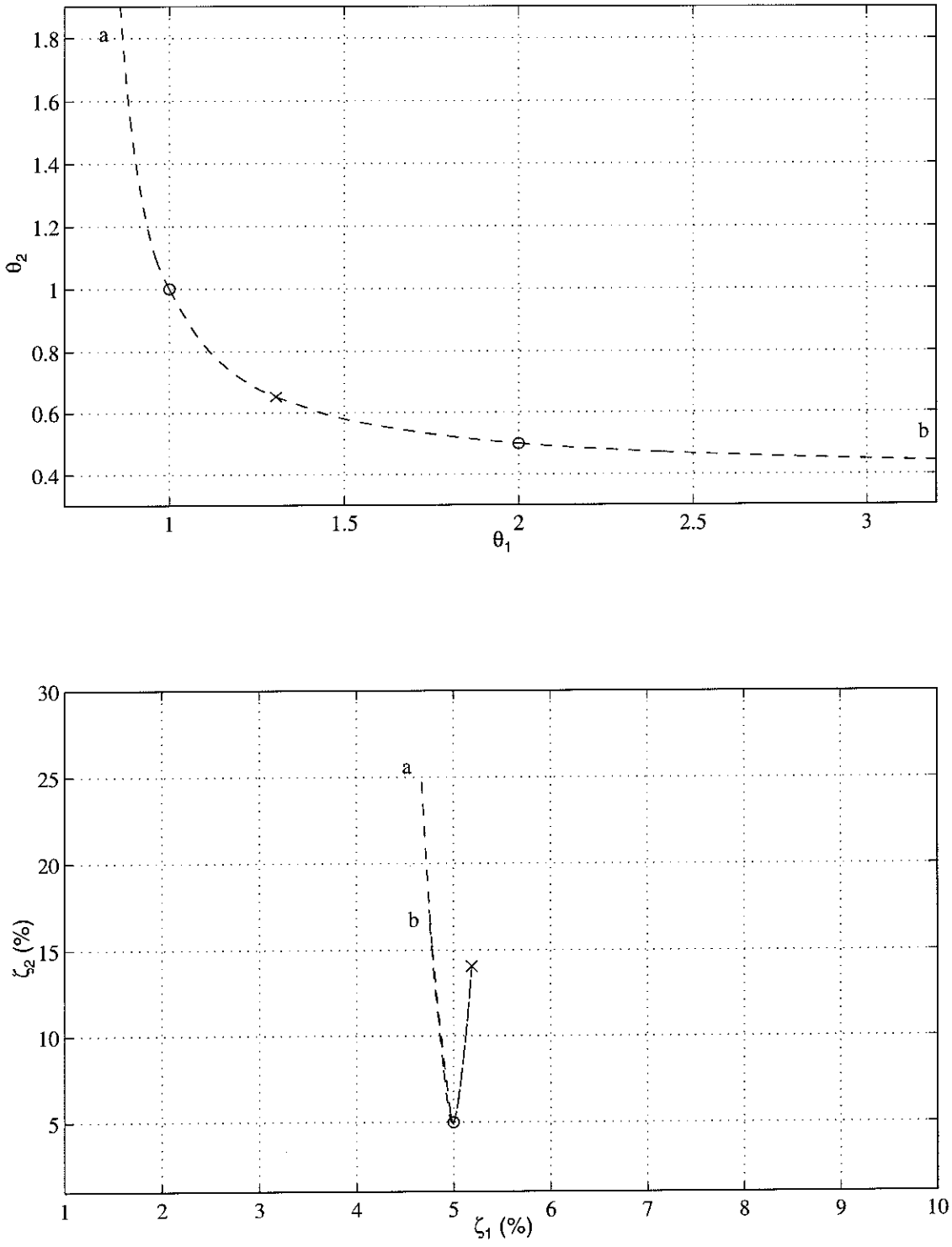

Figure 5.20: Projected Relaxation Trajectory ($\frac{\partial J_E(a)}{\partial \theta_1} = 0$ is relaxed) in the Identification of $\underline{\theta}_o$, $\underline{\theta}_e$, and $\underline{\zeta}_o$ (No Noise).

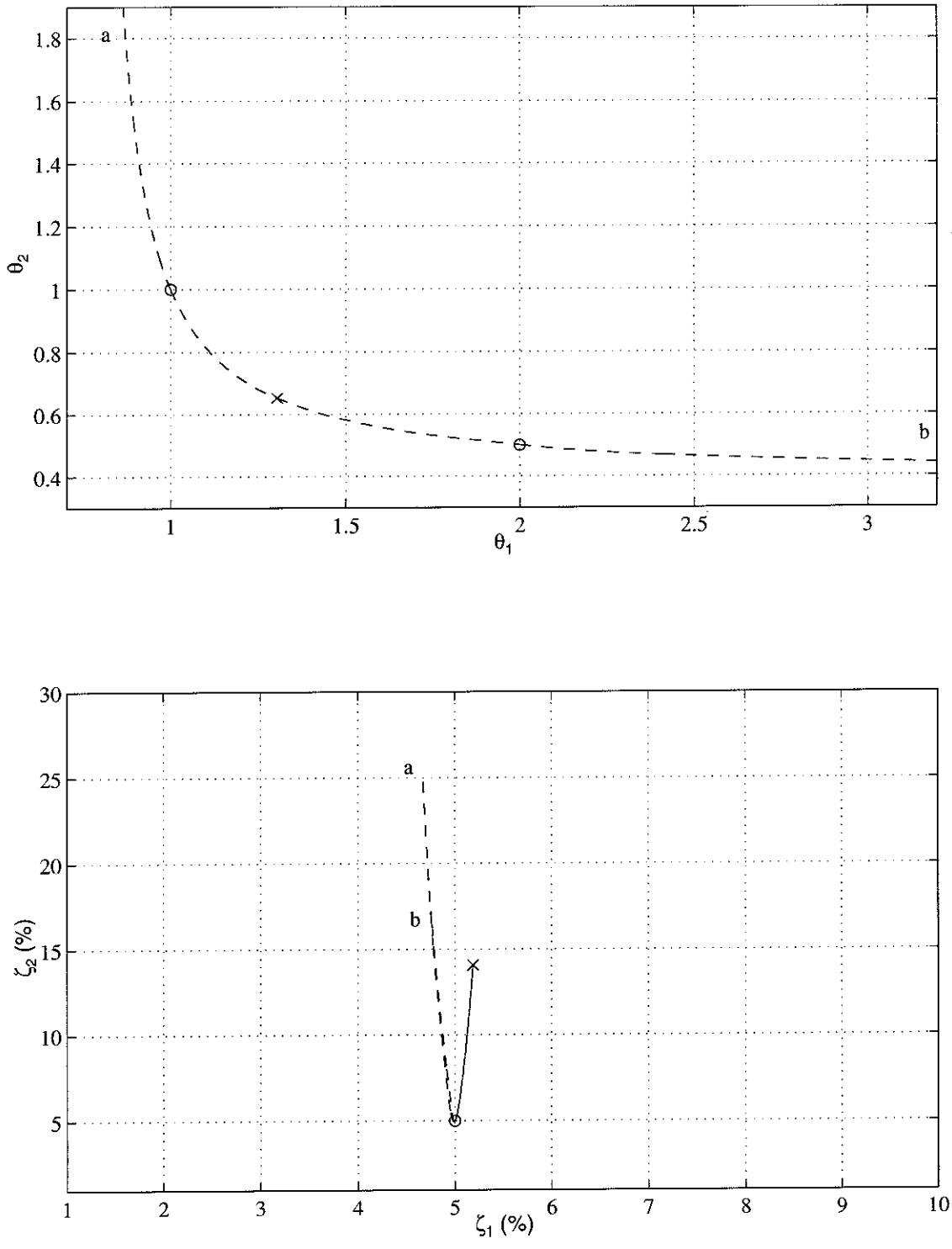

Figure 5.21: Projected Relaxation Trajectory ($\frac{\partial J_E(a)}{\partial \theta_2} = 0$ is relaxed) in the Identification of $\underline{\theta}_o$, $\underline{\theta}_e$, and $\underline{\zeta}_o$ (No Noise).

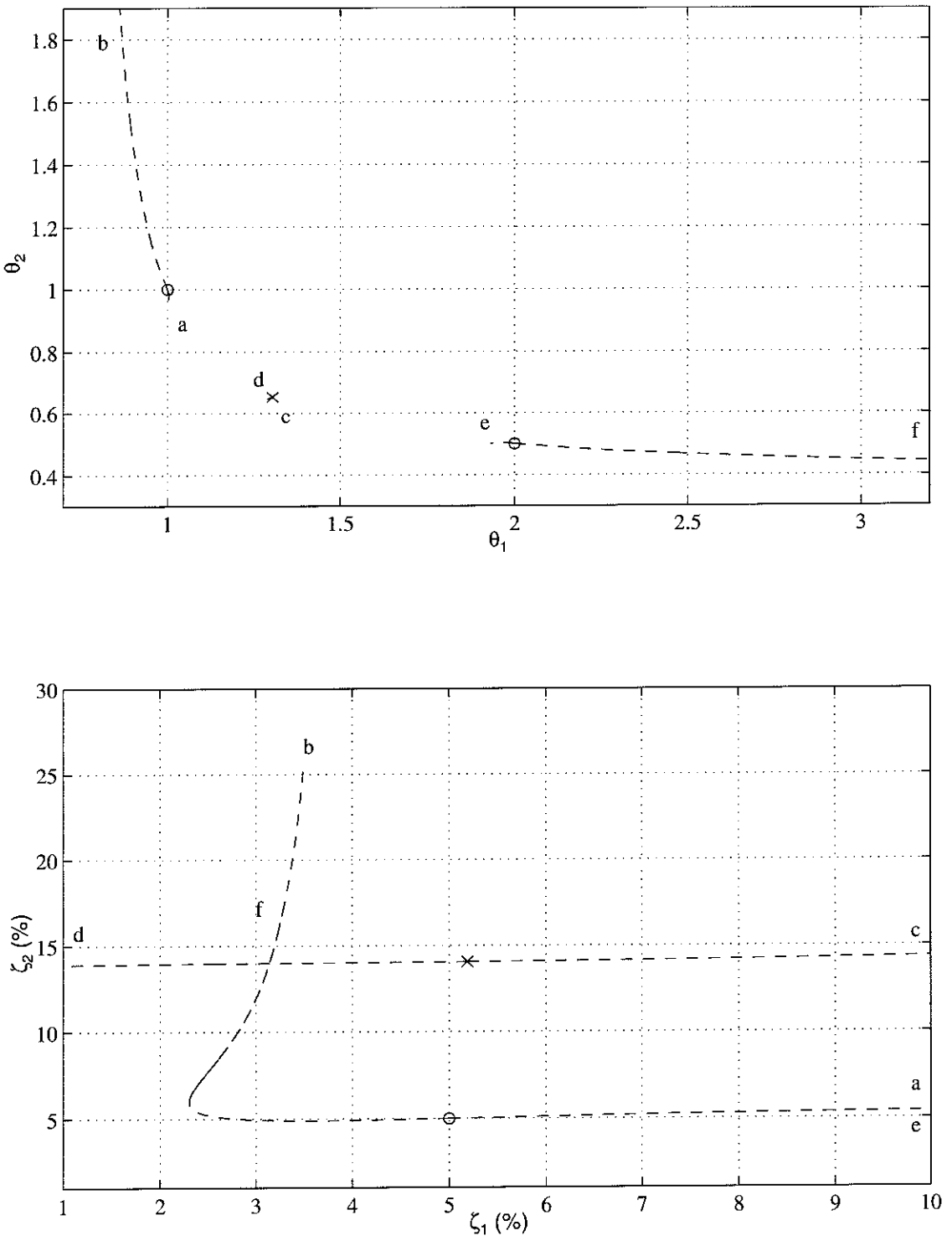

Figure 5.22: Projected Relaxation Trajectory ($\frac{\partial J_E(a)}{\partial \zeta_1} = 0$ is relaxed) in the Identification of $\underline{\theta}_o$, $\underline{\theta}_e$, and $\underline{\zeta}_o$ (No Noise).

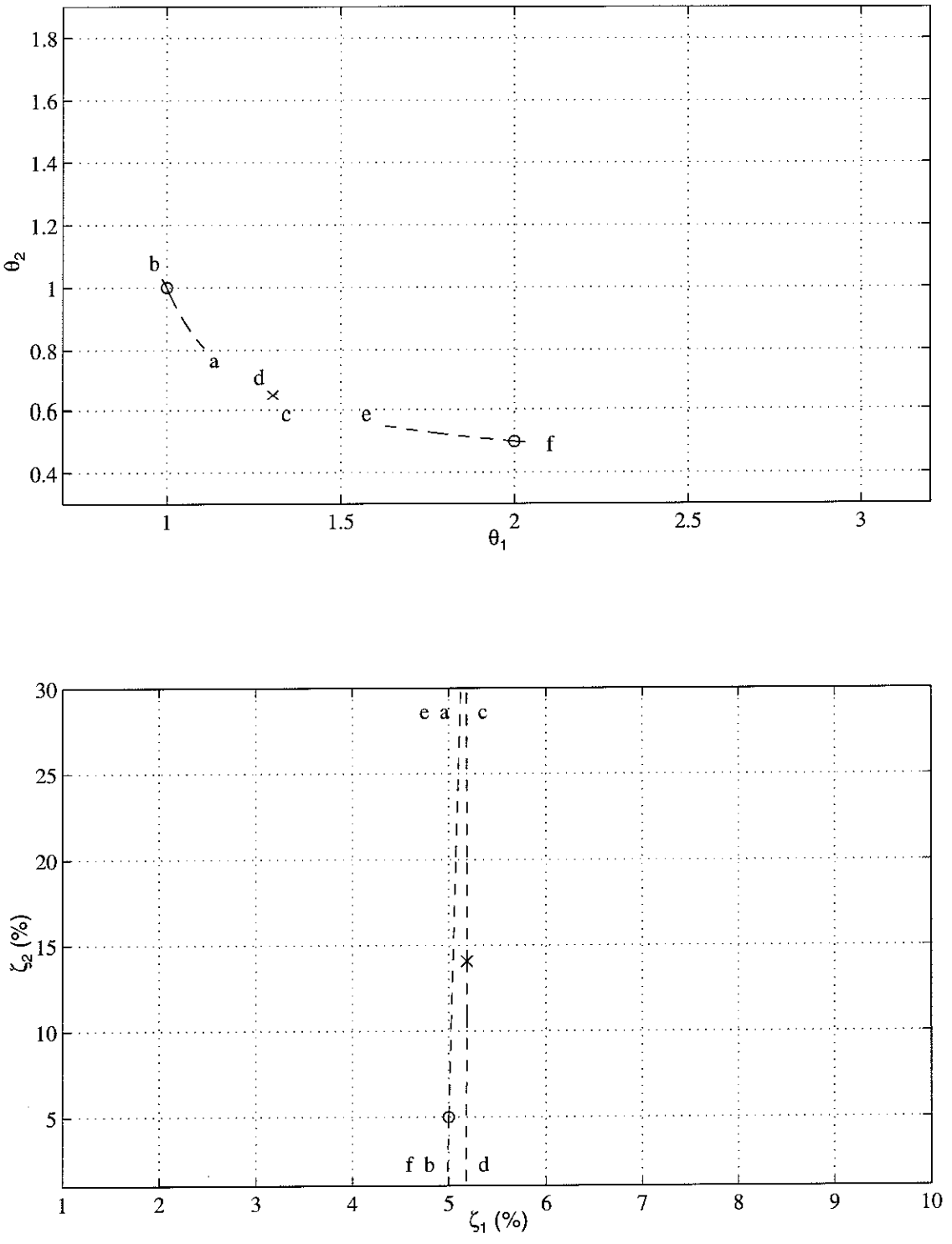

Figure 5.23: Projected Relaxation Trajectory ($\frac{\partial J_E(a)}{\partial \zeta_2} = 0$ is relaxed) in the Identification of $\underline{\theta}_o$, $\underline{\theta}_e$, and $\underline{\zeta}_o$ (No Noise).

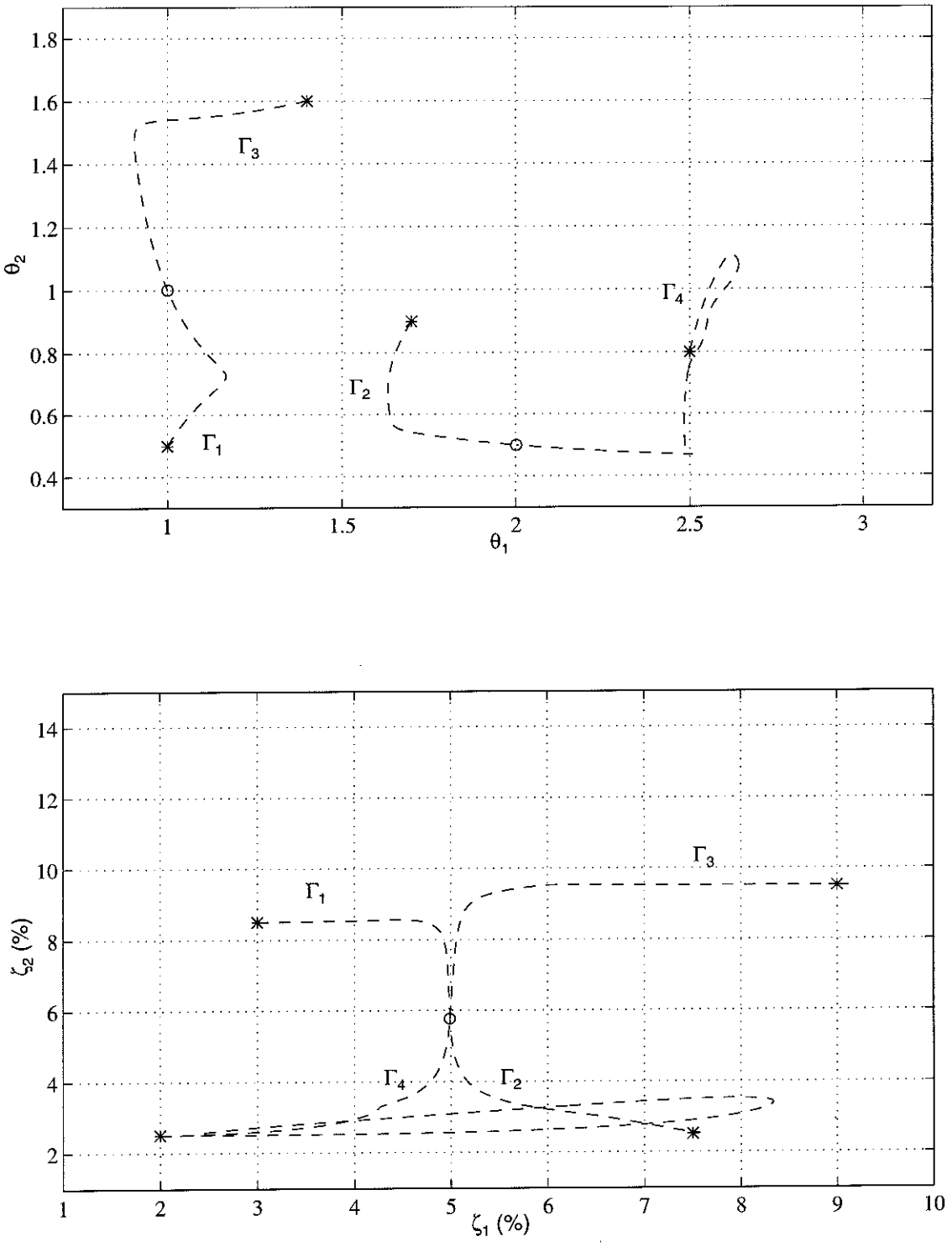

Figure 5.24: Projected Homotopy Trajectories in the Identification of $\hat{\underline{a}}$ (100% Noise).

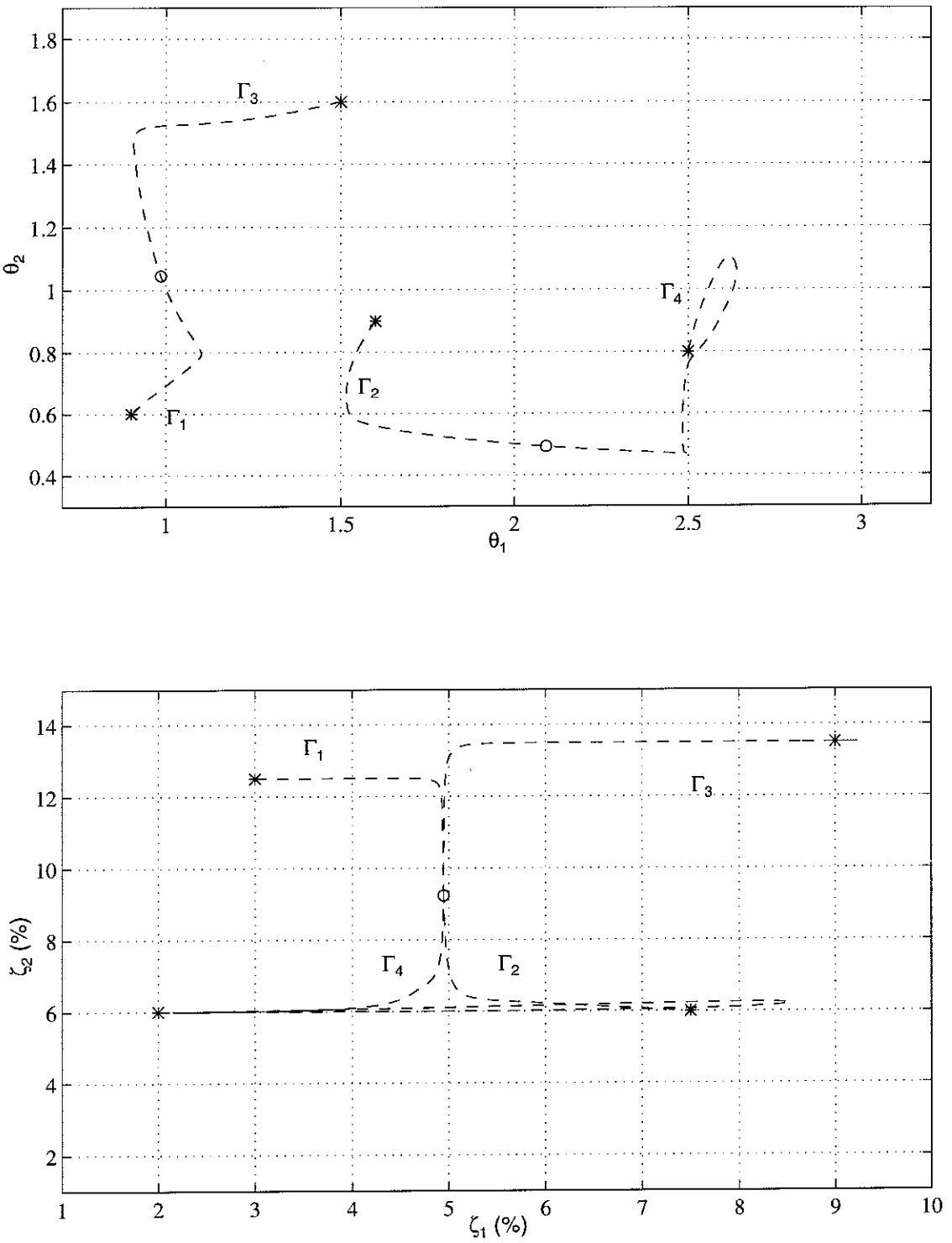

Figure 5.25: Projected Homotopy Trajectories in the Identification of $\hat{\underline{a}}$ (300% Noise).

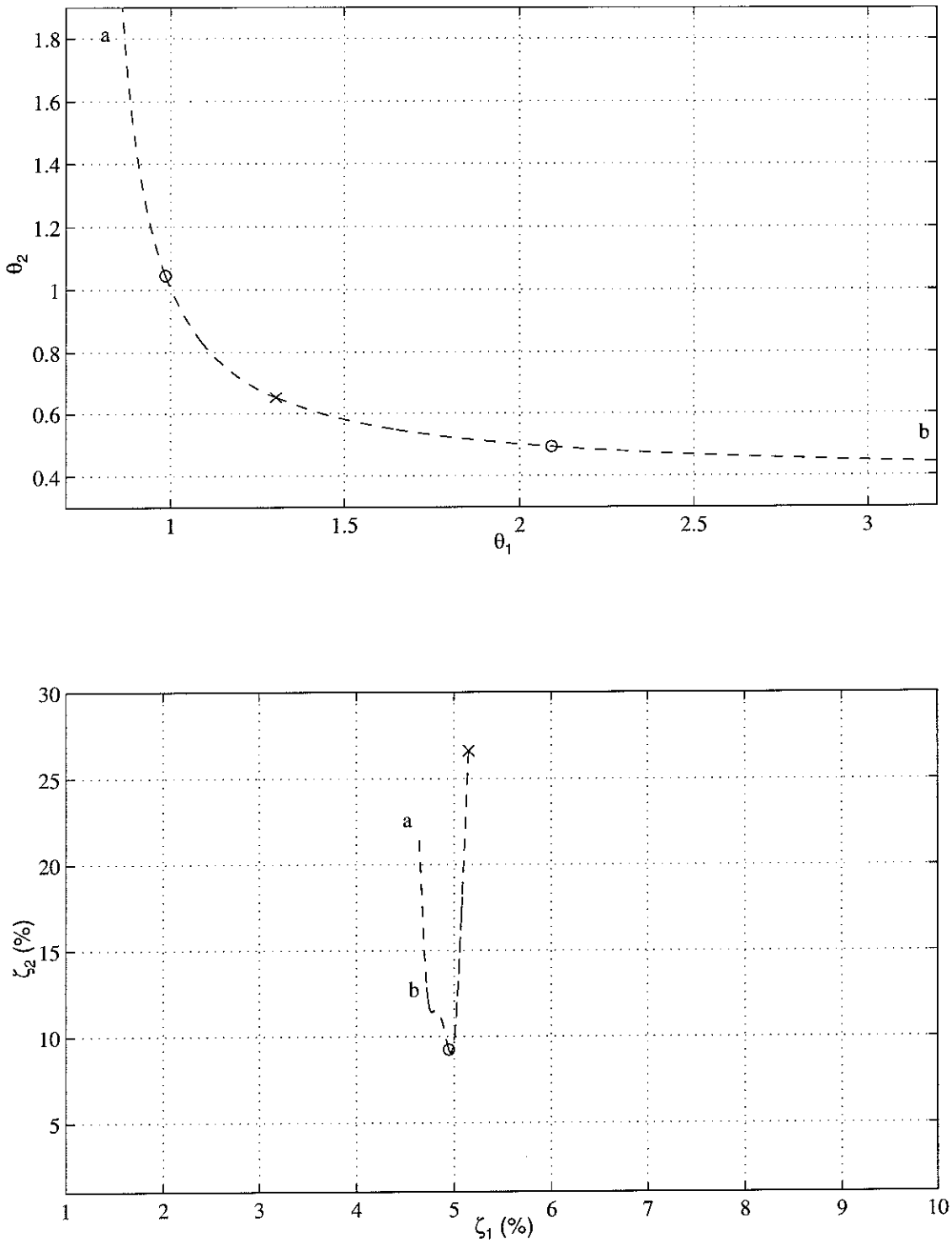

Figure 5.26: Projected Relaxation Trajectory ($\frac{\partial J_E(\underline{a})}{\partial \theta_1} = 0$ is relaxed) in the Identification of $\underline{\hat{a}}$ (300% Noise).

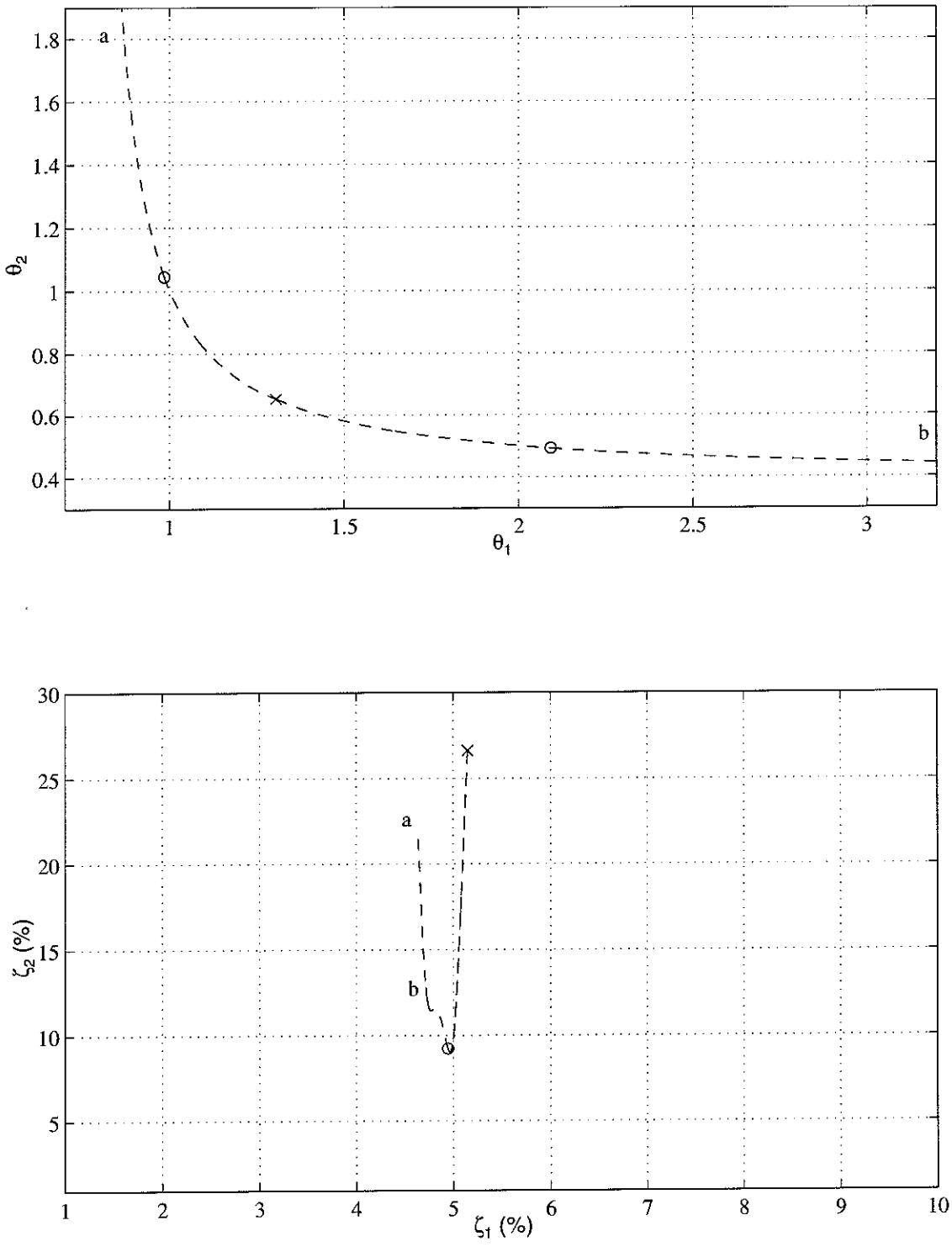

Figure 5.27: Projected Relaxation Trajectory ($\frac{\partial J_E(\underline{a})}{\partial \theta_2} = 0$ is relaxed) in the Identification of $\underline{\hat{a}}$ (300% Noise).

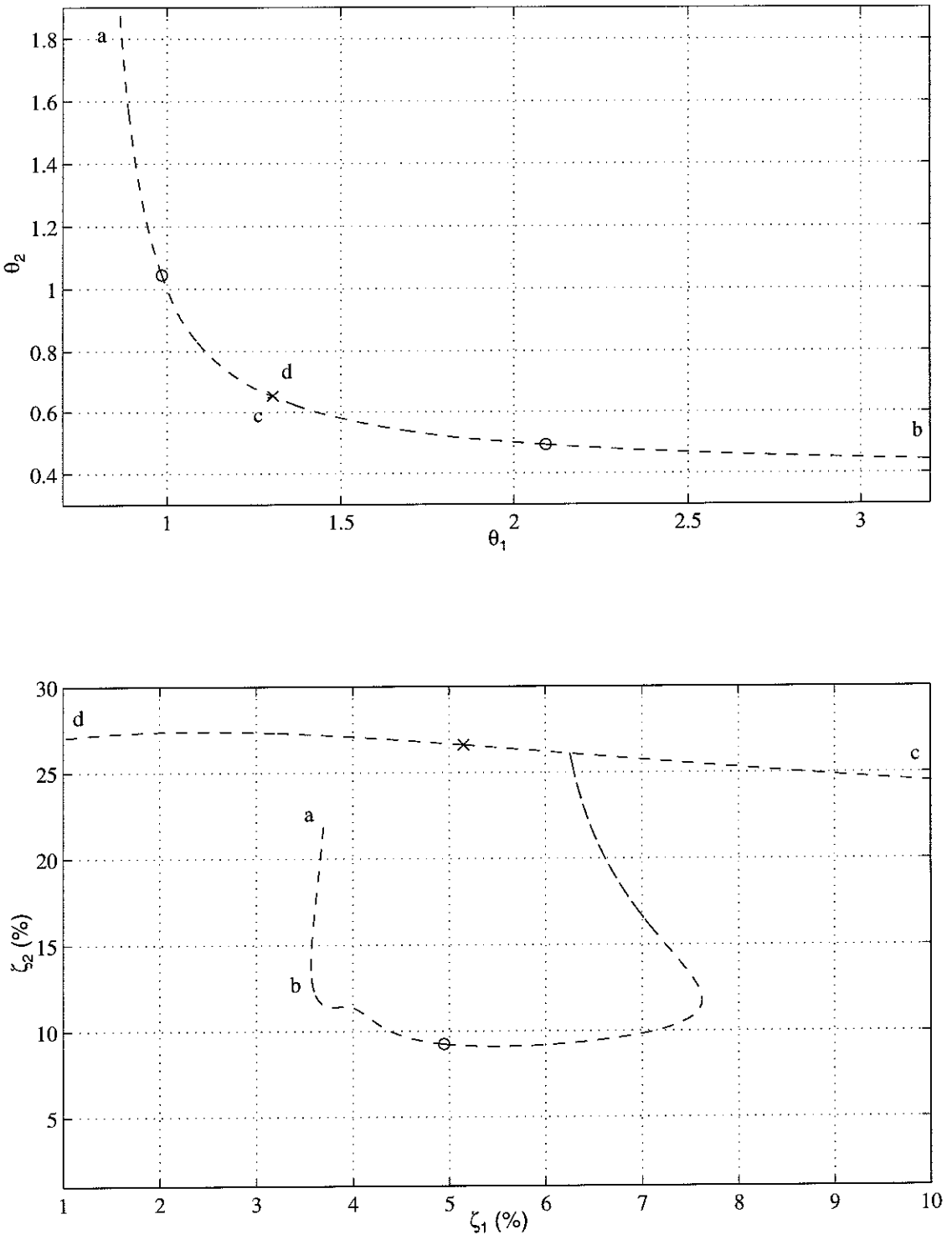

Figure 5.28: Projected Relaxation Trajectory ($\frac{\partial J_E(\underline{a})}{\partial \zeta_1} = 0$ is relaxed) in the Identification of $\underline{\hat{a}}$ (300% Noise).

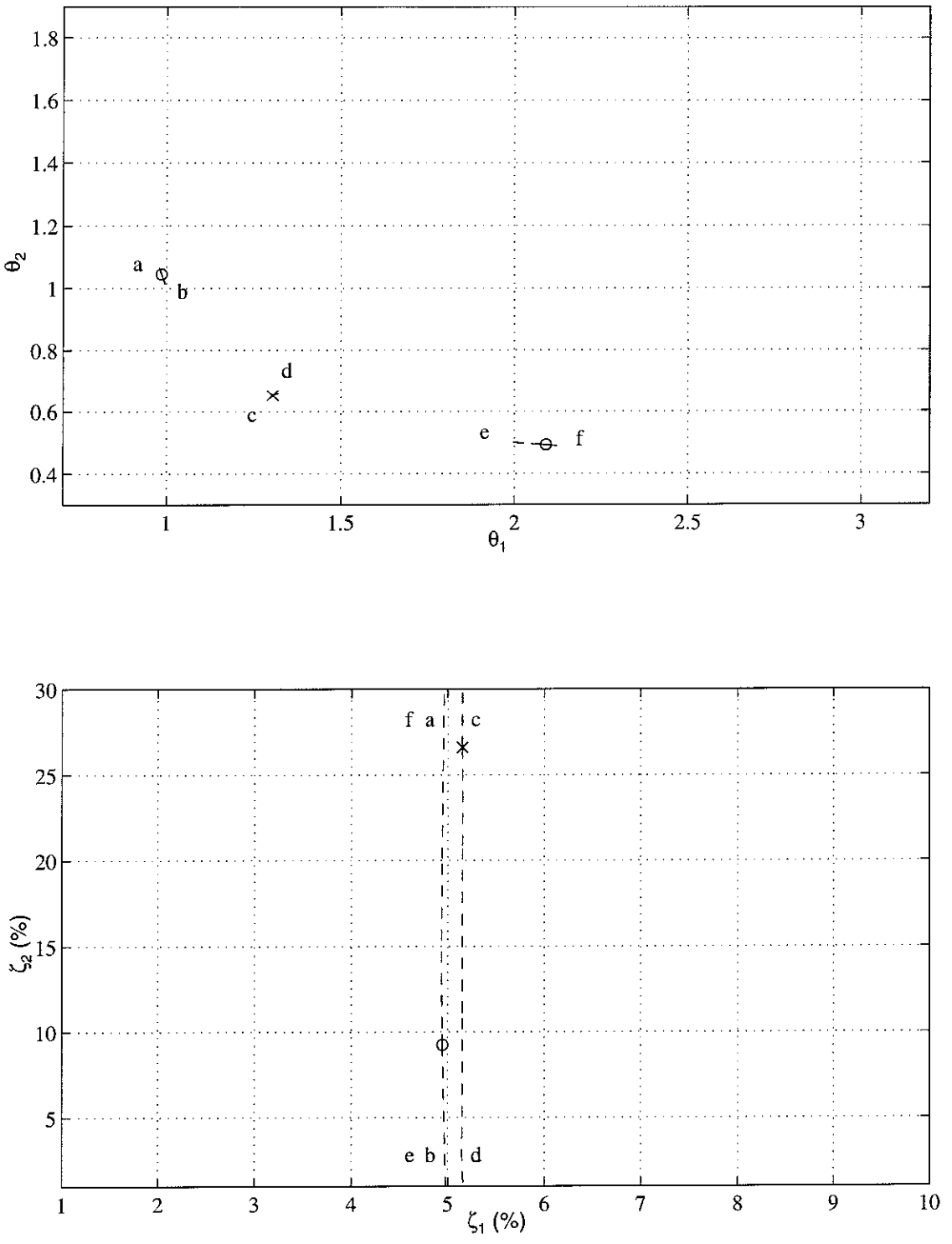

Figure 5.29: Projected Relaxation Trajectory ($\frac{\partial J_E(\underline{a})}{\partial \zeta_2} = 0$ is relaxed) in the Identification of $\underline{\hat{a}}$ (300% Noise).

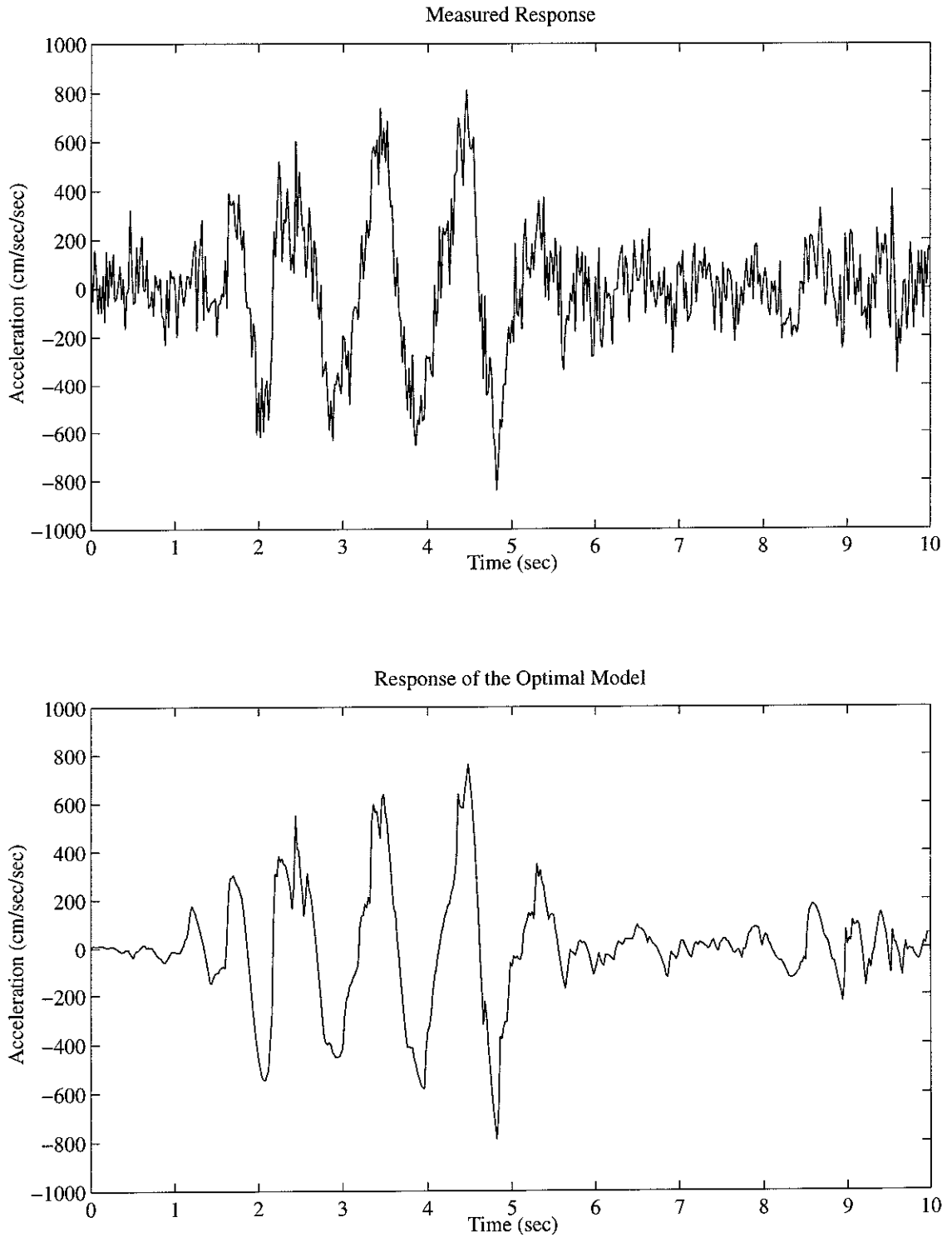

Figure 5.30: Measured "Roof" Response of the Two-Story Structure and the Response of the Optimal Linear Chain Models (300% Noise).

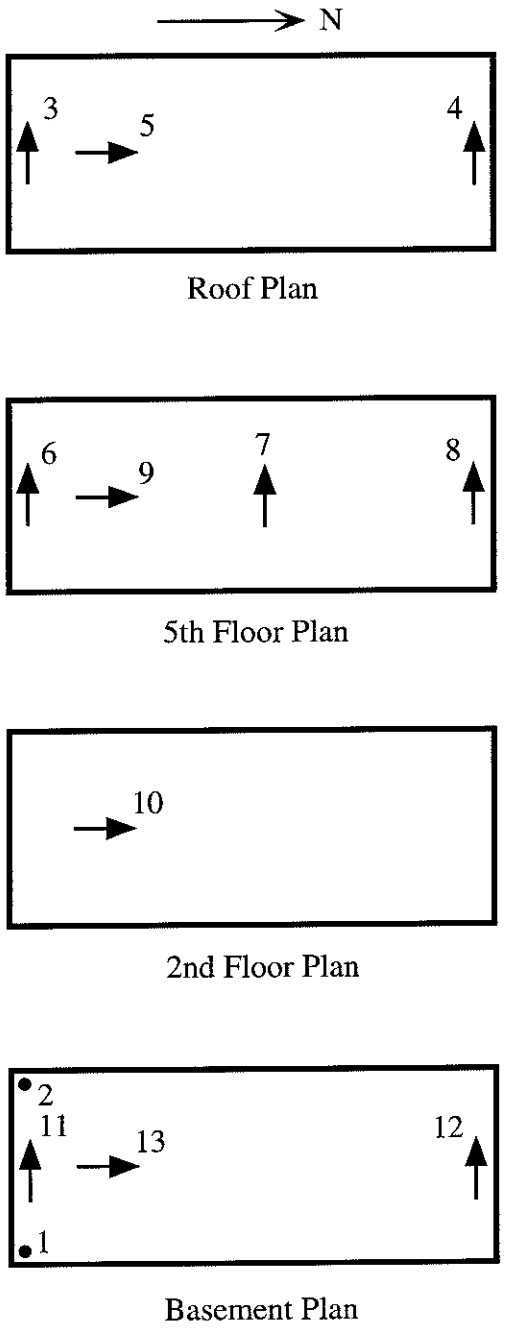

Figure 5.31: Illustration of Accelerometer Deployment in the Great Western Bank.

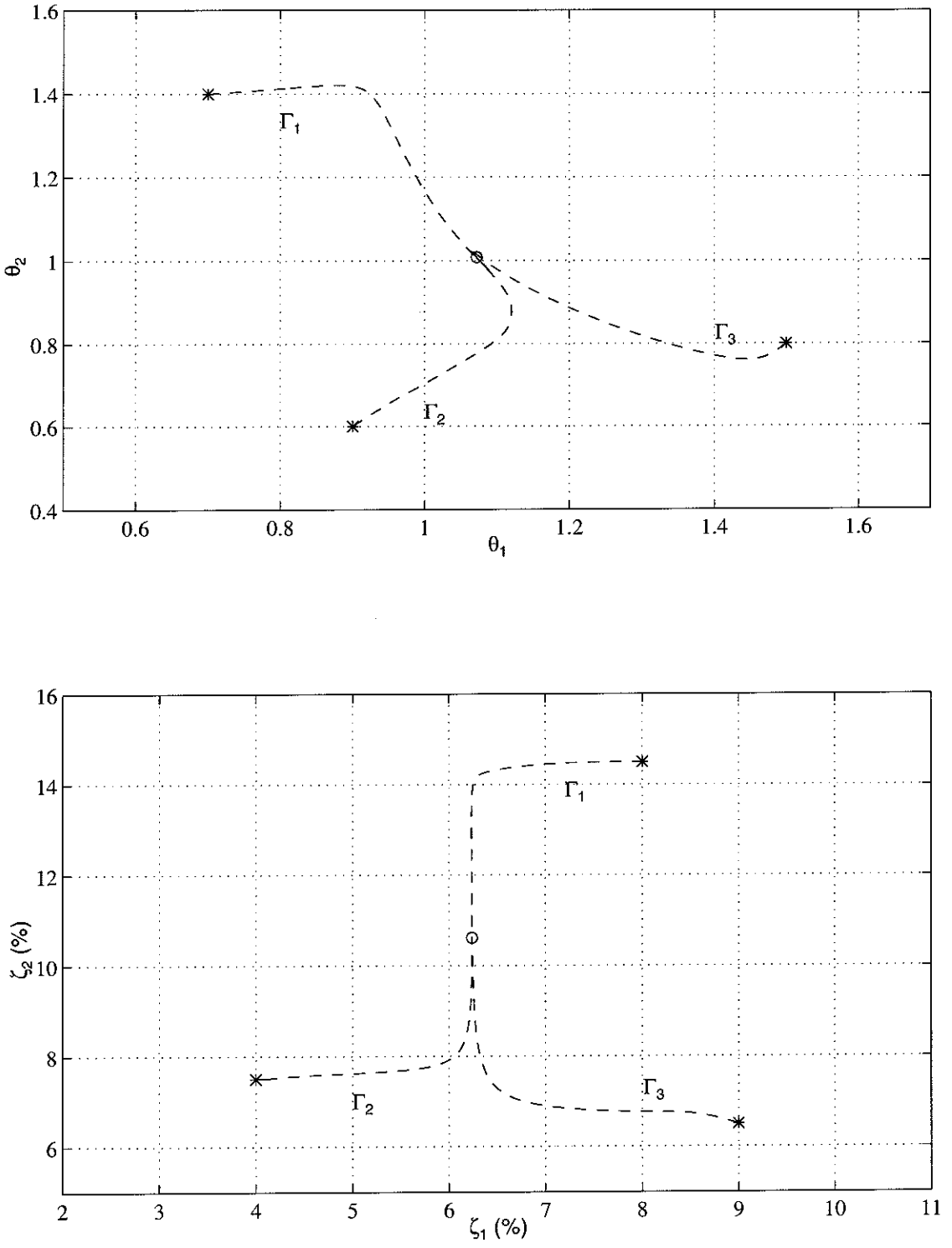

Figure 5.32: Projected Homotopy Trajectories in the Identification of the Optimal Model for the Great Western Bank (Transverse Direction) [Rocking-Base Model].

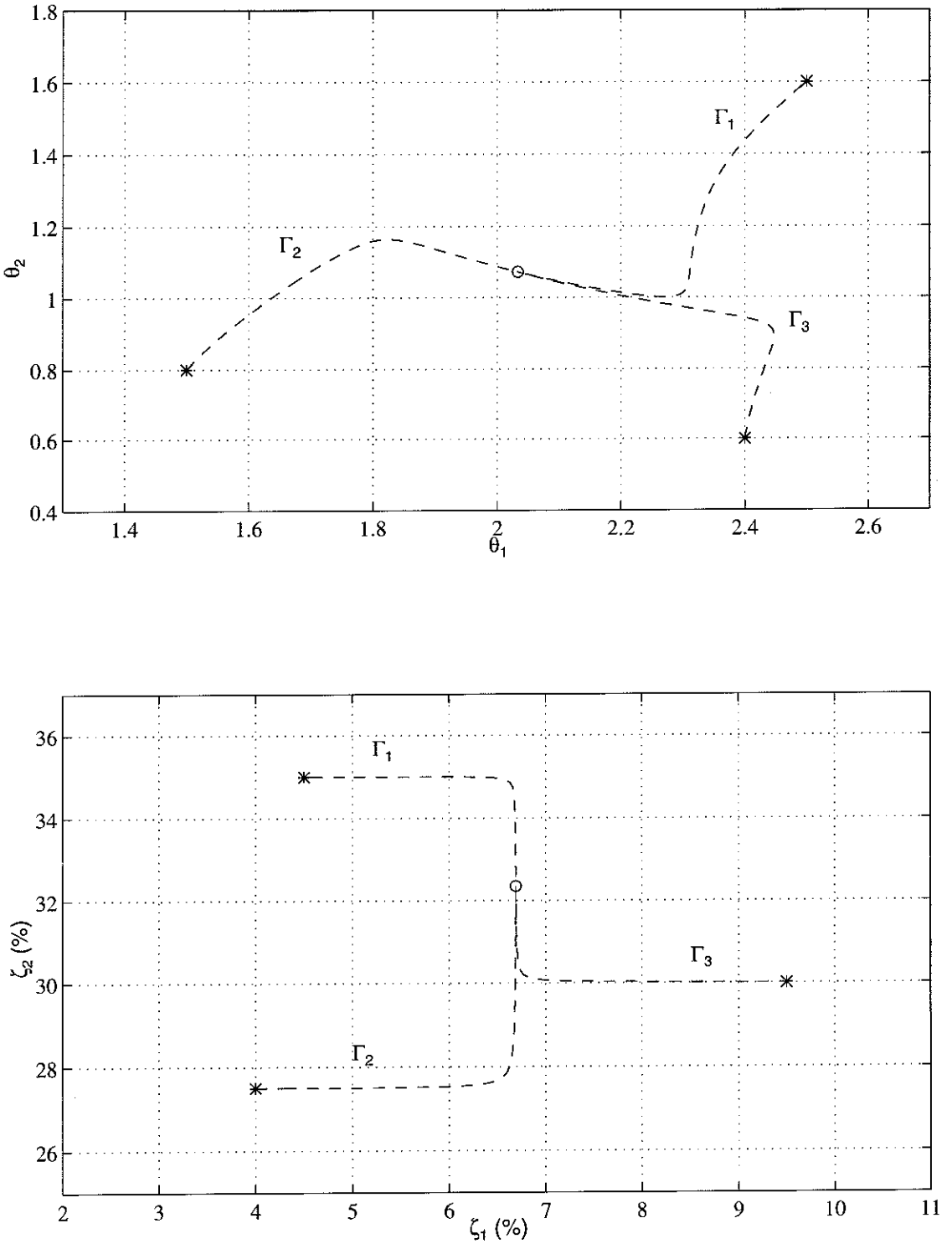

Figure 5.33: Projected Homotopy Trajectories in the Identification of the Optimal Model for the Great Western Bank (Transverse Direction) [Fixed-Base Model].

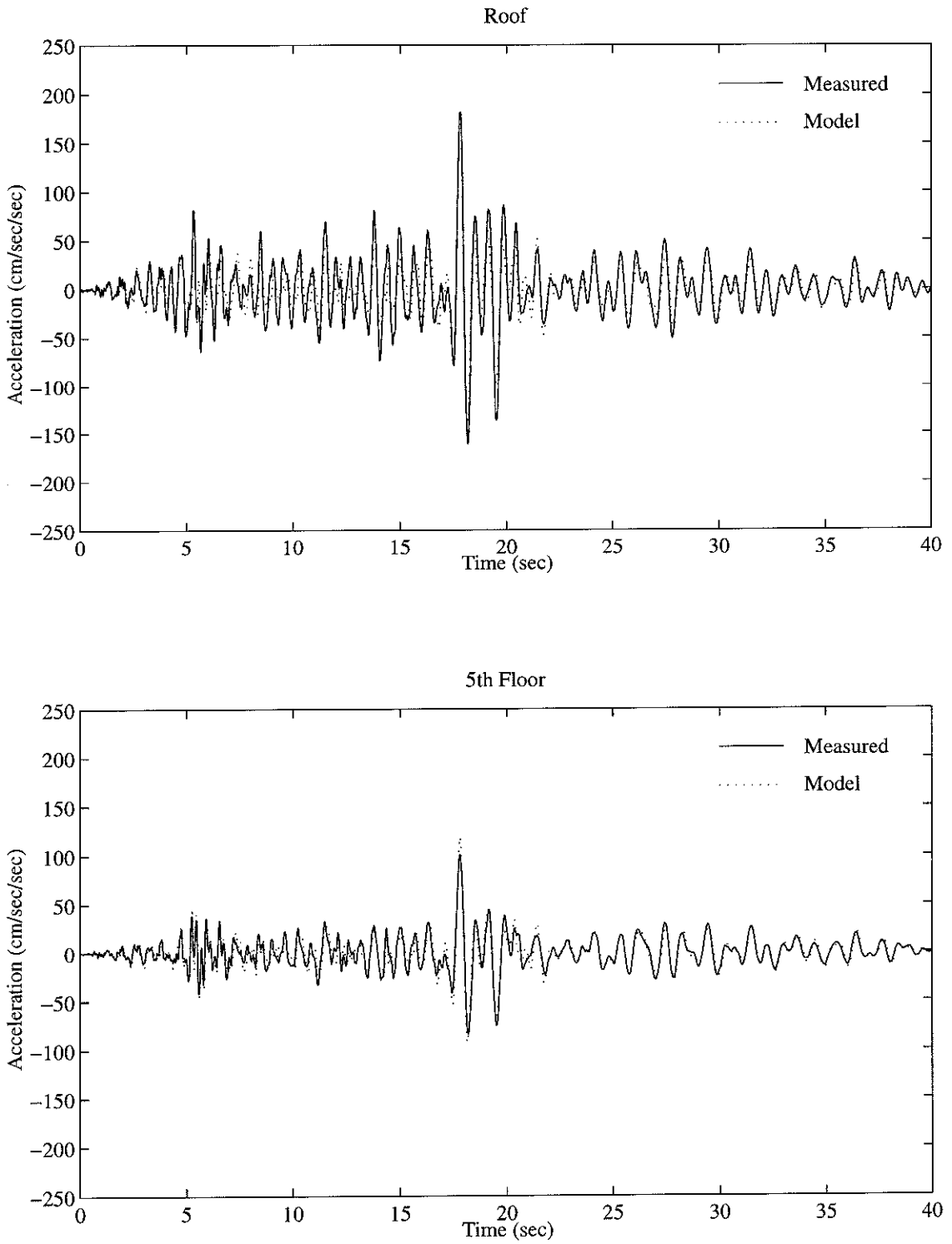

Figure 5.34: Comparison between Measured Response and Model Response (Transverse Direction) [Rocking-Base Model].

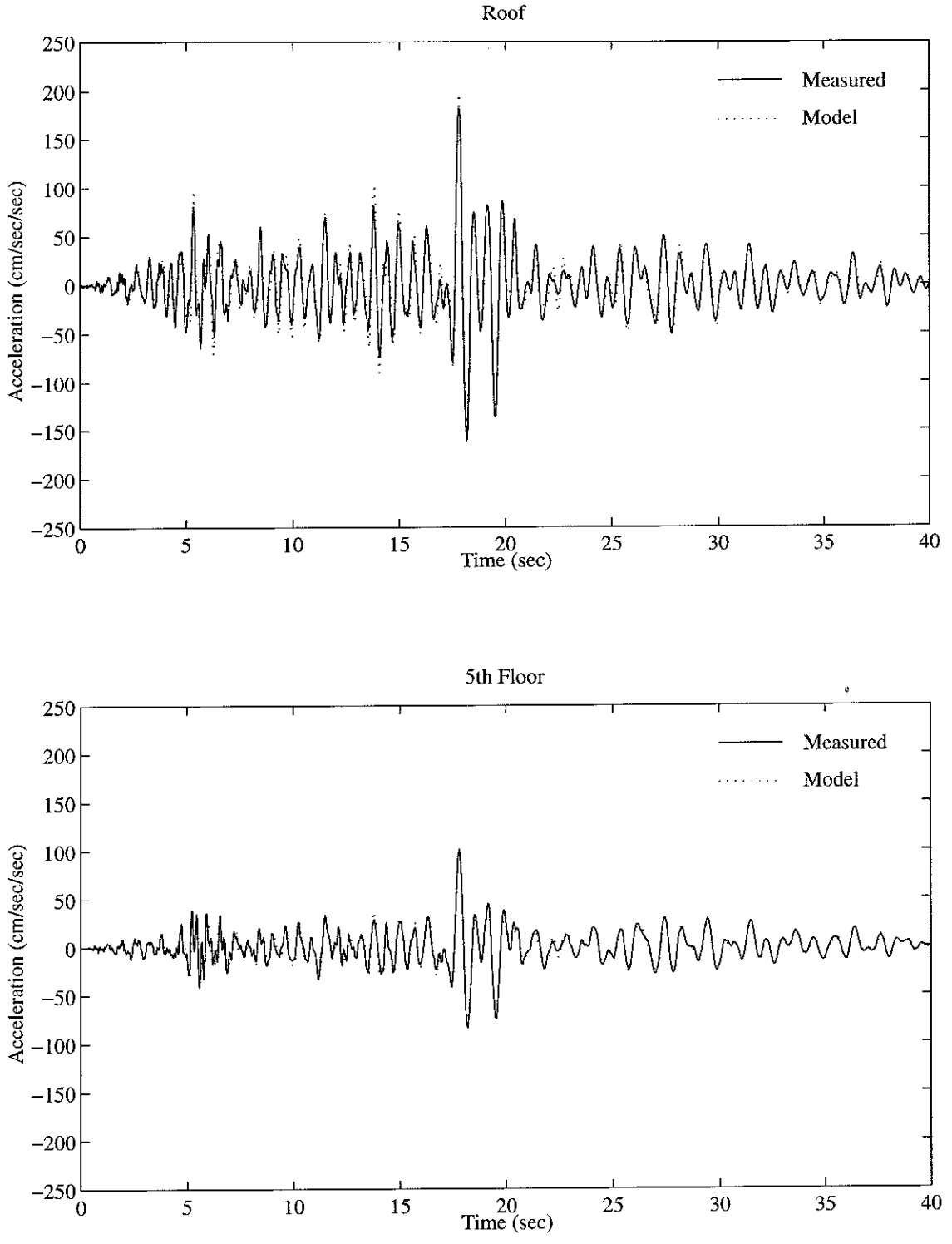

Figure 5.35: Comparison between Measured Response and Model Response (Transverse Direction) [Fixed-Base Model].

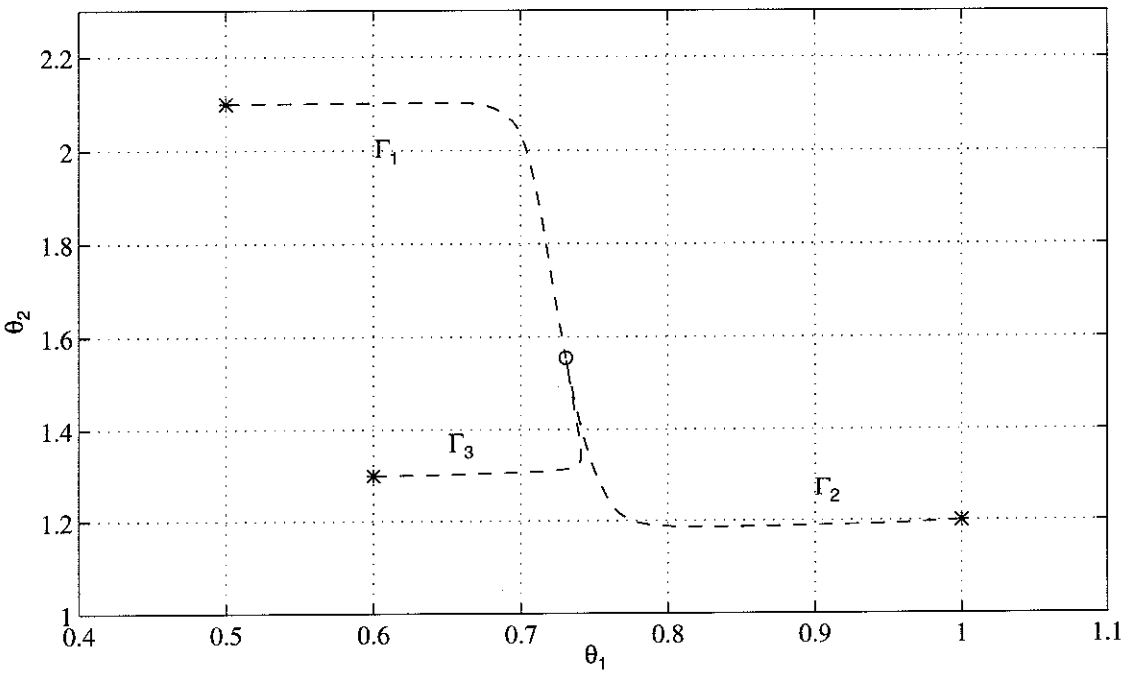

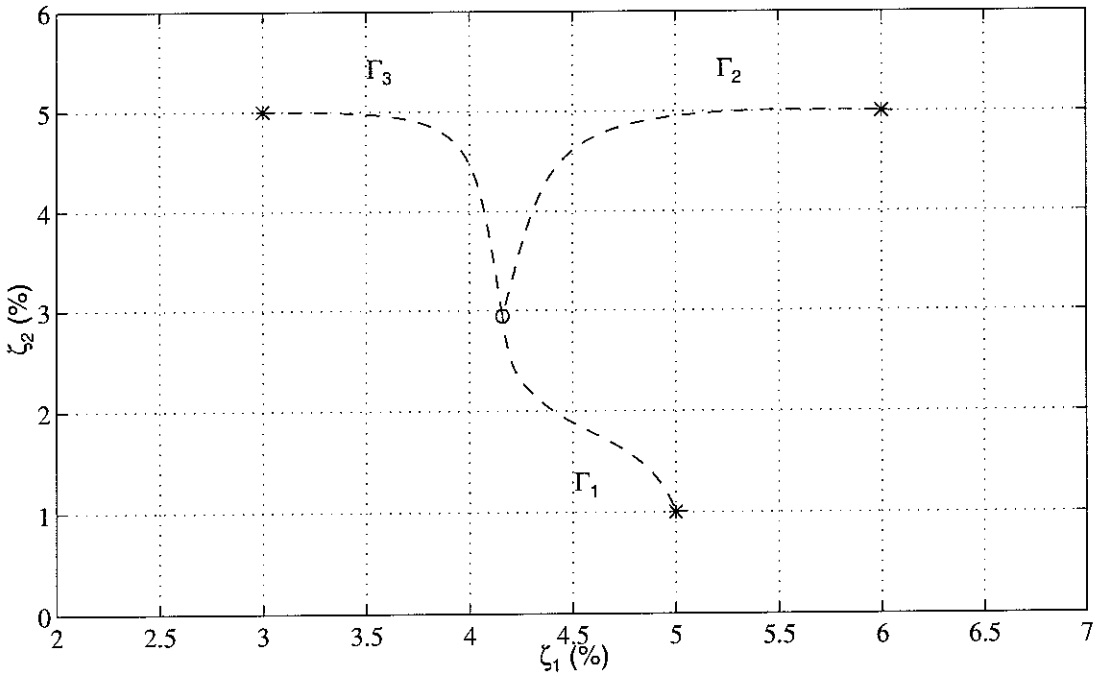

Figure 5.36: Projected Homotopy Trajectories in the Identification of the Optimal Model for the Great Western Bank (Longitudinal Direction).

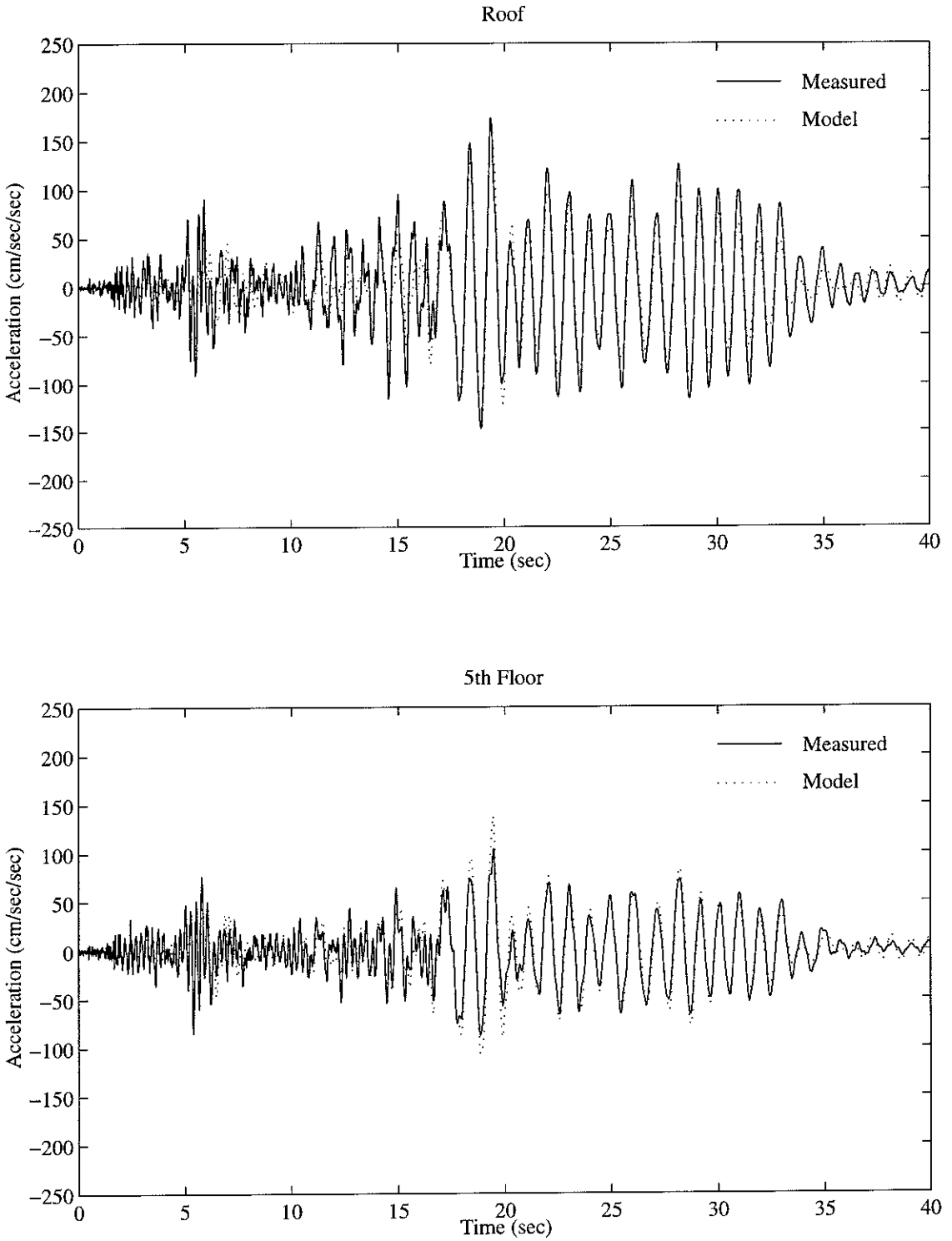

Figure 5.37: Comparison between Measured Response and Model Response (Longitudinal Direction).

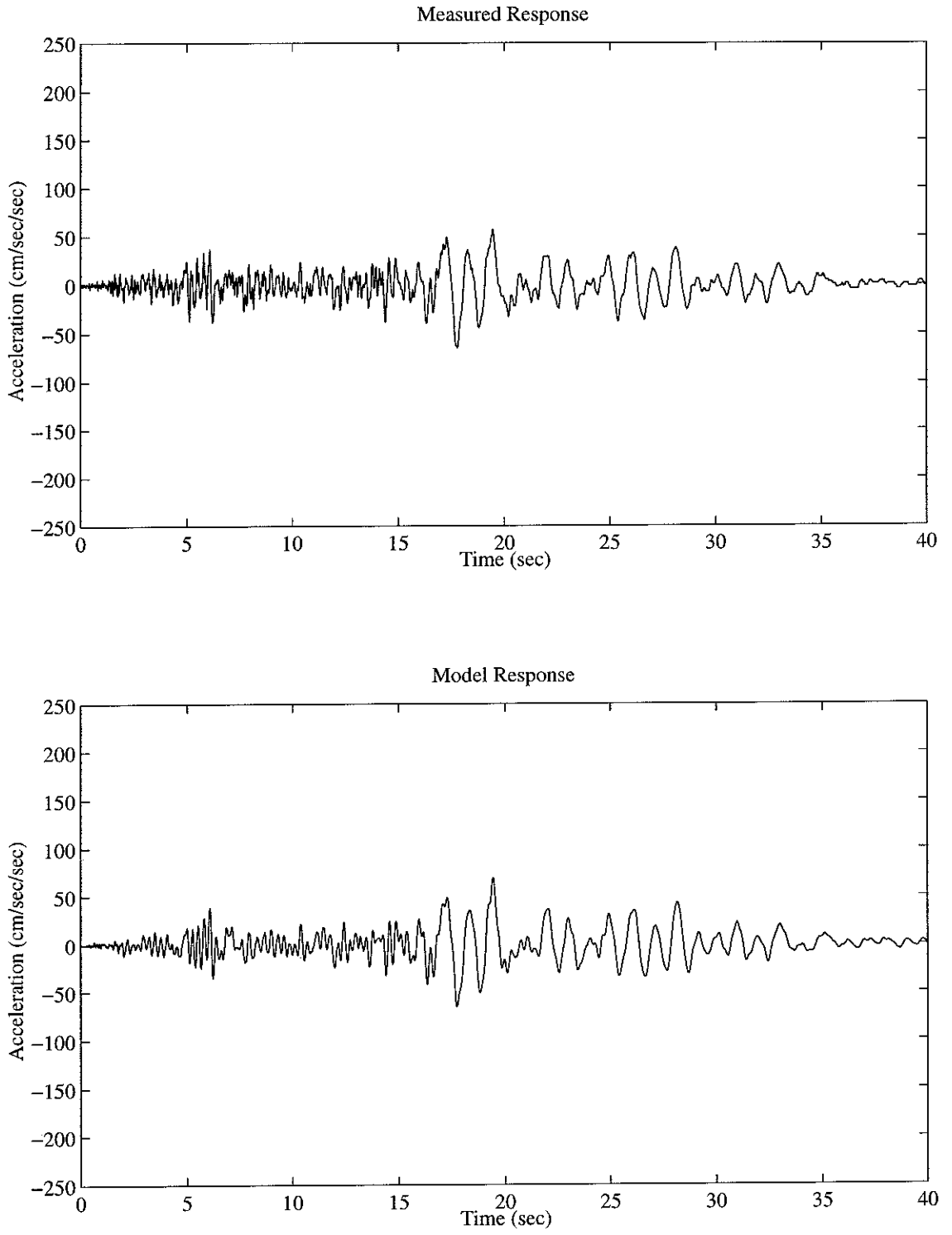

Figure 5.38: Comparison between Measured Response and Model Response at the 2nd Floor (Longitudinal Direction).

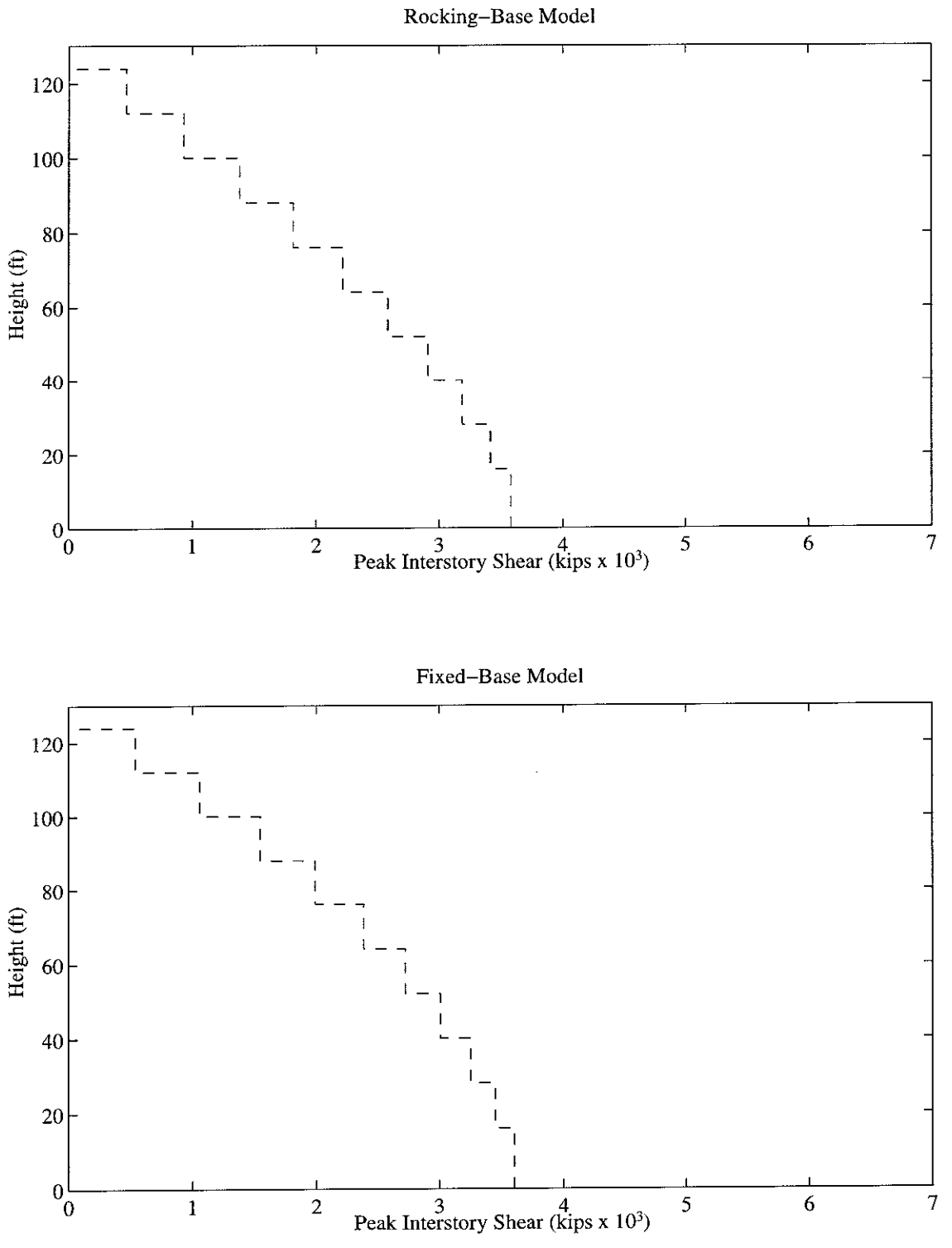

Figure 5.39: Envelope of Peak Interstory Shear Force (Transverse Direction).

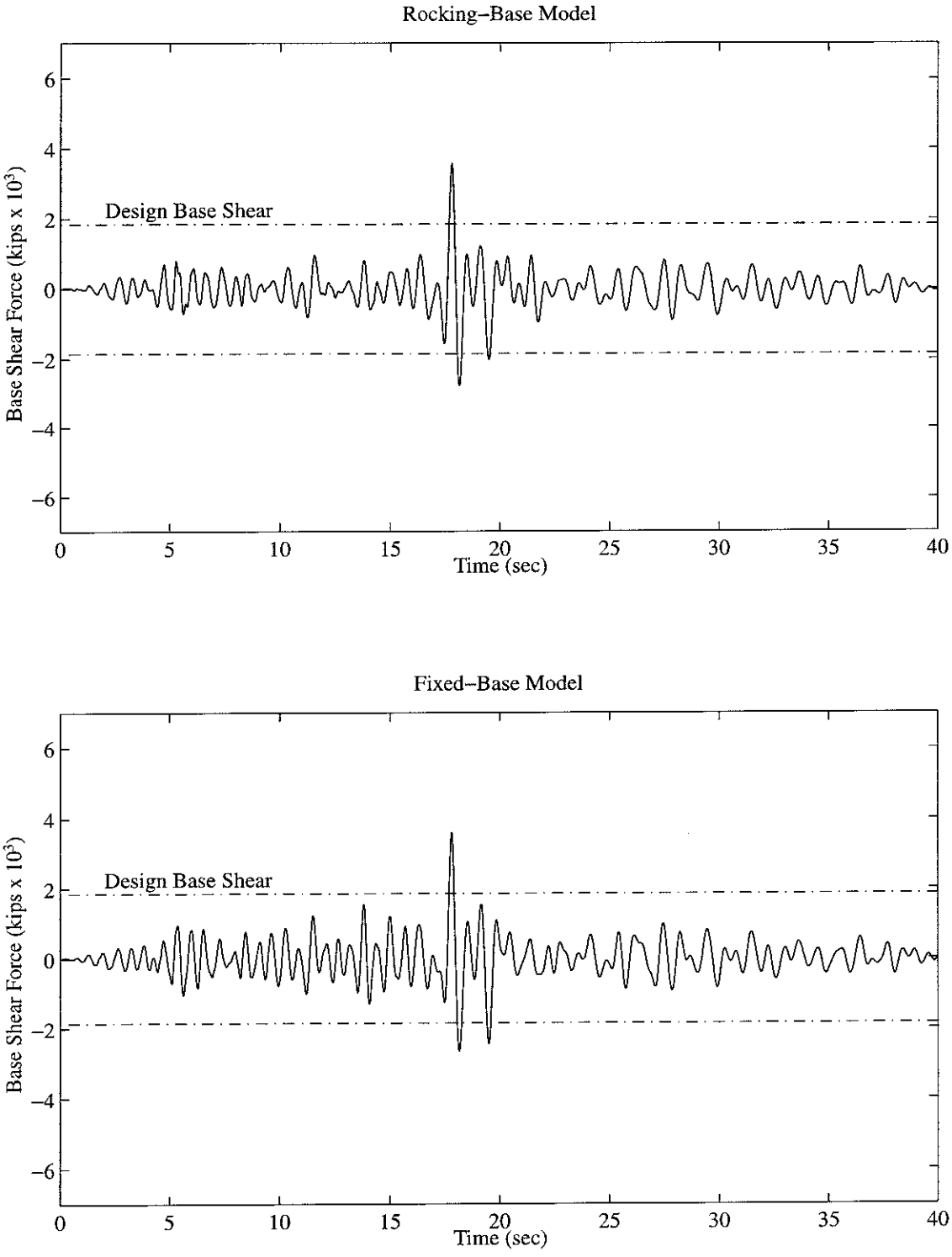

Figure 5.40: Time Histories of Base Shear Force (Transverse Direction).

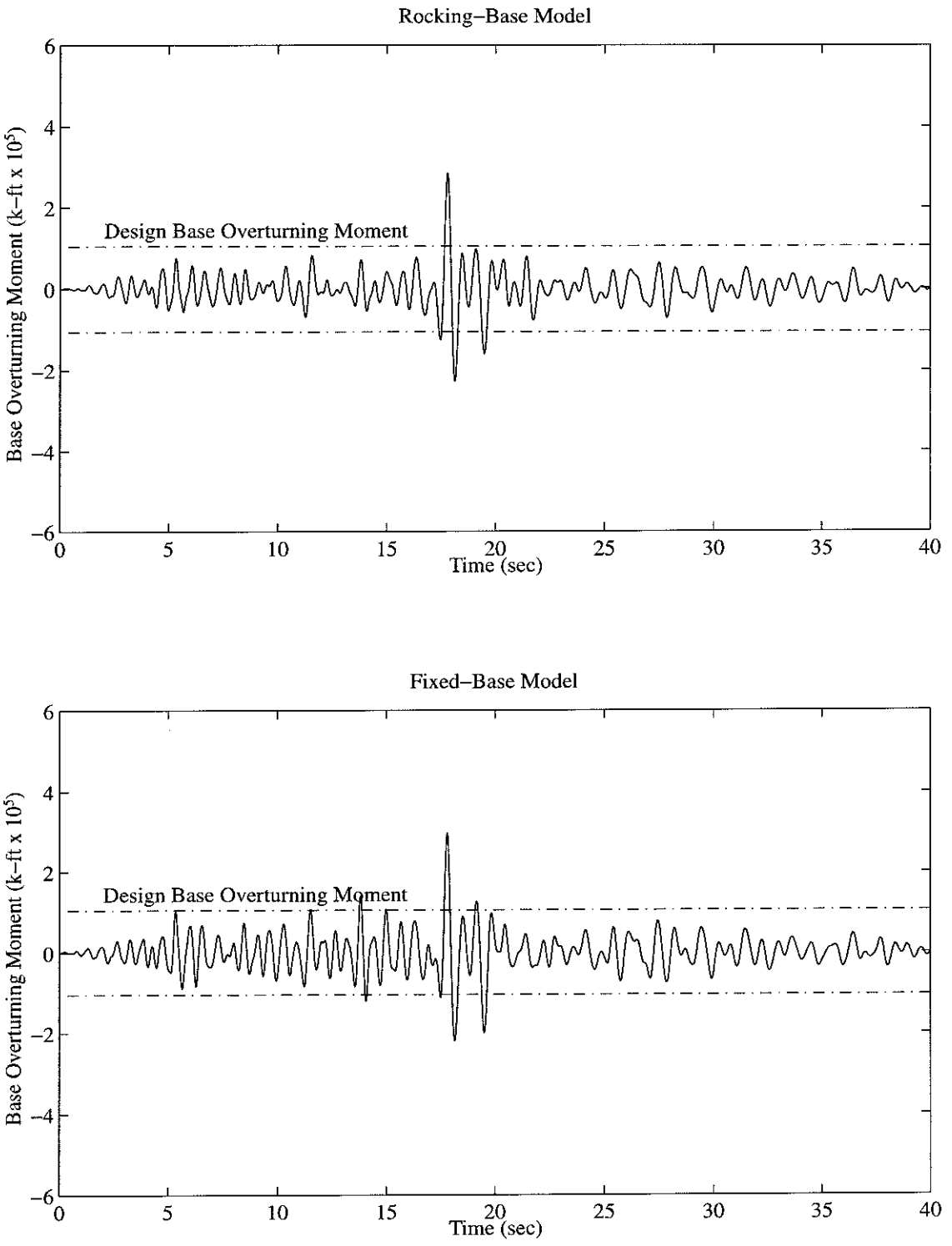

Figure 5.41: Time Histories of Base Overturning Moment (Transverse Direction).

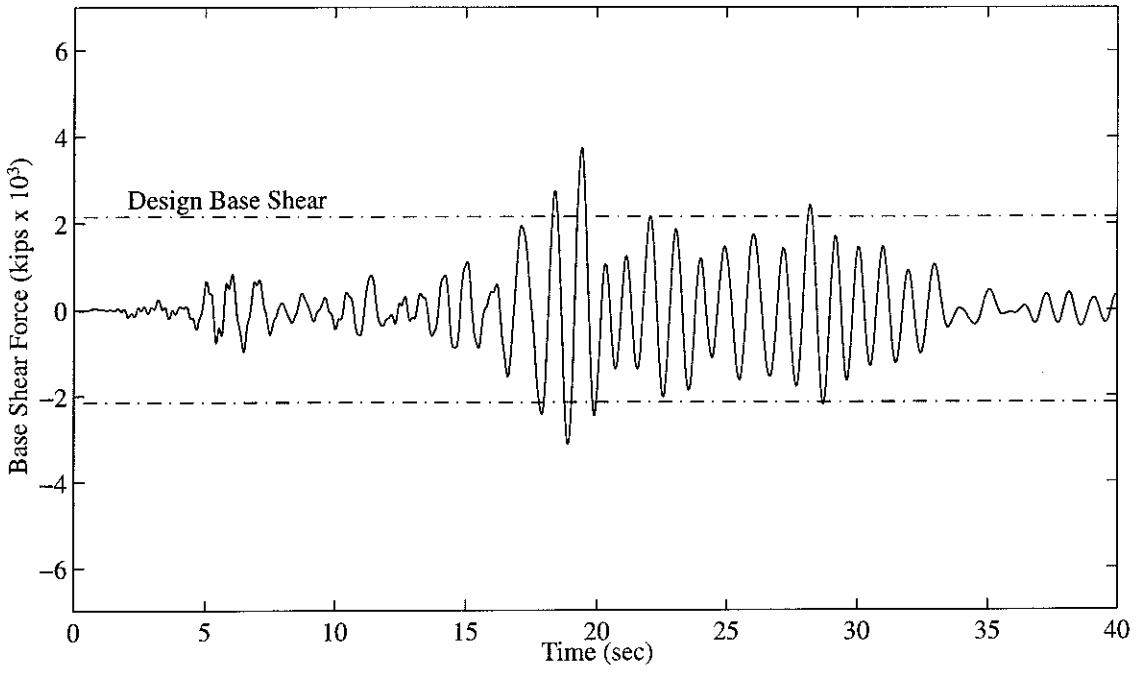

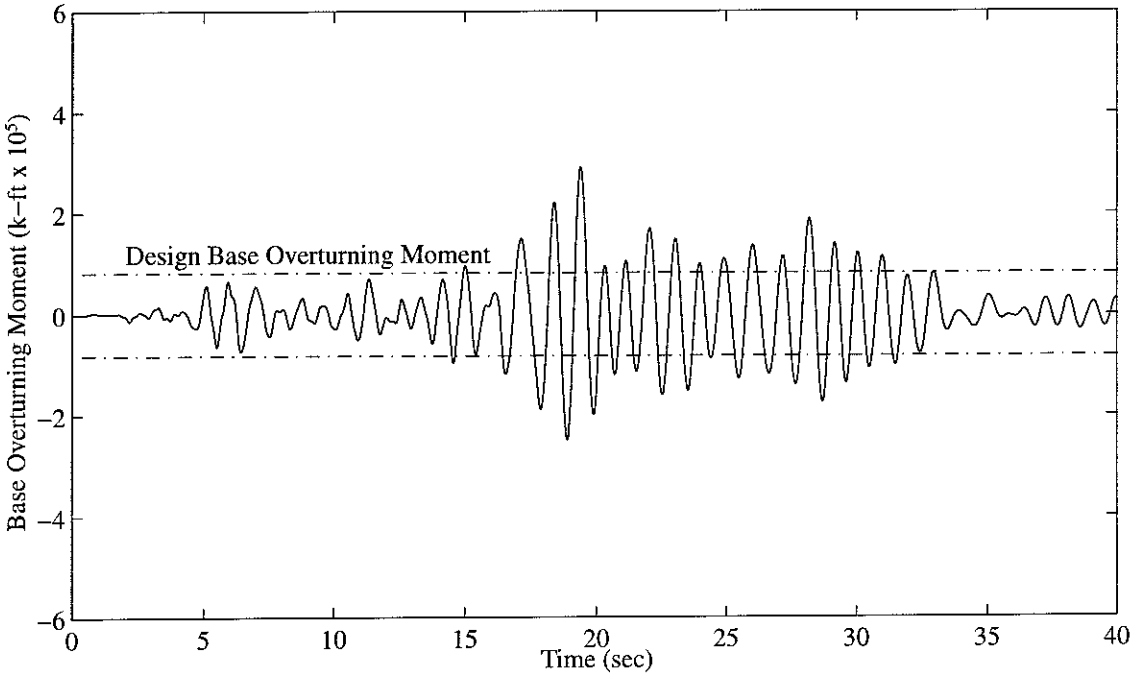

Figure 5.42: Time Histories of Base Shear Force and Base Overturning Moment (Longitudinal Direction).

Chapter 6

Conclusions and Future Research

6.1 Summary and Conclusions

In this dissertation, a pragmatic and versatile statistical system identification framework is presented and applied to seismic response records from structures. The framework is based on the interpretation of probability as a measure of plausibility and on Bayesian statistical inference. This interpretation of probability is more useful than the classical interpretation in terms of the limiting relative frequency of occurrence of events and is appropriate to describe the uncertainty in structural modeling, i.e., parameter uncertainty and modeling error. By making suitable choices for the class of probabilistic models in the framework, various classical system identification techniques can be derived and viewed as the special cases of the framework. However, the framework can provide a more informative interpretation of the identified optimal model than classical system identification techniques.

Even though the exact posterior probability distributions of model parameters and predicted system output in the statistical system identification framework do not require parameter estimation in the usual sense, the multi-dimensional integral cannot be evaluated analytically, nor numerically if the number of parameters is more than a few. Fortunately, when the number of sampled input and output data from structures is large, some useful asymptotic approximations of the analytical results are available. To incorporate these asymptotic approximations into the statistical system identification framework, definitions of system identifiability and model identifiability are presented. For the system identifiable case, existing asymptotic approximation formulas are described. The results are then extended to the system un-identifiable case to broaden the applicability of the statistical system identification framework.

From the viewpoint of asymptotic approximations, the system identification problem is then converted into a non-trivial global optimization problem. Because the objective function in the asymptotic approximations in the statistical system identification framework is not convex, there may be multiple optimal models in the parameter space. Two generalized trajectory methods, the homotopy scheme and the relaxation scheme, are presented which can be combined to provide a very robust numerical procedure for global optimization. The homotopy scheme provides a robust algorithm to find a stationary point of the objective function while the relaxation scheme starts from one stationary point and systematically connects other stationary points in the parameter space by a network of trajectories. Since both schemes actually solve the stationarity conditions, they can also be applied to find the roots of a set of nonlinear algebraic equations.

An efficient numerical algorithm for tracking both homotopy trajectories and relaxation trajectories is also proposed. Some properties and behavior of the homotopy trajectory and the relaxation trajectory are analyzed and results are presented. To deal with multiple trajectory components, a new approach is proposed in which multiple applications of the relaxation scheme are used in a systematic way so that the chance of finding all the stationary points increases. It is not easy to claim that one global optimization method is more efficient than another due to the lack of generally accepted criteria for comparing global optimization methods. With the advance of computer technology, however, robustness of global optimization methods has become more important than the efficiency, provided the computational effort is not prohibitive. From this perspective, the proposed generalized trajectory methods provide a very robust numerical procedure to find multiple local extrema as part of a strategy for global optimization.

The modal identification technique has been applied by using seismic response records from different types of civil structures to estimate their modal properties. In spite of its successful and broad applications, the modal identification technique has the limitations that no information can be directly extracted from the measured data

regarding the uninstrumented degrees of freedom of a structure and the search for optimal modal parameters is cumbersome when additional constraints are imposed on the stiffness matrix of a structure. Partially due to the limitations of modal identification, much attention has been drawn to the challenging problem of structural model updating in the system identification community. Structural model updating is useful because it can be applied to structural health monitoring which can provide early warning of damage of structural components. It is also desirable since the theoretically based stiffness matrix of a structure can be improved by using the measured data to give more accurate response predictions.

However, there are two intrinsic difficulties in structural model updating using real seismic structural response records. The first constraint is that seismic structural response is usually measured at only a few degrees of freedom in a structure because of economic reasons. Also, only a few dominant modes contribute to real seismic structural response. These two factors impose a severe limitation on the number of free parameters in the stiffness matrix if the identified stiffness matrix is to be accurate and at least locally unique. The number of dominant modes depends on the frequency content of the ground acceleration and the type of structure and it is unlikely that this number can be significantly increased. The only alternative, then, is to increase the number of measured degrees of freedom in a structure so that more mode shape information is incorporated if it is desired that the stiffness distribution of a structure be described in more detail by using more parameters.

Most research in structural model updating uses a two-stage approach in which a modal identification technique is first applied to identify the modal parameters of the dominant modes and then the stiffness matrix is adjusted according to various proposed methods so that it is consistent with the identified modal parameters. The main issue in the two-stage approach is that there is no well-accepted guideline in selecting the weight to give each dominant mode in the second stage. Different combinations of weights will give different estimated stiffness matrices. A single-stage structural model updating approach using the least-squares prediction-error method

and a substructuring technique is proposed. The advantage of the single-stage approach is that the identified stiffness matrix depends on the structural response time history directly and, therefore, only one class of probabilistic models is needed in the statistical system identification framework. Furthermore, the identified stiffness matrix is based on the directly measurable structural response rather than the modal parameters which can only be estimated indirectly.

In the proposed single-stage structural model updating approach, the damping factors of the dominant modes are also included as part of the model parameters so that the damping in a structure can be identified as well. Both the homotopy scheme and the relaxation scheme are applied to determine the optimal model parameters by minimizing the objective function in the least-squares prediction-error method. To reduce numerical round-off error and increase the accuracy in tracking both homotopy trajectories and relaxation trajectories, the gradient vector of the objective function is calculated by using analytical expressions instead of finite-difference approximations. The proposed structural model updating approach is applied to both simulated and real structural response data. It turns out the approach works well when simulated structural response data is used. However, another issue in structural model updating is noted when real structural response data is used.

Since there is only a small number of measured degrees of freedom in a structure with typical seismic instrumentation, the use of substructuring is necessary in order for the stiffness matrix to be at least locally identifiable. However, another important issue at stake is whether the identified optimal structural model can provide a physically feasible description of the stiffness distribution in the structure. Because each substructure has different scope of influence on the model behavior and a physically feasible stiffness distribution depends on the stiffness of all the substructures, there is no guarantee that the small set of measured degrees of freedom can provide enough constraints on the stiffness matrix so that the description of the stiffness distribution in the structure is physically feasible. It is possible that the model output of an identified optimal structural model may fit the measured structural response

reasonably well but it may not be considered plausible because its description of the stiffness distribution in the structure is not physically feasible. This discrepancy may be alleviated by increasing the number of measured degrees of freedom in a structure. However, the selection of appropriate structural models and proper choice of substructuring scheme are equally crucial as well.

6.2 Future Research

The proposed generalized trajectory methods are applicable when the stationary points of an objective function are isolated. In system identification, this situation corresponds to the system identifiable case in which there is a finite number of optimal models. It is of interest to explore if both methods are still applicable when the class of models is system un-identifiable and the set of optimal model parameters consists of a collection of smooth and non-intersecting curves.

It is desirable to have more applications of the proposed single-stage structural model updating approach using real structural response data. As discussed, seismic structural response records at more degrees of freedom in a structure are crucial for successful structural model updating. Since real seismic structural response records are usually available at only a few degrees of freedom in a structure, the use of experimental data remains as an alternative for future investigation of the structural model updating problem. Also, the planned dense seismic instrumentation of some structures using 50 to 100 sensors will provide better data for developing and testing structural model updating approaches. Besides, how to constrain the stiffness matrix such that the stiffness distribution remains physically realistic is also an important research issue.

Severe vibration of structures during earthquakes may reduce their serviceability or cause structural damage. Structural control consists of techniques to reduce structural vibration either by enhancing the energy dissipation capability of structures or isolating structures from external excitations. Various structural control algorithms and devices have been investigated and presented in the literature. Nevertheless, structural control design considering inherent uncertainty in structural modeling is

difficult to treat and it is recognized as an important area for research. From this perspective, robust structural control based on a probability distribution over the set of possible models, in conjunction with the statistical system identification framework presented here, is a promising area to explore.